# Application of inductively coupled plasma emission spectrometry in the analysis of environmental samples

by

Phillip Lyle Kempster

Submitted in partial fulfilment of the requirements for the degree

Master of Science

in the Faculty of Mathematics and Science
University of Pretoria,
Pretoria.
1986

Date of submission: 11 Feb 1986

# CONTENTS


| | | Page |
|---|---|---|
| ACKNOWLEDGEMENTS | | v |
| ABSTRACT | | vii |
| OPSOMMING | | ix |
| SYMBOLS | | xi |
| ABBREVIATIONS | | xvi |
| CHAPTER 1: | INTRODUCTION | |
| 1.1 | The analytical problem | 1 |
| 1.2 | Scope of this thesis | 3 |
| CHAPTER 2: | LITERATURE OVERVIEW | |
| 2.1 | Introduction | 9 |
| 2.2 | Atomic excitation and ionization | 15 |
| 2.3 | Temperatures within the argon plasma | 20 |
| 2.4 | Excitation mechanisms in the ICP source | 24 |
| 2.5 | Line broadening | 27 |
| 2.6 | Nature of the spectrum emitted by an ICP source | 30 |
| 2.7 | The height of observation | 34 |
| 2.8 | The plasma power | 36 |
| 2.9 | Sample introduction | 40 |
| 2.10 | Noise, precision and detection limit | 45 |
| 2.11 | Stability and drift | 55 |
| 2.12 | Calibration and accuracy | 59 |
| 2.13 | Quality control | 72 |
| 2.14 | Environmental sample analysis | 74 |
| 2.15 | Evaluation of present status | 76 |
| CHAPTER 3: | SAMPLING AND SAMPLE PREPARATION | |
| 3.1 | Introduction | 83 |
| 3.2 | Sampling and preservation | 84 |
| 3.3 | Acidification induced changes in water samples | 92 |
| 3.4 | Goals of sample pretreatment | 100 |
| 3.5 | The acid matrix effect | 106 |
| 3.6 | Matrix effect of surfactants | 117 |

CONTENTS


| | | Page |
|---|---|---|
| 3.7 | Matrix effect of tartaric acid | 118 |
| 3.8 | Sodium chloride matrix | 122 |
| 3.9 | Contamination at trace concentrations | 122 |
| 3.10 | Loss of analyte | 124 |
| 3.11 | Summary | 125 |
| CHAPTER 4: | INSTRUMENTATION, ANALYTICAL OPERATING CONDITIONS AND SOURCES OF ERROR | |
| 4.1 | Introduction | 127 |
| 4.2 | Instrumentation | 128 |
| 4.3 | Sample aspiration rate and signal intensity of manganese emission | 139 |
| 4.4 | Dependence of degree of ionization on plasma temperature | 161 |
| 4.5 | Excitation temperature and degree of ionization of zinc | 166 |
| 4.6 | Effect of rf generator input voltage on emission intensities | 171 |
| 4.7 | Effect of input voltage to ARL 34000 spectrometer on emission intensities | 185 |
| 4.8 | Effect of aerosol gas flow rate on emission intensities | 187 |
| 4.9 | Relationship between change of ionic line net intensity with aerosol gas flow rate change, and excitation potential | 200 |
| 4.10 | Summary | 203 |
| CHAPTER 5: | CALIBRATION AND INTERFERENCES ON THE POLYCHROMATOR | |
| 5.1 | Introduction | 206 |
| 5.2 | Calibration of intensity readout in concentration units | 207 |
| 5.3 | Analysis of the sample plate | 219 |
| 5.4 | Interelement interference correction | 226 |
| 5.5 | Memory effects in the sample transport system | 251 |

CONTENTS


| | | Page |
|---|---|---|
| 5.6 | Use of internal standardization to correct for error in ion-line readout caused by slight change in aerosol gas flow rate | 263 |
| 5.7 | Evaluation of internal standardization to correct for error in atomic-line readout caused by slight change in aerosol gas flow rate | 272 |
| 5.8 | Summary | 278 |
| CHAPTER 6: | QUANTITATIVE ANALYSIS NEAR THE DETECTION LIMIT ON THE SCANNING MONOCHROMATOR | |
| 6.1 | Introduction | 280 |
| 6.2 | Linearity and detection limit of the ARL scanning monochromator at line centre position | 281 |
| 6.3 | Use of an inverse Gaussian transformation for estimation of line centre intensity in the profile scan mode of measurement | 285 |
| 6.4 | Determination of the profile position of line centre | 288 |
| 6.5 | Application of the inverse Gaussian transform to profile scan data of the Co(II) 238,89 nm line | 291 |
| 6.6 | Treatment of profile scan data where baseline elevation occurs | 304 |
| 6.7 | Problem of relative profile shift for sloped or structured backgrounds in the profile scan mode of measurement | 309 |
| 6.8 | Detection limit from blank profile scan data | 318 |
| 6.9 | Assurance of analyte element identity by use of the profile scan technique at more than one analytical wavelength | 321 |
| 6.10 | Application of the inverse Gaussian transformation to the analysis of chromium and lead in a sediment digest | 322 |
| 6.11 | Summary | 332 |

# CONTENTS


| | | Page |
|---|---|---|
| CHAPTER 7: | QUALITY CONTROL | |
| 7.1 | Introduction | 334 |
| 7.2 | Internal quality control | 334 |
| 7.3 | Specific quality control procedures | 339 |
| 7.4 | External quality control | 342 |
| 7.5 | Approach to quality control in unusual matrices | 359 |
| 7.6 | Conclusion | 360 |
| CHAPTER 8: | CONCLUSIONS | |
| 8.1 | Significance of findings | 363 |
| 8.2 | Summary | 371 |
| LITERATURE REFERENCES | | 375 |

Acknowledgements

I am indebted to my supervisor, Professor A. Strasheim and co-supervisor, Professor R.G. Böhmer of the University of Pretoria for the many hours of enlightening discussion provided. I also express gratitude for the opportunity of working with Professor J.M. Mermet during his visit to the University of Pretoria in April 1985. I wish to thank Dr. Mermet for the illuminating discussions on excitation mechanisms, line-broadening and line-shape.

A work such as this is the culmination of many years of interest in emission spectroscopy, and I am indebted to Dr. L.R.P. Butler for originally stimulating my interest in the science of spectroscopy. My sincere gratitude is also extended to Dr. H.R. Van Vliet who encouraged me to undertake this work and provided a constant pillar of moral support.

My thanks go also to Miss. E. Davies, Miss R. Davies, Miss Y. Cronjé and Mrs. D. Portsmouth, the technical staff in the trace metal laboratory at the Hydrological Research Institute, for their dedicated assistance in the recording of the many analytical measurements. Mrs. A. Coleman is thanked for her care and effort in the drawing of the figures.

I wish to thank my father for his help in proof-reading the manuscript. I am further deeply indebted to Mrs. C. Edwards and Mrs. B. Sutton for their effort, patience and perseverance in the typing of the document.

Finally, I am indebted to the Department of Water Affairs for the use of their facilities.

## ABSTRACT

A discussion of the theory of inductively coupled plasma (ICP) emission spectrometry, with particular attention being paid to the question of detection limit, leads on to an overview of the analytical application of the ICP emission spectrometric technique in environmental sample analysis. Among the aspects which may influence accuracy are: (i) The sample matrix, in particular the acid matrix effect. (ii) The effect of sample uptake rate on excitation temperature and degree of ionization. Temperature was estimated by use of the two-line method. Inconsistencies in calculated temperatures illustrate the departure from local thermodynamic equilibrium in the ICP source. (iii) The effect of mains supply voltage change on analyte emission intensity; with the effect on the radio frequency generator and spectrometer being considered separately. (iv) The effect of aerosol argon flow rate change on analyte emission intensity, where a correlation with excitation potential is shown to exist. Thereafter follows a study on the calibration of a twenty eight channel ICP polychromator and the use of the software approach for interference correction. Second order polynomial interference correction coefficients were determined for interference from Ca, Mg, Fe and Mn. The importance of correction for drift in the concentration readout of a blank sample in analysis at trace concentrations is illustrated.

An investigation into the memory-effect in the sample transport system of the polychromator showed that the dead volume displacement time is followed by a biphasic washout curve with both the fast and slow phases having a linear double logarithmic plot. The use of a weighted internal standardization method to correct for sensitivity change consequent to aerosol argon flow rate change was investigated as a possible means of improving accuracy and avoiding frequent recalibration. An investigation is also undertaken into the use of a scanning monochromator for quantitative analysis in the profile scan mode of measurement, where interference correction is carried out by background subtraction. A study is included on the use of an inverse Gaussian transformation as a means of estimating precision from a profile scan, and a discussion on the establishment and the influence of background structure on detection limits. An example is given on the determination of Pb and Cr in a sediment digest. The study is concluded with a discussion on quality control.

## OPSOMMING

'n Bespreking van die teorie van induktiefgekoppeldeplasma (IGP) emissiespektrometrie, met spesiale verwysing na die onderwerp van deteksie-limiet, word gevolg deur 'n oorsig van die analitiese toepassing van die IGP emissiespektometriese tegniek vir die ontleding van omgewingsmonsters. Aandag is gegee aan die faktore wat akkuraatheid mag beïnvloed naamlik: (i) Die matriks van die monster, veral die suurtipe en konsentrasie. (ii) Die invloed van die monster opneemtempo op opwekkingstemperatuur en graad van ionisasie. Temperatuur is geskat met behulp van die tweelyn- metode. Teenstrydighede in die berekende temperature illustreer die afwyking van lokale termiese ewewig in die IGP bron. (iii) Die invloed van verandering in hooflynkrag- spanningstoevoer op die intensiteit van die analiet-emissie; met 'n afsonderlike beskouing van die effek op die radiofrekwensie-opwekker en spektrometer. (iv) Die effek van die vloeitempo van die aerosol-argon op die intensiteit van die analiet-emissie, waar 'n korrelasie met opwekkingspotensiaal gevind is. Daarna volg 'n studie van die kalibrering van 'n IGP polichromator met agt-en-twintigkanale en die gebruik van die programmatuur-benadering vir korrigering van interferensies. Tweede-orde polinoom interferensie korrigeringskoeffisiente is bepaal vir interferensies veroorsaak deur Ca, Mg, Fe en Mn. Die belangrikheid van 'n interpolasie-korreksie vir 'n verskuiwing in blanko-monster konsentrasie-uitlees wanneer spoorelement-konsentrasies bepaal word, word geïllustreer.

'n Ondersoek na die geheue-effek in die monstertransport-sisteem van die polichromator het getoon dat die verplasingstyd van die dooie volume deur 'n dubbelfase uitwas kurwe gevolg word, waar beide die vinnige en stadige fases 'n lineêre dubbele logaritmiese kurwe toon. Die gebruik van 'n geweegde interne-standardiseringsmetode om vir die sensitiwiteitsverandering wat intree wanneer die aerosol-argon se vloeitempo verander word, is ondersoek as 'n moontlike manier om die akkuraatheid te verbeter en gevolglik gereelde herkalibrasie te vermy. 'n Ondersoek is ook onderneem van die toepassing van 'n skandeermonochromator vir kwantitatiewe bepalings deur gebruik te maak van profielskanderings waar die korreksie vir interferensies deur blanko-aftrekking gedoen word. 'n Bespreking word ingesluit oor die gebruik van 'n omgekeerde Gaussiaanse transformasie om presisie te skat vanaf 'n profielskandering, en die daarstelling en die invloed van agtergrondstruktuur op deteksielimiet. 'n Voorbeeld is ingesluit van die bepaling van Pb en Cr in 'n sedimentvertering. Die studie word afgesluit met 'n bespreking oor kwaliteitsbeheer.

## SYMBOLS

| | | |
|---|---|---|
| $\alpha$ | – | level of significance. |
| $\beta_i$ | – | degree of ionization. |
| $\delta$ | – | differential. |
| $\Delta$ | – | difference, calculated minus observed value. |
| $\kappa$ | – | multiple of standard deviation adopted in definition of detection limit. |
| $\lambda$ | – | wavelength. |
| $\lambda_o$ | – | wavelength of centre of emission line. |
| $\Delta\lambda_D$ | – | Doppler broadened full line width at half-height. |
| $\mu$ | – | difference between population means; micro (as a prefix). |
| $\nu$ | – | frequency. |
| $\pi$ | – | ratio of circumference to diameter of a circle ca., 3,14159. |
| $\sigma$ | – | standard deviation. |
| $\sigma_b$ | – | std., deviation of background signal. |
| $\sigma_s$ | – | std., deviation of analyte signal in sample. |
| $\Sigma$ | – | sum. |
| $\phi$ | – | volume fraction. |
| $\phi_x$ | – | volume fraction of x. |
| $\phi_{HA}$ | – | volume fraction of acid HA. |
| $\Omega$ | – | ohm (unit of electrical resistance); omega function i.e., the std., deviation of a set of instensity readings taken across a wavelength window at successive wavelengths differing by $\delta\lambda$. |
| $\Omega_b$ | – | omega function for blank i.e., the std., deviation of a set of intensity readings taken across a wavelength window at successive wavelengths differing by $\delta\lambda$ for a blank sample. |

| | | |
|---|---|---|
| $A$ | – | transition probability. |
| $Ar_{meta}$ | – | metastable argon. |
| atm | – | atmosphere. |
| b | – | blank. |
| c | – | speed of light; corrected or current value (as a subscript). |
| C | – | concentration. |
| °C | – | degree Celcius. |
| $C_a$ | – | concentration of analyte a; apparent concentration of internal standard. |
| $C_b$ | – | apparent concentration of analyte before internal standardization. |
| $C_{ob}$ | – | analyte concentration after applying internal standardization. |
| $C_{oa}$ | – | true concentration of added internal standard. |
| $C_t$ | – | true analyte concentration. |
| $C_{i\phi}$ | – | concentration of analyte $\phi$ at aerosol flow rate $F_i$. |
| $\delta C_A$ | – | concentration equivalent to be subtracted from apparent (raw) concentration of element A in the software approach to interference correction. |
| $C(X)_{sn}$ | – | concentration of analyte X in sample number Sn. |
| $C^1$ | – | $1^{st}$ order interference coefficient (slope term). |
| $C^{11}$ | – | $2^{nd}$ order interference coefficient (curvature term). |
| $C_n$ | – | $n^{th}$ order interference coefficient. |
| $C^1_{XA}$ | – | linear interference coefficient of element X on element A. |
| $C^{11}_{XA}$ | – | $2^{nd}$ order interference coefficient of element X on element A. |
| $\overline{C}$ | – | mean concentration. |
| d | – | corrected for blank drift (subscript). |
| D | – | sum of squared residuals. |
| $D_1(X)$ | – | slope term for normalization of intensity of analyte X. |
| $D_2(X)$ | – | intercept term for normalization of intensity of analyte X. |

| | | |
|---|---|---|
| e | - | base of natural logarithms, ca., 2,71828. |
| $e^-$ | - | electron. |
| eV | - | electron volt. |
| E | - | excitation energy |
| $E_j$ | - | excitation energy of the $j^{th}$ state. |
| $E_a$ | - | excitation potential of internal standard element. |
| $E_b$ | - | excitation potential of analyte element. |
| f | - | atomic oscillator strength. |
| F | - | correction factor for internal standardization; F- statistic for comparison of variances. |
| $F_i$ | - | aerosol gas (inner gas) flow-rate. |
| $F_\ell$ | - | sample aspiration rate (liquid uptake rate). |
| f(x) | - | inverse Gaussian function. |
| g | - | statistical weight; gross (as a subscript); gram. |
| gj | - | statistical weight of $j^{th}$ state. |
| G | - | net intensity after transformation with the inverse Gaussian function, f(x). |
| h | - | Planck's constant; half-width at half-height of a wavelength profile; unit of time (hour). |
| $H_o$ | - | null hypothesis. |
| $H_1$ | - | alternative hypothesis. |
| I | - | Intensity. |
| $\bar{I}$ | - | mean intensity. |
| IA | - | analyte intensity in absence of an interfering element. |
| $I_b$ | - | background signal. |
| $I_{blank}$ | - | intensity of blank (usually $\phi$ = 0,01 $HNO_3$). |
| $I_{b,r}$ | - | regressed blank intensity. |
| $I_C$ | - | intensity of analyte signal for an analyte concentration of C $mg.\ell^{-1}$. |
| $I_g$ | - | gross signal. |
| $I_{gross}$ | - | gross analyte intensity. |
| $I_i$ | - | intensity recorded on the $i^{th}$ integration. |
| $I_{i\phi}$ | - | net intensity of analyte $\phi$ at an aerosol gas flow rate of $F_i$. |
| $I_n$ | - | net signal. |

| | | |
|---|---|---|
| $I_{net}$ | - | net analyte intensity. |
| Ip | - | analyte signal in presence of an interfering element. |
| $I_x$ | - | intensity recorded at profile offset position x from line centre, where x = 0. |
| $I_{xV}$ | - | intensity at x volt input to rf generator. |
| I(X) | - | gross intensity of analyte X prior to calibration normalization. |
| $I_t(X)$ | - | gross intensity of analyte X after the calibration normalization, wherein intensities are tranformed into those recorded at the time of full calibration. |
| I% | - | normalized relative intensity. |
| k | - | Boltzmann constant; kilo (as a prefix). |
| K | - | Kelvin (unit of temperature). |
| $K_i$ | - | ionization equilibrium constant (as a number density). |
| $K_x$ | - | ionization constant of analyte element x. |
| ℓ | - | litre. |
| ln | - | logarithm to base e. |
| log | - | logarithm to base 10. |
| m | - | metre; milli (as a prefix); electron mass. |
| M | - | memory factor; relative atomic mass. |
| n | - | number of integrations. |
| $n_{e^-}$ | - | free electron density. |
| nE-m | - | notation used for $n.10^{-m}$. |
| $N_j$ | - | number of atoms in excited state j. |
| $N_o$ | - | number of atoms in ground state o. |
| p | - | preserved. |
| P | - | instrument profile step setting, uncorrected. |
| Pa | - | pascal. |
| $P_o$ | - | apparent profile step position of maximum intensity. |
| $P_s$ | - | precision of analyte intensity in a sample. |
| $Q_A$ | - | interference on element A expressed in a concentration equivalent unit. |

| | | |
|---|---|---|
| r | - | linear correlation coefficient. |
| R | - | residual. |
| $R^o$ | - | ground state atom. |
| $R^{o*}$ | - | excited atom. |
| $R^+$ | - | ionized atom. |
| s | - | second (unit of time); sample/standard (as a subscript). |
| S | - | ionization equilibrium constant in pressure units (Saha constant). |
| Sn | - | counter denoting sequential number (n) of a sample on the sample plate of the autosampler. |
| $S_n$ | - | set of n data points (x, $I_x$) of a profile offset position from line centre (x) and the corresponding intensity ($I_x$). |
| t | - | time; t-statistic for comparison of means. |
| $t_x$ | - | washout time needed for signal to decay to x % of the initial value at t = 0. |
| † | - | constant used in conversion of the ionization equilibrium constant from pressure to number density units. |
| T | - | temperature; parameter used in evaluating the significance of a correlation (equation 34). |
| $T_{exc}$ | - | common excitation temperature. |
| $T_e$ | - | electron temperature. |
| $T_{gas}$ | - | kinetic gas temperature of neutral argon. |
| $T_{ion}$ | - | temperature associated with ionization of argon. |
| u | - | uncorrected; unpreserved; upper. |
| V | - | weighted degrees of freedom; volt. |
| $V_{exc}$ | - | excitation potential. |
| $V_i$ | - | ionization potential. |
| x | - | profile offset from line centre. |
| $x_{cor}$ | - | corrected profile step position. |
| Z | - | atomic partition function. |
| $Z_a$ | - | partition function of atom. |
| $Z_i$ | - | partition function of ion. |

## ABBREVIATIONS

| | | |
|---|---|---|
| AAS | - | atomic absorption spectrometry. |
| AES | - | atomic emission spectrometry. |
| AIR | - | aerosol ionic redestribution. |
| Aqt | - | digestion aliquot. |
| CEU | - | concentration equivalent unit. |
| DL | - | detection limit. |
| EIE | - | easily ionizable element. |
| GFAAS | - | graphite furnace atomic absorption spectrometry. |
| ICP | - | inductively coupled plasma. |
| LTE | - | local thermodynamic equilibrium. |
| min | - | minute. |
| ME | - | matrix effect. |
| MHDF | - | magnetic-hydrodynamic force. |
| MIBK | - | methyl-isobutyl-ketone. |
| MIP | - | microwave induced plasma. |
| MS | - | mass spectrometry. |
| NAA | - | neutron activation analysis. |
| PIC | - | percentage interference correction. |
| rf | - | radio frequency. |
| RSD | - | relative standard deviation. |
| S | - | Siemens (unit of electrical conductivity). |
| SBR | - | signal to background ratio. |
| XRS | - | X-ray spectroscopy. |

# CHAPTER 1: INTRODUCTION

## 1.1 The analytical problem

The analysis of environmental samples for trace metals necessitates firstly, an analytical technique which is sufficiently sensitive to detect the elements sought without, if possible, lengthy enrichment procedures, and secondly a method which should ideally be able to handle a wide spectrum of different sample types. Simultaneous analysis of a number of different elements is an added ideal, as this allows a whole range of elements to be studied in any given environmental problem without much additional effort.

When the inductively coupled plasma (ICP) emission spectrometric technique became commercially available in the mid-seventies, the multielement capability and relative sensitivity of the method lent the technique to applications in the environmental sample analysis field (Barnes, 1978; Dahlquist and Knoll, 1978), the attractiveness of the technique for this purpose being enhanced by the use of programmable process controllers to facilitate acquisition of multielement data (Capar and Dusold, 1979).

While ICP emission spectrometry provides a rapid method for acquiring multielement data, the technique must be used wisely and with caution if the data is to be accurate. The extremely

rich line spectra of an ICP source make the danger of error as a consequence of spectral interference ever present (Anderson et al, 1982) and correct use of the technique requires that the analyst address the possibility of interference, particularly when new or unusual matrices are encountered (EPA, 1982).

The ion and neutral atom rich line spectra of the ICP source provide the analyst with a wide choice of possible analytical lines, which allow for a versatility in the technique, particularly when used with a scanning monochromator. The analyst is, however, faced with the choice of which analytical line to use for a particular determination; and is required to weigh up the relative merits of the various possible analytical lines as regards sensitivity, freedom from spectral interference and stability of calibration with respect to profile change, in a given sample matrix. The question of the quantification of detection limit, particularly in the presence of interferences is another aspect of the analytical quantification process that should be addressed.

ICP emission spectrometry lends itself to the analysis of water samples, as the usual means of sample introduction is through nebulization of a liquid (Browner, 1978). Where solid samples such as sediments, plant tissue, fish, sludges etc., are presented for analysis, the analyst is faced with the problem of dissolution of the solids prior to introduction into an ICP emission spectrometer, a requirement shared by other

instrumental methods where nebulization is the usual means of sample introduction, e.g., in flame atomic absorption spectrometry (AAS).

The analytical problem in the use of ICP emission spectrometry for trace metal analysis centres firstly around the identification and quantification of sources of error and interferences, particularly of a spectroscopic nature (Anderson et al, 1982) which may seriously jeopardize the accuracy of reported results; and secondly the establishment of the blank emission intensities for a particular analytical emission line in a given matrix.

## 1.2 Scope of this thesis

The rapid evolution of the ICP emission spectrometric analysis method from discovery to wide application over little more than two decades (Dahlquist and Knoll, 1978; Greenfield et al, 1964; Greenfield et al, 1975; Reed, 1961; Reed, 1962; Taylor, 1983), without a parallel evolution in the understanding of excitation mechanisms in the ICP source (De Galan, 1984) has resulted in a relative lack of formalized text book type material to assist in the training of analytical staff who must run ICP spectrometric equipment. Trassy and Mermet (1984) have written a formal teaching text, but this being in French has limited usefulness outside French-speaking countries. Methodologies such as e.g.,

that published by the Environmental Protection Agency (EPA, 1982) are sketchy and assume familiarity with the ICP spectrometric technique. Nevertheless, much information can be gained, for instance, from compendia of papers on ICP spectrometry (Barnes, 1978; Barnes, 1983).

The scope of this thesis encompases the following:

An overview of the ICP emission spectroscopic literature is provided in Chapter 2. The early history of the technique is followed by a review of the excitation mechanisms, temperatures within the source, nature of the spectrum emitted by an ICP source, and sample introduction. Thereafter the determination of detection limit is discussed, followed by stability and drift, with special attention being given to the memory effect within the sample transport system. The problem of calibration and the methods employed for correction of interelement interference effects is discussed next, together with the practical difficulties encountered in the determination of interferences. A discussion on the need for quality control in the routine application of the ICP emission spectrometric analytical technique follows, with a brief note on the need to define the nature of a given analytical problem in environmental sample analysis. The literature overview is concluded with a summary of the present status of the technique in the analysis of water and related samples.

Chapter 3 is devoted to the collection, preservation and preparation of samples for analysis. Sample types included are water, sediment, macrophyte and fish. Acidification, while being regarded as a standard procedure in the preservation of water samples for trace metal determination, is not without its effects on sample composition. An example is included of the effect of acidification and sample filtration on analytical results. A discussion follows on the need to define goals of sample pretreatment in relation to the choice of sample preparation procedures. Thereafter the effect of acid concentration on analyte signal is discussed, for nitric, sulphuric and hydrochloric acids. Apart from the expected transport effects, part of the acid matrix effect is shown to have a correlation with excitation potential, and therefore ascribed to changes within the plasma itself. A brief investigation of the matrix effects of surfactants, tartaric acid and sodium chloride is included. The chapter is concluded with a note on two basic problems in sample preparation procedures viz., contamination and its reverse i.e., loss of analyte.

A description of the polychromator and monochromator type spectrometers employed for the experimental work, together with the analytical operating conditions used, is given in Chapter 4. This chapter deals at length with instrumental sources of error. The aspects which are included are firstly, the effect of sample uptake rate on excitation temperature as

illustrated for an atomic as well as ionic line pair of manganese, and an atomic line pair of zinc, with associated change in degree of ionization, showing the need for constancy of sample uptake rate. Also illlustrated is the lack of local thermodynamic equilibrium in the low power ICP source. Secondly, an investigation is given on the effect of change in mains input voltage to (a) the rf generator, and (b) the direct reading spectrometer on recorded analyte emission intensity. Lastly, the effect of change in inner (aerosol) gas flow rate to the plasma torch on analyte emission intensity was studied, where a correlation with excitation potential was shown to exist. This relationship allowed the formulation of a weighted internal standardization type correction equation, for use in sample analysis.

The calibration of the polychromator to give concentration readout is described in Chapter 5. Correction for drift in sensitivity and blank readout is discussed, followed by the establishment of 2nd order interference correction coefficients from the matrix elements Ca, Mg, Fe and Mn, together with a discussion on the stability of the correction coefficients. Thereafter the memory effect responsible for signal carry over following aspiration of a high analyte concentration was investigated, and the nature of the washout curve established. The memory effect has bearing on the time interval required between consecutive samples on a sample plate. The chapter is

concluded with an evaluation of the weighted internal standardization formula derived in Chapter 4, to correct for change in ion-line emission intensity consequent to change in inner (aerosol) gas flow to the plasma; togehter with the evaluation of an analagous formula for atomic line intensity standardization.

The sixth chapter discusses the use of a scanning monochromator for quantitative analysis near the limit of detection, firstly at line centre, and secondly through use of wavelength profile scans, which enable wing interference and background shifts to be detected. The use of an inverse Gaussian transformation to estimate precision from a profile scan is discussed, and the difficulties consequent to baseline elevation and relative profile shift between successive scans illustrated. The various methods of determining the detection limit are also given. A short note on the use of more than one analytical wavelength of an element to assure element identity, is given. The chapter is concluded with an illustration of the use of the inverse Gaussian transformation in the determination of Cr and Pb in a river sediment.

In the seventh chapter, a brief discussion is given on quality control, with its two facets i.e., internal quality control and external quality control. Examples are provided of the results achieved in external quality control exercises, showing that ICP emission spectrometry is suitable for analysis of trace elements in environmental samples where care is taken to correct for the interelement interferences inevitably present.

The thesis is concluded with a brief summary of the major findings which have relevance to the preservation of accuracy, and the estimation of precision and detection limit in the use of ICP emission spectrometry in environmental sample analysis. The two major findings of significance are firstly, the importance of maintaining a constant inner (aerosol) gas flow rate and constant mains voltage supply to the rf generator in the interest of a stable calibration. Both these parameters showing change in analyte emission intensity which correlates with excitation potential; and secondly, the demonstration that quantitative analysis, with calculation of precision, may be made from a single profile scan of a sample through the use of an inverse Gaussian transformation.

# CHAPTER 2: LITERATURE OVERVIEW

## 2.1 Introduction

In the early sixties, spectrochemical analysis was already extensively used for the analysis of environmental samples, particularly the atomic absorption spectrometric technique which provided sufficient sensitivity to detect pollutant metals at typical concentrations existing in water bodies. Despite its excellent detection limits for many metallic elements, however, atomic absorption spectrometry is essentially a single element technique and lacked the simultaneous multielement capability of emission techniques (Slavin, 1978). Emission techniques such as arc-plasma methods, while providing simultaneous multielement capabilities, lacked the sensitivity required for many elements of importance in environmental studies. The experiments of Greenfiled and co-workers in the United Kingdom and Fassel in the United States on the possibilities of using high-temperature induction plasmas as spectroscopic emission sources were of more than just passing interest to the environmentalist, as they provided hope of a stable emission source for use in emission spectrochemical analysis of environmental samples (Greenfield et al, 1964; Scott et al, 1974).

When commercial ICP emission spectrometers became available in the mid-seventies, the technique soon gained widespread use for environmental sample analysis (Dahlquist and Knoll, 1978; Berman et al, 1980; EPA, 1980; Taylor, 1983). In this chapter, an overview of the ICP emission technique is provided with particular attention being given to the question of detection limit, as well as procedures for correcting for interelement interference, as these two aspects are critical to the successful application of the technique in the determination of trace metals in water and related environmental samples. The chapter is concluded with a summary of the present status of the technique as applied to the analysis of water and related samples.

The induction heating of a gas at atmospheric pressure to form a stable plasma, where a sizeable fraction of the gas atoms present are ionized, was first achieved by Reed (1961). Reed showed that through tangential introduction of the feed gas (argon), vortex flow occurred and a stable fireball resulted when between 1 and 10 kW of radio-requency (rf) current at 4 MHz was passed through a copper coil surrounding a quartz tube containing the feed gas. Coupling of the rf current to the gas was initiated by the introduction of a graphite rod into the rf field, which through induction heating, served to ionize argon atoms and initiate a flow of induced current in the gas.

The temperature of the hot glowing fireball or plasma was estimated at 15 x $10^3$ K at the centre of the plasma from the intensity of the Ar 763,5 nm emission line, assuming a Boltzmann distribution of energy in the heated gas.

An inductively coupled plasma (ICP) produced in this manner, through induction heating of argon by the oscillation of a magnetic field along the axis of a coiled conductor, was initially but a scientific curiosity although Reed (1962) did suggest that this hot argon plasma would prove to be a useful spectroscopic source, especially by virtue of the fact that the plasma was free of contamination by electrode material. Such contamination, with deterioration in detection limits, is a problem in arc plasmas, where an electric current flows across the gap between carbon or metal electrodes, with consequent vaporisation of electrode material into the arc plasma.

Following the observations of Reed, the development of the ICP as a spectroscopic source was pursued independently by a number of workers. Greenfield and co-workers in the United Kingdom, after initial work on the low power plasma source as a means of overcoming classical flame interference phenomena such as the suppression of Ca emission by phosphate or aluminium (Greenfield et al, 1964), pursued the development of the high-powered nitrogen cooled argon plasma with rf power input in excess of 5 kW. This led to the demonstration in the mid-seventies that an

ICP source, coupled to a direct reading spectrometer, was a versatile multi-element analytical technique for a wide variety of different sample matrices, and had the added advantage of being readily amenable to automation, in the interests of rapid sample throughput (Greenfield et al, 1975). Fassel and co-workers in the United States of America followed the direction of the low power input pure argon plasma from the outset, employing rf power inputs around 1 or 2 kW. A major contribution of the American workers being the development of the Fassel torch, whereby sample introduction into the centre of the toroidal plasma was facilitated by use of a narrow aerosol injector tube, with an orifice diameter of 1,5 mm giving an injection velocity of 1,3 $m.s^{-1}$ for an aerosol gas* flow rate of 1,4 $\ell.min^{-1}$ at atmospheric pressure (Scott et al, 1974).

For penetration of the aerosol, carrying the analyte, into the plasma the flow velocity of the aerosol must exceed the magnetic-hydrodynamic force (MHDF) of the plasma (Chase, 1971). The MHDF is responsible for the so-called skin-effect whereby the aerosol gas tends to be deflected around the plasma rather than penetrating the hot ionized gas. The skin depth, which may be defined as the depth into the plasma where the induced current has decreased to 37% (or $e^{-1}$) of the surface current, is inversely proportional to the square-root of the generating frequency

---

* inner gas (Butler et al. 1985)

(Dickinson and Fassel, 1969). Thus increase of the radio-frequency from 4 MHz to 30 MHz results in a decrease in the skin depth by a factor of about 2,7 this being the inverse ratio of the square-root of the frequencies i.e. $\sqrt{30}/\sqrt{4}$. The smaller skin depth facilitates introduction of the sample into the plasma by virtue of the reduced effect of the MHDF at the axial position, as the MHDF and the consequent magnetic hydrodynamic force per unit area decreases as the diameter of the axial channel increases. The reliance on nebulization of the sample into an argon stream for introduction into the central axial region of the plasma naturally implies that viscosity and transport interference effects consequent to the nebulization process will be found in the ICP spectrometric method, as occur in flame atomic absorption spectrometry where nebulizers are likewise used to produce the sample aerosol. Both pneumatic (Dalquist and Knoll, 1978) and ultrasonic (Berman et al, 1980) nebulization have been used in ICP emission spectrometric analysis as the usual manner of introducing the sample.

The spectrometers used to resolve the light emitted by an ICP source into a line spectrum, may be classified into two broad groups: (i) Direct reading, polychromator type spectrometers where an array of detectors are positioned to receive light simultaneously from a number of analytical emission lines, thus making possible simultaneous

multi-element analysis (Mika and Török, 1974); and (ii) sequential, monochromator type spectrometers with a single detector which receives light from one analytical emission line only (Mika and Török, 1974). Wavelength selection in the latter case is usually achieved either by rotation of the grating or through shifting of the exit slit-detector combination.

The excellent excitation characteristics of an ICP source, with its ability to excite a wide range of elements to emit their characteristic atomic and/or ionic spectra (Boumans, 1974), coupled with the relative freedom from solute vaporization and easily ionizable element (EIE) inteferences when compared to atomic absorption spectrometry (Larson et al, 1975) make the ICP source an attractive spectroscopic tool. The use of programmable micro-processors to control multi-channel spectrometers interfaced to an ICP source (Capar and Dusold, 1979) make possible the analysis of a large number of samples for a whole suite of elements in a brief time span. Automation enhanced the attractiveness of the ICP emmission spectroscopic technique, and it has gained rapid acceptance as a valuable technique in the environmental sample analysis field, being used for elemental determination on a wide variety of matrices such as water (EPA, 1980; Taylor, 1983), plant tissues and soils (Dahlquist and Knoll, 1978), sea water (Berman et al, 1980) and oils (Merryfield and Runnels, 1983).

The ease with which the ICP source excites atomic and/or ionic spectra of the majority of elements in the periodic table thus facilitating multi-element determinations has, paradoxically, also been a major drawback as the line-rich spectra together with line-broadening phenomena within the source (Larson and Fassel, 1979) imply a high probability of spectral interferences from line coincidence or partial line overlap (Mermet and Trassy, 1981). Accurate analysis, particularly of trace elements in the presence of high concentrations of alkaline-earth elements, requires that spectral interference phenomena be closely addressed (EPA, 1982; Berman et al, 1983; Botto, 1983; Kempster et al, 1983).

## 2.2 Atomic excitation and ionization

Atomic emission may be defined as the process whereby an electromagnetic quantum of energy is emitted or released from an atom in an excited electronic state, when an electron returns from a quantum level of higher potential energy to a quantum level of lower potential energy. Where the state of lower potential energy is the ground state, then the characteristic emission line associated with the transition is termed a resonance line. The reverse process whereby an atom absorbs a photon of light and is thereby excited to an electronic state of higher potential energy is termed atomic absorption. The two processes may be symbolized as (Burrell, 1974):

$$R^{o} + h\nu \underset{b}{\overset{a}{\rightleftharpoons}} R^{o*} \qquad \ldots\ldots\ldots\ldots \qquad (1)$$

where $R^{o}$ represents the ground state atom,

$h\nu$ represents the energy quantum of the photon;

h is Planck's constant and $\nu$ is the frequency of the light,

$R^{o*}$ is the excited atom,

a is the atomic absorption process

and b is the atomic emission process.

Excitation of ground state atoms to excited energy states may not only be caused by absorption of characteristic photons of the required energy, but also occurs through thermal excitation where the kinetic energy of the gas particles is converted to electronic potential energy through collisional processes. The number of atoms in the excited state j, in chemical flames, is a function of the absolute temperature as given by the Boltzmann distribution (Burrell, 1974):

$$Nj = N_{o} \cdot \frac{gj}{Z} \cdot e^{(-Ej/kT)} \qquad \ldots\ldots\ldots\ldots \qquad (2)$$

where Nj = number of atoms in excited state j,

$N_o$ = number of atoms in ground state o,

gj = statistical weight of the jth state,

Z = atomic partition function,

Ej = excitation energy of the jth state,

k = Boltzmann constant

and T = temperature.

Nj and No are usually given in terms of number densities.

The Boltzmann distribution has particular bearing on the atomic emission intensity of a given electronic transition, as the emission intensity is proportional to the number of atoms in the excited energy state. The physical significance of the Boltsmann distribution in atomic spectrometry lies in the occurrence of the ratio Ej/T in the exponent, implying that for a given ratio of excited atoms to unexcited atoms a quantum transition of higher energy requires a correspondingly higher temperature, other factors remaining equal. In practice, the atomic partition function Z, is temperature dependent (Boumans, (a),1966). The latter complication does not, however, change the overall fact that higher temperature results in excitation of excited states of greater energy.

Reed (1961) indicated that the ICP would prove to be a useful spectroscopic emission source, capable of exciting quantum transitions of high associated energy, on the basis of a calculated temperature of 15 x $10^3$K assuming a Boltzmann distribution of excited energy states. While Reed was subsequently proved correct as regards the highly efficient excitation characteristics of the argon plasma, the assumption of local thermodynamic equilibrium (LTE) within the plasma and the associated Boltzmann distribution of excited energy states does not hold (Eckert and Pridmore-Brown, 1971) particularly in the low power, pure argon plasma (Goldfarb, 1983).The non-existence of LTE in the pure argon plasma has bearing not only on the estimation of number densities of excited neutral atoms, but also on the calculation of the degree of ionization ($\beta i$) from the Saha equation (Kornblum, 1977). The ionization of an atom may be symbolized as;

$$R^o \rightleftharpoons R^+ + e^- \qquad \ldots\ldots\ldots\ldots \qquad (3)$$

with the ionization constant Ki defined as;

$$Ki = \frac{[R^+] \,.\, [e^-]}{[R^o]} \qquad \ldots\ldots\ldots\ldots \qquad (4)$$

(Burrell, 1974), where

$R^o$ = ground state atom,

$R^+$ = ionized atom,

$e^-$ = electron,

Ki = ionization equilibrium constant

and $[\ ]$ denotes the concentration (usually expressed in this context as a number density) of the species concerned.

Burrell (1974) defines the degree of ionization ($\beta i$) as:

$$\beta i = \frac{[R^+]}{[R^o] + [R^+]} \qquad \ldots\ldots\ldots\ldots \qquad (5)$$

Using equation 4, $\beta i$ may be expressed in terms of the ionization constant Ki as:

$$\beta i = 1 - \frac{[e^-]}{[e^-] + Ki} \qquad \ldots\ldots\ldots\ldots \qquad (6)$$

The ionization constant Ki may also be expressed as a function of absolute temperature, the function concerned being known as the Saha or S function (Boumans, (b),1966).

Using the Saha function, the equilibrium constant may be written as a function of the absolute temperature. This equation, known as the Saha equation, like the Boltzmann equation 2, also assumes LTE (Kornblum, 1977):

$$Ki = \frac{(2\pi m k T)^{3/2}}{h^3} \cdot 2\frac{Zi}{Za} \cdot e^{-Vi/kT} \qquad \ldots\ldots \qquad (7)$$

where Ki = ionization equilibrium constant expressed as a number density, $cm^{-3}$

m = electron mass

k = Boltzmann constant

T = ionization temperature

h = Planck's constant

Zi = partition function of ion

Za = partition function of atom

Vi = ionization potential

The degree of ionization of introduced analyte atoms in the argon plasma is considerably greater than that indicated by equation 7 and is one of the reasons for believing that the ICP is not in LTE, particularly in the decaying tail flame region of the plasma, above the hot core (De Galan, 1984).

## 2.3 Temperatures within the argon plasma

Calorimetric measurements of heat release from argon or argon-nitrogen plasmas show fireball temperatures of around $9x10^3$ to $11x10^3$ K, with tail flame temperatures around $7,5x10^3$ K (Greenfield and McGeachin, 1978). Such mean temperatures have little practical use from the spectroscopic viewpoint, however, as the atoms and ions of argon, the various analyte atoms and ions, as well as free electrons and molecular species within the plasma show widely differing kinetic energies with associated

temperatures ranging from around $2x10^3$ K for the OH rotational temperature, to $4x10^3$ K for the Ar atom line temperature, to $8x10^3$ K for the temperature required to explain the degree of ionization of argon (Kornblum, 1977). For an observation point in the tail flame above the fireball Kornblum (1977) estimated excitation temperatures for analyte emission with the aid of the two-line technique using a formula based on the Boltzmann distribution, and thus assuming LTE;

$$\ln (Ip/Iq) = \ln \left( \frac{g_p \, . \, f_p \, . \, \nu_p^3}{g_q \, . \, fq \;\; \nu_q^3} \right) + (Eq-Ep)/k \; T_{exc} \quad ...(8)$$

where I = intensity of emission line

g = statistical weight

f = oscillator strength

$\nu$ = frequency of emission line

E = excitation energy of given state

k = Boltzmann's constant

$T_{exc}$ = common excitation temperature;

and p and q are the two transitions observed for the pair of emission lines observed, these both being of the same type i.e., atom-atom or ion-ion.

Kornblum found that the excitation temperatures for transitions involving analyte atoms or ions were between the two extremes of the OH rotational temperature and the Ar ionization temperature for his ICP source.

In the case of Ca and Mg, Kornblum (1977) looked at both the excitation temperatures of atom lines and ion lines, and found ion line temperatures around 500 K higher than the corresponding atom line excitation temperature. Kornblum summarized his findings as:

$$T_{gas} < T_{exc}\ (atom) < T_{exc}\ (ion) < T_{ion} \ldots\ldots \qquad (9)$$

where $T_{gas}$ = kinetic gas temperature of neutral argon as estimated from the OH rotational molecular emission temperature,

$T_{exc}$ (atom) = excitation temperature of an analyte atom transition using equation 8,

$T_{exc}$ (ion) = excitation temperature of an analyte ionic transition using equation 8,

and $T_{ion}$ = temperature associated with the ionization of argon using equation 7.

The inequality 9, is sufficient evidence for the non-existence of LTE in the ICP source. Further evidence may be obtained, however, from the measurement of free electron temperature. If excitation of the argon in an ICP source was only thermal, then the temperature of the electrons ($T_{e^-}$) produced through ionization of the argon would equal the argon ion temperature ($T_{ion}$). Departure

from this equality would indicate absence of LTE (Kornblum, 1977). In a 40 MHz plasma operated at 1,5 kW Batal et al (1983) calculated an electron temperature of $1x10^4$ K at between 2 and 3 mm from the axis of the plasma through measurement of the emission intensity of the argon ion - electron recombination continuum between 400 and 500 nm.

This electron temperature is more than $2x10^3$ K larger than an argon ionization temperature of between $7x10^3$ K and $8x10^3$ K, showing that $I_{ion} << T_{e-}$ and further illustrating lack of LTE in the ICP source.

The absence of thermal equilibrium is particularly apparent in low power, pure argon ICP sources. In high power argon-nitrogen ICP sources a closer approach to LTE occurs (Greenfield and Thorburn Burns, 1980). Goldfarb (1983) gives the criterion that plasmas with a power density of less than $10^2$ $W.cm^{-3}$ are not LTE.

The non-existence of LTE in the low power, pure argon plasma raises questions as to the significance of the temperatures derived for given species from emission intensity data. In a consideration of equilibrium processes in high frequency ICP sources and microwave induced plasma (MIP) sources, Van Montfort and Agterdenbos (1981) mention the possibility that more than one free electron population may occur and that the high energy

electron group may be responsible for exciting ion lines, while the low energy electron group is responsible for the excitation of atomic lines.

## 2.4 Excitation mechanisms in the ICP source

In a discussion on the mechanisms which have been proposed to explain observed spectral characteristics of an argon ICP source, De Galan (1984) states that any excitation model for the argon ICP should explain the following:

(i) The high free electron density ($n_{e^-}$), with values in the range of $10^{14}$ $cm^{-3}$ to $10^{16} cm^{-3}$.

(ii) The relative absence of ionization interferences from easily ionizable elements (EIE) such as potassium.

(iii) That values of excitation temperature ($T_{exc}$), calculated on the assumption of LTE and assuming a Boltzmann distribution, increase with an increase in the upper energy level of the transition considered, i.e. the relative overpopulation of energy levels increases with the excitation energy.

(iv) That the argon ICP provides effective excitation of ion lines, the ratio of the ion line to atom line intensities being considerably greater than the assumption of LTE would suggest.

In an attempt to account for the suprathermal population of excited energy states within the argon ICP, the existence of metastable argon ($Ar_{meta}$) has been evoked. Metastable argon is formed through absorption of ~ 100 nm photons in the hot plasma core (Blades, 1982; De Galan, 1984) and is able to ionize and excite analyte atoms (X) through a process known as Penning ionization (Greenfield and Thorburn Burns, 1980):

$$Ar_{meta} + X \longrightarrow Ar + X^{+} + e^{-}$$

and $$Ar_{meta} + X \longrightarrow Ar + X^{+*} + e^{-}$$

where the asterisk denotes an excited state of the analyte ion ($X^{+}$). Metastable argon is essentially an excited state of neutral argon of about 11,5 eV above the ground state, where the excited electron in a 4P orbital has a long lifetime of ~ 1,3 sec because the spin quantum number forbids coupling to the ground state. Blades and Heiftje (1982) have extended this concept of trapping of excitation energy within the neutral argon atoms by postulating that the $4^3P_o$ and $4^3P_2$ metastable states of argon exchange energy rapidly through collisional processes with the $4^3P_1$ and $4^1P_1$ radiative states of argon which have excitation potentials within 0,2 eV of the metastable states. This collisional interchange of energy at the ~ 11,5 eV level leads to a trapping of energy for approximately 1 ms, assuming a collisional frequency of $10^9$ $s^{-1}$.

While the existence of metastable argon and the phenomenon of radiation trapping are useful models in forming a point of departure in understanding the excitation process in the ICP source, the discussion would not be complete without a mention of the models taking the spatial inhomogeneity of the ICP source into account. In the latter models, the effects of the hot annular plasma surrounding the cooler central axial analyte channel are addressed. The radial inhomogeneity may result in the diffusion of analyte atoms or ions into the para-axial area, or diffusion of argon atoms, ions or electrons into the analyte channel in a process termed ambipolar diffusion (Blades and Horlick, 1981). De Galan (1984) postulated that at the normal observation height above the plasma core, in the decaying tail flame, that the diffusion of hot electrons, with an electron temperature of around $9x10^3$ K, plus argon ions into the axial channel may be the chief reason for efficient excitation of ionic lines of analyte atoms.

While there is still doubt as to the mechanisms of excitation occurring in the argon ICP, there is no doubt that it is an efficient excitation source, which is able to break even the most stable chemical bonds. Thus Northway and Fry (1980) reported that in the case of the carbon monoxide bond, with a dissociation energy of 11,1 eV, complete dissociation occurred at 2,0 kW power. The diatomic nitrogen bond (9,76 eV dissociation energy) is fully broken at 1 kW power (Northway *et al*, 1980). In

addition to the facile manner in which chemical bonds are broken, the ICP source is an efficient exciter for both atomic and ionic analytical emission lines for a wide variety of elements (Scott et al, 1974; Greenfield et al, 1975; Taylor and Floyd, 1980).

## 2.5 Line broadening

Line broadening with resultant overlap of line wings in the line-rich ICP spectrum is an important source of interference in the analytical application of ICP spectrometry. The major sources of line broadening (Larson and Fassel, 1979) are given in Table 1-1.

TABLE 1-1: Major sources of line broadening

(i) Natural
(ii) Doppler
(iii) Collisional or pressure
(iv) Self-absorption
(v) Instrumental

The natural line width, measured at half-height, has a minimum possible value of $1{,}19 \times 10^{-5}$ nm, based on the consideration of the emitting electron as a harmonic oscillator (Mika and Török, 1974). In practice the natural line width is, however, greater than this value due to the Heisenberg uncertainty principle (Mermet and Trassy, 1981).

Doppler broadening, resulting from the effect of the thermal motion of the radiating particles on the wavelength of the emitted light, becomes increasingly significant as the temperature of the emitting particles increases by virtue of increased kinetic energy. Doppler broadening is particularly pronounced for atoms of small atomic mass, as their velocity is greater for a given temperature (Mika and Török, 1974). Thus, for instance, Mermet and Trassy (1981) give Doppler broadening contributions to the full line width at half-height of the hydrogen 486,1 nm line and lithium 460,2 nm line as 0,0245 and 0,0088 nm respectively.

The Doppler broadening may be calculated from:

$$\Delta \lambda_D = 7{,}17 \times 10^{-7} \lambda_o \cdot \sqrt{\frac{T}{M}} \quad \ldots\ldots\ldots \quad (10)$$

where $\Delta \lambda_D$ = full line width at half-height,

$\lambda_o$ = central wavelength of emission line,

$T$ = absolute temperature

and $M$ = relative atomic mass.

Collisional broadening, which results in the gradual tailing-off of line wings and is of major concern as a source of background change in the ICP emission spectrum, may be futher subdivided into Stark broadening, Van der Waals broadening and resonance broadening; according to

whether the collision involves charged particles, neutral atoms, or emitting atoms resonating with the ground state (Larson and Fassel, 1979; Mermet and Trassy, 1981).

Stark broadening is important where the velocity of the charged particle involved in a collision is high (Mika and Török, 1974) and consequently affects primarily ions of low atomic mass, as these have greater velocities at a given kinetic gas temperature than ions of higher atomic mass. Mermet and Trassy (1981), for example, report that the Stark broadening contribution to the full width at half-maximum peak height for the hydrogen 486,1 nm emission line as 0,090 nm, whereas for the calcium 422,7 nm emission line the Stark broadening contribution is only 0,00006 nm.

Van der Waals broadening is usually insignificant as far as the effect on peak width at half-height is concerned, but does cause significant elevation of the far wings of an emission line profile (Mermet and Trassy, 1981).

Resonance broadening is possibly the most important source of wing interference from matrix elements such as calcium or magnesium in ICP emission spectrometry, as the resonance broadened contribution to lines from transitions coupling to the ground state may be as much as 0,02 nm e.g., for the Ca 422,7 nm line for full width at half-height (Mermet and Trassy, 1981). As resonance broadening is primarily the

result of collision of atoms or ions of the same element, it manifests at high concentrations, and is proportional to the density of the emitting species (Mika and Török, 1974).

The fourth source of line broadening is self-absorption (Table 1-1). Self-absorption, where the light emitted from a transition resonating with the ground state is reabsorbed by analyte atoms in the cooler region surrounding the emitting atoms as occurs in chemical flames and hollow cathode lamps, results in flattening or even self-reversal of line profiles (L'Vov, 1970; Mika and Török, 1974). Self-absorption is only of minor significance in an ICP source due firstly to the optically thin nature of the plasma and secondly to the axial analyte channel being surrounded by an annulus at higher temperature (Jones et al, 1974).

Lastly, line broadening also occurs as a consequence of the optical characteristics of the spectrometer used to resolve the light emitted by, for instance, an ICP source. The instrumental line broadening contribution to full width at half-height is a function of the optics of a spectrometer and will not be discussed here.

## 2.6 Nature of the spectrum emitted by an ICP source

The argon ICP source is a rich source of both atomic and ionic emission spectra of elements. Excited energy levels are readily populated where the excitation energy (or

excitation plus first ionization energy in the case of ion lines) is less than the ionization potential of argon i.e., 15,76 eV (Northway and Fry, 1980). The ICP source is able to produce around 160 000 spectral transitions between 180 and 600 nm. The probability of spectral line overlap interferences is therefore high (Anderson et al, 1982).

Apart from the spectra of introduced analyte elements, the source also produces atomic argon emission lines at wavelengths greater than 300 nm. Forster et al (1982) found 205 Ar I transitions between 317 nm and 600 nm, the ICP spectrum being free of Ar I emission lines in the wavelength region from 200 to 300 nm. No ionic argon emission lines were observed. Several of the Ar I emission lines had widths of several tenths of a nanometer, which Forster et al (1982) attributed to Stark broadening.

The atomic line spectrum of argon is superimposed on a continuum emission background resulting from recombination of $Ar^+$ and electrons (Roederer et al, 1982). The continuum emission is particularly prominent in the hot plasma core (Truitt and Robinson, 1970a).

The ICP spectrum further shows prominent hydroxyl molecular emission bands between 306 nm and 350 nm, particularly when water is aspirated into the plasma (Reeves et al, 1980). Molecular band heads, at 516,4 nm and 473,7 nm from the

Swan $C_2$ system; at 388,3nm from the cyanogen system; in the wavelength region from 200 to 280 nm from NO; as well as molecular emission from NH and $N_2$ at 336,0 nm and 337,1 nm respectively, have been reported (Truitt and Robinson, 1970a & 1970b; Reeves et al, 1980; Forster et al, 1982). Band spectra from N or C containing species are particularly prominent when nitrogen containing, or carbon containing, compounds are aspirated into the ICP. Such molecular band spectra also occur, however, in the absence of N or C containing compounds in the liquid aspirated, as a consequence of entrainment of atmospheric gases by the plasma, or as a consequence of impurities in the argon feed gas (Reeves et al, 1980). The appearance of molecular band spectra is obviously dependent on the existence of the given molecular species at a particular height and consequently temperature along the axial channel of the plasma. The high power $N_2$/Ar plasma may be less prone to certain molecular band spectra e.g., Greenfield and Thorburn Burns (1980) noted the absence of the Swan $C_2$ system.

Molecular emission from introduced analyte elements has also been described. Thus Roederer et al (1982) found molecular emission from MgOH at 383,5 nm; from ZrO at 571,8 nm, but none from CaOH, in a 1,25 kW argon ICP at an observation height of 15 mm above the load coil. The ZrO emission persisted further along the length of the axial

channel than the MgOH emission, consistent with the higher dissociation energy of the former molecule i.e., 7,8 eV as against 2,4 eV for MgOH. In the analysis of aqueous solutions, the OH band spectra predominate, however. On dissociation of the water molecule, hydrogen is also produced and atomic hydrogen emission lines are consequently observed. The atomic emission lines of hydrogen show pronounced broadening, by as much as 1,2 nm (Forster et al, 1982).

From the viewpoint of the analyst, the useful emission lines produced by the ICP source are the ionic and atomic line spectra of elements with excitation energy below the ionization potential of argon (Greenfield et al, 1964; Dickinson and Fassel, 1969; Scott et al, 1974; Greenfield and Jones, 1975; Northway and Fry, 1980; Anderson et al, 1982). The ICP source is able not only to excite a great number of atomic (I) and first ionization state (II) emission lines of elements as documented, for instance, in standard wavelength tables for arc and spark sources, but in addition is able to excite certain previously undocumented emission lines e.g., for Fe (Michaud and Mermet, 1982), for Ar (Forster and Anderson, 1982) and for Ca (Anderson et al, 1982).

## 2.7 The height of observation

The axial channel, within the hot plasma toroid, along which the analyte aerosol passes is subject to radiative heating from the hot surrounding plasma. The injected analyte aerosol is consequently exposed to rapid heating as it enters the base of the plasma, followed by gradual cooling in the tail region of the plasma. The central analyte channel of the ICP source was classified into the following four zones by Reeves et al (1980):

### (i) The preheating zone

This is the zone between 0 and 10 mm above the load coil where the analyte aerosol is subjected to desolvation, sublimation, melting, vaporization and molecular decomposition. This zone is also characterized by intense continuum emission from the surrounding plasma core.

### (ii) The monoxide emission zone

This is the zone between 10 and 15 mm above the load coil where molecular spectra are observed from stable monoxides of elements such as Y or Sc, which have not been fully dissociated in the preheating zone. Atomic spectra* of alkali metals are observed in this zone.

---

* Atomic spectra are also observed in the tail flame where exhaust gases leave the plasma.

(iii) The analytical zone

The zone between 15 and 25 mm above the load coil is characterized by favourable line to background intensity ratios of both atomic and ionic emission lines of the majority of elements, and is the region normally used for analytical purposes.

(iv) The plume zone

The zone above 25 mm is characterized by the reformation of molecular species as the exhaust gases cool to ambient temperature.

As a consequence of the temperature-height profile of the central axial channel of the plasma, and the differing molecular dissociation, excitation and ionization energies of different species, the height at which optimum line to background ratio is observed varies with the transition and element concerned. The temperature-height profile and optimum viewing height also depends on the plasma type (i.e., Ar. or $N_2$/Ar), as well as the gas flow rates, torch design, applied rf power, load coil design and characteristics of the nebulization/transport system (Greenfield and Thorburn Burns, 1980; Blades and Horlick, 1981; Montaser et al, 1981; Blades, 1982). For simultaneous multi-element analysis a compromise

observation height must be used. The height chosen not only affects the detection limit obtained for individual elements, but also the nature and extent of matrix interferences (Blades and Horlick, 1981).

## 2.8 The plasma power

In their original investigation of the inductively coupled plasma as a spectroscopic source, Greenfield et al (1964; 1975) reasoned that the aim should be to couple as much as 5 kW rf power into the plasma in order to excite elements with high excitation potentials. It was originally thought that the Greenfield high-power argon plasma with nitrogen coolant (Greenfield et al, 1975) had superior detection limits to the low-power pure argon plasma as developed by Fassel and co-workers (Scott et al, 1974). This idea was based on the assumption that the greater the power input, the greater the degree of excitation of especially the more refractory elements. This oversimplification has since been shown to be erroneous, however (Greenfield and Thorburn Burns, 1980; Montaser et al, 1981), with the low-power (~1 kW) pure argon Fassel type ICP and high-power (~5 kW) nitrogen/argon Greenfield type ICP having comparable limits of detection. A considerable portion of the applied rf power in the $N_2$/Ar plasma is consumed in the dissociation of the $N_2$ triple bond with a dissociation energy of 9,76 eV (Northway et al, 1980), while in the pure Ar plasma all the power is available for ionization and excitation of argon.

In the Greenfield plasma, nitrogen is used for the coolant gas only, the aerosol and plasma gases being argon (Greenfield et al, 1975). The nitrogen coolant causes a pinch effect, with narrowing of the plasma and aerosol channel, and consequently a greater efficiency of heat transfer from the plasma to the analyte in the axial channel. The high-power $N_2$ cooled Greenfield type plasma is thus less susceptible to solute vaporization type interferences than the pure argon plasma (Montaser et al, 1981). Where foreign diatomic gases are introduced into the axial analyte channel the high-power $N_2$/Ar plasma is preferable over the pure argon plasma as the former is less susceptible to plasma breakdown than the latter (Ohls and Sommer, 1983). The problem of plasma instability has for instance been experienced in the analysis of arsenic by the hydride method where hydrogen is introduced into the aerosol gas flow (Thompson et al, 1978; Nakahara, 1981). The $N_2$/Ar plasma is also useful where ultrasonic nebulization is employed instead of the usual pneumatic nebulization. Indeed, Ohls and Sommer (1983) make the statement: "You can put anything you want into the $N_2$/Ar plasma without a breakdown".

Other workers (Lowe, 1981; Rezaaiyaan et al, 1982, Meddings et al, 1985) have pursued the possibility of even lower powers, with associated low gas consumption rates, than the 1 to 2 kW power input used in the low-power pure

Ar plasma by Fassel and co-workers (Scott et al, 1974; Fassel et al, 1976); by the design of quartz torches employing less than 10 $\ell.min^{-1}$ cooling gas. Such low gas consumption torches have not, however, been adequately tested in the analytical application field, and it still remains to be seen how effective they are for routine analytical work. If the low gas consumption torches prove to have comparable analytical characteristics to the conventional Fassel-type torch, they will serve to decrease the operating cost of ICP emission spectrometry. Promising results in the use of a low gas consumption plasma have been achieved by Angleys and Mermet (1984), who showed that gas consumption may be reduced through reduction in the space between the outer and intermediate tubes. Angleys and Mermet reported a deterioration in detection limit of about five-fold for a 600 W rf input and 4 $\ell.min^{-1}$ gas flow rate and pnuematic nebulization, compared to a conventional plasma operating at a power > 1 kW and with > 12 $\ell.min^{-1}$ gas flow rate. These authors suggest the use of ultrasonic nebulization as a means of improving the detection limit.

With a given plasma torch, and a given set of aerosol, intermediate (plasma) and coolant gas* flows, the value of the rf power input influences the height above the load

---

* The IUPAC recommendations for nomenclature of the aerosol, plasma and coolant gas flows are the inner, intermediate and outer gas flows respectively (Butler et al, 1985).

coil at which the intensity of analyte atomic and ionic emission peaks. Thus Blades and Horlick (1981) found that the height of maximum emission for the Ca I 422,7 nm emission line shifted, from 17 mm to 13 mm above the load coil, as the rf power input was increased from 1,0 kW to 2,0 kW with flow rates of 0,85 $\ell.min.^{-1}$ for aerosol; 15 $\ell.min^{-1}$ for coolant and <1 $\ell.min^{-1}$ for auxiliary (intermediate) gas. The height of maximum emission for the Ca II 393,3 nm ion line likewise shifted from 23 mm to 20 mm above the load coil as the rf power input was increased from 1,0 kW to 2,0 kW. Changes in the rf power input to the ICP source, from the analytical chemists viewpoint, in essence influence the rate of energy transfer into the axial analyte channel, and consequently the point along the axis of the analyte channel at which the maximum excitation condition for a given spectral transition is reached. This point will also depend on any influence from matrix elements on excitation conditions of the surrounding plasma e.g., the presence of EIE's such as sodium (Blades and Horlick, 1981), as well as on the velocity of the aerosol gas flow along the axial channel. High aerosol gas flow rates would allow the analyte to pass further along the axial channel before a given state of excitation is reached, while low aerosol gas flow rates would have the opposite effect. Thus Kornblum (1977) found that for an argon plasma operated at 0,53 kW with an aerosol gas flow

of 1,4 $\ell.min^{-1}$ volatilization interference of phosphate on calcium emission was almost absent, whereas this matrix interference was pronounced when the aerosol gas flow was increased to 4,5 $\ell.min^{-1}$, a not unexpected observation.

The effect of plasma power on analytical characteristics such as detection limit or degree of matrix interferences are not only element specific, but also intimately related to other plasma variables such as observation height and gas flow rates. The oft confusing and contradictory reports on the effect of changing these variables on analytical characteristics is in part due to their interdependence. They should be considered synoptically (Greenfield and Thorburn Burns, 1980; Blades and Horlick, 1981).

## 2.9 Sample introduction

ICP spectrometry shares with flame AAS the most usual method of sample introduction *viz.*, as a nebulized aerosol. The ICP source has thus lent itself to the ready analysis of samples in the liquid form, where a nebulizer is used to introduce fine spray droplets of a liquid into the central argon flow (Barnes, 1978). The liquid is most usually water (Greenfield *et al*, 1975; Winge *et al*, 1977; Larson *et al*, 1983), although organic solvents have also been used e.g., in oil analysis (Fassel *et al*, 1976) or

where solvent extraction is employed (Motooka et al, 1979). While a few workers have mentioned techniques for introducing solid samples into the ICP source e.g., with laser (Abercrombie et al, 1978) or arc or spark (Barnes, 1978) vaporization, or by introducing a graphite cup containing the sample directly into the base of the plasma (Ohls and Sommer, 1983); the most common method of handling solids for ICP spectrometric analysis is by dissolution with a suitable digestion or fusion procedure, followed by nebulization of the resulting solution (Dahlquist and Knoll, 1978; Golightly, 1978; Zamechek et al, 1978). Solid samples present in a finely divided form as a suspension in a liquid i.e., a slurry, may also be directly nebulized with e.g., a GMK nebulizer using the V-notch principle (Garbarino and Taylor, 1980; McKinnon et al, 1983). Occasionally the sample may be present in a gaseous form e.g., where an ICP source is fed with the eluent from a gas chromatograph (Windsor and Denton, 1979), or where the analyte element is chemically converted into a gaseous species for introduction into the ICP source e.g., in the hydride method for the determination of arsenic (Thompson et al, 1978).

For the most common method of sample introduction i.e., nebulization, two main techniques are employed viz., (i) pneumatic nebulization and (ii) ultrasonic nebulization with or without desolvation (Greenfield et al, 1975;

Dahlquist and Knoll, 1978; Berman et al, 1980; Garbarino and Taylor, 1980; Goulden and Anthony, 1982). Pneumatic nebulization, by means of either the crossflow or Meinhard concentric glass nebulizer has the disadvantage that high salt concentrations such as found for instance in sea water, may evaporate on and block the nebulizer tip (Browner, 1978; Berman et al, 1980). The fine capillary orifice of the sample tube of conventional pneumatic nebulizers is also readily blocked by solid particles inadvertently present in suspension in the liquid sample, although this difficulty has been overcome, and indeed made use of, through the V-notch type GMK nebulizer design, based on the Babbington principle (Garbarino and Taylor, 1980; McKinnon and Giess, 1983). Through proper filtration of samples prior to analysis blocking of the capillary tip in the conventional pneumatic nebulizers may be avoided. Baginski and Meinhard (1984) made the interesting observation that the problem of salt deposition in the central tube of the plasma torch or at the capillary tip of a concentric pneumatic nebulizer may be minimised by taking care not to allow a plug of air to be aspirated between samples when analyzing saline solutions.

The main disadvantage of pneumatic nebulization is that the fraction of droplets that reach the plasma in the case of ICP emission spectrometry, or the flame in the case of AAS, is usually less than 10% with the remaining 90% or more of

the nebulized sample, having a droplet size in excess of 20 µm draining from the spray chamber (Burrell, 1974). In the case of the concentric, crossflow and GMK nebulizers efficiencies of less than 4% are reported (McKinnon and Giess, 1983). While the poor efficiency of fine droplet formation by pneumatic nebulizers does degrade the detection limits, the chief concern is in relation to transport nebulization interferences. Any change in the droplet size distribution e.g., as a consequence of viscosity changes between dilute and concentrated salt solutions may affect the nebulization efficiency. Interference may also occur without change in droplet size distribution when an analyte solution is nebulized in the presence of a matrix element at high concentration (> 1000 $mg.\ell^{-1}$) and differential migration of ions result in the finer droplets not having the same composition as the bulk solution. Browner et al (1983) refer to this interference as Aerosol Ionic Redistribution (AIR). The use of ultrasonic nebulization, with a greater efficiency of production of aerosol droplets with a droplet diameter less than 10 µm, while minimizing AIR interference, is nevertheless disappointing in regard to the improved detection limit expected from the greater efficiency of transport of sample into the plasma, a difficulty possibly attributable to instability of aerosol production (Berman et al, 1980). The greater mass of water injected into the plasma per unit time where ultrasonic

nebulization is used as opposed to pneumatic nebulization may also lead to instability or extinguishing of the plasma, and desolvation is usually employed in conjunction with ultrasonic nebulization. While desolvation does result in a fourfold improvement in detection limit, a drawback is the greater matrix effects from acids encountered (Berman et al, 1980). The susceptibility of ultrasonic nebulization with desolvation to matrix effects is due to the absence of the temperature buffering role water plays in nebulization without desolvation*. A similar criticism may be directed to the employment of desolvation in conjunction with pneumatic nebulization in an effort to improve detection limits (Goulden and Anthony, 1982). Ultrasonic nebulization also suffers from the drawback of greater memory effects following aspiration of a solution containing a high concentration of an analyte (Scott et al, 1974). As sample throughput time is often considered in economic/productivity terms, pneumatic nebulization, with the lesser memory effect is usually employed in routine analysis.

The problem of AIR interference in pneumatic nebulization may cause severe error e.g., Browner et al (1983) reported a 200% enhancement in Na 589,0 nm emission when present in a magnesium matrix of 5000 $mg.\ell^{-1}$ and with a Mg:Na

---

* (J.M. Mermet, personal communication, April 1985).

ratio of 200:1. Aerosol ionic redistribution interferences may be avoided where high salt content samples are diluted prior to nebulization.

The poor transport efficiency inherent in pneumatic nebulization (McKinnon et al, 1983) also creates the potential for other sources of change in the concentration of analyte in the introduced aerosol gas flow viz., where volatile analyte species are present. Thus enhancements of 50x have been observed in Os emission intensities when the osmium is present in solution as the volatile $OsO_4$ species (Summerhays et al, 1983). Similarly, enhancement of 80% in Hg analytical line emission intensities have been observed when mercury is present in the zero oxidation state as opposed to the oxidized ionic states, when Sn (II) is added to Hg(II) solutions (Kirkbright et al, 1973). The enhanced sensitivity when the analyte element is present in the sample in a volatile form may be put to good effect in the improvement of detection limits, and is for instance, purposely created in the hydride method for As (Thompson et al, 1978).

## 2.10 Noise, precision and detection limit

The greater the precision i.e., the greater the reproducibility of successive measurements of analyte emission intensity, the greater the ease with which small

differences in emission intensity are detected. Thus detection limit (DL) may be defined in terms of the noise of the background emission expressed in equivalent concentration units. It is customary to quantify the background noise at a given analytical wavelength for a sample-blank in terms of standard deviation units, where the detection limit is defined as a multiple of the standard deviation (Boumans et al, 1981):

$$DL = \kappa.\sigma_b \qquad \ldots\ldots\ldots\ldots \qquad (11)$$

where DL = Detection limit,

$\kappa$ = multiple of std., deviation adopted,

and $\sigma_b$ = standard deviation of the background.

Thus for a sample containing an analyte at the detection limit, the net analyte signal is equal to the multiple of $\sigma_b$ chosen (Greenfield, 1983):

$$I_g - I_b = \kappa.\ \sigma_b \qquad \ldots\ldots\ldots\ldots \qquad (12)$$

where $I_g$ = gross analyte signal,

$I_b$ = background signal,

and $\kappa$ and $\sigma_b$ are as defined for equation 11.

The value adopted for the factor $\kappa$ depends on the degree of certainty required in measuring analyte concentrations near the detection limit. Values of $\kappa$ chosen are for

instance 2 (Winge et al, 1977); $2\sqrt{2}$ (Greenfield, 1983) or 3 (Floyd et al, 1980; EPA, 1982). Winge et al (1977) also suggest a $\kappa$ value of 10 for quantitative analysis at trace concentration levels and name the corresponding DL the limit of quantifiable detection (LQD). The number of successive replicate measurements used in calculating $\sigma_b$ will obviously influence the value obtained, as the standard deviation of a subset drawn at random from a population is dependent on the number (n) of elements in the subset. The population standard deviation is only approached for large n. While 10 replicates give a good indication of the achievable detection limit (EPA, 1982), in routine analysis where speed is of the essence as few as 2 or 3 replicates are often used (Floyd, et al, 1980; Subramanian and Meranger, 1982; Larson et al, 1983).

Boumans et al, (1981) give the following formula for detection limit which contains terms for the relative standard deviation (RSD) and signal to background ratio (SBR):

$$DL = \kappa . (RSD)_b . \frac{C_o}{SBR} \qquad \ldots\ldots\ldots\ldots \qquad (13)$$

where DL and $\kappa$ are as defined in equation 11,

$(RSD)_b$ = the relative standard deviation of the background signal,

SBR = signal to background ratio in intensity units i.e., net signal ($I_o$) divided by net background ($I_b$),

and $C_o$ = concentration of analyte in solution giving the net signal concerned.

This formula creates the mistaken impression that DL is dependent on the SBR. This is a false impression, however, which can be seen if $(RSD)_b$ is expressed as:

$$(RSD)_b = \frac{\sigma_b}{I_b} \qquad \ldots\ldots\ldots\ldots \qquad (14)$$

and substituted into equation 13, and likewise expressing SBR as the ratio of the relevant intensities i.e. $I_o/I_b$, whereupon equation 13 becomes:

$$DL = \kappa . \sigma_b . \frac{C_o}{I_o} \qquad \ldots\ldots\ldots\ldots \qquad (15)$$

Equation 15 is essentially identical to equation 11, except that the ratio $C_o/I_o$ results in the DL value being expressed in concentration units rather than in intensity units.

In the analysis of real samples, the standard deviation of the background, $\sigma_b$, cannot of course be measured at the same time as the sample intensity is integrated. For this

reason the standard deviation of the sample analyte intensity, $\sigma_s$, is measured, with the precision $P_s$ of the sample being given by;

$$P_s = \kappa . \sigma_s \qquad \ldots\ldots\ldots\ldots \qquad (16)$$

where $\kappa$ is the multiple adopted as in equation 11.

When the concentration of analyte in the sample is small, then $\sigma_s \simeq \sigma_b$ and the precision $P_s$ of equation 16 becomes equal to the detection limit DL of equation 11, i.e;

$$\text{Limit } P_s \xrightarrow[0]{C_o} DL \qquad \ldots\ldots\ldots\ldots \qquad (17)$$

where the concentration, $C_o$, of analyte approaches zero. The concept of detection limit involves a grey area between quantitative and qualitative analysis. As the analyte concentration is reduced the analyte signal gradually disappears or merges into the background noise. Another way of stating this is that the relative standard deviation of the measured analyte concentration increases as the analyte's concentration approaches the detection limit. Butler expanded on the concept of the precision of analyte readout and blank readout in his analytical range idea (Butler et al, 1980; Greenfield, 1983), when he demonstrated that the relative standard deviation of the net signal, when plotted against log concentration, reveals the detection

limit of varying values of multiple $\kappa$ of equations 11 and 16. When $\kappa = 2$ for instance, then the detection limit is the concentration where the relative standard deviation of the net signal, $RSD_s$, is 50%. Butler's idea uses the limit (17) in equating the relative standard deviation of the net signal ($RSD_s$) with the $RSD_b$ for small analyte concentrations, and is in essence similar to Boumans et al (1981) idea as shown in equation 13 in bringing the RSD and SBR into the concept of precision. The analytical range concept of Butler also reveals the tendency of precision to deteriorate at high concentration, when relative standard deviations greater than the 1% RSD characteristic of the middle concentration range for analyte lines are considered (Butler et al, 1980).

In the grey area between the two extremes of quantitative analysis, where the analyte signal is several times greater than the standard deviation of the background noise, and zero analyte concentration; there is a zone where the presence of analyte may be confirmed, but where the background noise prohibits exact quantitation. Thus for signals barely discernable above the background noise, the analyte's concentration can only be expressed in probabilistic terms. The quantitative numerical concept that a sharply defined detection limit exists as implied by equation 11 may be modified to more suitably describe the analyte signal behaviour at trace concentrations if the

statistics of hypothesis testing between means is adopted. A useful statistic for this purpose being the t-statistic of the Student's t distribution given by the equation (Kenney and Keeping, 1964; Green and Margerison, (a),1978):

$$t = \frac{(\bar{I} - \bar{I}_b) - \mu}{\sigma/\sqrt{n}} \qquad \ldots\ldots\ldots\ldots \qquad (18)$$

Where $\bar{I}$ = mean gross analyte signal,

$\bar{I}_b$ = mean blank signal,

$\sigma$ = standard deviation of blank signal,

n = number of integrations used in calculating $\bar{I}$ and $\bar{I}_b$,

and $\mu$ = difference between population means.

If the hypotheses to be tested are:

(i) The null hypothesis, $H_o$: There is no analyte present i.e., $\mu = 0$, and the difference observed between $\bar{I}$ and $\bar{I}_b$ is due to chance, and

(ii) the alternative hypothesis, $H_1$: Analyte is present i.e. $\mu > 0$.

The null hypothesis is rejected when the modulus of the experimental value of t from equation 18 is greater than or equal to the critical value of t for a given level of

significance, or as read from a table of values for the t-distribution (Green and Margerison, (a), 1978). In this way a probabilistic statement on the presence of analyte at the detection limit may be made. Other hypotheses may also be set up to test if the population difference between analyte and blank values is greater than a given value i.e.;

(i) null hypothesis, $H_o$: $\mu = \mu_o$

and (ii) alternative hypothesis, $H_1$: $\mu > \mu_o$;

thus providing information on the quantity of analyte present.

The concept of detection limit in the ICP spectrometric literature has primarily been limited to consideration of the standard deviation of the background noise for n replicate measurements at a single, fixed wavelength. Thus an unstated assumption of $\sigma_b$ in equation 11 for instance, is that it applies to successive intensity measurements at the analytical line centre i.e.;

$$\sigma_b = \left( \frac{\sum_1^n (\bar{I} - I_i)^2}{n-1} \right)^{1/2} \quad \ldots\ldots\ldots\ldots \quad (19)$$

where n = no's of readings at the central wavelength position $\lambda_o$,

$I_i$ = intensity of the $i^{th}$ measurement

$\bar{I}$ = mean of the $I_i$'s.

With the advent of high resolution graphic screens, and the ease with which profile scans of analytical emission lines may be recorded, the profile mode of measurement may be used for routine analysis of samples instead of the conventional measurement at line centre i.e.; profile peak position, only. This necessitates an expression for detection limit in the profile mode i.e., when does the scan of a sample across the analyte wavelength $\lambda_o$ differ significantly (in the positive direction) from a scan of a blank solution across $\lambda_o$? While n repetitive scans may be performed on a blank solution and the intensities at central profile position used to calculate the detection limit in the usual manner (equations 11 and 19), this is impractical in routine analysis as firstly, the profile scan mode is generally time consuming and secondly, a single scan of 2m + 1 steps across the central profile position $\lambda_o$ already contains repetitive measurements of blank intensity albeit at wavelength intervals of $\delta\lambda$.

If a function $\Omega_b$ is defined as follows:

$$\Omega_b = \left( \frac{\sum_{-m}^{+m} (\bar{I} - Im)^2}{(2m+1)-1} \right)^{1/2} \qquad \ldots\ldots\ldots\ldots \qquad (20)$$

Where Im = the intensity of the blank at step position m, i.e., at wavelength position $\lambda_o + m.\ \delta\lambda$ where $\lambda_o$ is the central wavelength, and $\delta\lambda$ is the wavelength difference for one profile step,

and $\bar{I}$ = the mean blank intensity i.e.,

$$\bar{I} = \left( \sum_{-m}^{+m} Im \right) \div (2m+1) \quad \ldots\ldots\ldots\ldots \quad (21)$$

Then it follows that the usual method of defining the standard deviation of the background $\sigma_b$ in equation 19, is the limiting case of equation 20 when $\delta\lambda$ approaches zero and n = 2m+1. This may be written:

$$\text{Limit: } \Omega_b \xrightarrow[0]{\delta\lambda} \sigma_b \quad \text{where } n=2m+1 \quad \ldots\ldots\ldots \quad (22)$$

Expression 20, to be practically useful in determining detection limit in the profile mode of analysis at trace levels, must be considered in relation to background slope. This will be discussed further in chapter 6, where the interpretation of scan data near the limit of detection is dealt with. While a definition of the detection limit in the profile scan mode of analysis is needed in practical analysis, the approach as suggested by equations 20 and 22 has not previously been described in the literature.

As for the source of the background noise responsible for the typically 1% RSD background noise in ICP emission spectrometric instrumentation, Watters and Norris (1978) divide the sources of noise into the following three groups:

(i) Noise in the measuring system i.e., photomultiplier tubes and associated electronics, together with noise in the conversion of analogue to digital data,

(ii) Noise in the ICP source i.e. gas flows to plasma, radio frequency power generation and coupling.

(iii) Noise in the sample introduction system i.e., spray chamber and nebulizer.

Related to the question of noise i.e., short term variability in signals, is the variation in signals in the long term i.e., stability and the associated concept of drift, where the long term variation shows a bias in a given direction. These are discussed below.

## 2.11 Stability and drift

Stability of source conditions over time enhances accuracy and facilitates calibration of the instrument. Invariance of plasma conditions is particularly important where interelement interference corrections are used (Berman et al, 1983). The reproducibility of gas flow rates to the

plasma, particularly the aerosol gas flow rate is important as regards stability of calibration sensitivities (Broekaert, et al, 1982). Botto (1983; 1984) suggested the use of the emission intensity ratio of Cu(I) 324,754 nm to Mn(II) 257,610 nm as an aid in adjusting aerosol gas flow and achieving reproducible plasma excitation conditions over time.

While stability of plasma excitation conditions is important where interelement effects are considered, a more serious problem in trace analysis is drift in blank emission intensity between samples. The usual procedure in analysis of samples is to subtract the last updated blank intensity or concentration (Winge et al, 1977), but any drift in the blank signal will naturally result in an error in accuracy for the concentration measured for a subsequently aspirated sample. Interpolation between blanks may partially solve this difficulty, but relies on the assumption of linear drift of blank intensity with time. While true blank drift is due to change in the emission intensity of the recombination continuum and thus to change in the free electron number density or electron temperature (Kornblum, 1977), change in apparent blank intensity due to memory effect or carry-over in the nebulization/transport system is often a more serious problem in routine analysis. The memory effect is responsible for elevation in blank intensity of sample blanks run immediately after a high

concentration of standard or sample (Garbarino and Taylor, 1980). While chromatographic effects may contribute to the memory phenomenon, the major cause is the inability of the nebulizer to dissipate the aerosol fog in the spray chamber (Dobb and Jenke, 1983). The degree of memory varies also with the type of nebulizer employed. Thus pneumatic nebulization exhibits the memory effect to a lesser degree than ultrasonic nebulization with desolvation, and is probably the reason for the greater employment of the former method by ICP spectrometric analysts (Scott et al, 1974).

The use of acid wash solutions between samples has been suggested as a means of reducing the time needed to reach true blank intensity levels (Winge et al, 1977). While the assumption of an exponential decay curve to describe the washout portion of an analyte intensity readout, with expression of the memory effect in terms of the half-life tau ($\tau$), has for instance been used by Garbarino and Taylor (1980); the shape of the washout curve is more closely approximated by a hyperbolic function (Dobb and Jenke, 1983). Dobb and Jenke (1983) found that the washout curve could be described by a hyperbolic function of the form:

$$I = A + B/t \qquad \ldots\ldots\ldots\ldots \qquad (23)$$

where I = gross intensity signal (analyte plus blank),

A = constant (true blank intensity),

B = constant (units of s x intensity),

and t = washout time (s).

Dobb and Jenke (1983) further defined a memory factor M as:

$$M = B/I_n \qquad \ldots\ldots\ldots\ldots \qquad (24)$$

where B is the constant as given in equation 23, and $I_n$ is the intensity of the previously analyzed sample responsible for the memory effect.

Alternatively the memory effect may be expressed as the time needed for the net analyte signal to decay to x% of the initial intensity, symbolized by $t_x$. For a Meinhard concentric glass nebulizer Dobb and Jenke (1983) report typical $t_{o,1}$ values varying between 150 s for K to 290 s for Pb.

A problem of stability characteristic of Czerny-Turner type scanning monochromators is the difficulty in exact positioning of the wavelength setting. This may be overcome through fine-tuning of the wavelength position e.g., with a peak-search software routine (Floyd et al, 1980). Once the analytical line maximum has been found, however, it may not necessarily remain exactly on the exit slit if any thermal

drift occurs (Taylor et al, 1984). Any drift from the centre of the emission line peak will result firstly in a decrease in analytical sensitivity and secondly in a change in background emission intensity unless the background beneath the analytical emission line is horizontal.

## 2.12 Calibration and accuracy

Calibration of analytical emission line intensity, as measured with a photomultiplier tube (PMT) in analyte concentration units is at first sight simple, as the ICP source characteristically shows linear proportionality between emission intensity (I), and concentration (C) over several orders of magnitude (Jones et al, 1974; Kirkbright and Ward, 1974).

Calibration with a blank and a single standard using the relationship,

$$C = aI + b \qquad \ldots\ldots\ldots\ldots \qquad (25)$$

where C = concentration of analyte
a = proportionality constant
I = emission intensity,
and b = intercept,

has been used in routine ICP spectrometric analysis (Kuennen et al, 1982). While a linear relationship such as given by equation 25 may be used for concentrations below 10 $mg.\ell^{-1}$ (Larson et al, 1983) this approach is not advisable at greater concentrations as departure from linearity may occur. Thus Garbarino and Taylor (1979) found that curvature of the Ca(II) 396,8 nm emission line response can be observed at concentrations above 100 $mg.\ell^{-1}$. Depending on the concentration range covered therefore, polynomial curve fitting software routines of 1st, 2nd or 3rd order may be used for calibration (Floyd et al, 1980).

If calibration were merely limited to the above, ICP spectrometric analysis would be simple indeed. The extremely rich line spectrum of the ICP source results in a high probability of line overlap interferences, and any analytical emission line must therefore be studied for possible interferences from matrix elements before routine analysis is carried out (Anderson et al, 1982). The various approaches to the problem of spectral interferences were summarized by Berman et al (1983):

(i) Avoid the interference by choice of an alternative analytical wavelength, or through use of chemical separation techniques prior to introduction of the sample in the ICP spectrometer.

(ii) Use of interference filters in front of the photomultipliers. While this approach may be used to reduce for stray light (crosstalk) e.g., from Ca or Mg emission, it has no effect on interferences due to spectral line coincidence or overlap from neighbouring line wings (near stray light).

(iii) Use of matrix matching for major elements, so that the interference is the same for the calibration as for the samples. This suffers from the disadvantage that it does not allow for variation in sample composition, and secondly is economically undesirable as a consequence of the high cost of ultrapure chemicals.

(iv) The software approach i.e., use of intereference correction coefficients. This approach necessitates invariant plasma conditions.

(v) The measurement of off-peak background intensity as an estimate of background intensity at the analytical wavelength.

(vi) The use of wavelength profile scans to detect spectral interference.

The first approach to the problem of spectral interferences is particularly important when the wavelength suite for a polychromator is chosen. Choice of interference free lines is, however, not always possible, and interference from calcium and magnesium, with their very bright resonance lines (Anderson et al, 1982) is common (Garbarino and Taylor, 1979; Thompson et al, 1982; Winge et al, 1977; Berman et al, 1983). As the choice of analytical wavelengths is to a large extent dictated by the principle of maximum sensitivity with least spectral interference (Johnson et al, 1979), the wavelength suite chosen will also influence the choice of which elements are mixed together in multielement standard solutions used for calibrating under compromise conditions (EPA, 1982; Ohls et al, 1977).

The second approach i.e., use of interference filters is not suitable for near stray light (i.e., wing overlap) interference, which is the major problem with the line rich ICP spectrum, and will not be discussed further here.

The third approach i.e., matrix matching has limited usefulness for dealing with true spectral interferences as mentioned by Berman et al (1983), but is of great importance as far as avoiding error due to sensitivity change interferences between different matrices, i.e. changes in the magnitude of the constant "a" in equation 25. While matrix effect due to viscosity and change in nebulization

efficiency may be relatively easily solved through ratioing to an internal standard, the sensitivity changes resulting from different response of elements in the suite to changed plasma excitation conditions is not so readily solved, and internal standardization has been reported to degrade analytical precision without materially improving accuracy (Dahlquist and Knoll, 1978). Use of forced aspiration to minimise variation in sample uptake rate has been used as an alternative to internal standardization in ICP spectrometric analysis (Kuennen et al, 1982; Wolnik et al, 1983), Internal standardization is particularly useful where preconcentration techniques, such as evaporation are used, with a variable preconcentration factor, eg., lanthanum has been used for this purpose by Thompson et al (1982) to quantify the evaporative preconcentration factor. A reasonable degree of matrix matching with respect to major salt concentration is advisable in ICP spectrometric analysis, particularly in view of the non-additivity of sensitivity changes (Maessen et al, 1982). The latter workers found that the relative change in line intensity of an analyte element is proportional to the square root of the concentration of the matrix element. Maessen et al (1982), in studying the effect of high concentrations of the alkali and alkaline-earth elements on analyte sensitivity defined the matrix effect (ME) as follows:

$$ME = \left(\frac{100 \quad (IA - Ip)}{(IA)}\right) \% \qquad \ldots\ldots\ldots\ldots \quad (26)$$

where IA = analyte intensity in the absence of interfering salt.

Ip = analyte intensity in the presence of interfering salt.

The fourth approach to interelement interference phenomena in ICP spectrometry i.e., the use of interference correction coefficients, also known as the software approach (Berman et al, 1983), is widely used in routine ICP spectrometry, particularly on multielement polychromator type instruments (Garbarino and Taylor, 1979; Botto, 1983; Larson et al, 1983; Munter and Grande, 1983). The basis of the interference approach is to analyze pure, single cation standards for the suite of elements for which a polychromator has analyte channels and record the readings obtained for the suite of element channels in concentration equivalent units (CEU). Thus the cross-talk between analyte channels may be quantified. If a concentration $C_X$ of analyte X results in a CEU reading of $Q_A$ for element A, then the linear interference coefficient $C^1_{XA}$ for interference of X on A is given by:

$$C^{1}_{XA} = \frac{Q_A}{C_X} \qquad \ldots\ldots\ldots\ldots \quad (27)$$

In routine analysis, coefficients of the type given by equation 27 may be used to correct the apparent (raw) concentration readout as follows (Botto, 1983):

$$C_{A(corrected)} = C_{A(raw)} - C^{1}_{XA} \cdot C_X \qquad (28)$$

where $C_{A(corrected)}$ = corrected concentration of analyte A,

$C_{A(raw)}$ = concentration readout for A uncorrected for interference of X on A,

$C_X$ = concentration of interfering element X,

$C^{1}_{XA}$ = dimensionless linear interference correction coefficient of X on A.

Linear interference corrections of the type used by Botto (1983) have also been employed by Subramanian and Méranger (1982) in the analysis of autopsy samples, and by Munter and Grande (1983) in the analysis of plant tissue digests and soil extracts. The assumption of linearity of interelement interferences is only valid, however, as a first approximation. Curvature of interelement interference is particularly pronounced, for example for the spectral interference of Ca on the Al 396,15 nm analytical line, with a quadratic function providing a better fit for the experimental data than a linear function (Dahlquist and Knoll, 1978). Garbarino and Taylor (1979) found that first

order interference corrections are ineffective when the electrical conductivity of the sample is greater than 200 $mS.m^{-1}$ (25°C). Larson et al (1983) reported that non-linear corrections from stray light arising from the intense ionic calcium emission at 393,4 and 396,8 nm are frequently required. Kempster et al (1983) used quadratic interference corrections of the form:

$$\delta C_A = C^1_{XA} . C_X + C^{11}_{XA} . (C_X)^2 \quad \ldots\ldots \quad (29)$$

where $\delta C_A$ = concentration equivalent to be subtracted from raw concentration A.

$C^1_{XA}$ = dimensionless first order interference coefficient of X on A.

$C^{11}_{XA}$ = second order interference coefficient of X on A, dimension : reciprocal of concentration

$C_X$ = concentration of interfering element, X.

Kempster et al (1983) used equation 29 to correct the raw analyte concentrations as follows:

$$C_{A(corrected)} = C_{A(raw)} - \delta C_A \quad \ldots\ldots\ldots \quad (30)$$

One of the problems in the use of the software or interference coefficient approach is that the validity of the technique depends on invariance of the relative emission intensities of pairs of elements involved in the correction calculation. This implies that plasma excitation conditions must be as reproducible as possible from one day to the next. One method of achieving this reproducibility has been by adjusting aerosol flow to achieve a given intensity ratio between two elements with

different excitation energies. Botto (1983) used the ratio between an atom line of copper i.e., Cu(I) 324,75 nm and an ion line of manganese Mn(II) 257,61 nm, and reported reproducibility of linear correction coefficients of around 5%.

A major problem in the interference correction approach is the determination of the coefficients, as this rests on the assumption that pure single cation standards are used. This is equivalent to the assumption that the signal obtained for an element not present in the single cation standard is due entirely to spectral interference and not to any impurities. In practice, absolute purity of single cation standards is not achievable, and concentration values for impurities must be subtracted before the interference coefficients are calculated. The certificate of analysis accompanying so called spectroscopically pure chemicals provides an indication of what impurities can be expected in the single cation standards used for interference coefficient determinations. It should not be forgotten, however, that to these impurities must be added the impurities arising by leaching from the containers used in preparing the standards. The effect of impurities in redistilled acids or deionized water used to dissolve the spectroscopically pure material are usually negated through use of the same batch of acid or deionized water in the blanks run with the single cation standards. Impurities in

ultra pure acids are not always insignificant, for instance Iyengar and Sansoni (1980) report the following impurities in ultrapure acids: 52 $\mu g.\ell^{-1}$ Ca in HF; 8 $\mu g.\ell^{-1}$ S in $HNO_3$; 200 $\mu g.\ell^{-1}$ Se in $H_2SO_4$ and 9 $\mu g.\ell^{-1}$ Cr in $HClO_4$.

Iyengar and Sansoni (1980) found ultra pure HCl to be the most free of impurities of the acids, the maximum impurity being sulphur at 3 $\mu g.\ell^{-1}$. Wing overlap or background shift spectral interferences can readily be distinguished from impurities in single cation standards, except in the case of exact spectral emission wavelength coincidence; through the use of profile offset measurements, or profile scan techniques to obtain information of the shape of the observed emission line (Dahlquist and Knoll, 1978; Floyd et al, 1980; Kempster et al, 1983; Winge et al, 1977). Exact emission line coincidence between two different elements can be distinguished from an impurity, through comparison of emission intensity at the wavelength where coincidence is suspected for a number of different salts of the given cation, as the possibility that an impurity is present in different salts at the same concentration is low (Michaud and Mermet, 1982). Alternative approaches are to compare values with other analytical emission lines of the element concerned, or with analytical results obtained by alternative instrumental techniques. Failure to identify and quantify impurities in single cation standards used for

determining interference correction coefficients for use in routine analysis, will result in over correction on real samples, one sign of which is the occurrence of negative concentration readout which cannot be accounted for by the background noise (Kempster et al, 1983).

Botto (1984) points out that the accuracy of determination is influenced by the magnitude of spectral interference correction, and defines the percentage interference correction (PIC) as follows:

$$PIC = \frac{C_{A(corrected)} - C_{A(raw)}}{C_{A(corrected)}} \times 100\ \% \quad ..... \quad (31)$$

where $C_{A(corrected)}$ = corrected concentration of analyte A, using interference correction coefficients,

and $C_{A(raw)}$ = uncorrected concentration readout for analyte A.

Botto (1984) further defines the corrected concentration value for analyte A as quantitative where PIC $\leq$ 100%, as semi quantitative where PIC is between 100% and 500%, and as unreliable where PIC $\geq$ 500%.

The use of wavelength tables (Zaidel' et al, 1970; Parsons et al, 1980) are of great value in the establishment of interference correction coefficients, as such tables assist in the identification of possible spectral interferences on the analytical channels of a polychromator.

The fifth approach, i.e., measurement of off-peak background emission intensity in order to perform background correction has been used by Kuennen et al (1982) at a background position of ± 0,03 nm from central profile position and by Skogerboe et al (1976) who used an automated technique employing a tuning fork to vibrate a refractor plate across the light path. A major problem in the use of the background measurement approach is the difficulty of measuring true background emission consequent to the high probability of overlap of a spectral line of some other element at the position chosen for background correction as a consequence of the line rich ICP spectrum (Larson et al, 1983) as well as the problem presented by background structure (Garbarino and Taylor, 1974) or where the background is sloped (Larson et al, 1983).

The sixth approach, i.e., the identification of spectral interference through the use of wavelength profile scans is related to the approaches mentioned above, e.g., in choosing a suitable analytical emission line; in distinguishing between impurity and wing-spectral interference; and in choosing suitable wavelength offset positions for background correction. The wavelength profile scan approach has, however, been primarily employed as a means of qualitatively investigating the nature of the ICP spectrum in the region of each analytical emission line and the type of interferences occurring, rather than in quantitative analysis per se (Berman et al, 1983; Dahlquist and Knoll, 1978; Floyd et al, 1980; Kempster et al, 1983; Larson and Fassel, 1979; Winge et al, 1977). The advent

of high resolution graphic video screens in ICP spectrometric scanning monochromator instrumentation, by which the analyst may readily obtain quantitative measurement on wavelength profile scans, opens the way to use of such scans for quantitative analysis.

This section on calibration and accuracy would not be complete without a discussion on the problem of contamination. A sine qua non of accurate analysis at trace concentration levels is the prevention of elemental contamination (Kuennen et al, 1982). While this is commonly recognised as a problem where preconcentration techniques are employed due to impurities in reagents used (Iyengar and Sansoni, 1980) it also presents a problem in establishing the blank emission intensities for the analytes. Any contamination in the deionized water will result in elevation of blank emission intensity for the relevant analytical channel, and as blank concentrations are subtracted from sample concentration readouts, will result in over correction for the blank. This is primarily a problem in water analysis. Where solid samples are digested, the same contamination from acids or deionized water is added to both sample and blank, and is subtracted out on analysis. Larson et al (1983) point out that particular care should be taken in ensuring that where automatic samplers are used, that cups containing the blank solution should be free of contamination, else a negative bias in the samples following will result.

## 2.13 Quality Control

Quality control is an essential requirement in any analytical service, particularly where modern day instrumentation is used with its accompanying microprocessor or process controller, as computers can readily produce numbers, which may have little value if adequate care is not taken to ensure invariant conditions as far as possible, so that the analytical conditions occurring at the time of calibration are also valid where unknown samples are analyzed. Quality control may be subdivided into (i) instrumental quality control which entails the regular analysis of instrumental check standards, also termed mid-range standards (MRS) as well as blank check samples with each batch of samples (EPA, 1982); (ii) Intralaboratory quality control which includes instrumental quality control as well as quality control within a given laboratory through comparison with other methods used in that laboratory and (iii) Interlaboratory quality control, also termed external quality control (Standard Methods (a), 1980), which involves the analysis of aliquots of a given sample by a number of different laboratories and subsequent comparison of results. The Environmental Protection Agency, in their guide for trace element analysis of environmental samples (EPA, 1982) emaphasize the importance of quality control techniques such as serial dilution, recovery of an added spike, comparison with other techniques such as atomic absorption spectrometry and wavelength scanning to detect potential interferences whenever a new or unusual sample matrix is encountered.

In the early days of ICP emission spectrometry, before the technique was well established and widely used, atomic absorption spectrometry was the recognised standard technique for metal analysis of water samples, together with polarographic and colorimetric methods (Standard Methods,* 1975). With improvements in spectrometers to reduce channel cross-talk e.g., by the use of a holographic grating in place of the older ruled grating replica, the ability of spectrometers to reduce stray light problems associated with matrix elements such as calcium and magnesium, with their extremely intense ICP emission lines, was improved (Taylor and Floyd, 1980). Despite such improvements, the statement of Boumans (1974) that it is much easier to obtain correct analytical results with AAS than with most optical emission spectrometric techniques is still valid and interelement interference is a problem which cannot be ignored in ICP spectrometric analysis (Bremmer, 1985). Nevertheless, ICP emission spectrometry has shown itself capable of accurate analysis of environmental samples, as shown for instance through the analysis of standard reference materials such as the National Bureau of Standards (NBS) orchard leaves standard reference material SRM 1571, and bovine liver NBS-SRM 1577 (Dahlquist and Knoll, 1978); geological reference materials such as NBS-SRM 69, USGS 51 and SARM-NIM 65 (Church, 1983; as

---

* Standard Methods for the examination of water and wastewater, published by the American Public Health Association.

well as NBS and Environmental Protection Agency reference water samples (Ronan, undated; Winge et al, 1977). Of great value in assessing the accuracy of ICP spectrometric analysis results in comparison with other analytical techniques are interlaboratory quality control exercises such as those organised by the International Atomic Energy Agency (IAEA) Analytical Quality Control Service in Vienna, as a wide spectrum of techniques is included. As solid samples must be brought into solution prior to ICP spectrometric analysis, such interlaboratory comparison also assists the emission spectroscopist in evaluating the sample preparation technique and identifying any problem elements (Pszonicki et al, 1983a and b).

## 2.14 Environmental sample analysis

Clarity on the nature of the problem for which an analysis is being sought is essential when samples are submitted for analysis. The nature of the problem not only determines the analytical technique, the elements and detection limits required, but also has an influence on the type, number and location of sampling points as well as on the sample preparation procedures used. Thus for example if a water sample is submitted for the determination of copper in domestic water supply, a $2\sigma$ detection limit of around 1 $\mu g.\ell^{-1}$ for the Cu 324,3 nm analytical line on a typical multichannel ICP spectrometer (Larson et al, 1983) is more than adequate for

direct analysis of the water sample, if the question is merely whether the copper concentration lies within the recommended drinking water limit for Cu of 500 $\mu g.\ell^{-1}$ (SABS, 1984). On the other hand, if the question posed is whether the copper concentration in the water may represent a threat to fish aquaculture, then it is necessary to analyze for Cu in the low $\mu g.\ell^{-1}$ range, close to the detection limit of the ICP spectrometric technique for copper, and in addition the pH and alkalinity of the sample should be determined as the copper species present, rather than total copper has a marked effect on the threshold limits for copper toxicity to aquatic life (Train, 1979).

Where solid samples are submitted for analysis, it is even more important to define clearly the aim for which analysis is sought. For example, if a solid sample from a waste dump is submitted, the analyst should find out what the requester's problem is, if an explanation of this is not supplied with the sample. Thus sulphur, for example, may be present in a sample in a variety of species of varying solubility, and if the requester's problem is sulphate pollution by rain washout from the dump then an indication of sulphur species present and their concentrations is of greater relevance than total sulphur determined following complete dissolution of the sample and ICP spectrometric analysis of the resultant solution for sulphur. Use of the selective extraction techniques of soil science in the sample preparation stage allow such questions to be answered (Hesse, 1971).

As the field of environmental sample analysis is a very wide one, involving many interactions in the biosphere, the questions posed in relation to a particular section of the environment may require a multidisciplinary analytical approach in order to clarify the issues (Bruwer et al, 1985). The wide variety of sample materials characteristic of environmental chemistry demands that the objective of the analysis, sampling in the field, and sample preparation should receive as great attention as is applied to the instrumental facet of the analytical process (Hamilton, 1980).

## 2.15 Evaluation of present status

The literature overview provided a summary of various aspects of the theory and analytical application of ICP emission spectrometry. The field covered was rather wide as correct practical analytical use of the technique requires an understanding of many subjects from excitation mechanisms and line broadening with its influence on wing overlap interference as well as the effects of observation height and plasma power on the problems of calibration and interference correction, as well as establishment of detection limits. A critical evaluation of each of these aspects is beyond the scope of this thesis. By way of indicating the present status of the application of ICP emission spectrometry in the analysis of water and related samples, and forming a link between the literature and the experimental work which follows in the succeeding chapters, however, the analytical problem may be summarized as follows:

The problem is the determination of a wide spectrum of metal pollutants at trace concentration levels, i.e. less than 1 $mg.\ell^{-1}$, in the presence of high concentrations of major matrix elements. The successful achievement of this goal requires that the following corollaries must be dealt with:

(i) The analytical technique employed should be sufficiently sensitive to determine the wide range of elements sought, if possible without preconcentration procedures.

(ii) Calibration procedures to provide concentration readout should ideally be simple and invariant to change in sample composition as well as insensitive to small changes in operating parameters, i.e., the calibration should be stable in the interests of high sample throughput, as environmental surveys often require the analysis of a great number of samples.

(iii) The major matrix elements should ideally not interfere in the determination of the trace constituents. If such interferences are present, then they require quantification and correction for accurate analysis.

(iv) The precision and exact detection limit must be known for each element sought in whatever matrix is being analysed, and not only for pure single cation standards.

(v) As decisions following environmental surveys of the presence and extent of metal pollution are often made on elemental analytical data which lie near the limit of detection in the given matrix, elemental identity of toxic trace elements must be established with absolute certainty.

How does the ICP emission spectrometric technique measure up to these requirements?

As far as the first requirement is concerned, i.e., the need for sufficient sensitivity for many elements, the multielement sensitivity of the ICP emission technique with the detection limit for many elements lying in the low $\mu g.\ell^{-1}$ range, together with the simultaneous capability of polychromator type emission spectrometers, provided the main impetus to the application of the technique for environmental sample analysis.

The second corollary, i.e., the ideal of simple, stable calibration procedures, is as far as ICP emission spectrometry is concerned deceptively easily achieved. The near-linearity over several orders of concentration magnitude of intensity readout is strictly valid only when a number of conditions remain invariant viz., (a) sample uptake rate and nebulization efficiency, (b) the concentration of acid preservative used, (c) the plasma excitation conditions at the point of observation, implying invariance of rf input power and gas flow rates, and

(d) linearity of spectrometer/detector response, implying among other factors, that no profile drift occurs. While the ICP emission spectrometric technique shows a far greater linear dynamic range than AAS for example, attention must be given in practical analysis to the four provisos mentioned, as variation in these conditions is often found. The use of a peristaltic pump to control sample uptake rate to the nebulizer, while minimizing the effects of viscosity differences, does not eliminate the effects of matrix variation. As will be shown in Chapter 3, residual matrix effects e.g., in the case of change in acid preservative concentration remain, which show a correlation with excitation potential. A degree of matrix matching is thus required. Invariance of sample uptake rate is not only important as regards the delivery of a constant quantity of analyte to the plasma, but also as regards the effects of the solvent (usually water) on excitation temperatures and on degree of ionization as will be shown in Chapter 4. The importance of stabilizing the mains voltage supply to the rf generator as well as maintaining a constant inner (aerosol) gas flow rate to the plasma will also be shown. The use of internal standardization through ratioing of analyte intensities to that of an added internal standard, while classically used to minimize the detrimental effects of variation in calibration slope, is of little use where element specific changes occur. Establishment of the manner in which specific analyte elements respond to change in operating parameters may allow the development of empirical correction techniques as will be demonstrated in Chapters 4 and 5. An

aspect of the calibration procedure which requires attention in the sequential analysis of a set of samples on either a polychromator or monochromator type instrument is that of establishing the character of the memory within the system following aspiration of a sample containing a high concentration of a given analyte. As memory results in carry over of signal to the next sample, correction must either be done mathematically, or else sufficient time must be allowed for the signal to decay to an acceptable value before the next sample is measured. The memory effect as well as the related questions of establishment of blank intensity and blank drift will be discussed in Chapter 5.

As far as the third corollary is concerned, i.e. the ideal that matrix elements should not interfere in the determination of trace elements, the ICP emission technique fares poorly, and the problem of interelement spectral overlap interferences remains one of the major difficulties in the analytical application of the technique. The very rich line spectra emitted by an ICP source imply that interelement interference is almost inevitable, and that correction procedures must be employed for the interference of many major matrix elements on the trace metal determinands. While the use of high resolution spectrometers is essential, and does somewhat ameliorate the problem of line overlap interference, it does not provide a complete solution, as the emission lines have a significant width as a consequence of the various broadening processes

within the ICP source. The software approach for interelement interference correction which is commonly employed on polychromator instruments is critically dependent on the maintenance of constant relative emission intensity ratios between element pairs as well as on the reproducibility of exact profile setting. The determination of the interelement interference correction coefficients is discussed in Chapter 5. In the case of sequential monochromator type spectormeters the interference problem may be dealt with by off-peak background correction. Structured backgrounds create problems, however, as the background intensity at the analytical line wavelength may not necessarily be readily related to the background at offset profile positions.

The fourth corollary i.e., the need to know the analyte detection limits in the sample types being analyzed, is closely allied with the third corollary. This is because the detection limit deteriorates when interference corrections are made as a consequence of the uncertainty present in the exact quantitation of the extent of a given interference on a given analyte channel. While detection limit is relatively easily estimated in real samples in the absence of significant interference, this is not the case where interference is present. The use of profile scans to detect wing overlap interferences is well known, but the use of profile scans for quantitative measurement is less developed than the customary integration at line centre. A discussion on the various means

of estimating precision and detection limit where the profile scan mode is used for quantitative analysis is given in Chapter 6. The fifth corollary i.e., the need for certainty of element identity at trace concentration levels arises out of the fact that interferences become progressively more important as the concentration level sought is decreased, as well as from the danger that unidentified interferences my be present which have not been considered in the calibration of the ICP spectrometer. Element identity may be confirmed by demonstation of the presence of more that one of the characteristic analytical wavelengths of a given element, as well as by confirmation using other analytical methods.

In conclusion, the successful analytical use of ICP emission spectrometry in environmental sample analysis depends on (a) the invariance of the calibration between standards and samples, failing which it becomes necessary to use suitable internal standardization procedures; (b) the identification and quantification of all significant interelement interferences and correction for such interferences; and (c) the establishment of the detection limit in the real sample matrix. It also follows that whatever procedures will assist in assuring invariant conditions of analytical and instrumental parameters will enhance the precision and accuracy of the analytical results produced.

# CHAPTER 3: SAMPLING AND SAMPLE PREPARATION

## 3.1 Introduction

The subjects of sample collection and preparation of samples for analysis, by for instance the ICP emission spectrometric technique, are of formidable dimensions especially in the field of environmental chemistry, as a consequence of the variety of sample matrices encountered as well as the oft present heterogeneity in concentration both in space and in time. This heterogeneity is of particular relevance in the water environment. If a typical sample of raw water from a water source such as the Vaal River is considered, for instance, it is muddy in appearance, and obviously contains not only liquid water, but suspended material as well. In solution, in the liquid phase, are present a variety of inorganic as well as organic chemicals and complexes; while the suspended solid material is equally diverse on closer inspection, containing clay particles as well as microscopic biological material such as algae, zooplankton and bacteria (Bruwer et al, 1985). While water, in itself, presents a problem in sampling, preservation and preparation to the analyst, the hydrologist's field of interest is of necessity inclusive of the materials with which water comes into contact, either naturally or as a consequence of man-made pollution. The scope of sample types thus encompasses sediments, sludge and waste-dump materials, plant material

and fish material, as well as the atmospheric, surface and ground water phases per se. The vastness of the subject prohibits all but a brief overview of aspects which are of particular relevance to the determination of metals in environmental samples by ICP emission spectrometry. This chapter will firstly describe briefly the requirements of sampling and preservation, secondly the goals in sample pretreatment; for when the aim is defined, a necessary pretreatment may be devised for almost any sample type, given time, expertise and equipment. Lastly the effect of certain matrix types on analyte emission intensity will be demonstrated, thereby illustrating the need for a degree of matrix matching in the preparation procedures. Finally, a brief mention of contamination and the reverse problem of loss of analyte will be made.

## 3.2 Sampling and preservation

The aim of sampling is firstly to collect representative aliquots or samples from the medium that the analyst wishes to quantify in chemical analytical terms, and secondly, to treat the samples in such a way that the change in sample composition, in the interval between sample collection and analysis, is kept to a minimum in respect of the analytes to be quantified.

The requirement of representativeness requires a knowledge of the temporal and spatial variability of the analyte concentration. Where this is not known, it is customary to collect a series of samples at different points or times. If the goal is merely assuring representativeness and not studying the temporal and spatial variation, samples may be composited to lower the work load on the analytical service (Standard Methods (b), 1980). Representativeness is not limited to chemical characterization, however, and a knowledge of the physical conditions pertaining to the sampling site is also helpful. Thus for a sampling site in a river close to a point of pollution; whether direct e.g., from an effluent point source, or indirect via a diffuse source of pollution e.g., where a smoke stack adjacent to a river releases particulates which may fall onto the water surface; the siting of the point may materially influence the results obtained, due to the concentration gradients occurring near sources of pollution. If the goal of sampling is establishing long term trends or background quality, then sampling sites should where possible be selected at points far removed from sources of pollution (NHRMWDA,* 1977). In the case of river water samples, selection of a sampling site just below a weir serves

---

* NHRMWDA = National handbook of recommended methods for water-data acquisition, U.S. Dept., of the interior, Reston, Virginia (1977).

two purposes: viz., (i) Flow data may be obtained simultaneously, which enables loads to be calculated, and (ii) the turbulence created by water flowing over the weir serves to mix the water and so ensures a greater degree of homogeneity. While sampling at sites where related flow data may be obtained, represents an ideal, the dynamics of water quality variability often requires sampling points at additional sites, especially where sources of possible pollution must be evaluated (Bruwer et al, 1985). The obtaining of representative samples of the bottom sediments using either grab-type samplers or corer-type samplers presents a problem not readily overcome, as a consequence of the ease with which the solid liquid interface is disturbed in the sampling process (NHRMWDA, 1977).

The type of sampling procedures for trace metal analysis used in a typical riverine water quality survey are as follows (Bruwer et al, 1985):

(a) Water samples:

Grab, hosepipe integrated depth samples, or depth samples collected with a depth sampling bottle consisting of plastic materials are subsampled into:

(i) A subsample for dissolved metals, which is filtered through a 0,45 µm membrane filter into a 335 mℓ* high density polyethylene bottle, with a polyethylene cap with no liner. The first 20 mℓ of sample filtered is discarded. Immediately after filtration the sample is preserved with 3 mℓ redistilled nitric acid, which has been sealed in the laboratory into small pre-cleaned glass ampoules for field use. The sample bottle likewise has been pre-cleaned in the laboratory by soaking in hydrochloric acid volume fraction 0,05 for 24 h and rinsed 4x with distilled-deionised water. The nitric acid preservative serves to decrease the pH-value of the water to less than 2, and thus discourage adsorption/ hydrolysis of metals. Analyte material passing through a 0,45 µm pore-size membrane filter is by convention termed the dissolved material (NHRMWDA, 1977). The use of concentrated acid,

---

* In terms of a decision made by the SABS, following a note from the International Standards Organization, the usage mℓ and ℓ is allowed for $cm^3$ and $dm^3$ respectively in the water and environmental analysis field.

usually nitric, as preservative for water samples collected for trace metal analysis is also customary (Standard Methods, (c),1980). While the use of lowered pH as a means of preserving a water sample for trace metal analysis is widely used, it is not without its drawbacks. The common presence of natural organic complexing agents such as humic acids, particularly in coloured waters (Christman and Ghassemi, 1966), together with the tendency for part of the organic material to precipitate at acidic pH values (Black et al, 1963) may result in co-precipitation of trace metals on acidification. A similar phenomenon may occur in some waters containing high dissolved silica concentrations, for as much as 40% of the dissolved silica in surface waters may be in polymeric form or in association with dissolved organic matter, and may likewise show change on acidification.

A separate subsample of the 0,45 µm filtered sample to which suprapur sulphuric acid has been added to give a volume fraction $\phi_{H_2SO_4}$ of 0,01 is collected for mercury analysis.

(ii) An unfiltered water sample to which nitric acid has been added at the same concentration ratio as for the dissolved metals sample i.e., $\phi$ = 0,01. The added acid serves to dissolve some of the metals adsorbed on the particulate fraction. Where an unfiltered and acid preserved sample is subsequently treated in the laboratory with some acid-digestion or acid-oxidation-digestion procedure, the analyte concentrations obtained on analysis are refered to as "total recoverable" concentrations (NHRMWDA, 1977). The total recoverable concentrations represent only part of the true total analyte concentrations.

(iii) An unfiltered water sample to which mercury (II) chloride is added to give a mercury concentration of 20 $mg.\ell^{-1}$ Hg(II). The mercury (II) ion serves to stop biological activity in the sample. The mercury- preserved sample is used for analysis of nutrients and major ions, and as these analyses are mostly done by non-emission techniques e.g., by colorimetry, they will not be discussed further. The very fact of the use of high concentrations of mercury to preserve samples

for major ion analyses, poses extreme risk of contamination of samples collected for mercury analysis *per se*. In order to detect contamination, the mercury (II) chloride solution used for preserving the samples for major ion analyses is spiked in the laboratory with lanthanum (III) chloride to give a mass ratio of Hg:La of 15:1. Whenever any sample for mercury analysis shows the presence of high mercury concentrations, the sample is screened for the presence of lanthanum by ICP emission spectrometry. In this way any samples inadvertently contaminated with mercury at the time of sampling may be detected.

(b) Sediment samples

River or reservoir bottom sediments are normally collected with an Eckman grab-sampler, placed in 500 mℓ glass bottles with teflon lined caps and frozen on site (Bruwer *et al*, 1985).

(c) Macrophyte samples

Samples of aquatic macrophytes are subdivided on site, in the case of floating macrophytes, into the aerial (leaf) and submerged (root) portions, washed with

distilled water, placed in plastic bags and frozen on site (Bruwer et al, 1985). It is important to attempt to dislodge sediment particles from the submerged portions of an aquatic plant at the time of sampling.

(d) Fish samples

Freshly netted fish are gutted, cleaned, wrapped in aluminium foil and frozen immediately on site (Bruwer et al, 1985). Ungutted fish decay extremely rapidly after death, which renders fish tissue analyses futile unless samples are absolutely fresh and frozen immediately on collection. This makes fish sample analyses e.g., in the case of a fish-kill difficult unless fresh material can be obtained.

Apart from these samples, the environmental chemist may be called upon to analyze a variety of sludge or waste-dump materials. Here sampling must be approached on an ad-hoc basis, bearing the basic requirements of sampling in mind i.e., representativeness and minimum change between sampling and laboratory analysis. This may, for instance, require exclusion of oxygen where oxidizable materials such as sulphide bearing substances are sampled.

## 3.3 Acidification induced changes in water samples

As mentioned in Section 3.2, despite the fact that acidification of 0,45 µm membrane filtered water samples with $\phi_{HNO_3}$ = 0,01 nitric acid is a widely used procedure (NHRWDA, 1977; Standard Methods, (c), 1980) it is not without its effects on the concentrations of metal analytes in solution, and while hydrolosis is minimized, change in analyte concentration may occur. The problem may be illustrated by the following experiment:

A one litre sample of tap water, originating from the Hydrological Research Institute's borehole, was filtered twice through 0,45 µm membrane filters (Millipore type HAWP-047, mixed cellulose acetate/nitrate), which had been precleaned with $\phi_{HNO_3}$ = 0,05 redistilled nitric acid and rinsed with distilled-deionised water. The filtered sample was divided into two aliquots, one of which was left unpreserved (u), and the second of which was preserved (p) with $\phi_{HNO_3}$ = 0,01 redistilled nitric acid. The pH value as determined by a glass electrode, was 6,6 for the unpreserved aliquot and 1,2 for the nitric acid preserved aliquot. Five replicates of each of these two treatments, u and p, were analyzed immediately on a 34000 ARL ICP polychromator which had been calibrated for multielement analysis (Chapter 5), the unpreserved aliquot being analyzed first. Distilled-deionised water was used for

blank subtraction in the case of the unpreserved aliquot, and $\phi_{HNO_3}$ = 0,01 redistilled nitric acid in distilled-deionised water for subtraction in the case of the acid preserved aliquot. As both aliquots had been identically treated apart from the presence of nitric acid preservative in the second aliquot, differences found may be ascribed to the effects of preservation or non-preservation, assuming no significant acid matrix effect difference between deionized water and $\phi$ = 0,01 nitric acid.

The concentration differences of the means of the five replicates of each treatment were compared using a two-tailed Student-t type test, where allowance had been made for possibly unequal variance between the two data sets by calculating a weighted degrees of freedom (V) as follows (Green and Margerison, (b), 1978);

$$V = \left( \frac{1}{V_1} \left( \frac{\sigma_1^2/n_1}{(\sigma_1^2/n_1 + \sigma_2^2/n_2)} \right)^2 + \frac{1}{V_2} \left( \frac{\sigma_2^2/n_2}{(\sigma_1^2/n_1 + \sigma_2^2/n_2)} \right)^2 \right)^{-1} \quad \ldots\ldots\ldots \quad (32)$$

where $V$ = weighted degrees of freedom,

$n_1$ = no's of data points in group 1,

$\sigma_1$ = standard deviation of group 1,

$V_1$ = degrees of freedom of group 1, i.e., $(n_1-1)$,

$n_2$ = no's of data points in group 2,

$\sigma_2$ = standard deviation of group 2,

and $V_2$ = degrees of freedom of group 2, i.e., $(n_2-1)$.

The Student-t value being calculated as:

$$t = (\bar{C}_1 - \bar{C}_2) \cdot (\sigma_1^2/n_1 + \sigma_2^2/n_2)^{-\frac{1}{2}} \quad \ldots\ldots\ldots \quad (33)$$

where $\bar{C}_1$ = mean concentration of group 1,

$\bar{C}_2$ = mean concentration of group 2,

and the $\sigma$ and $n$ terms are as defined for equation 32 above.

The null hypothesis being;

$$H_0 : C_1 - C_2 = 0$$

and the alternative hypothesis being;

$H_1 : C_1 - C_2 \neq 0$

where $C_1$ and $C_2$ are the corresponding population means as opposed to the sample means $\overline{C}_1$ and $\overline{C}_2$.

$H_0$ was rejected where:

$|t| \geq t_{critical}$

where $t_{critical} = t_V(1-\alpha/2)$,

V being the weighted degrees of freedom and $\alpha$ the level of significance adopted (Green and Margerison, (b), 1978). As V was often non-integral, the $t_{critical}$ value corresponding to the integral portion of V in tables of the t distribution was used (Netter and Wasserman, (a), 1974). An $\alpha$ value of 1% was adopted for this comparison, i.e., the probability of falsely rejecting the null hypothesis is 0,01.

The results on the comparison of differences in analyte concentration between unpreserved (u) and $\phi$ = 0,01 nitric acid preserved (p) treatment of a tap water sample are shown in Table 3-1. The number of figures reported for mean concentration ($\overline{C}$) and standard deviation ($\sigma$) are greater than is customary. This was done in order to

TABLE 3-1: Difference in analyte concentration ($mg.\ell^{-1}$) readout for 0,45 µm twice filtered tap water for unpreserved (u) and $\phi$ = 0,01 nitric acid preserved (p) aliquots, as evaluated by a Student-t test with weighted degrees of freedom, for 5 replicate analyses (each the mean of 3 x 10 s integrations) on the two treatments, u and p.@

| | Al | | B | | Ba | | Ca | | Cr | |
|---|---|---|---|---|---|---|---|---|---|---|
| | u | p | u | p | u | p | u | p | u | p |
| | 0,166 | 0,098 | 0,088 | 0,072 | 0,046 | 0,045 | 39,1 | 39,0 | 0,013 | 0,011 |
| | 0,209 | 0,101 | 0,093 | 0,072 | 0,048 | 0,044 | 39,3 | 38,6 | 0,017 | 0,013 |
| | 0,152 | 0,102 | 0,095 | 0,072 | 0,049 | 0,044 | 39,5 | 38,4 | 0,017 | 0,013 |
| | 0,164 | 0,125 | 0,090 | 0,074 | 0,048 | 0,044 | 39,3 | 38,4 | 0,017 | 0,012 |
| | 0,166 | 0,106 | 0,090 | 0,074 | 0,048 | 0,044 | 39,1 | 38,7 | 0,012 | 0,018 |
| $\overline{C}$ | 0,1714 | 0,1064 | 0,0912 | 0,0728 | 0,0478 | 0,0442 | 39,26 | 38,62 | 0,0152 | 0,0134 |
| $\sigma$ | 2,18E-2 | 1,08E-2 | 2,78E-3 | 1,10E-3 | 1,1E-3 | 4,5E-4 | 1,67E-1 | 2,49E-1 | 2,49E-3 | 2,70E-3 |
| V | 5,8 | | 5,2 | | 5,3 | | 7,0 | | 7,9 | |
| t | 5,97* | | 13,8* | | 6,80* | | 4,77* | | 1,09 | |
| $t_{crit}$ | 4,03 | | 4,03 | | 4,03 | | 3,50 | | 3,50 | |

@: $\overline{C}$ = mean concentration; $\sigma$ = std., deviation; V = weighted degrees of freedom; t = calculated Student-t value; and $t_{crit}$ = critical t value for 1% significance (two-tailed) at the integral portion of V. For $10^{-n}$ the symbolism E-n is used.

*: significant at 1% level.

TABLE 3-1 (continued)

| | Cu | | Fe | | Mg | | Mn | | Si | |
|---|---|---|---|---|---|---|---|---|---|---|
| | u | p | u | p | u | p | u | p | u | p |
| | 0,019 | 0,036 | 0,051 | 0,006 | 13,03 | 12,72 | 0,071 | 0,066 | 53,0 | 61,4 |
| | 0,018 | 0,042 | 0,055 | 0,011 | 13,02 | 12,71 | 0,070 | 0,067 | 50,5 | 59,8 |
| | 0,022 | 0,035 | 0,046 | 0,012 | 12,97 | 12,65 | 0,070 | 0,065 | 51,1 | 58,7 |
| | 0,024 | 0,037 | 0,042 | 0,014 | 12,98 | 12,67 | 0,070 | 0,067 | 57,0 | 58,4 |
| | 0,024 | 0,037 | 0,050 | 0,024 | 12,99 | 12,70 | 0,069 | 0,067 | 58,5 | 55,8 |
| $\overline{C}$ | 0,0214 | 0,0374 | 0,0488 | 0,0134 | 12,998 | 12,690 | 0,070 | 0,0664 | 54,0 | 58,8 |
| $\sigma$ | 2,79E-3 | 2,70E-3 | 4,97E-3 | 6,62E-3 | 2,59E-2 | 2,92E-2 | 7,1E-4 | 8,94E-4 | 3,57 | 2,06 |
| V | 8,0 | | 7,4 | | 7,9 | | 7,6 | | 6,4 | |
| t | -9,22* | | 9,56* | | 17,7* | | 7,06* | | -2,60 | |
| $t_{crit}$ | 3,36 | | 3,50 | | 3,50 | | 3,50 | | 3,71 | |

*significant at 1% level.

TABLE 3-1 (continued)

| | Sr | | Zn | |
|---|---|---|---|---|
| | u | p | u | p |
| | 2,711 | 2,661 | 1,002 | 1,124 |
| | 2,706 | 2,650 | 1,190 | 1,198 |
| | 2,703 | 2,631 | 1,211 | 1,111 |
| | 2,695 | 2,641 | 1,212 | 1,109 |
| | 2,694 | 2,647 | 1,193 | 1,114 |
| $\bar{C}$ | 2,702 | 2,646 | 1,162 | 1,131 |
| $\sigma$ | 7,26E-3 | 1,11E-2 | 8,98E-2 | 3,78E-2 |
| V | 6,9 | | 5,4 | |
| t | 9,41* | | 0,71 | |
| $t_{crit}$ | 3,71 | | 4,03 | |

*significant at 1% level.

prevent propagation of rounding-off errors in the calculation of the weighted degrees of freedom (V) and Student-t value (t). Table 3-1 clearly shows that acid preservation significantly altered the concentration readout for Al, B, Ba, Ca, Cu, Fe, Mg, Mn and Sr for this particular sample, the null hypothesis that the differences are due to chance being rejected with 99% certainty for the 1% level of significance for the two-tailed test-employed. The preserved values were less than the unpreserved values for Al, B, Ba, Ca, Fe, Mg, Mn and Sr. The analyte concentrations of Cr, Si and Zn were not altered significantly. While it can be argued that the observed concentration differences between the two treatments u and p may be due to an acid effect within the ICP source, this is unlikely in view of the absence of an observed difference in zinc readout between the two treatments. As will be shown in Section 3.5, zinc usually shows the acid matrix effect to a greater degree than Cu for instance. The use of blank subtraction with deionized water/nitric acid ($\phi$ = 0,01) blanks for the u/p treated aliquots respectively also argues for true analyte concentration differences.

While in the example given the precision between the two treatments u and p, as reflected in the std., deviation values, are similar, and the more usual form of the t-test with $n_1 + n_2 - 2$ degrees of freedom and pooled variance may have been used, the more general form for comparison of

means with unknown, unequal variance, known as a Fisher-Behrens type problem (Green and Margerison, (b), 1978) is given. The differences found in analyte concentration on acidification will obviously depend on the type of water sample. The acidification change in analyte readout for a clear, uncoloured sample as illustrated, are relatively minor. For coloured samples containing colloidal material, a visible flocculation is on occassion observed, and greater differences may be expected.

Despite the changes in sample composition that may result from acidification, the prevention of losses by adsorption onto container surfaces when there is a time delay between sampling and analysis is essential. The fact that the analyst determines what analyte concentrations are in solution in the acidified sample as received by the laboratory rather than in the original state in the water body must not be forgotten.

## 3.4 Goals of sample pretreatment

The primary aim of sample pretreatment is to ensure that the sample is in aqueous solution, with ideally no solid particles present. This in practice amounts to the absence of suspended particles of diameter greater than 0,45 µm, i.e., the pore size of membrane filters usually employed to filter aqueous environmental samples for analysis (EPA, 1982). A corollary to the requirement of a liquid

sample-form where nebulization is the means of sample introduction is, naturally, that solids must be dissolved prior to analysis using for example appropriate wet or dry oxidation procedures in the case of biological materials, and often fusion techniques in the case of inorganic solids such as silicate based minerals. The spectrum of available sample dissolution methods is legion (Bock, 1979).

Before deciding on a given solid decomposition technique, the analyst must have a clear picture of the purpose for which the analysis on a solid sample is being performed. Thus, is a total dissolution technqiue called for, or a partial dissolution technique; and is the total sample or a certain particle size fraction to be analyzed? Thus the analysis of a riverine sediment may involve chemical characterisation by carrying out a series of dissolution/-extraction procedures ranging from relatively mild treatments such as sodium acetate extracts, weak acid extracts or complexing agent extracts, to concentrated acid digestions; with or without prior physical separation into different particle size fractions (De Groot et al, 1982). The enrichment of pollutant metals in the sediment fines e.g., in the clay particle fraction (Förstner et al, 1979) provides a sensitive indicator of pollution where the clay particle fraction is selectively analyzed e.g., in riverine surveys (Bruwer et al, 1985).

In the studying of pollution by leaching from industrial waste dumps, the use of a variety of extraction and dissolution procedures provides an indication of the potential hazard to the water environment. Thus a deionized water extract will provide an indication of immediate leaching by rain water, while weak acid extracts may provide an indication of the short term pollution possibilities. Strong acid/oxidizing acid digests e.g., with aqua regia or mixtures containing perchloric acid, provide data on the total available metals. The residue which is only soluble e.g., in fusion techniques, is not normally of interest in pollution *per se*, but may be of vital importance where baseline values of trace metals in environmental studies are needed.

Fractionation-extraction methods are usually based on the principle of successive attack on lithological fractions from, "the most mobile to those strongly bound to the support mineral" (Boust and Saas, 1981) and a variety of extractants are available to dissolve specific phases such as the carbonate phase, reducible phase and organic and sulphide phases (Förstner *et al*, 1981).

Biological samples such as fish tissue or plant samples are usually decomposed by wet ashing techniques such as nitric/perchloric acid digestion e.g., in the case of fish

tissue or dry ashing techniques e.g., for plant samples. Dry ashing has the disadvantage, however that volatile elements may be lost (Iyengar and Sansoni, 1980).

In the use of dissolution procedures to dissolve solid samples the aim should be to have the final analysis solution in a similar matrix to that used for the calibration standards so as thereby to minimize the possibility of matrix effects on calibration sensitivity. The total cation concentration should not exceed 3400 $mg.\ell^{-1}$ if transport problems are to be avoided especially if a peristaltic pump has not been used to keep sample uptake rate invariant (Butler et al, 1980).

In any pretreatment procedure, whether for a water or solid sample, the limitation of contamination especially where trace concentration levels are being analyzed is absolutely essential. In addition to the provision of a clean, dust-free laboratory environment, this entails an awareness of contamination possibilities at each step in the preparation procedure from all reagents used as well as all materials and containers with which the sample comes into contact (Hamilton, 1980). Membrane filters should be prewashed, either with deionised water, a sample aliquot, or with dilute acid (Wallace et al, 1977). Sample containers and all laboratory glassware used in trace metal analysis should be cleaned with an appropriate acid followed by several rinses with distilled-deionised water.

For water blanks in trace metal analysis, high purity water is required, prepared for instance by distillation followed by passage through a Millipore Milli-Q deionizing system giving water with resistivity >18 $M\Omega.cm^{-1}$. As non-charged species do not contribute to the conductivity, however, leak-through of colloids or organically bound metals may occur without a decrease in resistivity (Knott, 1975). The activated carbon column should therefore at least be replaced at the same time as ion exchange columns.

Where a metal analyte's concentration in a sample lies below the detection limit, and a more sensitive emission line than the one currently in use for the given element is not available, then the analyst is faced with two possible alternatives viz., (i) use of an enrichment procedure in the sample preparation stage prior to introduction of the sample into the ICP source, or (ii) analysis of the sample by a more sensitive analytical technique, such as for instance graphite furnace atomic absorption spectrometry (GFAAS). In the case of water samples, enrichment techniques designed for AAS such as ion exchange resin preconcentration (Kempster and Van Vliet, 1978), or chelation and liquid-liquid extraction (Watling and Watling, 1976) may be relatively easily adapted for use in ICP spectrometric analysis. While evaporative preconcentration may be used for enrichment of fresh water samples for ICP spectrometry (Thompson et al, 1982), this is not suitable for saline samples. Berman et al (1980)

used Chelex-100 resin for extracting trace metals from sea water, but found difficulties in achieving complete recovery, and suggested that carrier precipitation may provide a solution for sea water. Complexation followed by extraction into an organic solvent such as methyl-isobutyl-ketone (MIBK) with direct aspiration into the ICP source may also be used, however, reduction of intensities of ion-lines when MIBK is aspirated has been reported (Motooka et al, 1979).

The goals of sample pretreatment for pneumatic nebulization may be summarized as:

(i) The sample should be in homogenous liquid, ideally water, solution with no particles of greater diameter than 0,45 µm.

(ii) The sample solution for most elements should be acidic to prevent hydrolysis. Acid matrices of samples, blanks and standards should be approximately matched to avoid matrix changes in sensitivity.

(iii) Total cation concentration should not exceed approximately 3400 $mg.\ell^{-1}$. Where this does occur, then dilution or selective extraction may be required.

(iv) Where the analyte concentration is below the limit of detection then either a more sensitive technique is called for, or an enrichment technique may be used.

(v) In the choice of an enrichment technique, the possibility of contamination with each step should be considered. The number of sample manipulations should be kept to a minimum.

(vi) In the choice of pretreatment techniques, particularly for solid samples, the analytical goal must be clearly defined i.e., is a total digestion called for, or a selective or partial extraction?

## 3.5 The acid matrix effect

Dahlquist and Knoll (1978) clearly demonstrated the analyte signal suppression which occurs, particularly in sulphuric acid matrices as a result of viscosity effects. The use of forced sample introduction by means of a peristaltic pump may overcome viscosity induced changes in aspiration rate, but does not, however, solve the changes in nebulization efficiency or plasma excitation changes consequent to varying acid volume fractions as demonstrated by the following experiment:

The effect of acid strengths with volume fraction between 0,01 and 0,10 of nitric, sulphuric and hydrochloric acids on Fe, Mn, Cu, Zn and Cr analyte emission was studied by preparing standards containing these five elements in acid matrices of varying concentration. These standards were then analyzed on a 34000 ARL ICP polychromator under compromise analytical conditions. The recovery of $\phi$ = 0,01 nitric acid was taken as 100% and all recoveries were normalized to this matrix, as it constituted the calibration matrix used for the spectrometer. Aspiration was forced by means of a Gilson Minipuls II peristaltic pump. Aspiration rate was measured by means of a 10 mℓ measuring cylinder and a stop-watch, by recording the time needed to aspirate 3,0 mℓ of each respective acid/volume fraction. The aspiration rate was found in all cases to be in the range 1,21 to 1,25 $m\ell.min^{-1}$ i.e., a variation of less than 4% for all three acids (nitric, sulphuric and hydrochloric) over the volume fraction range of 0,01 to 0,10. The nebulizer employed was a Meinhard concentric glass nebulizer. The analytical emission lines used are shown in Table 3-2. Redistilled (Quartz and Silice subboiling distillation) nitric acid, Aristar hydrochloric acid and Analar sulphuric acid were used for preparing the acid matrices. The analyte concentrations employed were Fe 210 $mg.\ell^{-1}$; Mn 110 $mg.\ell^{-1}$; Cu 10,0 $mg.\ell^{-1}$; Zn 10,0 $mg.\ell^{-1}$ and Cr 10,0 $mg.\ell^{-1}$. Titrisol standards were used for preparing 1 000 $mg.\ell^{-1}$ stock solutions. On analysis of the prepared standards, blank solutions were run to check for change in blank emission intensity.

TABLE 3-2: Analytical wavelengths, λ, of Fe, Mn, Cu, Zn and Cr used for studying the acid matrix effect on the 34000 ARL ICP polychromator, together with excitation potentials ($V_{exc}$) corresponding to the emission lines.

| Element* | λ/nm | $V_{exc}$/eV** |
|---|---|---|
| Fe (II) | 259,940 | 4,77 |
| Mn (II) | 257,610 | 4,81 |
| Cu (I) | 327,396 | 3,78 |
| Zn (I) | 213,856 | 5,80 |
| Cr (II) | 267,719 | 6,18 |

*(I) = atom line of element, and (II) = ion line.
**Zaidel' et al (1970).

TABLE 3-3: Percentage recovery of Fe, Mn, Cu, Zn and Cr in nitric acid matrix, with respect to the $\phi$ = 0,01 nitric acid calibration matrix taken as 100% recovery. Analyses carried out on a 34000 ARL ICP polychromator under compromise analytical conditions using forced sample aspiration at 1,2 mℓ.min$^{-1}$.

| $\phi_{HNO_3}$ x 100 | Percentage recovery of analyte elements | | | | |
|---|---|---|---|---|---|
| | Fe | Mn | Cu | Zn | Cr |
| 2,5 | 99,6 | 99,8 | 99,5 | 98,1 | 99,9 |
| 5,0 | 95,6 | 96,5 | 98,4 | 94,0 | 95,6 |
| 7,5 | 95,5 | 96,2 | 98,1 | 92,4 | 95,5 |
| 10,0 | 91,0 | 92,2 | 97,2 | 88,1 | 90,1 |
| *Drift in calibration: | -0,3 | -0,3 | +0,3 | -0,9 | -1,3 |

*The drift in the calibration is expressed as the % change in calibration sensitivity as measured by a control standard in the $\phi$ = 0,01 nitric acid matrix run before and after the sample plate.

TABLE 3-4: Percentage recovery of Fe, Mn, Cu, Zn and Cr in sulphuric acid matrix, with respect to the $\phi$ = 0,01 nitric acid calibration matrix taken as 100% recovery. Analyses carried out on a 34000 ARL ICP polychromator under compromise analytical conditions using forced sample aspiration at 1,2 mℓ.min$^{-1}$.

| $\phi_{H_2SO_4}$ x 100 | Percentage recovery of analyte elements | | | | |
|---|---|---|---|---|---|
| | Fe | Mn | Cu | Zn | Cr |
| 1,0 | 92,7 | 93,3 | 97,2 | 92,0 | 90,2 |
| 2,5 | 91,3 | 92,1 | 95,3 | 87,3 | 89,1 |
| 5,0 | 86,0 | 87,8 | 93,4 | 80,4 | 83,9 |
| 7,5 | 82,7 | 84,5 | 92,3 | 76,1 | 80,8 |
| 10,0 | 79,6 | 81,8 | 91,4 | 72,6 | 78,4 |
| *Drift in calibration: | -4,0 | -3,5 | -0,1 | -2,7 | -4,6 |

*The drift in the calibration is expressed as the % change in calibration sensitivity as measured by a control standard in the $\phi$ = 0,01 nitric and matrix run before and after the sulphuric acid matrix samples.

TABLE 3-5: Percentage recovery of Fe, Mn, Cu, Zn and Cr in hydrochloric acid matrix, with respect to the $\phi$ = 0,01 nitric acid calibration matrix taken as 100% recovery. Analyses carried out on a 34000 ARL ICP polychromator under compromise analytical conditions using forced sample aspiration at 1,2 mℓ.min$^{-1}$.

| $\phi_{HCl}$ x 100 | Percentage recovery of analyte elements | | | | |
|---|---|---|---|---|---|
| | Fe | Mn | Cu | Zn | Cr |
| 1,0 | 98,2 | 99,1 | 99,7 | 100,4 | 98,7 |
| 2,5 | 100,4 | 100,9 | 99,5 | 100,9 | 101,0 |
| 5,0 | 101,1 | 101,4 | 99,5 | 100,6 | 101,1 |
| 7,5 | 99,3 | 100,6 | 98,8 | 99,9 | 100,5 |
| 10,0 | 100,1 | 101,8 | 98,4 | 100,8 | 102,6 |
| *Drift in calibration: | +1,2 | +1,4 | -0,1 | +0,3 | +1,6 |

*The drift in the calibration is expressed as the % change in calibration sensitivity as measured by a control standard in the $\phi$ = 0,01 nitric acid matrix run before and after the hydrochloric acid matrix samples.

The recoveries obtained are shown in Tables 3-3 to 3-5, with the results presented graphically for the nitric acid effect in Figure 3-1 and for the sulphuric acid effect in Figure 3-2. Three 10 s integrations were read on each standard, and precision was ≤1% RSD with the exception of Cr in the hydrochloric acid matrix, where RSD values of around 1,1 % were obtained.

The drift in calibration sensitivity was determined by analyzing a mixed control standard containing the five elements in ϕ = 0,01 nitric acid before and after each set of standards. As calibration drift may not necessarily be linear, the results have not been corrected for calibration drift. The drift for each analyte element has been reported in the tabulated data (Tables 3-3 to 3-5). A perusal of these tables and Figures 3-1 and 3-2 shows the following:

(a) Sulphuric acid showed the greatest matrix effect on analyte emission intensity, and hydrochloric acid the least effect.

(b) In both sulphuric and nitric acids the least suppression is shown for Cu (I) 327,396 nm emission and the greatest suppression for Zn (I) 213,856 nm emission. The recoveries of Cu and Zn were 91,4% and 72,6% respectively in a ϕ = 0,10 sulphuric acid matrix; and 97,2% and 88,1% respectively in a

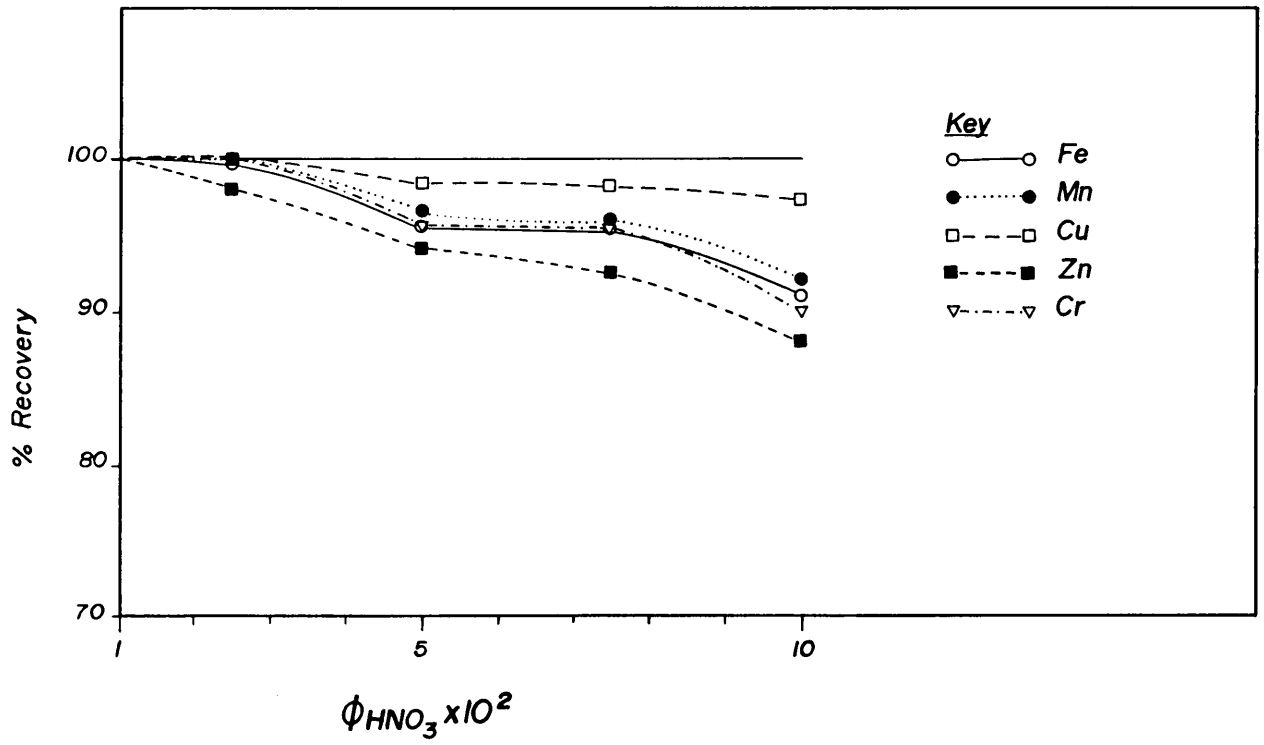


**Figure 3-1:** The nitric acid matrix effect showing suppression of recovery with respect to the $\phi$ = 0,01 nitric acid calibration matrix at 1,2 $m\ell.min^{-1}$ aspiration rate on the 34000 ICP polychromator. Data plotted from Table 3-3.

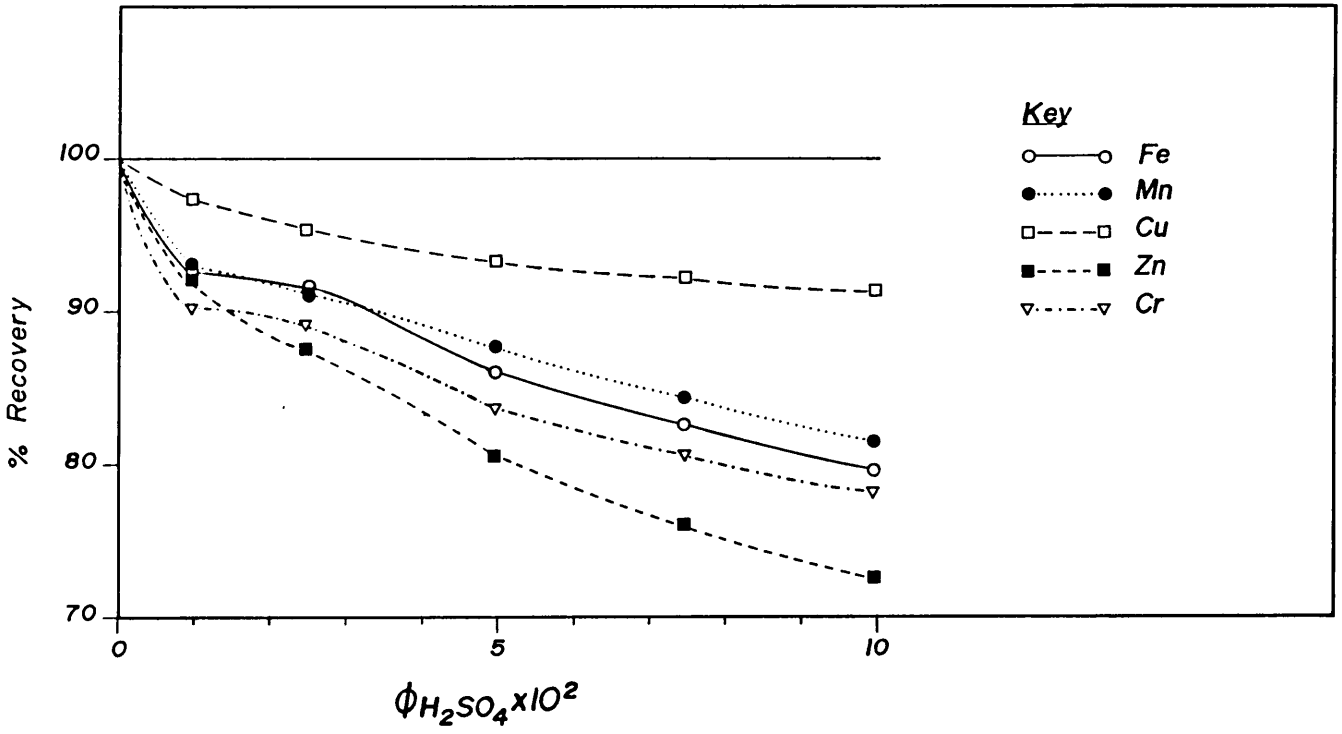


Figure 3-2: The sulphuric acid matrix effect showing suppression of recovery with respect to the $\phi$ = 0,01 nitric acid calibration matrix at 1,2 $m\ell.min^{-1}$ aspiration rate on the 34000 ARL ICP polychromator. Data plotted from Table 3-4.

$\phi$ = 0,10 nitric acid matrix. It is interesting to note that of the five elements considered, the Cu (I) 327,396 nm line has the lowest excitation potential. This is possibly suggestive that the suppression effect observed may be partly due to changes in plasma excitation conditions and not just to changes in nebulization efficiency. It should be emphasized that the Gilson Minipuls II pump maintained an aspiration rate at a value of 1,2 $m\ell.min^{-1}$, with <4% variation and that the acid effect cannot therefore be entirely ascribed to changes in uptake rate, unless the situation were present that nebulization efficiency changed by several times this amount, for the <4% change in uptake rate.

(c) An observable matrix effect was slight or absent in the case of hydrochloric acid up to $\phi$ = 0,10, at least within the experimental error resulting from the sensitivity drift of up to 1,6% (Table 3-5). An exception was the matrix effect of hydrochloric acid on copper emission which showed a suppression of 1,6% which is considered significant in view of the calibration sensitivity drift for Cu of only -0,1%. The precision of the copper recoveries was <4% RSD.

The near-absence of a hydrochloric acid matrix effect is in contrast to recoveries of around 85% reported by Dahlquist and Knoll (1978) in $\phi$ = 0,10 hydrochloric acid using a coaxial pneumatic nebulizer but using free sample aspiration. This clearly demonstrates the effectiveness of controlling aspiration rate by means of a peristaltic pump to reduce sample uptake change effects.

(d) The acid matrix effect curves for nitric acid show smaller change with concentration at low acid strengths for nitric acid than for sulphuric acid (Figure 3-1 and 3-2).

The possibility of a relation between percentage recovery in nitric and sulphuric acid media and the excitation potential of the analyte atomic or ionic transitions is numerically demonstrated in Table 3-6. This table was prepared by taking the recovery data for Fe, Mn, Cu, Zn and Cr at a given acid concentration from Table 3-3 (for nitric acid and Table 3-4 (for sulphuric acid) and calculating the linear correlation coefficient, r, between the recoveries for the set of five elements and their corresponding excitation potentials (Table 3-2) at each acid volume fraction.

TABLE 3-6: Linear correlation coefficients (r) between percentage recovery of Fe, Mn, Cu, Zn and Cr and the corresponding excitation potentials (eV) in sulphuric and nitric acid matrices. (Data for calculation of r taken from Tables 3-2, 3-3 and 3-4) at a given acid strength.

| | Correlation coefficient (r) | |
|---|---|---|
| $\Phi_{HA}$ x 100 | in nitric acid | in sulphuric acid |
| 1 | - | -0,95* |
| 2,5 | -0,33 | -0,93* |
| 5,0 | -0,82 | -0,90* |
| 7,5 | -0,75 | -0,88* |
| 10,0 | -0,88* | -0,86 |

*Significant at the 5% level.

The significance of these correlations (Table 3-6) was evaluated by calculating the parameter T defined as (Green and Margerison, (c), 1978);

$$T = r\left(\frac{n-2}{1-r^2}\right)^{\frac{1}{2}} \quad \ldots\ldots\ldots \quad (34)$$

where r = correlation coefficient,

and n = number of data pairs.

The significance of T was evaluated using the Student-t distribution, by comparing the T value to the critical value of Student-t for n-2 degrees of freedom at a significance level of $\alpha$:

$$t_{critical} = t_{(n-2)}(1-\alpha/2) \quad \ldots\ldots\ldots \quad (35)$$

where the null hypothesis, that the true population correlation is zero, being rejected when $|T| > t_{critical}$.

Using equations 34 and 35, the negative correlation between percentage recovery and excitation potential is significant at the 5% level (i.e., the probability that the observed correlation is due to chance is <0,05 or, in other terminology, the confidence with which the null hypothesis of "no real correlation" is rejected is 95%) for sulphuric acid volume fractions up to 0,075.. The correlation in the case of nitric acid only showed significance at a volume fraction of 0,10.

As can be seen from Table 3-6, the correlation in the case of sulphuric acid decreases with increasing volume fraction, implying that non-plasma (i.e., nebulizer efficiency change) reasons for decreased recovery become important at high volume fractions of sulphuric acid. The definite correlation between excitation potential and percentage recovery of analyte in sulphuric acid medium can be construed as evidence that plasma excitation changes are involved in causation of the residual acid matrix effect where aspiration rate has been held constant with a peristaltic pump, over and above the expected contribution of nebulizer efficiency change.

## 3.6 Matrix effect of surfactants

As surfactants may be present in environmental water samples, it is important to know whether they influence calibration sensitivity through a possible change in nebulization efficiency. A similar experiment was carried out as for the investigation of the acid matrix effect i.e., the measurement of recoveries of added analyte elements in the presence of a surfactant. A mixed standard containing 210 $mg.\ell^{-1}$ Fe; 110 $mg.\ell^{-1}$ Mn, 10 $mg.\ell^{-1}$ Cu; 10 $mg.\ell^{-1}$ Zn and 10 $mg.\ell^{-1}$ Cr in $\phi$ = 0,01 nitric acid was prepared from Titrisol standards. An aliquot of this mixed standard was spiked with a cationic detergent and analyzed under compromise analytical conditions on the 34000 ARL ICP spectrometer and the recoveries calculated. The experiment was repeated with an anionic detergent. The results of this experiment are given in Table 3-7. The effect of surfactants at moderate concentration (12,6 $mmol.\ell^{-1}$ for the cationic surfactant, alkylbenzyldimethylammonium chloride; and 17,3 $mmol.\ell^{-1}$ for the anionic surfactant, dodecylhydrogensulphate sodium salt) was minimal, with sensitivity changes of less than 4%.

TABLE 3-7: Matrix effect on calibration sensitivity caused by surfactants. Percentage recovery for Fe, Mn, Cu, Zn and Cr in the presence of 12,6 mmol.$\ell^{-1}$ cationic surfactant* and 17,3 mmol.$\ell^{-1}$ anionic surfactant** as compared to the $\phi$ = 0,01 nitric acid calibration matrix alone. Aspiration was forced by means of a Gilson Minipuls II pump at 1,3 m$\ell$.min$^{-1}$.

| | Percentage recovery | | | | |
|---|---|---|---|---|---|
| Surfactant | Fe | Mn | Cu | Zn | Cr |
| Cationic* | 98,0 | 98,8 | 101,0 | 99,5 | 97,0 |
| Anionic** | 96,1 | 98,2 | 101,0 | 100,4 | 97,4 |

*Alkylbenzyldimethylammonium chloride.
**Dodecylhydrogensulphate, sodium salt.

## 3.7 Matrix effect of tartaric acid

The suppression of analyte emission intensity by acids is not limited to the mineral acids as shown in Section 3-5, but also occurs with organic acids, as shown by an analagous experiment on the suppression of recoveries of a mixed standard, consisting of 210 mg.$\ell^{-1}$ Fe; 110 mg.$\ell^{-1}$ Mn; 10 mg.$\ell^{-1}$ Cu; 10 mg.$\ell^{-1}$ Zn and 10 mg.$\ell^{-1}$ Cr, in tartaric acid matrix. As in the case of the mineral acid matrix experiment, the aspiration rate was held invariant ( <2% change) through the use of a Gilson Minipuls II peristaltic pump. Analytical precision of the triplicate integrations was better than 0,7% RSD except for chromium where a precision of <1,3% RSD was found. The recoveries obtained in L(+) tartaric acid

medium are shown in Table 3-8 and illustrated graphically in Figure 3-3. The suppression of recovery at tartaric acid concentrations greater than 40 mmol.$\ell^{-1}$ was least for Cu (I) 327,396 nm with an excitation potential of 3,78 eV (Table 3-2), and greatest for Cr (II) with an excitation potential of 6,18 eV. The linear correlation between percentage recovery of Fe, Mn, Cu, Zn and Cr in tartaric acid medium and the excitation potentials corresponding to the analyte lines is shown in Tabel 3-9, with significance tested in the same manner as for the mineral acid matrix effect using equations 34 and 35. The most significant correlation was observed at a tartaric acid concentration of 67 mmol.$\ell^{-1}$, with an r value of -0,98 again indicating the importance of plasma excitation changes in the matrix effect at invariant aspiration rate.

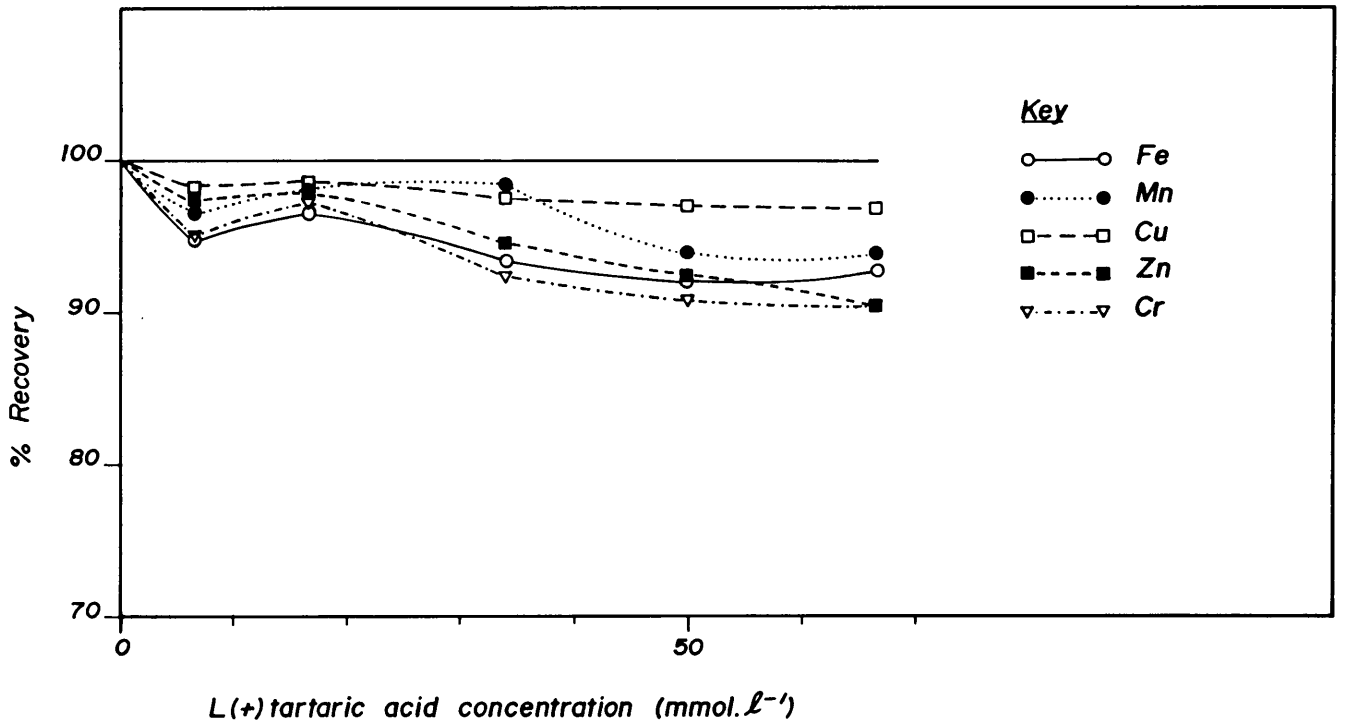


Figure 3-3: The tartaric acid matrix effect showing suppression of recovery with respect to the $\phi$ = 0,01 nitric acid calibration matrix at 1,25 $m\ell.min^{-1}$ aspiration rate on the 34000 ARL ICP polychromator. Data plotted from Table 3-8.

TABLE 3-8: Percentage recovery of Fe, Mn, Cu, Zn and Cr in L(+) tartaric acid matrix, with respect to the $\phi$ = 0,01 nitric acid calibration matrix taken as 100% recovery. Analyses carried out on a 34000 ARL ICP polychromator under compromise analytical conditions using forced sample aspiration at 1,2 $m\ell.min^{-1}$.

| L(+) tartaric acid ($mmol.\ell^{-1}$) | Percentage recovery of analyte elements | | | | |
|---|---|---|---|---|---|
| | Fe | Mn | Cu | Zn | Cr |
| 7 | 94,8 | 96,8 | 98,3 | 97,9 | 95,2 |
| 17 | 97,1 | 98,3 | 98,6 | 98,2 | 97,4 |
| 34 | 93,6 | 98,3 | 97,5 | 94,6 | 92,5 |
| 50 | 92,3 | 94,0 | 97,0 | 92,5 | 90,9 |
| 67 | 93,0 | 93,8 | 96,8 | 90,6 | 90,6 |
| *Drift in calibration: | -1,3 | -0,7 | -0,8 | -2,4 | -1,5 |

*The drift in the calibration is expressed as the % change in calibration sensitivity as measured by a control standard in the $\phi$ = 0,01 nitric acid matrix run before and after the tartaric acid matrix samples.

TABLE 3.9: Linear correlation coefficients (r) between percentage recovery of Fe, Mn, Cu, Zn and Cr and the corresponding excitation potentials (eV) in L(+) tartaric acid medium. (Data for calculation of r taken from Tables 3-2 and 3-8).

| Tartaric acid concentration ($mmol.\ell^{-1}$) | Correlation coefficient, r, between % recovery and excitation potential |
|---|---|
| 7 | -0,41 |
| 17 | -0,46 |
| 34 | -0,71 |
| 50 | -0,90* |
| 67 | -0,98** |

*Significant at the 5% level.
**Significant at the 1% level.

## 3.8 Sodium chloride matrix

The relative absence of matrix effects from EIE's under compromise analytical conditions on the 34000 ICP spectrometer was shown by the analysis of a solution containing 85,6 mmol.$\ell^{-1}$ (0,5% m/v) NaCl which had been spiked with Fe, Mn, Cu, Zn and Cr, in an analagous manner to the experiment done in Section 3.5 to demonstrate the acid matrix effect. Recoveries obtained were 91% for Fe; 96% for Mn; 97% for Cr, 101% for Cu and 101% for Zn. The major difficulty with high salt concentration matrices is salt deposition with consequent transport changes either around the nebulizer capillary, or near the tip of the inner sample introduction tube of the ICP quartz torch rather than effects in the plasma *per se*.

## 3.9 Contamination at trace concentrations

The issue of contamination as discussed in Section 3.4 with sample preparation must be seen in a wider synoptic context, from the collection of the sample at the sampling site to the final spectrometric analysis of the sample. Gross contamination at any one step may render the remainder of the analytical procedure an exercise in futility. The trace metal analyst should suspect every material with which the sample comes into contact with, or in proximity to, as a possible source of contamination.

While sample bottles of polyethylene or other plastic material are commonly used for containers for trace metal sampling, they should be precleaned with dilute acid (Klopper and Marchant, 1977). Note, however, that various metal containing additives may be used in the manufacture of plastic polymers, with consequent leaching possibilities into contained water e.g., in water distribution systems (WHO*, 1973; Kempster, 1979), and likewise pose a hazard of leaching when used as water sample containers. It has been the practice at the Hydrological Research Institute to have polyethylene sampling bottles manufactured to specification, and containing the absolute minimum quantity of metal stabilizer, usually a zinc compound.

The degree of effort to avoid all possible sources of contamination should be kept in proportion to the desired detection limit of an analyte, as well as the number of precautions taken in sampling. The issue of contamination should be seriously considered and reasonable precautions taken with e.g., cleanliness of reagents and laboratory ware, to reduce blank analyte readings to acceptably low levels, and the analyst should be continually on the guard against obvious sources of contamination.

---

* WHO = World Health Organisation.

## 3.10 Loss of Analyte

The reverse of contamination, i.e., the loss of analyte is perhaps more difficult to solve than the former. The major type of losses encountered are, (i) hydrolysis and the related aspects of adsorption or even precipitation e.g., of metal hydroxides; (ii) loss of volatile species especially where a sample is heated at some stage during the pretreatment process. The first is relatively easily solved e.g., by ensuring that the pH is sufficiently acid to minimize hydrolysis and adsorption. The second is a problem in all ashing procedures whether wet or dry, and is also particularly a problem in the drying of biological materials where loss of volatile metal compounds may occur even at temperatures below 100°C. Some workers have attempted to minimizing this problem by freeze-drying biological samples.

The loss of mercury in environmental water samples at the $\mu g.\ell^{-1}$ concentration level and below has been studied extensively (Christmann and Ingle, 1976; Sanemasa *et al*, 1976; Weiss *et al*, 1976). An important reason for a high probability of mercury loss from water samples, is the ease with which Hg(O) may be lost as the vapour when Hg (II) is reduced, particularly in deoxygenated waters, and an oxidizing agent such as potassium dichromate is therefore

often added to samples for mercury analysis (Mahan and Mahan, 1977), in addition to the customary acid preservative; nitric or sulphuric acid being suitable for this purpose (Bureau International Technique du Chlore, 1979). Differences in composition of polyethylene bottles may influence the stability of stored mercury containing samples (Heiden and Aikens, 1977), and the analyst is advised to check new containers as regards suitability for storing water samples for mercury analysis prior to use.

## 3.11 Summary

In this chapter, after an overview of sample collection procedures for water, sediment, macrophyte and fish samples, the problem of preservation was discussed, and an experiment carried out to show that acidification may influence the trace metal composition of a water sample. The goals of sample pretreatment were then discussed, and the point emphasized that sample pretreatment must be considered in relation to the analytical question being asked, particularly for solid samples, where selective or partial extraction may be desired rather than a total dissolution procedure.

A study of the acid matrix effect was then undertaken, it being shown that the use of a peristaltic pump to assure constant sample uptake rate resulted in a smaller acid matrix effect than that reported by Dahlquist and Knoll (1978). A residual acid matrix effect remained, however, particularly in the case of sulphuric acid. The suppression of Zn(I) 213,856 nm emission was greater than that of Cu(I) 327,396 nm emission both in the case of sulphuric and nitric acids. A correlation between the percentage recovery of Fe, Mn, Cu, Zn and Cr and the corresponding excitation potentials suggested that the emission signal for analyte elements with high excitation potential show a greater acid matrix effect than those with low excitation potential.

An investigation into sensitivity changes occurring in other matrices showed that the matrix effect was minimal for hydrochloric acid and surfactants. The matrix effect for tartaric acid showed a significant correlation with excitation potential at tartaric acid concentrations of 50 $mmol.^{-1}$ and greater. A matrix effect from sodium chloride was minimal for NaCl concentrations below 85,6 $mmol.^{-1}$ (0,5% m/v).

The chapter was concluded with a discussion of contamination and loss of analyte during sample preparation procedures.

# CHAPTER 4: INSTRUMENTATION, ANALYTICAL OPERATING CONDITIONS AND SOURCES OF ERROR

## 4.1 Introduction

In this chapter, a description of the instrumentation used is given together with the compromise analytical operating conditions used on the polychromator and scanning monochromator; followed by experiments to show the effect of change in certain variables on for instance analyte emission intensity viz.,

(a) Sample aspiration rate as it affects emission intensity, excitation temperature and degree of ionization,

(b) effect of mains input voltage change on emission intensity, with separate consideration of the effect on the source conditions and measuring electronics, and

(c) effect of change in aerosol gas flow rate on emission intensity, and the relationship to excitation potential.

The latter relationship allows the development of a modified internal standardization type formula as is described in Section 4.8 and 4.9.

## 4.2 Instrumentation

The instrumental data for the two ICP emission spectrometers utilized in this work i.e., a 1978 Applied Research Laboratories (ARL) Model 34000 polychromator, and a 1983 Model ARL 3510 scanning monochromator are given in Table 4-1. In addition to the standard instrumentation, both instruments have been fitted with two separate, dedicated Watford voltage stabilizers, one for the rf generator mains supply, and the second for the spectrometer mains. The spectrometers are housed in air-conditioned rooms at around 20°C. Each instrument has also been supplied with a Gilson Minipuls II pump to control sample aspiration rate.

The analytical wavelength programme for the 28 channels of the ARL 34000 polychromator is shown in Table 4-2, and the compromise operating conditions in Table 4-3. The profile setting of the polychromator is checked daily by scanning across the Y (II) 360,07 nm line with the micrometer screw for adjusting the entrance slit position while aspirating an yttrium solution of approximately 10 $mg.\ell^{-1}$ concentration. One drawback of the 34000 polychromator is the use of needle valves rather than mass flow controllers for adjustment of the argon gas flow rates. The needle valves are fully opened for a few seconds before igniting the plasma to dislodge any fine particulate matter that may

have collected between the needle and the surrounding housing, when any rotameter flow instability is observed. In addition, the needle valve controlling the aerosol gas flow is opened and carefully cleansed on a regular basis.

The compromise operating conditions of the ARL 3510 scanning monochromator are also shown in Table 4-3. The largely solid state type rf generator of the ARL 3510 spectrometer reaches operating stability more rapidly on ignition of the torch than the older conventional rf generator on the ARL 34000 spectrometer. On the former calibration and analysis may be commenced within approximately 10 min, of ignition of the plasma, whereas on the latter a delay of at least 60 min, between plasma ignition and calibration is required before stable background and analyte intensity readings are reached. Apart from the rf generator as a possible source of this prolonged warm-up period on the polychromator, the 2 ℓ capacity heat-exchanger with water as coolant opposed to the silicone oil heat exchanger of only a few hundred mℓ capacity on the ARL 3510 spectrometer may also be an important contributing factor to the different warm-up periods.

TABLE 4-1: Characteristics of the ARL 34000 polychromator and ARL 3510 monochromator

| | | ARL 34000 | ARL 3510 |
|---|---|---|---|
| 1. | rf Generator | | |
| | Model | 2000 PGC27, conventional | Solid state type except radio valve |
| | Phases | single | single |
| | Input | 220 volt | 220 volt |
| | Cooling | air | air |
| | Radio frequency | 27,12 MHz | 27 MHz |
| 2. | ICP source | | |
| | Torch | standard ARL, quartz glass | standard ARL, quartz glass |
| | Induction coil | 2-turn copper, plated with silver | 3-turn copper |
| | Coolant | water | silicone-oil |
| | Observation height | 14; 18; 22 or 26 mm above coil | fixed |
| | Ignition | Tesla coil | Tesla coil |

TABLE 4-1 Continued

| | ARL 34000 | ARL 3510 |
|---|---|---|
| 3. Gas | | |
| Gas type | argon, apectroscopic grade | argon, spectroscopic grade |
| Inner (aerosol) argon wetted | no | yes |
| Adjustment of gas flow | needle valve for inner, intermediate and outer gases gas flow lines | compression type regulators on inner, intermediate and outer gas flow lines |
| Measurement of gas delivery | rotameters | pressure gauges except for rotameter on inner gas flow line |
| Tip washer on aerosol gas flow line | no | yes |
| 4. Spectrometer: | | |
| Type | Paschen-Runge, air | Czerny-Turner, argon flushed |
| Focal length | 1,0 m | 1,0 m |
| Grating | Replica; 1920 lines, $mm^{-1}$ | Holographic; 2400 lines, $mm^{-1}$ |
| Entrance slit | 20 µm | 20 µm |
| Entrance slit filters | none | Two filters for:<br>(a) 320 to 510 nm and<br>(b) 510 to 800 nm to exclude higher order reflections |

TABLE 4-1 Continued

| | ARL 34000 | ARL 3510 |
|---|---|---|
| Exit slit | 37; 50; 75 or 100 µm depending on element channel (Table 4-2) | 20 µm |
| Reciprocal linear dispersion | 0,52 nm. $mm^{-1}$ | 0,67 nm. $mm^{-1}$ |
| Resolution | 76800 | 124 800 |
| Wavelength coverage | 191 to 458 nm (1st order) | 160 to 800 nm (1st order) |
| Bandpass | Dependent on element channel | 0,0134 nm |
| Wavelength selection | Fixed exit slits | Grating rotation |
| Stepping motor | none | One measuring step = 5 motor steps = 0,0028 nm |
| Reference wavelength | Not applicable | Ar(I) 355,431 nm |
| Photomultiplier tube | Various | Type R955 |
| Photomultiplier high voltage attenuation | Channel specific; manually selectable between 514 and 1000 volt with bridges | Attenuation software selectable in 15 steps from 1 to 15 |
| Spectrometer thermostated | Yes | Yes |

TABLE 4-1 Continued

| | ARL 34000 | ARL 3510 |
|---|---|---|
| 5. Sample transport | | |
| Autosampler | Yes, carousel type | No |
| Control of sample aspiration rate | Gilson Minipuls II peristaltic pump | Gilson Minipuls II peristaltic pump |
| Nebulizer | Meinhard, concentric glass | Meinhard, concentric glass |
| Spray chamber | Cylindrical, with inner sleeve, no spoiler | Conical, no inner sleeve, with glass bead spoiler |
| 6. Control | | |
| Processor | PDP 11/04, 32 K memory, controls autosampler, torch height, integration and readout electronics and data processing | DEC 11/03, 32 K memory, controls wavelength selection, scanning and integration routines and data processing |
| Data storage | two RX01 15 cm floppy disc storage devices | two 13 cm Micropolis floppy disc storage devices |
| Terminals | a) LAP 36 Decwriter for printout of data and communication with processor | a) standard ASCII keyboard to communicate with processor |

TABLE 4-1 Continued

| | ARL 34000 | ARL 3510 |
|---|---|---|
| | b) VT100 video display with keyboard as alternate terminal | b) High resolution colour graphics display terminal |
| | c) Data transfer to a mainframe computer via a RS 232-20 mA current loop interface | c) Prism 80 colour printer |
| Language | ARL Extended BASIC | ARL Extended BASIC |

TABLE 4-2: Analytical channels on ARL 34000 ICP polychromator

| Channel No. | Element* | λ/nm | Exit slit/µm | Attenuator/V |
|---|---|---|---|---|
| 1 | Se (I) | 203,98 | 50 | 726 |
| 2 | Zn (I) | 213,85 | 37 | 696 |
| 3 | Cd (II) | 226,50 | 75 | 696 |
| 4 | Hg (I) | 253,65 | 75 | 848 |
| 5 | Cr (II) | 267,72 | 75 | 709 |
| 6 | Mo (II) | 281,62 | 50 | 741 |
| 7 | Si (I) | 288,16 | 75 | 687 |
| 8 | Mn (II) | 257,61 | 75 | 525 |
| 9 | V (II) | 311,07 | 75 | 687 |
| 10 | Ti (II) | 334,94 | 75 | 621 |
| 11 | Ni (I) | 352,45 | 75 | 621 |
| 12 | As (I) | 193,76 | 50 | 784 |
| 13 | Sb (I) | 206,83 | 37 | 805 |
| 14 | Co (I) | 340,51 | 75 | 726 |
| 15 | Be (I) | 234,86 | 75 | 657 |

* (I) = atomic line.

(II) = ion line.

TABLE 4-2: (continued)

| Channel No. | Element* | λ/nm | Exit slit/μm | Attenuator/V |
|---|---|---|---|---|
| 16 | B (I) | 249,68 | 50 | 687 |
| 17 | Fe (II) | 259,94 | 75 | 530 |
| 18 | Ca (II) | 315,89 | 100 | 657 |
| 19 | Na (I) | 588,99 | @ | 784 |
| 20 | Mg (I) | 383,83 | 75 | 586 |
| 21 | K (I) | 766,49 | @ | 880 |
| 22 | Pb (I) | 368,35 | 75 | 829 |
| 23 | Cu (I) | 237,39 | 75 | 687 |
| 24 | Al (I) | 396,15 | 75 | 750 |
| 25 | Sr (II) | 421,55 | 75 | 530 |
| 26 | Y (II) | 360,07 | 50 | 709 |
| 27 | Ba (II) | 455,40 | 50 | 580 |
| 28 | Zr (II) | 349,62 | 50 | 805 |

@ Na and K are determined using fibre optics to transmit light from the tail flame of the plasma to the respective Na and K photomultiplier tubes, through interference filters, and not through the spectrometer *per se*.

* (I) = atomic line.
(II) = ion line.

TABLE 4-3: Compromise operating conditions used for analysis on the ARL 34000 polychromator and ARL 3510 scanning monochromator

| | ARL 34000 | ARL 3510 |
|---|---|---|
| 1. Gas | | |
| Argon feed pressure | 500 k Pa | 480 kPa |
| Secondary regulator in source box | 340 kPa; being the inlet pressure to the rotameters | a) 238 kPa for outer gas<br>b) 152 kPa for intermediate gas |
| Inner (aerosol) gas flow | 0,40 $\ell.min^{-1}$ | 0,36 rotameter units, nominally 1 $\ell.min^{-1}$ as stated by manaufacturer |
| Intermediate (plasma) gas | 0,40 $\ell,min^{-1}$ | 0,8 $\ell.min^{-1}$ as stated by manufacturer |
| Outer (coolant) gas | 11,0 $\ell.min^{-1}$ | 12 $\ell.min^{-1}$ as stated by manufacturer |
| 2. Observation height | 18 mm above coil | fixed, ca. 15 mm above coil |
| 3, Sample uptake | 1,27 $m\ell.min^{-1}$ | 1,14 $m\ell.min^{-1}$ |
| 4. rf power | | |
| Incident | 1250 watt | 1200 watt |
| Reflected | <5 watt | <5 watt |

TABLE 4-3 Continued

| | ARL 34000 | ARL 35120 |
|---|---|---|
| 5. A.C. mains | | |
| Stabilizer | separate Watford stabilizers on gen., and spect., supplies | separate Watford stabilizers on gen., and spect., supplies |
| rf Generator | 216 ± 1 volt | 220 ± 1 volt |
| Spectrometer | 225 ± 1 volt | 220 ± 1 volt |
| 6. Integration | | |
| Time | 10 s. | to suit particular analytical line |
| Replicates | 3 | to suit particular problem |
| 7. Analytical wavelengths | Fixed, see Table 4-2 | Chosen to suit particular analytical problem. |

## 4.3 Sample aspiration rate and signal intensity of Mn emission

In order to demonstrate the effect of nebulizer uptake rate on analyte emission line intensity, using the ARL 3510 spectrometer, the behaviour of emission intensity of four manganese lines was studied at sample uptake rates from 0,60 to 1,40 $m\ell.min^{-1}$. The manganese emission lines used are given in Table 4-4.

TABLE 4-4: The manganese emission lines used to study sample uptake rate changes on the ARL 3510 ICP (data from Zaidel' et al, 1970)

| Element | λ/nm | $V_{exc}$/eV |
|---|---|---|
| Mn (I) | 401,810 | 5,20 |
| Mn (I) | 403,076 | 3,08 |
| Mn (II) | 257,610 | 4,81 |
| Mn (II) | 294,921 | 5,37 |

As the two ionic lines of manganese have considerably greater emission intensities than the two atomic lines, a weaker manganese standard solution was used for the ionic lines, i.e., $10mg.\ell^{-1}$ Mn, as against 100 $mg.\ell^{-1}$ Mn for the atomic line measurements. In addition, the attenuator was set at 3 for the ionic lines, as against 5 for the atomic lines.

The ARL 3510 scanning monochromator was used under compromise operating conditions (Table 4-3), with the observation height lying between the height profile maxima for Mn (I) and Mn (II) emission (Figure 4-1). Aspiration rate was measured by recording the time necessary to aspirate 3,0 mℓ of the test solution using a stop watch and 10 mℓ measuring cylinder. At each aspiration rate, standard and blank intensity readings were recorded for 27 x 5 s integrations. Nitric acid, $\phi$ = 0,01 was used as blank. The wavelength profile was checked before and after each set of readings, and operating parameters such as gas pressures and rf power readings were checked. No significant changes were observed in instrumental parameters during a run.

The data obtained for the Mn (I) lines is presented in Tables 4-5 to 4-6 and in Figures 4-2 to 4-4. As seen in Table 4-5 the relative standard deviation of gross analyte intensity of the Mn(I) 401,81 nm was lowest for aspiration rates between 0,87 and 0,97 $m\ell.min^{-1}$, with poorer precision at aspiration rates outside this range. The precision of gross analyte intensity for the Mn(I) 403,076 nm line was more uniform over the range of aspiration rates tested, the relative standard deviation lying between 2% and 4% (Table 4-6). The precision of these two atomic lines of manganese is poorer than that of the Mn(II) 257,61 nm line, which is the emission line of

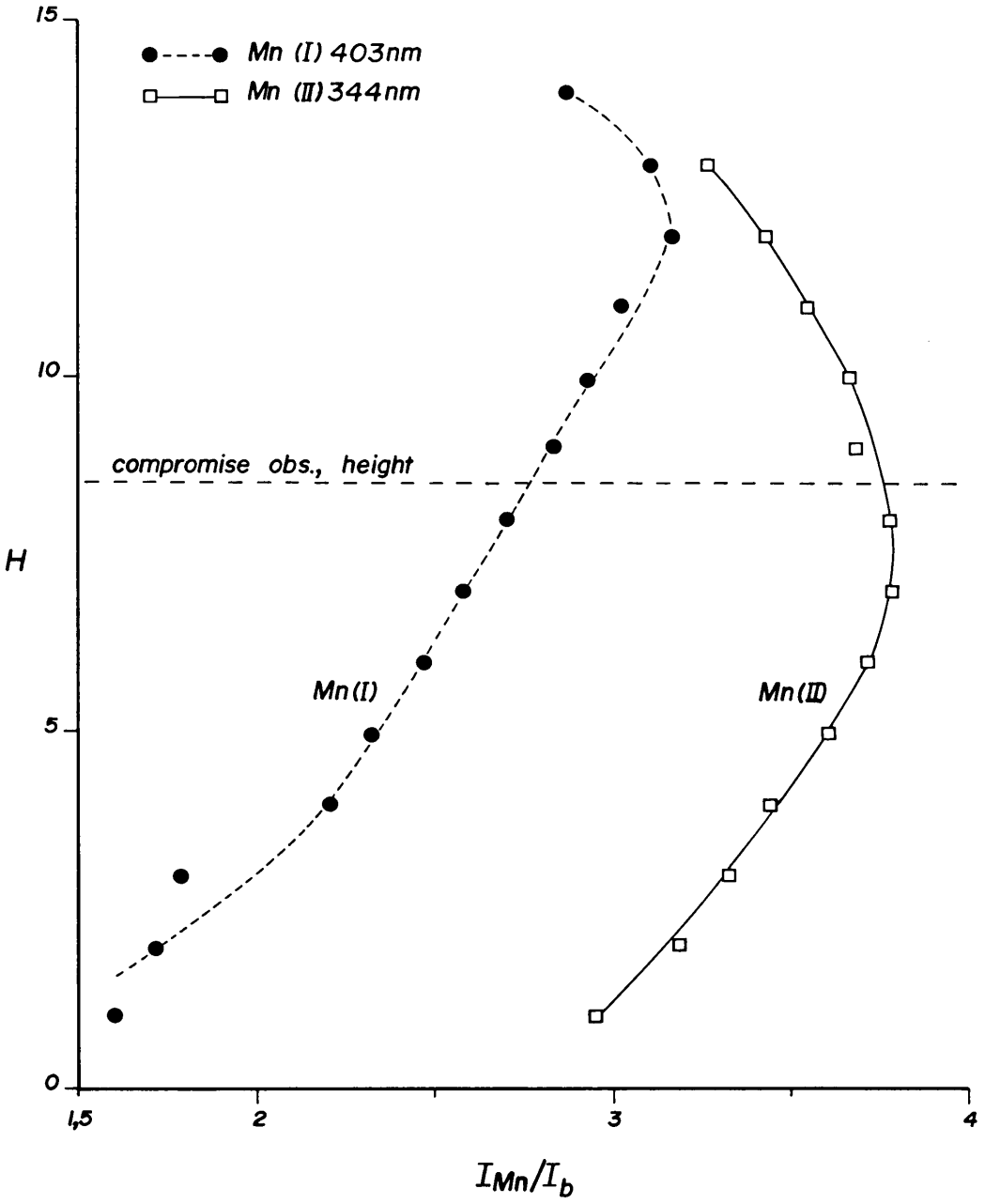


**Figure 4-1:** Relationship between line to background intensity ratio ($I_{Mn}/I_b$) and observation height above rim of torch, in turns of the adjusting screw, for the Mn(I) 403,076 nm and Mn(II) 344,198 nm emission lines on the ARL 3510 spectrometer, as determined at the time of installation (March 1983).

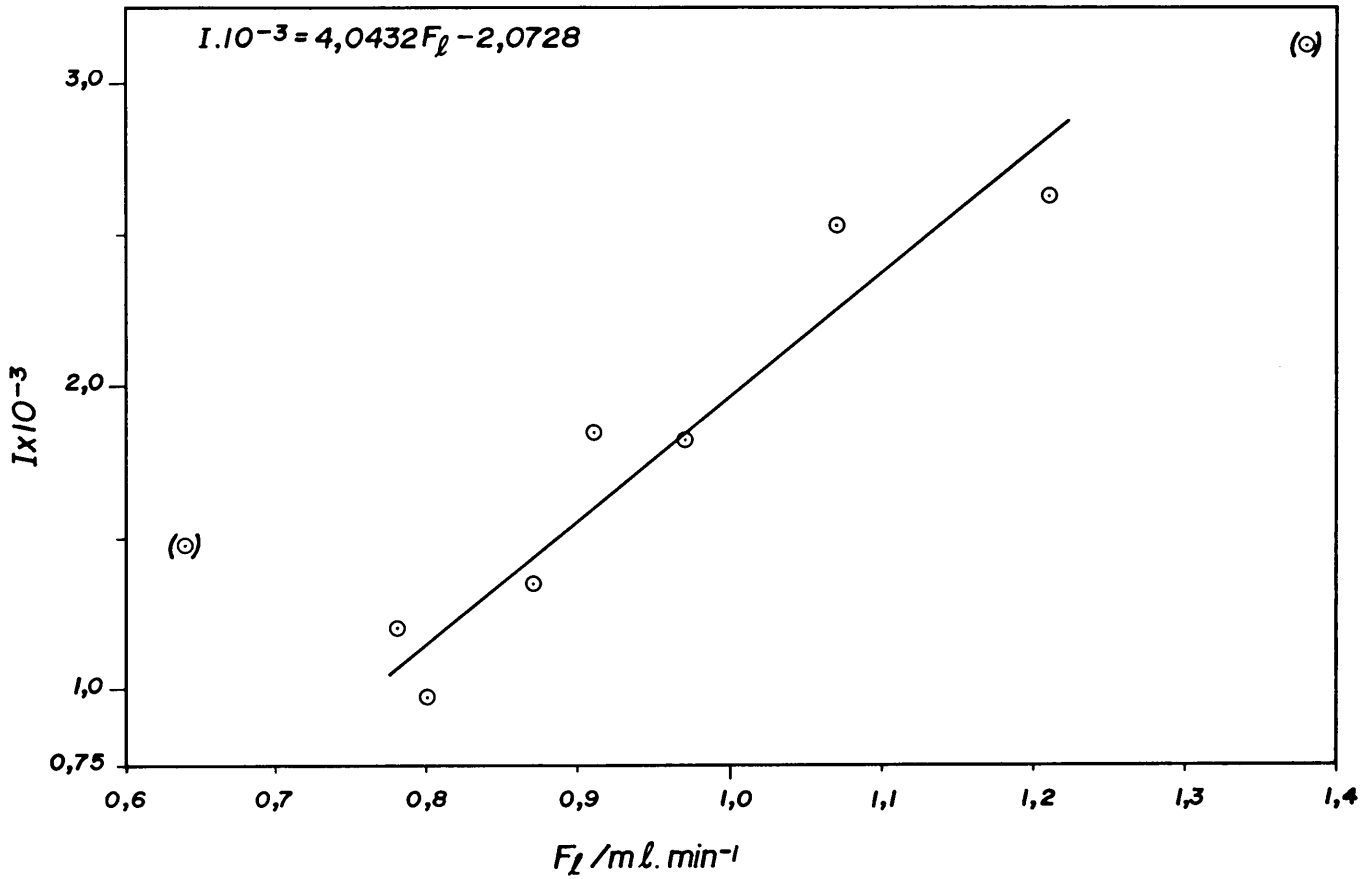


Figure 4-2: Effect of aspiration rate ($F_\ell$) on net emission intensity (I) of Mn (I) 401,81 nm at attenuator setting 5. The least squares linear regression with r = 0,95 excludes the two outlying points given in parentheses.

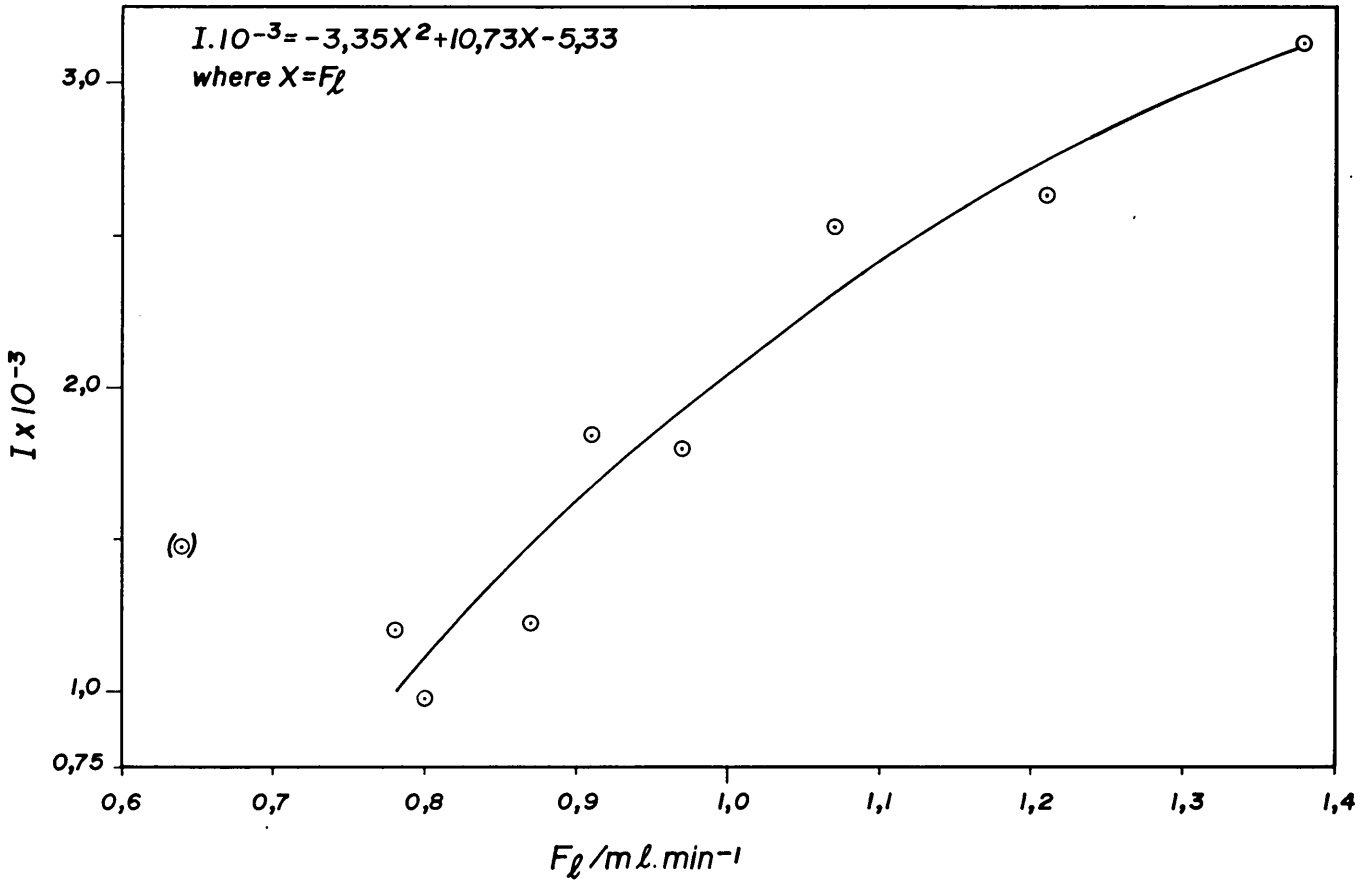


Figure 4-3: Effect of aspiration rate ($F_\ell$) on net emission intensity (I) of Mn (I) 401,81 nm at attenuator setting 5. A quadratic regression has been fitted to the data points, with the exception of the point in parentheses.

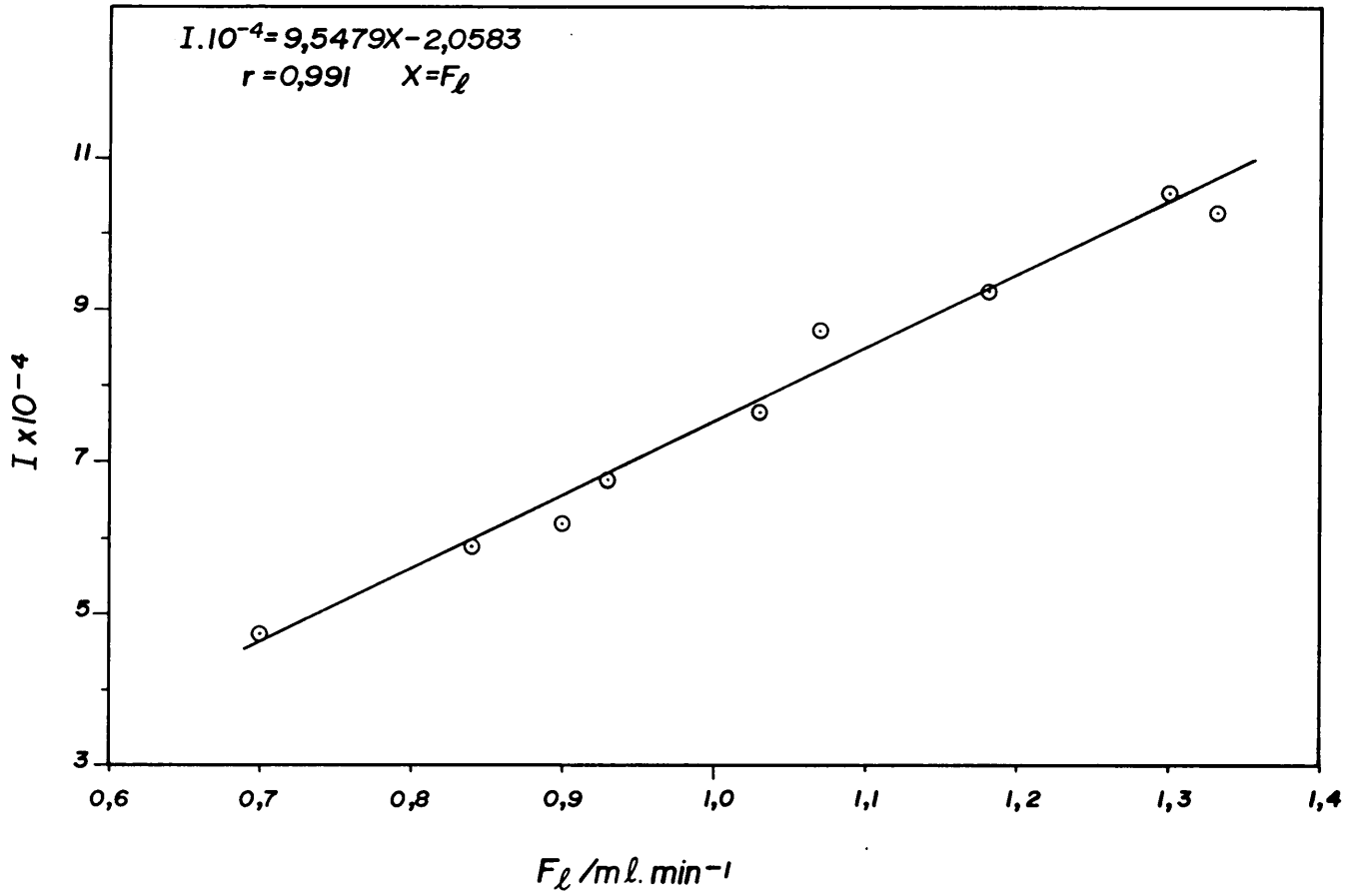


Figure 4-4: Effect of aspiration rate ($F_\ell$) on net emission intensity (I) of Mn (I) 403,076 nm at attenuator setting 5. A least squares linear regression gave a correlation coefficient r, of 0,991.

manganese normally used in routine analysis of water samples (Table 4-7). The 1% precision achievable in ICP emission spectrometric analysis is characteristic of the intense analytical lines in the middle of the analytical concentration range, when source conditions have been optimised for the line in question (Butler et al, 1980). The Mn (I) 401,81 nm atomic line showed a linear dependence of net intensity on aspiration rate between 0,8 and 1,2 $m\ell.min^{-1}$ (Figure 4-2), except for two outlying points at 0,64 $m\ell.min^{-1}$ and 1,38 $m\ell.min^{-1}$, with a correlation coefficient, r = 0,947 and the net intensity (I) showing the following dependence on aspiration rate ($F_\ell$) of:

$$I_{401} \cdot 10^{-3} = 4{,}04.F_\ell - 2{,}07 \quad \ldots\ldots\ldots\ldots \quad (36)$$

where I = net intensity of Mn 401,81 nm for 5 s integration time at attenuator setting 5,

and $F_\ell$ = sample aspiration rate ($m\ell.min^{-1}$).

TABLE 4-5: Emission intensity data for Mn(I) 401,81 nm on ARL 3510 spectrometer at a concentration of 100 $mg.\ell^{-1}$. An attenuator setting of 5 was used with 27 x 5 s integrations.*

| $F_\ell/m\ell.min^{-1}$** | $\bar{I}_{gross}$ | σ | RSD% | $\bar{I}_{blank}$ | σ | RSD% | $\bar{I}_{net}$ | DL(2σ)/$mg.\ell^{-1}$ |
|---|---|---|---|---|---|---|---|---|
| 0,64 | 2580 | 184 | 7% | 1100 | 166 | 15% | 1480 | 22 |
| 0,78 | 2242 | 41 | 2% | 1040 | 5 | 0,5% | 1200 | 0,8 |
| 0,80 | 2055 | 60 | 3% | 1082 | 6 | 0,6% | 973 | 1,2 |
| 0,87 | 2297 | 15 | 0,6% | 1072 | 7 | 0,6% | 1225 | 1,1 |
| 0,91 | 2621 | 54 | 2% | 784 | 8 | 1,0% | 1840 | 0,9 |
| 0,97 | 2632 | 20 | 0,8% | 816 | 5 | 0,6% | 1820 | 0,5 |
| 1,07 | 3527 | 153 | 4% | 996 | 8 | 0,8% | 2530 | 0,6 |
| 1,21 | 3622 | 194 | 5% | 990 | 8 | 0,8% | 2630 | 0,6 |
| 1.38 | 4099 | 104 | 2% | 981 | 9 | 0,9% | 3120 | 0,6 |

* rf Power at 1200 watt; $\bar{I}_{gross}$ = mean gross analyte intensity; $\bar{I}_{blank}$ = mean blank intensity; $\bar{I}_{net}$ = mean net analyte intensity; σ = standard deviation; RSD% = relative standard deviation percent; DL = detection limit. The Mn(I) 401,81 nm line is a weak line, showing poor precision under the compromise analytical conditions used (Table 4-3).

** $F_\ell$: aspiration rate (rate of liquid uptake)

TABLE 4-6: Emission intensity data for Mn(I) 403,076 nm on ARL 3510 spectrometer at a concentration of 100 mg.$\ell^{-1}$. An attenuator setting of 5 was used with 27 x 5 s integrations.*

| $F_\ell$/mℓ.min$^{-1}$** | $\bar{I}_{gross}$ | σ | RSD% | $\bar{I}_{blank}$ | σ | RSD% | $\bar{I}_{net}$ | DL(2σ)/mg.$\ell^{-1}$ |
|---|---|---|---|---|---|---|---|---|
| 0,70 | 47900 | 2000 | 4% | 604 | 5 | 0,8% | 47300 | 0,021 |
| 0,84 | 59900 | 1500 | 2% | 600 | 4 | 0,7% | 59300 | 0,013 |
| 0,90 | 62400 | 1400 | 2% | 601 | 4 | 0,7% | 61800 | 0,013 |
| 0,93 | 68100 | 2100 | 3% | 613 | 5 | 0,8% | 67500 | 0,015 |
| 1,03 | 77400 | 1600 | 2% | 599 | 4 | 0,7% | 76800 | 0,010 |
| 1,07 | 88000 | 2800 | 3% | 585 | 4 | 0,7% | 87400 | 0,009 |
| 1,18 | 92900 | 1400 | 2% | 574 | 8 | 1,4% | 92300 | 0,017 |
| 1,30 | 105800 | 2300 | 2% | 556 | 7 | 1,2% | 105200 | 0,013 |
| 1,33 | 103700 | 2000 | 2% | 545 | 6 | 1,1% | 103200 | 0,012 |

* rf Power at 1200 watt; $\bar{I}_{gross}$ = mean gross analyte intensity; $\bar{I}_{blank}$ = mean blank intensity; $\bar{I}_{net}$ = mean net analyte intensity; σ = standard deviation; RDS% = relative standard deviation percent; DL = detection limit. The Mn(I) 403,076 nm line is considerably stronger than the Mn(I) 401,81 nm line (Table 4-5).

** $F_\ell$ : aspiration rate (rate of liquid uptake)

The outlying point at 0,64 mℓ. $min^{-1}$ aspiration rate is uncertain due to poor precision in the readings for the low uptake rate (Table 4-5) whereas the point at 1,38 mℓ. $min^{-1}$ is associated with better than 3% precision. Including the latter point in a 2nd order regression provides the following equation (Figure 4-3):

$$I_{401} \cdot 10^{-3} = -3,35.F_{\ell}^{2} + 10,7.F_{\ell} - 5,33 \quad \ldots\ldots \quad (37)$$

covering the uptake range 0,8 to 1,4 mℓ. $min^{-1}$, where $F_{\ell}$ and I are as defined for equation 36.

The data for the 403,076 nm atomic line of manganese (Table 4-6) showed greater linearity with aspiration rate change than the 401,81 nm line. The linear regression equation;

$$I_{403} \cdot 10^{-4} = 9.548.F_{\ell} - 2,058 \quad \ldots\ldots\ldots\ldots \quad (38)$$

where $I_{403}$ = net intensity of Mn 403,073 nm line for 5 s integration time at attenuator setting 5,

and $F_{\ell}$ = aspiration rate ($m\ell.min^{-1}$),

had a correlation coefficient value r of 0,991 (Figure 4-4) for the aspiration rate range 0,70 to 1,33 $m\ell.min^{-1}$. The linear response of the 403 nm Mn (I) line implies that the associated transition excitation conditions for this

line did not change significantly, whereas the deviation from linearity of the Mn (I) 401 nm data (Figures 4-2 and 4-3) imply change in excitation conditions at different aspiration rates.

Using equation 8 (Chapter 2), the common excitation temperature may be calculated from the intensity ratio of the Mn 401 and 403 nm atomic lines. Equation 8 may be written:

$$\ln ( Ip/Iq) = \ln\left( \frac{g^u_p . A_p}{\lambda_p} . \frac{\lambda_q}{g^u_q . A_q} \right) - (V_{exc,p} - V_{exc,q})/k\ T_{exc} \quad ..... (39)$$

where $Ip$ = net intensity of line p,
$Iq$ = net intensity of line q,
$\lambda_p$ = wavelength of line p,
$\lambda_q$ = wavelength of line q,
$A_p$ = transition probability associated with line p,
$A_q$ = transition probability associated with line q,
$g^u_p$ = upper statistical weight associated with line p,
$g^u_q$ = upper statistical weight associated with line q,
$V_{exc,p}$ = excitation potential for line p
$k$ = Boltzmann constant
and $T_{exc}$ = common excitation temperature

by using the relationships (Weast, 1980):

(a) $g_i.f = 1{,}499 \times 10^{-8} . \lambda^2 . g^u_i . A$

where $g_i$ = lower statistical weight

$g^u_i$ = upper statistical weight

$\lambda$ = wavelength (Angstroms)

f = atomic oscillator strength

and A = transition probability,

and (b) $c = \nu \lambda$

where c = speed of light

$\nu$ = frequency

and $\lambda$ = wavelength

The excitation potentials may be converted from eV units (Table 4-4) to Joule or erg units using

$1\ eV = 1{,}602 \times 10^{-19}\ J$

or $1\ eV = 1{,}602 \times 10^{-12}\ erg$ (Wehr and Richards, 1964).

Values for the product of statistical weight and transition probability (Weast, 1980) are:

for Mn 401,81 nm $gA = 8x0{,}33x10^{8}\ s^{-1}$

and for Mn 403,076 nm $gA = 8x0{,}19x10^{8}\ s^{-1}$.

Substituting in equation (39):

$$\ln (I_{401}/I_{403}) = \ln (1{,}7423) - (3{,}396x10^{-12}/k\ T_{exc})$$

i.e. $$\ln (I_{401}/I_{403}) = \ln (1{,}7423) - (2{,}461x10^{4}/T_{exc})$$

whence, by rearrangement:

$$T_{exc} = \frac{2{,}461x10^{4}}{\ln 1{,}7423 - \ln (I_{401}/I_{403})} \quad \ldots\ldots\ldots\ldots\ (40)$$

For the ratio of $I_{401}/I_{403}$ in equation 40, an expression for $I_{403}$ obtained from equation 38 may be substituted; and for $I_{401}$ either a linear expression from equation 36, or a quadratic expression from equation 37 might be employed. A plot of $T_{exc}$ against aspiration

rate $F_{\ell}$, for these two cases, as obtained from equation 40 is shown in Figure 4-5 where the linear expression for $I_{403}$ was used, and in Figure 4-6 where the quadratic expression for $I_{403}$ was taken. Both these figures show that the excitation temperature for the Mn 401/Mn 403 nm line pair increases rapidly with flow rate between 0,8 $m\ell.min^{-1}$ and 1,0 $m\ell.min^{-1}$ whereafter the curve flattens off, reaching a maximum of approx., 6000 K at around 1,2 $m\ell.\ min^{-1}$ sample uptake rate.

The data for the two ionic lines of manganese viz., Mn(II)257,61 nm and Mn(II)294,92 nm is shown in Tables 4-7 and 4-8, and Figures 4-7 and 4-8 respectively. The relative standard deviation of gross analyte intensity for the Mn(II) 257,61 nm line lay between 1% and 4%, with a mean precision of 2% (Table 4-7). The Mn(II) 257,61 nm line is the usual emission line of manganese employed for analytical determination of manganese, and its precision is better than the Mn(II) 294,921 nm line (Table 4-8) as well as that of the two atomic lines of manganese tested viz., Mn(I) 401,81 nm (Table 4-5) and Mn(I) 403,076 nm (Table 4-6). For Mn(II) 257,61 nm the following relationship between aspiration rate and net intensity, with a correlation coefficient of 0,92 was found:

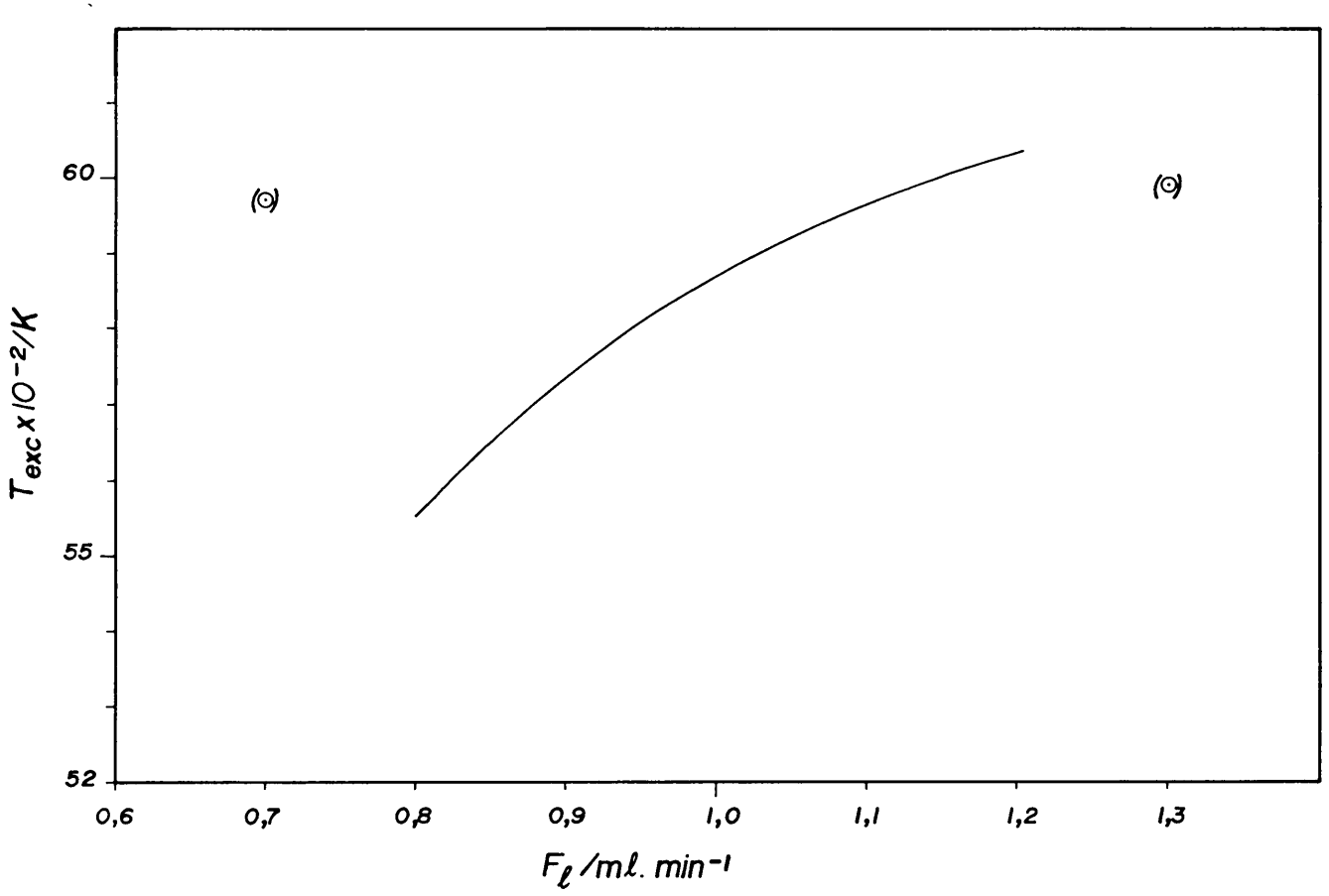


Figure 4-5: Common excitation temperature ($T_{exc}$) of the Mn 401,81 nm and 403,076 nm line pair as a function of aspiration rate ($F_\ell$), as determined by the two-line method from the data of Figure 4-2 and Figure 4-4.

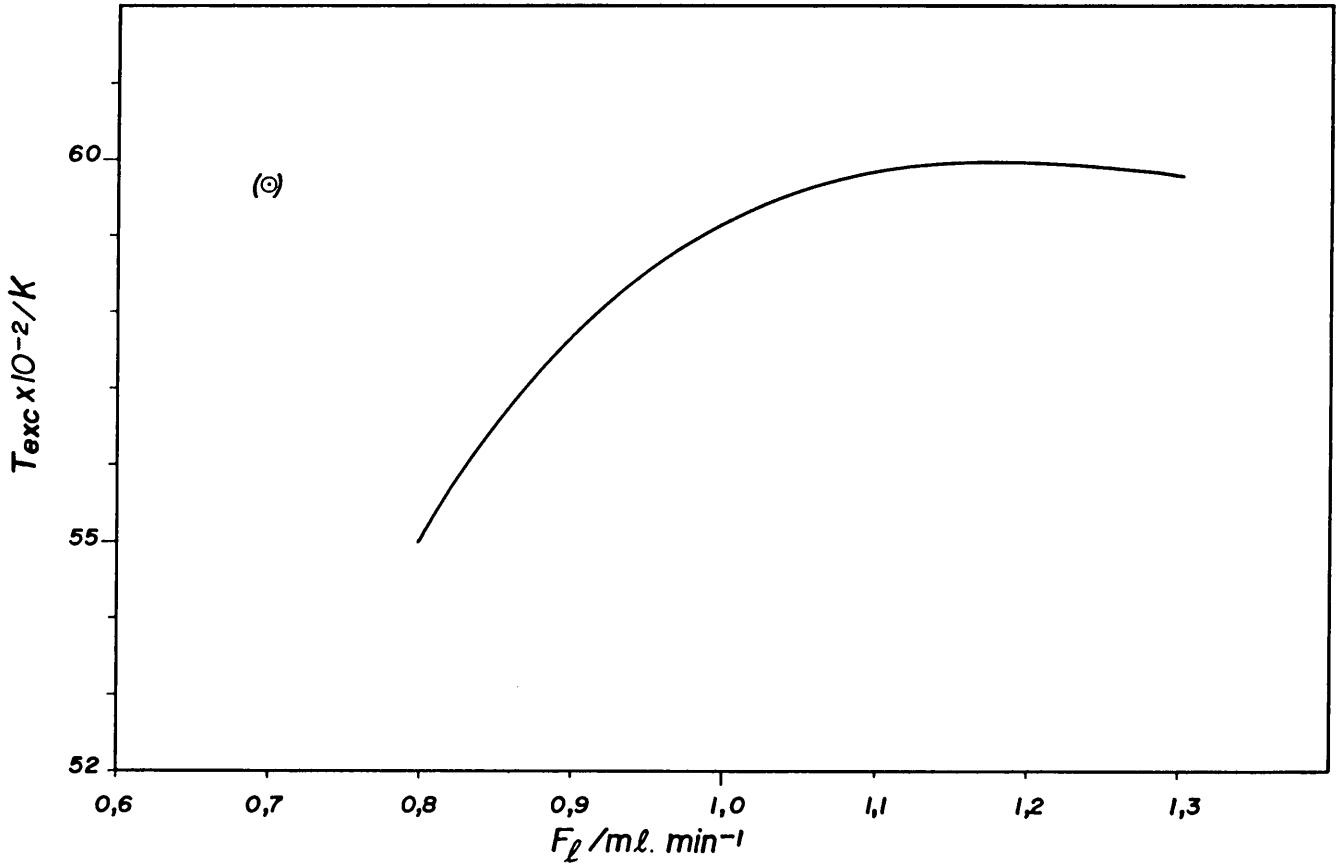


Figure 4-6: Common excitation temperature ($T_{exc}$) of the Mn 401,81 nm and 403,076 nm line pair as a function of aspiration rate ($F_\ell$), as determined by the two-line method from the data of Figure 4-3 and Figure 4-4.

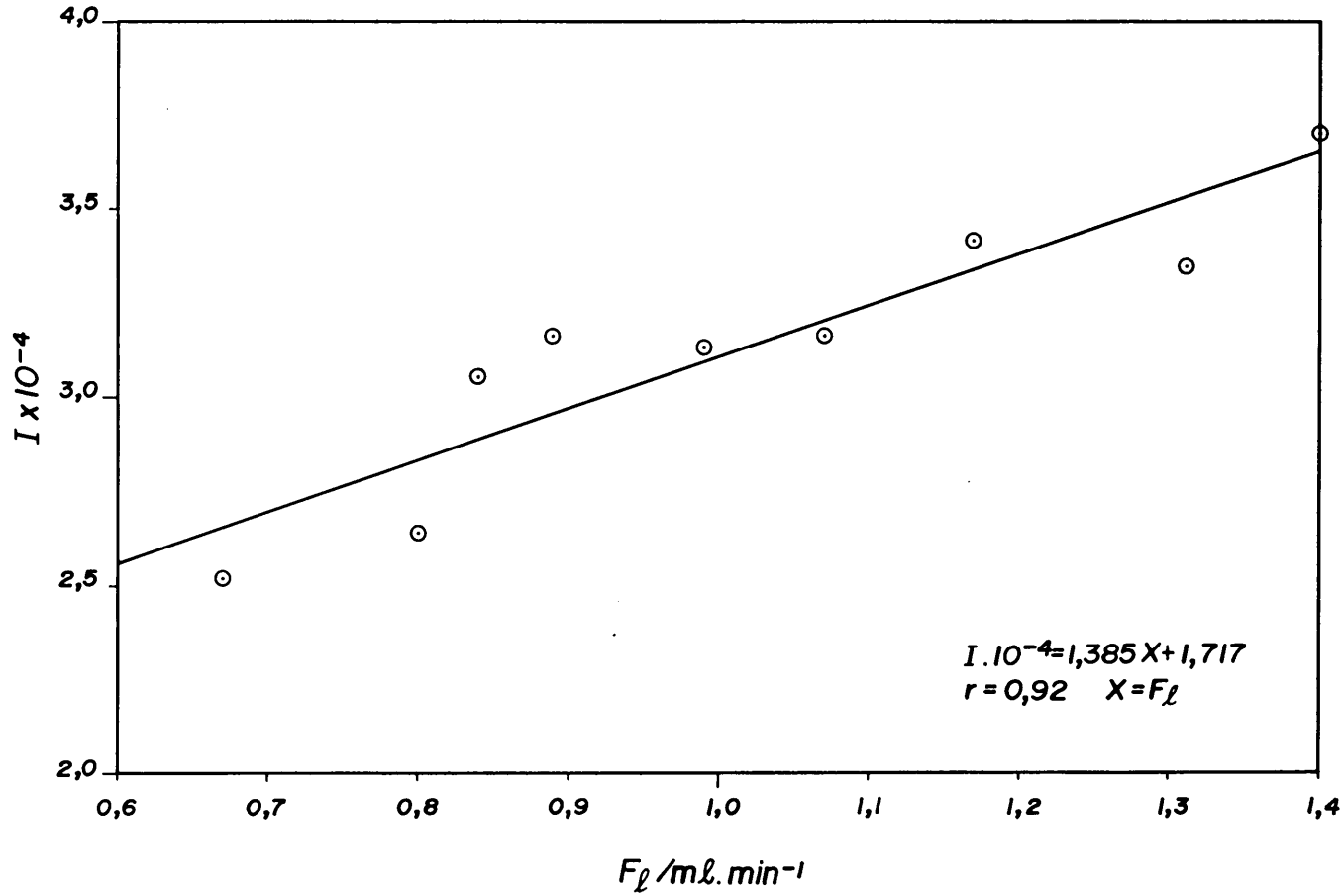


Figure 4-7: Effect of aspiration rate ($F_\ell$/mℓ.min$^{-1}$) on net emission intensity (I) of Mn (II) 257,61 nm at attenuator setting 3. A least squares linear regression gave a correlation coefficient r, of 0,92.

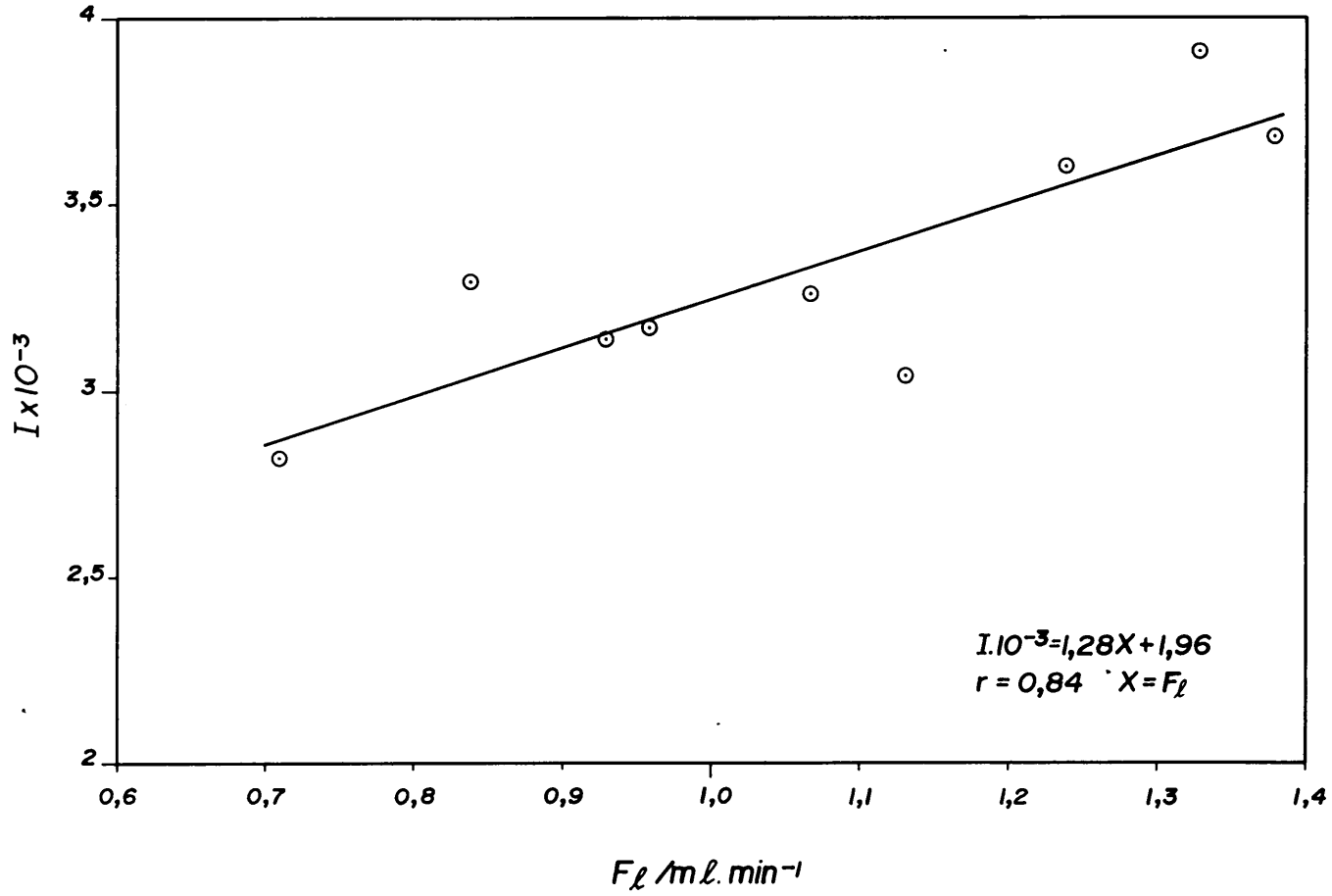


Figure 4-8: Effect of aspiration rate ($F_\ell$) on net emission intensity (I) of Mn (II) 294,92 nm at attenuator setting 3. A least squares linear regression gave a correlation coefficient r, of 0,84.

$$I_{257} \cdot 10^{-4} = 1,38.F_{\ell} + 1,72 \quad \ldots\ldots\ldots \quad (41)$$

where $I_{257}$ = net intensity of Mn 257,61 nm for 5 s integration time at attenuator setting 3,

and $F_{\ell}$ = aspiration rate*.

For Mn(II) 294,92 nm the relationship is;

$$I_{294} \cdot 10^{-3} = 1,28.F_{\ell} + 1,96 \quad \ldots\ldots\ldots \quad (42)$$

where $I_{294}$ = net intensity of Mn 294,92 nm for 5 s integration time at attenuator setting 3,

and $F_{\ell}$ = aspiration rate*,

with a correlation coefficient, r, of 0,84.

Using values for the product, gA of $80 \times 10^{8}$ $s^{-1}$ for Mn(II) 257,61 nm and $66 \times 10^{8}$ $s^{-1}$ for Mn(II) 294,92 nm (Rezaaiyaan and Hieftje, 1985), together with the relevant excitation potentials (Table 4-4); an expression for temperature may be obtained using equation 39 and substituting the expressions for $I_{257}$ and $I_{294}$ from equations 41 and 42, in an analagous fashion as calculated for the atomic line pair previously.

---

* The constants in equations 41 and 42 are applicable if $F_{\ell}$ is measured as $m\ell.min^{-1}$.

TABLE 4-7: Emission intensity data for Mn(II) 257,61 nm on ARL 3510 spectrometer at a concentration of 10 mg.$\ell^{-1}$. An attenuator setting of 3 was used with 27 x 5 s integrations.*

| $F_\ell$/mℓ.min$^{-1}$** | $\bar{I}_{gross}$ | σ | RSD% | $\bar{I}_{blank}$ | σ | RSD% | $\bar{I}_{net}$ | DL(2σ)/mg.$\ell^{-1}$ |
|---|---|---|---|---|---|---|---|---|
| 0,67 | 25600 | 332 | 1% | 416 | 2 | 0,5% | 25180 | 0,002 |
| 0,80 | 26810 | 744 | 3% | 424 | 6 | 1,4% | 26390 | 0,005 |
| 0,84 | 30910 | 550 | 2% | 424 | 4 | 0,9% | 30490 | 0,003 |
| 0,89 | 31990 | 283 | 1% | 441 | 16 | 3,6% | 31550 | 0,010 |
| 0,99 | 31710 | 439 | 1% | 411 | 3 | 0,7% | 31300 | 0,002 |
| 1,07 | 31980 | 505 | 2% | 410 | 3 | 0,7% | 31570 | 0,002 |
| 1,17 | 34510 | 1350 | 4% | 406 | 4 | 1,0% | 34100 | 0,002 |
| 1,31 | 33880 | 819 | 2% | 411 | 3 | 0,7% | 33470 | 0,002 |
| 1,40 | 37430 | 882 | 2% | 412 | 6 | 1,5% | 37020 | 0,003 |

* rf Power at 1200 watt; $\bar{I}_{gross}$ = mean gross analyte intensity; $\bar{I}_{blank}$ = mean blank intensity; $\bar{I}_{net}$ = mean net analyte intensity; σ = standard deviation; RDS% = relative standard deviation percent; DL = detection limit; Mn concentration 10 mg.$\ell^{-1}$. The Mn(II) 257,61 nm line is the emission line of manganese employed in routine analysis of water samples, and shows the best precision of the lines tested (Table 4-4).

** $F_\ell$ : aspiration rate (liquid uptake rate).

TABLE 4-8: Emission intensity data for Mn(II) 294,921 nm on ARL 3510 spectrometer at a concentration of 10 mg.$\ell^{-1}$. An attenuator setting of 3 was used with 27 x 5 s integrations.*

| $F_\ell$/mℓ.min$^{-1}$** | $\overline{I}_{gross}$ | σ | RSD% | $\overline{I}_{blank}$ | σ | RSD% | $\overline{I}_{net}$ | DL(2σ)/mg.$\ell^{-1}$ |
|---|---|---|---|---|---|---|---|---|
| 0,71 | 3164 | 87 | 3% | 342 | 3 | 0,9% | 2820 | 0,02 |
| 0,84 | 3629 | 82 | 2% | 343 | 2 | 0,6% | 3290 | 0,01 |
| 0,93 | 3486 | 86 | 2% | 341 | 2 | 0,6% | 3140 | 0,01 |
| 0,97 | 3510 | 97 | 3% | 341 | 2 | 0,6% | 3170 | 0,01 |
| 1,07 | 3571 | 92 | 3% | 312 | 2 | 0,6% | 3260 | 0,01 |
| 1,13 | 3377 | 103 | 3% | 342 | 2 | 0,6% | 3040 | 0,01 |
| 1,24 | 3937 | 151 | 4% | 340 | 2 | 0,6% | 3600 | 0,01 |
| 1,33 | 4259 | 112 | 3% | 345 | 2 | 0,6% | 3910 | 0,01 |
| 1,38 | 4023 | 162 | 4% | 343 | 3 | 0,9% | 3680 | 0,02 |

* rf Power at 1200 watt; $\overline{I}_{gross}$ = mean gross analyte intensity; $\overline{I}_{blank}$ = mean blank intensity; $\overline{I}_{net}$ = mean net analyte intensity; σ = standard deviation; RDS% = relative standard deviation percent; DL = detection limit; Mn concentration 10 mg.$\ell^{-1}$. The Mn(II) 294,921 nm line is a weak ion line with poorer precision than the Mn(II) 257,61 nm line (Table 4-7).

** $F_\ell$ : aspiration rate (liquid uptake rate).

The expression for excitation temperature ($T_{exc}$) for the manganese ionic line pair is:

$$T_{exc} = \frac{6501}{\ln 1{,}388 - \ln (I_{257}/I_{294})} \qquad \ldots\ldots\ldots \quad (43)$$

where $\frac{I_{257}}{I_{294}} = \frac{13{,}8.F_{\ell} + 17{,}2}{1{,}28.F_{\ell} + 1{,}96}$ from 41 & 42.

A plot of the function for $T_{exc}$ is shown in Figure 4-9. This shows a decrease in common excitation temperature for the Mn(II) ion lines from 3400 K at 0,7 $m\ell.min^{-1}$ aspiration rate to around 3300 K at 1,4 $m\ell.min^{-1}$ aspiration rate. This result is quite different from the temperature found for the Mn(I) atomic line pair of between 5500 and 6000 K (Figure 4-6), demonstrating the lack of LTE in the low power argon plasma. The finding of a lower temperature for ion line excitation than for atomic line excitation also implies departure from a Boltzmann distribution of energies.

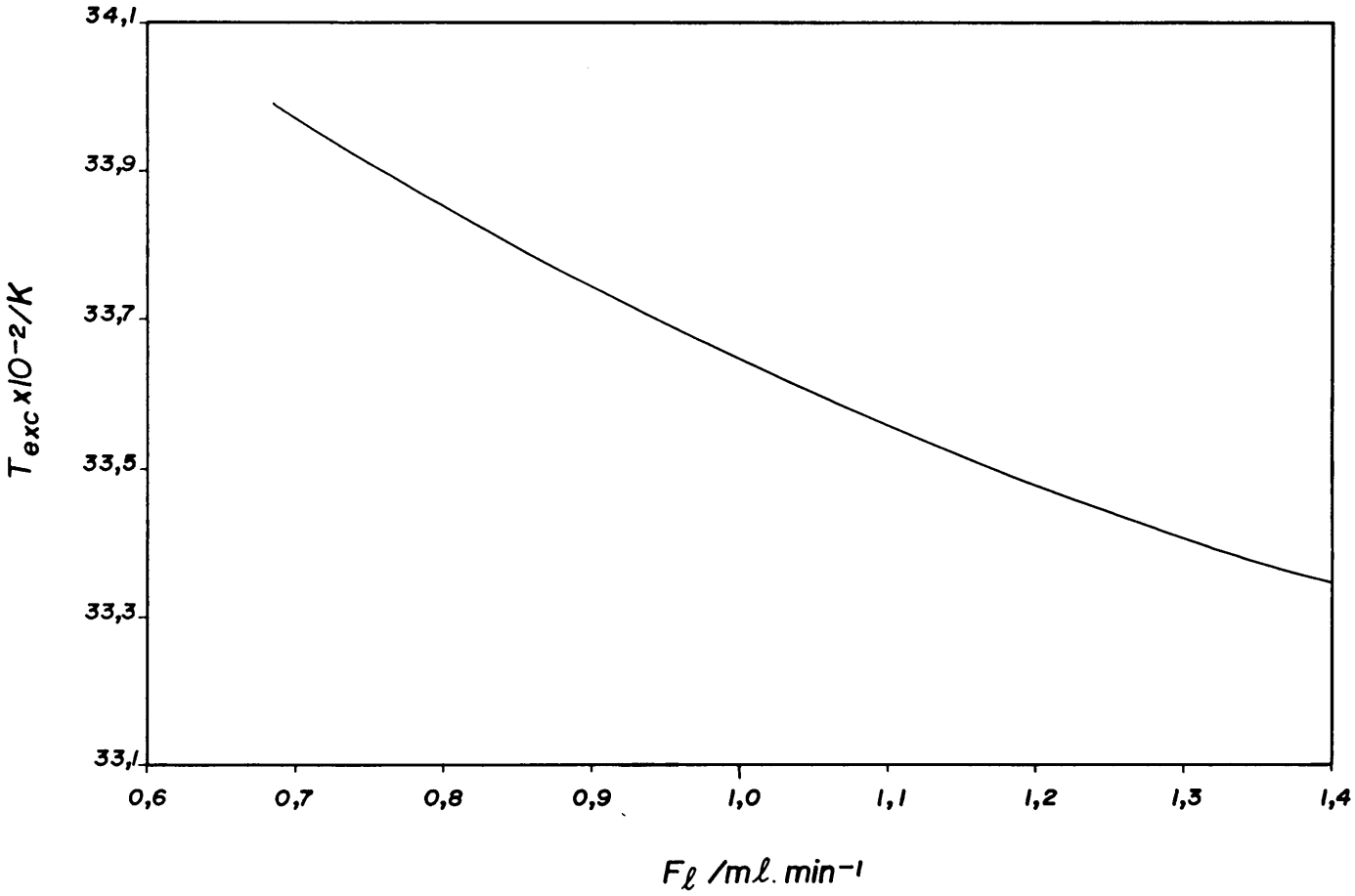


Figure 4-9: Variation of excitation temperature ($T_{exc}$) for the Mn 257/295 nm ion line pair with aspiration rate ($F_\ell$), as plotted from equation 43.

## 4.4 Dependence of degree of ionization on plasma temperature

In the use of ICP emission spectrometry as an analytical technique, it is important that plasma temperatures should remain invariant, as temperature has a direct effect on the ionization equilibrium constant as expressed by the Saha equation (7) as given in Chapter 2.

By substituting the values for the physical constants (Wehr and Richards, 1964), equation 7 may be written in practical form as;

$$K_i = 4{,}829\times10^{15}.T^{3/2}.\ \frac{Z_i}{Z_a}\ .\ e^{(-1{,}161\times10^{4}V_i)/T} \quad \ldots\ldots\ (44)$$

where $K_i$ = ionization equilibrium constant as number density, $cm^{-3}$,

$T$ = temperature,

$Z_i$ = partition function of ion.

$Z_a$ = partition function of atom,

and $V_i$ = ionization potential, as eV.

using the conversion factor 1eV = $1{,}602\times10^{-12}$ erg to convert ionization potential in erg to ionization potential in electron volts, or 1 eV = $1{,}602\times10^{-19}$ J to convert from ionization potential in Joule to ionization potential in electron volts.

The Saha equation as given e.g., by Boumans, (a),(1966) or L'Vov, (b),(1970) at first sight looks quite different from the form given by equation 7; the former containing the term $T^{5/2}$ instead of the term $T^{3/2}$ as given by equation 7. It may be readily shown, however, that the two forms are essentially identical, bearing in mind that the ionization equilibrium constant is defined in partial pressure (atmosphere) units by Boumans, (b),(1966) and L'Vov, (b),(1970), whereas Kornblum (1977) uses units of number density ($cm^{-3}$) for $K_i$. From the ideal gas equation and the definition of Boltzmann's constant (Moore, 1966) it follows that;

$$K_i = \left( \frac{S.\dagger}{T.k} \right) \qquad \ldots\ldots\ldots\ldots\ldots\ldots \quad (45)$$

where $K_i$ = ionization constant as $cm^{-3}$,

$S$ = ionization constant in atm,

$T$ = temperature,

$k$ = Boltzmann's constant as erg. $K^{-1}$,

and the factor $\dagger$ = 1,0133 x $10^6 cm^{-3}.atm^{-1}.erg$, is to convert pressure in atm., to $dyne.cm^{-2}$ (Wehr and Richards, 1964).

If equation 44 is applied to the ionization of manganese, by substituting the values for the partition functions $Z_i$ and $Z_a$ of 8,4 and 6,9 respectively (Boumans, (c),1966), together with a value for the ionization potential of Mn of 7,432 eV (Zaidel' et al, 1970) the result is:

$$K_{Mn} = 5,879 \times 10^{15} . T^{3/2} . e^{(-8,629 \times 10^{4}/T)} \quad \ldots\ldots\ldots\ldots \quad (46)$$

where $K_{Mn}$ = ionization equilibrium constant for manganese in $cm^{-3}$,

and T = temperature.

If the assumption of LTE is made, i.e., that the inequality (9) of Chapter 2 becomes an equality, with the temperature of the atomic and ionic species being identical, then a temperature value found by the two-line method (Figure 4-6) may be substituted in equation 46 and the value of $K_{Mn}$ calculated. For instance, at an aspiration rate of 1,2 $m\ell.min^{-1}$ the temperature derived by the two-line method for atomic manganese was $6 \times 10^{3}$ K (Figure 4-6). Substituting this value in equation 46 gives a $K_{Mn}$ value of $1,55 \times 10^{15} cm^{-3}$. Substituting this value for the ionization constant in equation 6 (Chapter 2), together with a representative value for electron number density in the conventional torch of $1,6 \times 10^{15} cm^{-3}$ (Rezaaiyaan and Hieftje, 1985), the degree of ionization of manganese, $\beta i$ is 0,49:

$$\beta_i = 1 - \frac{[e^-]}{[e^-] + K_{Mn}}$$

$$= 1 - 0,51$$

$$= 0,49$$

thus approximately half of the manganese atoms have been ionized.

If we consider the effect on manganese ionization of a temperature 100° lower i.e., 5900 K, then calculating as above, the ionization constant $K_{Mn}$ is $1,18x10^{15}cm^{-3}$ and the degree of ionization 0,42. Thus for a decrease in temperature from $6x10^{3}$ K to $5,9x10^{3}$ K, the degree of ionization of manganese decreases by 14%!

While calculations of this type may be criticised becasue of the lack of LTE in the argon plasma, they nevertheless assist in gaining insight into the behaviour of the source, illustrating in this instance how slight change in plasma temperature may result in marked change in ionic/atomic partition ratios and consequently in the observed analytical emission line intensity of a given ionic or atomic transition.

If the exercise of calculating the ionization equilibrium constant $K_i$ from the Saha equation (44) is repeated using the temperature of around 3350 K obtained for excitation of the Mn (II) lines (Figure 4-9) assuming the partition functions do not change significantly from the values given for Mn at 5000 K by Boumans, (c),(1966) of 7,7 for $Z_i$ and 6,4 for $Z_a$; a $K_i$ value of $7,3x10^{9}cm^{-3}$ is obtained, From this value for $K_i$, using equation 6, the degree of ionization $\beta_i$, is calculated as $4,9x10^{-6}$ i.e., practically none of the Mn atoms are ionized!. This is obviously an untenable conclusion in view of the observed

intensities of ionic manganese lines and implies that the assumption of local thermodynamic equilibrium on which both the temperature calculation and calculation of the ionization constant from the Saha equation are based, does not hold under the observed source conditions.

Great deviation from LTE conditions in the low-power ICP is also found in the low-flow, low-power ICP (Rezaaiyaan and Hieftje, 1985). The magnitude of this deviation from equilibrium conditions places a large question mark on the meaning of temperatures for species derived from the Boltzmann or Saha equations in the pure argon plasma.

## 4.5 Excitation temperature and degree of ionization of zinc

The common excitation temperature of the Zn (I) 307,59 nm and Zn (I) 328,23 nm line pair was determined in an analagous manner to that employed for manganese in Section 4.3. The filter normally used for wavelengths above 320nm on the ARL 3510 spectrometer (Table 4-1) was removed from the light path to avoid the possibility of reduction of the intensity of the Zn 328,23 nm line. The net intensity of the atomic line zinc pair at an aspiration rate of 0,83 $m\ell.min^{-1}$ and 1,63 $m\ell.min^{-1}$ is given in Table 4-9. The calculated excitation temperature, ionization constant and degree of ionization are given in Table 4-11, using the values for excitation potential and transition probability from Table 4-10, and equations 39, 50 and 6 respectively.

The excitation temperature found for atomic zinc emission at an aspiration rate of around 0,8 $m\ell.min^{-1}$ is several hundred K higher than that for atomic manganese emission (Figure 4-6). The mean excitation potential of the zinc line pair is 5,9 eV as compared to a mean excitation potential for the manganese atomic line pair of 4,14 eV (Table 4-4). The difference in excitation temperatures of atomic line pairs of these two elements is in keeping with the observation of De Galan (1984) that the excitation tempterature is greater for higher energy states than for

lower energy states. The degree of ionization for Zn of less than 10% (Table 4-11) is to be expected from the high 1st ionization potential of 9,39eV (Zaidel' et al, 1970), although this is probably underestimated due to the departure from LTE and the tendency of higher energy and ionic states to be overpopulated in excess of the degree of ionization expected from the Saha equation.

TABLE 4-9: Net intensities of the Zn 307,59 nm and Zn 328,23 nm atomic lines versus aspiration rate, $F_\ell$ for 30x5 s integrations at attenuator setting of 12 on the ARL 3510 spectrometer. Intensities given as mean ± std., deviation. Blank solution was $\phi$ = 0,01 nitric acid and concentration of zinc standard 100 $mg.\ell^{-1}$.

| $F_\ell/m\ell.min^{-1}$: | 0,83 | 1,63 |
|---|---|---|
| Zn(I) 307,59 nm | 15800 ± 300 | 38900 ± 1500 |
| Zn(I) 328,23 nm | 25100 ± 640 | 45800 ± 1300 |
| $I_{307}/I_{328}$* | 0,63 ± 0,02 | 0,85 ± 0,04 |

* ratio of intensity of Zn 307,59 nm line to that of the 328,23 nm line.

TABLE 4-10: Excitation potential and the product of transition probability and statistical weight data for the Zn 307,59 and Zn 328,23 nm line pair.

| Emission line, λ/nm | [a] $V_{exc}/eV$ | [b] $gA/s^{-1}$ |
|---|---|---|
| Zn(I)307,59 | 4,03 | $3,15x10^5$ |
| Zn(I)328,23 | 7,78 | $5,76x10^8$ |

(a) Excitation potentials from Zaidel' et al, (1970)
(b) Product of upper statistical weight (g) and transition probability (A), from Kornblum (1977).

**TABLE 4-11:** Common excitation temperature, $T_{exc}$/K for the Zn 307,59; Zn 328,23 nm line pair, together with the ionization equilibrium constant, $K_{Zn}/cm^{-3}$ and degree of ionization $\beta$, assuming LTE at two aspiration rates, $F_\ell$, on the ARL 3510 spectrometer.

| $F_\ell/m\ell.min^{-1}$: | 0,83 | 1,63 |
|---|---|---|
| $T_{exc}$/K [a] | 6230 ± 30 | 5980 ± 40 |
| $K_{Zn}/cm^{-3}$ [b] | $1,2x10^{14}$ $\pm 0,1x10^{14}$ | $5,4x10^{13}$ $\pm 0,7x10^{13}$ |
| $\beta$ [c] | 0,070 ±0,005 | 0,033 ±0,004 |

(a) Using equation 39 and the data for gA and excitation potential from Table 4-10, and the intensity ratio data from Table 4-9.

(b) Using equation 44 and assuming LTE, with Zi = 2,0 and Za = 1,0 at $6x10^3$ K (Boumans, (c),1966), and an ionization potential for zinc of 9,391 eV (Zaidel' et al, 1970).

(c) Using equation 6 and assuming an electron number density of $1,6x10^{15}.cm^{-3}$.

Ionic zinc emission is readily detected e.g., the Zn (II) 206,191 nm line gave a net emission intensity of $2,03x10^4$ with an RSD of 2,5% for 10 $mg.\ell^{-1}$ Zn at an attenuator setting of 9; 5 s integration time and 0,80 $m\ell.min^{-1}$ aspiration rate, other parameters being those of the compromise operating conditions on the ARL 3510 spectrometer (Table 4-3). The intensity of the Zn(II) 206,191 nm ion line, bearing in mind the attenuator setting and concentration of zinc, is considerably greater than that observed for the Zn(I) lines (Table 4-9), which is somewhat unexpected considering the low degree of ionization of zinc (Table 4-11). This example clearly illustrates the high intensity of ion line emission from an ICP source i.e., the overpopulation of upper energy states and ionic states.

Kornblum (1977) observing intensities at different lateral co-ordinates followed by application of the Abel inversion technique to obtain radial intensities, found the common excitation temperature of the Zn 307,59/Zn 328,23 nm line pair to vary from around $4x10^3$ K at the axis of the plasma to around $8x10^3$ K at a radial co-ordinate of 5 mm, using the two-line method. The application of the two-line method to net intensity data integrated over the depth of the plasma as done here, provides a mean excitation temperature. As, however, depth integrated mean intensities are employed in routine ICP spectrometric

analysis of real samples, the behaviour of the mean as opposed to the temperature at specific radial coordinate positions is of interest in this work. Radial coordinate temperatures would be of interest in investigating the cause and mechanisms of the observed effects, but the analytical behaviour of depth integrated intensities/ temperatures is of obvious interest in practical analytical applications.

## 4.6 Effect of rf generator input voltage on emission intensities

As the ARL 34000 spectrometer was fitted with separate Watford stabilizers on the voltage supply to the generator and spectrometer, this provided an ideal opportunity to study the effect of input voltage change on the ICP source and measuring electronics separately. Each Watford stabilizer ensures that the mains voltage supply is stabilized to within 0,5% i.e., 220 $\pm$ 1 volt. The output voltage from each stabilizer may be changed independently with a potentiometer.

In this experiment the voltage input to the rf generator was set at values between 206 V and 221 V, the value being measured with a digital readout voltmeter (Gould Alpha III), and the effect on the net signal intensity for 20 elements recorded (Table 4-12). The concentrations of the

four groups of mixed standards used are as given in Table 5-1, for mixed standard sets 1 to 4. Apart from this variation of the rf generator input voltage, the instrumental operation conditions were the compromise conditions normally used for analysis (Table 4-3).

Despite the decrease in input voltage from 221 V to 206 V i.e., a decrease of 6,8%, no change in incident power or reflected power was observed on the meters of the rf generator. Nevertheless the blank intensities of 14 of the 20 elements tested showed significantly lower blank intensities at 206 V as compared to 221 V as determined with a t-test (Table 4-13). This may be taken as evidence that a change in incident rf power to the ICP torch did indeed occur.

TABLE 4-12: Effect of input voltage to rf generator of ARL 34000 spectrometer on net signal intensity (mean ± std., dev.) of the mixed calibration standards for 5x10 s integrations.

| Input voltage/V: | | 206 | 211 | 216 | 221 |
|---|---|---|---|---|---|
| Group | | | | | |
| | Ba* | 1709± 14 | 1724± 5 | 1730± 5 | 1729± 4 |
| | Ca | 2295± 9 | 2368±11 | 2344±11 | 2446±16 |
| 1 | K | 575± 6 | 568± 3 | 563± 2 | 565± 8 |
| | Mg | 3814± 14 | 3846± 8 | 3900± 9 | 3886± 8 |
| | Na | 917± 6 | 909± 2 | 907± 4 | 905± 7 |
| | Cr | 639± 4 | 657± 4 | 660± 6 | 679± 2 |
| | Cu | 196,6±0,5 | 197,8±0,7 | 193,9± 3 | 194,7±0,7 |
| 2 | Fe | 966± 5 | 988± 4 | 989± 9 | 1013± 2 |
| | Mn | 3047± 19 | 3117±15 | 3112±29 | 3207± 9 |
| | Zn | 1098± 3 | 1124± 2 | 1135±11 | 1157± 2 |
| | Be | 9031±140 | 9221±48 | 9386±10 | 9470±13 |
| | Cd | 708± 18 | 727± 9 | 741± 2 | 749± 3 |
| 3 | Mo | 332± 27 | 360± 4 | 364± 1 | 367± 2 |
| | Ti | 2635± 66 | 2696±32 | 2733± 7 | 2754±13 |
| | V | 1048± 27 | 1074±13 | 1091± 3 | 1100± 5 |
| | Al | 77,7±0,3 | 78,1±0,3 | 77,7±0,2 | 77,9±0,5 |
| | Co | 390± 2 | 390± 4 | 388± 1 | 390± 1 |
| 4 | Ni | 320± 1 | 320± 2 | 317± 1 | 318± 1 |
| | Pb | 13,2±0,1 | 13,2±0,1 | 13,2±0,1 | 13,3±0,1 |
| | Sr | 1564± 17 | 1545±26 | 1537± 5 | 1536± 9 |

* Analytical wavelengths shown in Table 4-2

TABLE 4-13: Change in blank (nitric acid, $\phi$ = 0,01) intensity between 221 V and 206 V input voltage to rf generator of analyte channel readout on ARL 34000 spectrometer for 5x10 s., integrations [a].

| Group | | $I_b$,206 V | $I_b$,221 V | $\Delta I_b$ | t-test value |
|---|---|---|---|---|---|
| | Ba** | 2,2 ±0,1 | 2,18±0,01 | −0,02±0,10 | − 0,44 |
| | Ca | 27,4 ±0,2 | 27,60±0,01 | 0,20±0,20 | 2,23 |
| 1 | K | 39,1 ±0,2 | 39,8 ±0,1 | 0,70±0,22 | * 7,00 |
| | Mg | 8,3 ±0,3 | 8,40±0,01 | 0,10±0,30 | 0,74 |
| | Na | 8,54±0,04 | 8,66±0,04 | 0,12±0,06 | * 4,74 |
| | Cr | 46,8 ±0,2 | 49,4 ±0,3 | 2,6±0,4 | *16,1 |
| | Cu | 4,87±0,01 | 5,08±0,01 | 0,21±0,01 | *33,2 |
| 2 | Fe | 2,67±0,02 | 2,71±0,01 | 0,04±0,02 | * 4,00 |
| | Mn | 7,05±0,06 | 7,09±0,08 | 0,04±0,10 | 0,89 |
| | Zn | 51,6 ±0,3 | 54,2 ±0,04 | 2,6 ±0,5 | *11,6 |
| | Be | 48,6 ±0,2 | 51,3 ±0,2 | 2,7 ±0,3 | *21,3 |
| | Cd | 60,9 ±0,4 | 64,1 ±0,1 | 3,2 ±0,4 | *17,4 |
| 3 | Mo | 48,3 ±0,1 | 50,6 ±0,2 | 2,3 ±0,2 | *23,0 |
| | Ti | 30,9 ±0,1 | 32,9 ±0,1 | 2,0 ±0,1 | *31,6 |
| | V | 45,4 ±0,1 | 47,2 ±0,1 | 1,8 ±0,1 | *28,5 |
| | Al | 2,71±0,07 | 2,76±0,03 | 0,05±0,08 | 1,47 |
| | Co | 18,0 ±0,2 | 18,57±0,02 | 0,57±0,2 | * 6,34 |
| 4 | Ni | 13,2 ±0,1 | 13,62±0,05 | 0,42±0,1 | * 8,40 |
| | Pb | 3,55±0,04 | 3,59±0,03 | 0,04±0,05 | 1,79 |
| | Sr | 4,10±0,05 | 4,22±0,01 | 0,12±0,05 | * 5,26 |

(a) $I_{b,x\ V}$ = blank intensity at x volt input to rf generator; $\Delta I_b$ = difference in blank intensity.

* Significant at 1% level (two-tailed test with pooled variance and 8 degrees freedom; t-critical = 3,36).

** Analytical wavelengths shown in Table 4-2.

The net intensity data for the mixed standards (Table 4-12) was normalized into percent change in intensity relative to the signal at 221 V using the formula:

$$\bar{I} = \frac{\bar{I}_a}{\bar{I}_b} \cdot 100 \pm \frac{100}{\bar{I}_b^{\,2}} \cdot \left( \bar{I}_b^{\,2} \cdot \sigma_a^2 + \bar{I}_a^{\,2} \cdot \sigma_b^2 \right)^{1/2} \quad \ldots \quad (47)$$

where $\bar{\bar{I}}$ = normalised net intensity at voltage a, as a percent of net intensity at voltage b, given as mean $\pm$ std., deviation,

$\bar{I}_a$ = mean net intensity at voltage a,

$\bar{I}_b$ = mean net intensity at voltage b,

$\sigma_a$ = std., deviation of mean of net intensity at voltage a,

$\sigma_b$ = std., deviation of mean of net intensity at voltage b.

The normalised percent net intensity data is given in Table 4-14.

The equation for std., deviation of a ratio of two values, as a function of the individual std., deviations (47) was derived from the formula for the theory of errors for the general function as given by Eckschlager (1969) and Sachs (1982). Note that the specific formula for the std., deviation of a quotient in both these references contain misprints, with either subscripts or power terms omitted or incorrect.

TABLE 4-14: Effect of input voltage of rf generator of ARL 34000 spectrometer on net signal intensity (mean ± std., dev.) expressed as a percentage of the signal at 221 volts, taken as 100%.

| Input voltage/V: | | 206 | 211 | 216 |
|---|---|---|---|---|
| Group | | | | |
| | Ba** | 98,8±0,8% | 99,7±0,4% | 100,0±0,4% |
| | Ca | * 93,8±0,7% | * 96,8±0,8% | *95,8±0,8% |
| 1 | K | 102 ±2% | 101 ±2% | 100 ±1% |
| | Mg | * 98,1±0,4% | * 99,0±0,3% | 100,4±0,3% |
| | Na | 101 ±1% | 100,4±0,8% | 100,2±0,9% |
| | Cr | * 94,1±0,6% | * 96,8±0,6% | *97,2±0,9% |
| | Cu | *101,0±0,4% | *101,6±0,5% | 99,6±1,6% |
| 2 | Fe | * 98,3±0,5% | * 97,5±0,4% | *97,6±0,9% |
| | Mn | * 95,0±0,6% | * 97,2±0,5% | *97,0±0,9% |
| | Zn | * 94,9±0,3% | * 97,1±0,2% | *98,1±1,0% |
| | Be | * 95,4±1,5% | * 97,4±0,5% | * 99,1±0,2% |
| | Cd | * 94,5±2,4% | * 97,1±1,3% | * 98,9±0,5% |
| 3 | Mo | 90,5±7,4% | * 98,1±1,2% | 99,2±0,6% |
| | Ti | * 95,7±2,4% | * 97,9±1,2% | 99,2±0,5% |
| | V | * 95,3±2,5% | * 97,6±1,3% | * 99,2±0,5% |
| | Al | 99,7±0,7% | 100,3±0,7% | 99,7±0,7% |
| | Co | 100,0±0,6% | 100,0±1,0% | 99,5±0,4% |
| 4 | Ni | 100,6±0,4% | 100,6±0,7% | 99,7±0,4% |
| | Pb | 99,2±1,1% | 99,2±1,1% | 99,2±1,1% |
| | Sr | 101,8±1,2% | 100,6±1,8% | 100,1±0,7% |

* Significant t at the $\alpha$ = 1% level.
(See Table 4-15 for |t| values).
** Analytical wavelengths of elements listed shown in Table 4-2.

TABLE 4-15: Modulus of t-values for comparison of net signal at different input voltages to rf generator of ARL 34000 spectrometer with signal at 221 volt input, of the data given in Table 4-13[a].

| Input voltage/V: | | 206 | 211 | 216 |
|---|---|---|---|---|
| Group | | | | |
| | Ba[b] | ° 3,07 | 1,75 | 0,35 |
| | Ca | *18,4 | * 8,98 | *11,7 |
| 1 | K | 2,24 | 0,78 | 0,54 |
| | Mg | * 9,98 | * 7,91 | ° 2,60 |
| | Na | ° 2,91 | 1,23 | 0,56 |
| | Cr | *20,0 | *11,0 | * 6,72 |
| | Cu | * 4,94 | * 7,00 | 0,58 |
| 2 | Fe | *19,5 | *12,5 | * 5,82 |
| | Mn | *17,0 | *11,5 | * 7,00 |
| | Zn | *36,6 | *26.1 | * 4,40 |
| | Be | * 6,98 | *11,2 | *11,4 |
| | Cd | * 5,02 | * 5,18 | * 4,96 |
| 3 | Mo | ° 2,89 | * 3,50 | ° 3,00 |
| | Ti | * 3,96 | * 3,75 | ° 3,18 |
| | V | * 4,23 | * 4,17 | * 3,45 |
| | Al | 0,77 | 0,77 | 0,83 |
| | Co | 0,0 | 0,0 | ° 3,16 |
| 4 | Ni | ° 3,16 | 2,00 | 1,58 |
| | Pb | 1,58 | 1,58 | 1,58 |
| | Sr | ° 3,25 | 0,73 | 0,22 |

* Significant at 1% level ° Significant at 5% level

(a) t-critical = 3,36 for two-tailed t-test at 1% significance level for 8 degrees of freedom (pooled variance form of t-test). The critical value for 5% significance is 2,31.

(b) Analytical wavelengths of elements listed shown in Table 4-2.

The significance of the difference in observed net intensities of the data in Table 4-12 was determined by use of the t-test statistic with pooled variance and 2n-2 degrees of freedom (Green and Margerison, (a), 1978). The |t| values of this comparison are given in Table 4-15.

A perusal of Table 4-14 shows that the analytical channels for elements whose emission is readily excited, such as Na or K showed little change; whereas for elements such as Cr, Mo or Zn, with high excitation potentials, greater change in emission intensity was observed. This observation raised the question as to whether a correlation, if any, was present between change in emission intensity and excitation potential of the associated quantum level.

To investigate this hypothesis, the normalized intensities at 206V input power were tabulated together with excitation potentials (Table 4-16).

TABLE 4-16: Net intensity at 206 volt ($I_{206}$) rf input voltage as a percentage of intensity at 221 volt (from Table 4-14), with analytical channel wavelengths and excitation potentials (Zaidel' et al, 1970).

| Analytical channel, λ/nm | $I_{206}$ | $V_{exc}$/eV |
|---|---|---|
| Ba(II)455,404nm | ° 98,8% | 2,72 |
| Ca(II)315,887nm | * 93,8% | 7,05 |
| K (I) 766,490nm | 102, % | 1,62 |
| Mg(I) 383,829nm | * 98,1% | 5,94 |
| Na(I) 588,995nm | °101, % | 2,11 |
| Cr(II)267,716nm | * 94,1% | 6,18 |
| Cu(I) 327,396nm | *101,0% | 3,78 |
| Fe(II)259,940nm | * 98,3% | 4,77 |
| Mn(II)257,610nm | * 95,0% | 4,81 |
| Zn(I) 213,856nm | * 94,9% | 5,80 |
| Be(I) 234,861nm | * 95,4% | 5,28 |
| Cd(II)226,502nm | * 94,5% | 5,47 |
| Mo(II)281,615nm | ° 90,5% | 6,06 |
| Ti(II)334,940nm | * 95,7% | 3,74 |
| V (II)311,071nm | * 95,3% | 4,33 |
| Al(I) 396,152nm | 99,7% | 3,14 |
| Co(I) 340,512nm | 100,0% | 4,07 |
| Ni(I) 352,454nm | °100,6% | 3,54 |
| Pb(I) 368,347nm | 99,2% | 4,34 |
| Sr(II)421,552nm | °101,8% | 2,94 |

* = Significant at 1% level (two-tailed)
° = Significant at 5% level (two-tailed)

The linear correlation coefficient, r, was calculated between the normalised intensities and excitation potentials with the significance determined using equation 34 (Chapter 3). The results of this comparison are shown in Table 4-17 and illustrated graphically in Figure 4-10. The hypothesis was confirmed; there being an inverse correlation between the normalized intensity at 206 volt and the excitation potential. Sodium and potassium were not included in the correlations given in Table 4-17 and Figure 4-10, as their intensity readings correspond to a different observation height in the plasma viz., the tail flame (with the aid of fibre optics), rather than the 18 mm observation height of the other elements (see footnotes to Table 4-2).

While the inverse correlation between normalized signal and excitation potential was found to be significant at the 1% level (two tailed) for the atomic and ionic line data together (Table 4-17 (a), and Figure 4-10); significant correlations were also found for the atomic line data at the 10% level, and the ionic line data at the 5% level (Table 4-17(c), and (d) ). The correlation between the net normalized intensity of ionic lines at 206 volt rf generator input voltage and total excitation potential i.e., the first ionization potential plus the line excitation potential was also calculated, and a correlation

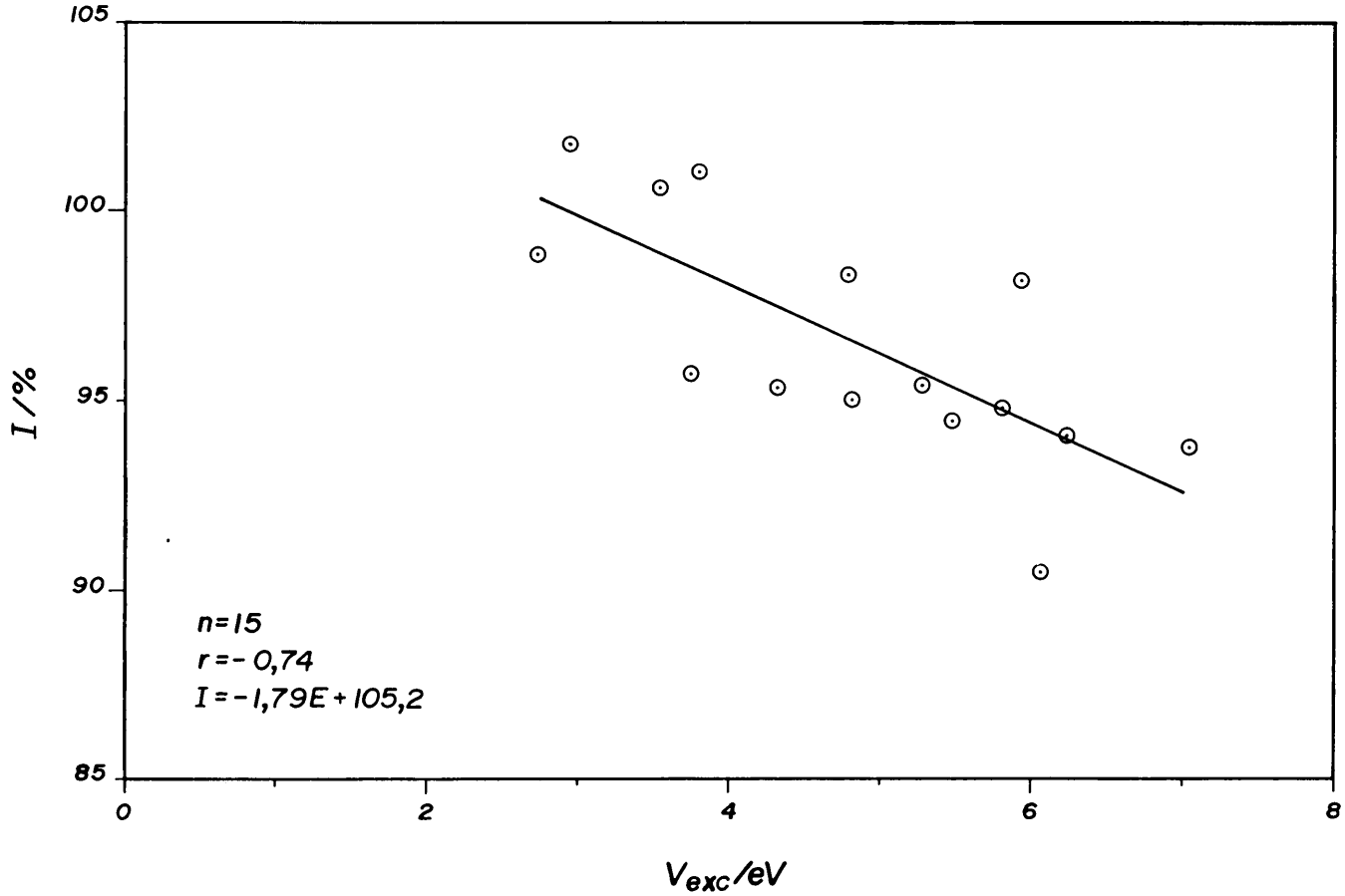


Figure 4-10: Relationship between excitation potential ($V_{exc}$) and net signal at 206 V rf input voltage expressed as a percentage of the signal at an rf input voltage of 221 V (I). The data points with a significance of 5% or better, except Na, plotted from Table 4-16.

coefficient value r of -0,735 (for n = 10) found. The correlation is poorer than the r value of -0,786 (for n = 10) found between the net normalized intensity and line excitation potential for ion lines (Table 4-17).

Eight analyte channels, viz., Ca, Cr, Fe, Mn, Zn, Be, Cd and V showed significant change in intensity at the 1% two-tailed significance level for a decrease of rf input voltage of only 2,3% i.e., a change in voltage from 221 V to 216 V (Table 4-14); the magnitude of the change in intensity being greatest for Ca (II) 315,887 nm, i.e., a 4,2% change in intensity. This implies that fluctuations in mains voltage supply to the rf generator may be an important source of error in routine ICP spectrometric analysis when stability of the input voltage supply is not assured.

The conclusion drawn from this experiment is that the emission intensity of analyte emission lines with associated high excitation potentials is more sensitive to changes in incident rf power than the intensity of analyte lines with associated lower excitation potentials at the compromise operating conditions used on the ARL 34000 spectrometer.

TABLE 4-17: Correlation between excitation potential /eV and net intensity at 206 volt rf generator input voltage as a percentage of intensity at 221 volt input (Table 4-16), using equation 34 to test significance.

(a) For all analyte channels (Table 4-16), except Na and K:
n = 18; r = -0,755; T = -4,61; $t_{critical}$ = 2,92 for $\alpha$ = 0,005.
$|T| > t_{crit.}$, i.e., correlation significant at 1% (two-tailed) level.

(b) For data with 5% or better significance (° and * in Table 4-16), except Na:
n = 15; r = -0,736; T = -3,92; $t_{critical}$ = 3,01 for $\alpha$ = 0,005.
$|T| > t_{crit.}$, i.e., correlation significant at 1% (two-tailed) level.

(c) For atomic line (I) data, except Na, with 5% or better significance (Table 4-16):
n = 5; r = -0,823; T = -2,51; $t_{critical}$ = 3,18 for $\alpha$ = 0,025.
$|T| < t_{crit.}$, i.e., correlation not significant at 5% (two-tailed) level. The correlation is, however, significant at 10% (two-tailed) level, with $t_{crit.}$ = 2,35.

(d) For ionic line (II) data with 5% or better significance (Table 4-16):
n = 10; r = -0,786; T = -3,60; $t_{critical}$ = 2,31 for $\alpha$ = 0,025
$|T| > t_{crit.}$, i.e., correlation is significant at 5% (two-tailed) level.

## 4.7 Effect of input voltage to ARL 34000 spectrometer on emission intensities.

The effect of input mains voltage to the ARL 34000 spectrometer itself was investigated by recording net intensity for mixed calibration standards 1 to 4 (Table 5-1) while the Watford stabilizer output to the spectrometer was set at 226 and 211 volt respectively (Table 4-18). The separate stabilizer on the rf generator ensured that source incident power did not change. In contrast to the effect of changing input voltage to the rf generator as discussed in Section 4.6, the effect of a 15 volt change in spectrometer input voltage was negligible (Table 4-18), no intensity difference being greater than 2,3%. The apparently significant change in Ca (II) 315,887 nm and Cd (II) 226,502 nm emission may possibly be due to slight change in aerosol gas flow rate during the experiment. As will be shown in Section 4.8, these two emission lines are particularly sensitive to change in aerosol gas flow rate.

The insensitivity of the measuring electronics to change in mains input voltage implies that the constant power supplies for the photomultiplier, attenuator and measuring circuits are stable, and reflect a higher state of the art than the rf generator electronics.

TABLE 4-18: Effect of input voltage to measuring electronics of ARL 34000 spectrometer on net signal intensity (mean ± std., deviation) of the mixed calibration stds. (Table 5-1) for 5x10 s integrations[a].

| Element | $I_{211}$ V | $I_{226}$ V | ΔI | % ΔI |
|---|---|---|---|---|
| Ba** | 1671 ± 6 | 1681 ± 7 | 10 | 0,6% |
| Ca | 4976 ± 5 | 5015 ± 15 | 39* | 0,8% |
| K | 309 ± 2 | 313 ± 3 | 4 | 1,3% |
| Mg | 3754 ± 22 | 3770 ± 21 | 16 | 0,4% |
| Na | 555 ± 3 | 560 ± 5 | 5 | 0,9% |
| Cr | 1477 ± 39 | 1502 ± 4 | 25 | 1,7% |
| Cu | 162,3± 0,6 | 162,4± 1,0 | 0,1 | 0,1% |
| Fe | 1938 ± 44 | 1970 ± 7 | 32 | 1,6% |
| Mn | 6590 ±170 | 6724 ± 21 | 152 | 2,3% |
| Zn | 2092 ± 42 | 2125 ± 8 | 33 | 1,6% |
| Be | 13250 ± 70 | 13300 ± 50 | 50 | 0,4% |
| Cd | 1747 ± 7 | 1780 ± 14 | 33* | 1,8% |
| Mo | 652 ± 33 | 666 ± 22 | 14 | 2,1% |
| Ti | 4021 ± 27 | 4047 ± 12 | 26 | 0,6% |
| V | 1730 ± 10 | 1745 ± 6 | 15 | 0,8% |
| Al | 64,4± 0,7 | 64,3± 0,4 | - 0,1 | -0,2% |
| Co | 413,0± 2,4 | 414,1± 2,3 | 1,1 | 0,3% |
| Ni | 283,6± 1,9 | 284,0± 1,6 | 0,4 | 0,1% |
| Pb | 14,3± 0,2 | 14,4± 0,1 | 0,1 | 0,7% |
| Sr | 1812 ± 10 | 1811 ± 7 | - 1 | -0,1% |

(a) $I_x$ V = net intensity at x volt input to measuring electronics;
ΔI = difference in intensity;
% ΔI = percentage difference in intensity.

* Significant at 1% level (two-tailed) for 8 degrees of freedom, as determined by t-test.
** Analytical wavelengths shown in Table 4-2.

## 4.8 Effect of aerosol gas flow rate on emission intensities

The critical role played by the aerosol (nebulizer) argon gas flow rate on analyte signal intensity of the ARL 34000 ICP polychromator was investigated by recording the analyte signal and blank intensities for the mixed standards 1 to 4 (Table 5-1) under compromise analytical conditions (Table 4-3); and then adjusting only the aerosol gas rotameter needle valve setting and again recording intensities.

The net analyte signal intensities found are given in Table 4-19. The measurements were normalized to show relative magnitudes by ratioing to the mean net intensity at the compromise aerosol gas flow rate of 400 $m\ell.min^{-1}$ (Table 4-20). Use of the t-test in the manner illustrated in Section 4.6 showed that all the intensity ratios shown in Table 4-20 were significantly different from 100% at the 1% (two-tailed) level except for the intensity of barium at 200 $m\ell.min^{-1}$ aerosol gas flow rate, and the intensity of copper at 300 $m\ell.min^{-1}$ as indicated in Table 4-20.

In Table 4-21 the relative intensity at an aerosol gas flow rate of 350 $m\ell.min^{-1}$ as a percentage of the intensity at a flow rate of 400 $m\ell.min^{-1}$ has been tabulated together with excitation potentials of the respective atomic (I) or ionic (II) analyte lines.

TABLE 4-19: Effect of aerosol (nebulizer) gas flow rate ($F_g$/mℓ.min$^{-1}$) at 340 kPa[a] on the net signal intensity (mean ± std., deviation) on the ARL 34000 spectrometer for 5x10 s integrations of the mixed calibration stds (Table 5-1).

| $F_g$/mℓ.min$^{-1}$: | 200 | 250 | 300 | 350 | 400 |
|---|---|---|---|---|---|
| | Intensity | | | | |
| Ba* | 1749 ± 9 | 2017 ± 13 | 2264 ± 10 | 2170 ± 10 | 1743 ± 8 |
| Ca | 8640 ± 34 | 8854 ± 47 | 7914 + 24 | 4764 ± 12 | 2356 ± 11 |
| K | 280 ± 6 | 339 ± 5 | 427 ± 3 | 502 ± 7 | 549 ± 3 |
| Mg | 3661 ± 14 | 4178 ± 29 | 4653 ± 23 | 4517 ± 20 | 4004 ± 15 |
| Na | 451 ± 4 | 548 ± 4 | 690 ± 4 | 820 ± 6 | 906 ± 4 |
| Cr | 2197 ± 10 | 2399 ± 12 | 2231 ± 3 | 1475 ± 6 | 712 ± 6 |
| Cu | 161,0 ± 0,8 | 187,5 ± 1,1 | 203,7 ± 0,9 | 206,8 ± 1,0 | 202,0 ± 0,9 |
| Fe | 2676 ± 11 | 2954 ± 16 | 2796 ± 4 | 1970 ± 7 | 1064 ± 7 |
| Mn | 9261 ± 41 | 10264 ± 64 | 9717 ± 17 | 6656 ± 29 | 3416 ± 28 |
| Zn | 2913 ± 13 | 3105 ± 15 | 2839 ± 3 | 2045 ± 3 | 1202 ± 4 |

* Analytical wavelengths shown in Table 4-2.
(a) Input pressure to rotameters of ARL 34000 spectrometer.

TABLE 4-19 (Continued)

| $F_g$/mℓ.min$^{-1}$: | 200 | 250 | 300 | 350 | 400 |
|---|---|---|---|---|---|
| | Intensity | | | | |
| Be* | 13055 ± 84 | 14878 ± 8 | >15000[a] | 13711 ± 27 | 9549 ± 75 |
| Cd | 3274 ± 17 | 3238 ± 9 | 2643 ± 5 | 1540 ± 3 | 776 ± 12 |
| Mo | 923 ± 7 | 1004 ± 17 | 954 ± 23 | 671 ± 18 | 373 ± 10 |
| Ti | 4588 ± 24 | 5290 ± 18 | 5539 ± 15 | 4570 ± 14 | 2840 ± 39 |
| V | 2086 ± 12 | 2370 ± 8 | 2436 ± 7 | 1922 ± 4 | 1138 ± 16 |
| Al | 58,2 ± 0,2 | 67,2 ± 0,2 | 75,9 ± 0,3 | 82,3 ± 0,5 | 77, 1 ± 0,2 |
| Co | 449,2 ± 1,7 | 514,2 ± 1,5 | 538,8 ± 2,0 | 485,7 ± 1,7 | 381, 4 ± 0,7 |
| Ni | 297,3 ± 0,9 | 338,3 ± 1,2 | 369,9 ± 1,4 | 364,8 ± 1,3 | 315, 9 ± 0,8 |
| Pb | 14,5 ± 0,1 | 15,6 ± 0,1 | 15,9 ± 0,1 | 14,7 ± 0,1 | 13,15 ± 0,05 |
| Sr | 1870 ± 6 | 2166 ± 8 | 2387 ± 11 | 2171 ± 5 | 1531 ± 5 |

(a) Photomultiplier saturated.
* Analytical wavelengths shown in Table 4-2.

TABLE 4-20: Effect of aerosol (nebulizer) gas flow rate ($F_g$/mℓ.min$^{-1}$) at 340 kPa[a] on the net signal intensity (mean ± std., deviation) expressed as a percentage of the intensity at a flow rate of 400 mℓ.min$^{-1}$, taken as 100%. Data calculated from Table 4-19.

| $F_g$/mℓ.min$^{-1}$: | 200 | 250 | 300 | 350 |
|---|---|---|---|---|
| | Intensity | | | |
| Ba** | *100,3 ± 0,7% | 115,7 ± 0,9% | 129,9 ± 0,8% | 124,5 ± 0,8% |
| Ca | 366,7 ± 2,2% | 375,8 ± 2,6% | 335,9 ± 1,9% | 202,2 ± 1,1% |
| K | 51,0 ± 1,1% | 61,7 ± 1,0% | 77,8 ± 0,7% | 91,4 ± 1,4% |
| Mg | 91,4 ± 0,5% | 104,3 ± 0,8% | 116,2 ± 0,7% | 112,8 ± 0,6% |
| Na | 49,8 ± 0,5% | 60,5 ± 0,5% | 76,2 ± 0,6% | 90,5 ± 0,8% |
| Cr | 308,6 ± 3,0% | 336,9 ± 3,3% | 313,3 ± 2,7% | 207,2 ± 1,9% |
| Cu | 79,7 ± 0,5% | 92,8 ± 0,7% | *100,8 ± 0,6% | 102,4 ± 0,7% |
| Fe | 251,5 ± 2,0% | 277,6 ± 2,4% | 262,8 ± 1,8% | 185,2 ± 1,4% |
| Mn | 271,1 ± 2,5% | 300,5 ± 3,1% | 284,4 ± 2,4% | 194,8 ± 1,8% |
| Zn | 242,3 ± 1,3% | 258,3 ± 1,5% | 236,2 ± 0,8% | 170,1 ± 0,6% |

* Not significantly different from 100% at the 1% two-tailed level. (All values not marked with an asterisk are significantly different from 100%).

** Analytical wavelengths shown in Table 4-2.

(a) Input pressure to rotameters of ARL 34000 spectrometer.

TABLE 4-20 (Continued)

| $F_g$/mℓ.mim$^{-1}$: | 200 | 250 | 300 | 350 |
|---|---|---|---|---|
| | Intensity | | | |
| Be** | 136,7 ± 1,4% | 155,8 ± 1,2% | >157% | 143,6 ± 1,2% |
| Cd | 421,9 ± 6,9% | 417,3 ± 6,6% | 340,6 ± 5,3% | 198,4 ± 3,1% |
| Mo | 247,4 ± 6,9% | 269,2 ± 8,5% | 255,8 ± 9,2% | 179,9 ± 6,8% |
| Ti | 161,5 ± 2,4% | 186,3 ± 2,6% | 195,0 ± 2,7% | 160,9 ± 2,3% |
| V | 183,3 ± 2,8% | 208,3 ± 3,0% | 214,1 ± 3,1% | 168,9 ± 2,4% |
| Al | 75,5 ± 0,3% | 87,2 ± 0,3% | 98,4 ± 0,5% | 106,7 ± 0,7% |
| Co | 117,8 ± 0,5% | 134,8 ± 0,5% | 141,3 ± 0,6% | 127,3 ± 0,5% |
| Ni | 94,1 ± 0,4% | 107,1 ± 0,5% | 117,1 ± 0,5% | 115,5 ± 0,5% |
| Pb | 110,3 ± 0,9% | 118,6 ± 0,9% | 120,9 ± 0,9% | 111,8 ± 0,9% |
| Sr | 122,1 ± 0,6% | 141,5 ± 0,7% | 155,9 ± 0,9% | 141,8 ± 0,7% |

** Analytical wavelengths shown in Table 4-2.

TABLE 4-21: Net intensity at 350 mℓ.min$^{-1}$ aerosol gas flow rate as a percentage of the intensity at 400 mℓ.min$^{-1}$ flow rate (I%) for the ARL 34000 ICP spectrometer, showing excitation potentials (Zaidel' et al, 1970).

| Analyte | I%* | $V_{exc}$/eV |
|---|---|---|
| Ba(II)** | 124,5% | 2,72 |
| Ca(II) | 202,2% | 7,05 |
| K (I) | 91,4% | 1,62 |
| Mg(I) | 112,8% | 5,94 |
| Na(I) | 90,5% | 2,11 |
| Cr(II) | 207,2% | 6,18 |
| Cu(I) | 102,4% | 3,78 |
| Fe(II) | 185,2% | 4,77 |
| Mn(II) | 194,8% | 4,81 |
| Zn(I) | 170,1% | 5,80 |
| Be(I) | 143,6% | 5,28 |
| Cd(II) | 198,4% | 5,47 |
| Mo(II) | 179,9% | 6,06 |
| Ti(II) | 170,9% | 3,74 |
| V (II) | 178,9% | 4,33 |
| Al(I) | 106,7% | 3,14 |
| Co(I) | 127,3% | 4,07 |
| Ni(I) | 115,5% | 3,54 |
| Pb(I) | 111,8% | 4,34 |
| Sr(II) | 141,8% | 2,94 |

* All values significantly different from I% = 100% at the 1% (two-tailed) significance level.
** Analytical wavelengths shown in Table 4-2.

The 12,5% decrease in aerosol argon flow rate caused a dramatic increase in intensity of the Ca(II) 315,887 nm emission of 202%, whereas the Cu(I) 327,396 nm emission was hardly affected as shown by the measured intensity ratio of 102%.

A plot of the data from Table 4-21 shows that a linear correlation, which is particularly pronounced in the case of ionic analyte emission, exsits between the normalized intensity at 350 $m\ell.min^{-1}$ aerosol flow and the excitation potential associated with the observed transition (Figure 4-11). The Na and K data were omitted from this correlation as their emission does not correspond to the same observation height of 18 mm as used for the other element channels as mentioned previously (Table 4-2).

The following linear regression equations were found (Figure 4-11):

(a) Ionic lines only:

$$I = 17,2.E + 94 \quad \text{.....} \quad (48)$$

where I = net intensity at an aerosol flow of 350 $m\ell.min^{-1}$ as a percentage of the net intensity at 400 $m\ell.min^{-1}$,

and E = excitation potential in electron-volts.

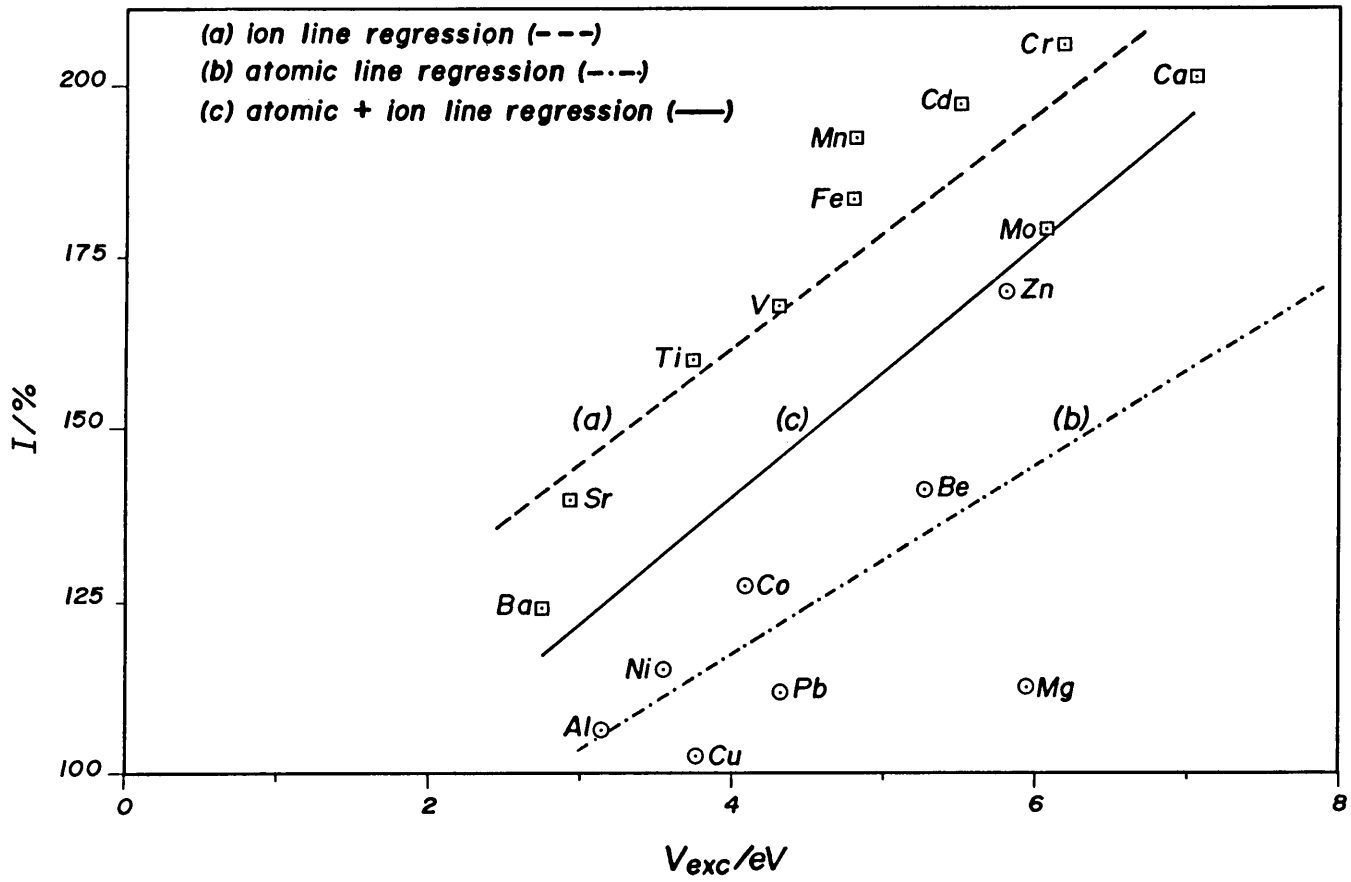


Figure 4-11: Effect of a 12,5% decrease in aerosol gas flow rate on analyte net emission intensities, expressed as a percentage of the intensity at the original aerosol gas flow rate of 400 mℓ.min$^{-1}$ at 340 kPa, showing the correlation with excitation potential, for analytical channels on the ARL 34000 polychromator. The ion lines ( ⊡ ) are more sensitive to change in aerosol gas flow rate than the atomic lines ( ⊙ ). Data plotted from Table 4-21.

The regression (48) had a correlation coefficient, r, of 0,89 giving a T value (from equation 34) of 5,6. The $t_{critical}$ value of 3,36 for the 1% (two-tailed) level and n-2 i.e., 8 degrees of freedom implied a significant correlation at the 1% level.

(b) Atomic lines only:

$$I = 13,6.E + 63 \quad \ldots\ldots\ldots\ldots\ldots \quad (49)$$

where I and E are as defined above.

For r = 0,63 and n = 8, this regression is just significant at the 10% level, but not at the 1% level.

(c) Both atomic and ionic lines:

$$I = 18,7.E + 66 \quad \ldots\ldots\ldots\ldots\ldots \quad (50)$$

which is significant at the 1% level for r = 0,64 and n = 18.

The implication of the existence of a good correlation between percentage change in analyte emission intensity with change in aerosol gas flow rate and excitation potential, particularly for ionic (II) emission lines implies that equation 48 should prove useful in internal

standardization or mid range calibration correction as the change in intensity of one ionic species would then allow calculation of the change in intensity for other ionic transitions. The derivation of the required correction formula is given in Section 4.10.

Normalized intensity data from Table 4-20 is graphically illustrated in Figure 4-12. This figure shows how analyte emission lines with associated high excitation potential (E) such as Ca(II) 315,887 nm with E = 7,05 eV are very sensitive to changes in aerosol flow rate; whereas lines with associated small excitation potential e.g., Cu(I) 327,396 nm with E = 3,78 eV are insensitive to change in aerosol gas flow rate. The tendency of ionic lines of high excitation potential to have considerably greater sensitivity at an aerosol flow rate of 200 $m\ell.min^{-1}$ as opposed to the compromise flow of 400 $m\ell.min^{-1}$ implies that the magnitude of spectral interferences of ion lines on atomic lines may be expected to be more pronounced at low aerosol gas flow rates.

The effect of aerosol gas flow rates on detection limit (DL) expressed as the concentration equivalent value of twice the standard deviation of the signal for the blank standard is given in Table 4-22. The choice of the compromise aerosol flow rate of 400 $m\ell.min^{-1}$ is

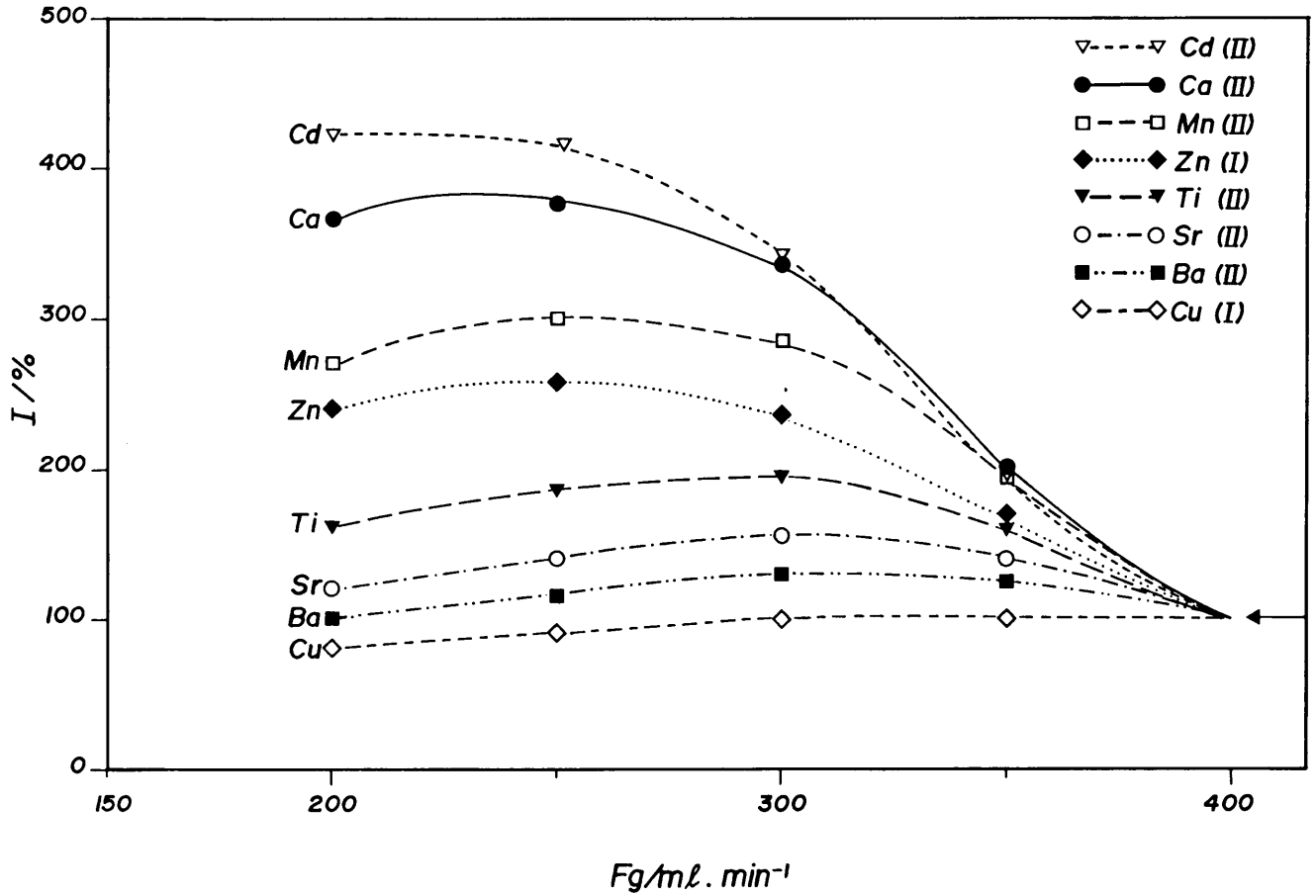


Figure 4-12: Effect of aerosol (nebulizer) gas flow rate (Fg) at 340 kPa on the net analyte emission intensity expressed as a percentage of the intensity at an aerosol gas flow rate of 400 mℓ.min$^{-1}$ taken as 100%.

governed by the need to obtain adequately sensitive detection limits for such elements as Al, while at the same time minimizing the intensity of ionic emission from matrix analyte elements such as calcium, in order to reduce the magnitude of ionic line emission which is particularly intense in the ICP source at low aerosol flow rates (Figure 4-12).

TABLE 4-22: Effect of aerosol (nebulizer) gas flow rate ($F_g$/mℓ.min$^{-1}$) at 340 kPa[a] on the detection limit (DL) expressed as twice the standard deviation of the nitric acid ϕ = 0,01, blank signal in concentration equivalent units of μg.ℓ$^{-1}$, for 5x10 s integrations on the ARL 34000 polychromator*.

| $F_g$/mℓ.min$^{-1}$: | 200 | 250 | 300 | 350 | 400 |
|---|---|---|---|---|---|
| | DL/μg.ℓ$^{-1}$ | | | | |
| Ba** | 1,0 | 0,6 | 0,2 | 0,7 | 1,5 |
| Ca | 15 | 16 | 14 | 35 | 28 |
| K | 640 | 670 | 900 | 290 | 180 |
| Mg | 11 | 23 | 17 | 26 | 24 |
| Na | 190 | 96 | 40 | 50 | 85 |
| Cr | 2,6 | 2,1 | 1,7 | 4,2 | 8,4 |
| Cu | 9,9 | 5,3 | 3,9 | 4,0 | 3,5 |
| Fe | 6,3 | 2,3 | 14 | 2,3 | 32 |
| Mn | 1,4 | 1,5 | 2,9 | 4,0 | 12 |
| Zn | 2,6 | 1,7 | 3,4 | 4,0 | 3,8 |
| Be | 0,5 | 0,5 | < 0,5 | 0,4 | 0,5 |
| Cd | 2,3 | 2,7 | 3,8 | 4,2 | 5,7 |
| Mo | 5,6 | 3,8 | 8,6 | 4,8 | 12 |
| Ti | 0,6 | 0,6 | 1,6 | 0,3 | 0,5 |
| V | 3,4 | 2,7 | 4,3 | 1,0 | 1,8 |
| Al | 105 | 82 | 45 | 51 | 19 |
| Co | 24 | 58 | 22 | 10 | 16 |
| Ni | 22 | 35 | 30 | 8 | 18 |
| Pb | 370 | 480 | 350 | 240 | 160 |
| Sr | 0,18 | 0,22 | 0,12 | 0,03 | <0,03 |

* Smallest D.L., for each element underlined.
** Analytical wavelengths shown in Table 4-2.
(a) Input pressure to rotameters of ARL 34000 spectrometer.

## 4.9 Relationship between change of ionic line net intensity with aerosol gas flow rate change, and excitation potential.

If $I_{i\phi}$ = net intensity of analyte $\phi$ at aerosol flow rate $F_i$, and the assumption is made that for small change in net intensity ($\delta I_{i\phi}$), the change in intensity is proportional to change in aerosol gas flow rate ($\delta F_i$) i.e.,

$$\delta I_{i\phi} = K_1 . \delta F_i \qquad \ldots\ldots\ldots\ldots\ldots \quad (51)$$

which yields on integration:

$$I_{i\phi} = K_1 . F_i + c \qquad \ldots\ldots\ldots\ldots\ldots \quad (52)$$

where c is the integration constant.

From equation 52 the following expression is readily derived;

$$\frac{I_{ia} - I_{oa}}{I_{ib} - I_{ob}} = \frac{I_{1a} - I_{oa}}{I_{1b} - I_{ob}} \qquad \ldots\ldots\ldots\ldots\ldots \quad (53)$$

for the relationship between the net intensities of two analytes, a and b, at aerosol flow rates $F_o$, $F_1$ and $F_i$. If $F_1$ = 350 $m\ell.min^{-1}$ and $F_o$ = 400 $m\ell.min^{-1}$, then from equation 48 in Section 4.9;

$$\frac{I_{1\phi}}{I_{o\phi}} \times 100 = 17{,}2.E_{\phi} + 94 \quad \ldots\ldots\ldots\ldots \quad (54)$$

where $\phi$ = a or b, and $E_{\phi}$ is the excitation potential in eV of analyte $\phi$.

Equation 54 may be written:

$$I_{1\phi} = (m.E_{\phi} + \ell)\, I_{o\phi} \quad \ldots\ldots\ldots\ldots\ldots \quad (55)$$

where m = 17,2/100

and $\ell$ = 94/100

Substituting for $I_{1\phi}$ where $\phi$ = a or b from 55 into equation 53. and collecting like terms:

$$\frac{I_{ia} - I_{oa}}{I_{ib} - I_{ob}} = \frac{I_{oa}\,(m.E_a + \ell - 1)}{I_{ob}\,(m.E_b + \ell - 1)} \quad \ldots\ldots \quad (56)$$

Now let $A = (m.E_a + \ell - 1)$,

and $B = (m.E_b + \ell - 1)$.

equation 56 may then be written:

$$\frac{I_{ia} - I_{oa}}{I_{ib} - I_{ob}} = \frac{I_{oa} \cdot A}{I_{ob} \cdot B} \quad \ldots\ldots\ldots\ldots \quad (57)$$

If the substitution (assuming linearity of calibration);

$$C_{i\phi} = k_{\phi} \cdot I_{i\phi} + C_{\phi} \quad \ldots\ldots\ldots\ldots\ldots \quad (58)$$

where $C_{\phi} = 0$ because $I_{i\phi}$ is net analyte intensity; where $C_{i\phi}$ is the apparent concentration readout of analyte $\phi$ at aerosol flow rate $F_i$, and $k_{\phi}$ is the proportionality constant, is made, then 57 becomes;

$$\frac{C_{ia} - C_{oa}}{C_{ib} - C_{ob}} = \frac{C_{oa} \cdot A}{C_{ob} \cdot B} \quad \ldots\ldots\ldots \quad (59)$$

which by multiplying out and solving for $C_{ob}$ yields;

$$C_{ob} = C_b \cdot \left( \frac{A}{A - B + B\left(\frac{C_a}{C_{oa}}\right)} \right) \quad \ldots\ldots \quad (60)$$

which on substitution for A and B yields;

$$C_{ob} = C_b \cdot \left( \frac{m.E_a + \ell - 1}{m(E_a - E_b) + (m.E_b + \ell - 1).\left(\frac{C_a}{C_{oa}}\right)} \right) \quad \ldots\ldots\ldots \quad (61)$$

which in the case of the operating source conditions used on the ARL 34000 spectrometer, with the values for m and $\ell$ yields:

$$C_{ob} = C_b \cdot \left( \frac{0{,}172E_a - 0{,}06}{0{,}172(E_a - E_b) + (0{,}172E_b - 0{,}06)\left(\frac{C_a}{C_{oa}}\right)} \right) \quad \ldots\ldots\ldots \quad (62)$$

Equation 62 reduces to the usual formula for internal standardization where $E_a = E_b$:

$$C_{ob} = C_b \cdot \frac{C_{oa}}{C_a} \quad \ldots\ldots\ldots\ldots \quad (63)$$

Where $C_{oa}$ = true concentration of internal standard (analyte a) at aerosol flow rate $F_o$; $C_a$ = apparent concentration of analyte a; $C_b$ = apparent concentration of analyte b; and $C_{ob}$ = calculated true concentration of analyte b.

Equation 62 may be used for correction of ionic line concentration readout either by using the reference analyte, analyte a, as an internal std., or as a mid range drift correction std., where one wishes to correct for drift in sensitivity caused by change in aerosol gas flow rate. The use of this procedure for internal standardization is illustrated in Chapter 5 (section 5.6) for ionic line concentration readout correction. An analagous expression for atomic lines is evaluated for internal standardization in section 5.7 of Chapter 5.

## 4.10 Summary

In this chapter the following was demonstrated:

(a) That excitation temperature and degree of ionization of Mn and Zn are affected by the sample aspiration rate. As only one analytical line, either atomic or ionic per element is usually employed in routine analysis, it is important that the degree of ionization of an analyte element should remain invariant between calibration standard and samples. Thus the need to keep sample aspiration rate constant.

(b) That a decrease in the mains supply voltage input to the rf generator of the ARL 34000 spectrometer of only 2,3% resulted in a significant change in net intensity of eight analyte channels, viz., Ca, Cr, Fe, Mn, Zn, Be, Cd and V. This change in net intensity occurred despite no visible decrease in rf input power or change in reflected power being observed on the meters on the rf generator. Lines with high excitation potential in general showed greater change than lines with low excitation potential. The practical significance of this is that the mains supply voltage to the rf generator must be suitably stabilized.

By contrast, the measuring electronics of the ARL 34000 spectrometer were shown to be insensitive to variation in mains supply voltage, thus demonstrating a high state-of-the-art of the constant voltage supply to the photomultiplier tubes.

(c) That change in inner (aerosol) argon flow rate causes a change in net intensity of analyte emission which is particularly marked in the case of lines with associated high excitation potential, and was greater for ion lines than for atomic lines. The change in normalized net intensity showed a strong correlation with excitation potential in the case of ion lines ($r = 0,89$ for $n = 10$). A weaker correlation was shown

for atomic line emission. The practical analytical significance of this finding is that the inner argon flow rate must be kept invariant if relative intensities between different analyte channels are to remain constant, as such relative intensities are fundamental to the application of the software method of interference correction as discussed in Chapter five. The high correlation in the case of ion-lines allows the development of a weighted formula for internal standardization as discussed in section 4.9.

# CHAPTER 5: CALIBRATION AND INTERFERENCES ON THE POLYCHROMATOR

## 5.1 Introduction

In this chapter the essential procedures for calibration of the ARL 34000 ICP polychromator are discussed. These involve (i) the determination of the relationship between intensity readout and analyte concentration, and the procedure for correction of drift in sensitivity (Section 5.2); (ii) the setup of the sample plate on the autosampler and the necessity for blank subtraction and blank drift correction (Section 5.3); (iii) the determination of the interelement interference correction coefficients using the software approach for interference correction from the matrix elements Ca, Mg, Fe and Mn (Section 5.4); and (iv) the determination of the washout time necessary to reduce analyte signal intensity to less than 1% of initial intensity i.e., the memory effect (Section 5.5). In addition, the use of the weighted internal standardization relationship derived in Section 4.9 is tested for ability to correct for error consequent to aerosol gas flow change with ionic lines (Section 5.6). Lastly, the application of internal standardization to correct for error consequent to aerosol flow change for atomic lines is evaluated (Section 5.7).

## 5.2 Calibration of intensity readout in concentration units.

The calibration of the polychromator to provide concentration equivalent readout for each analyte intensity signal is relatively elementary, as a consequence of the close approach to linearity over several orders of magnitude which is characteristic of the ICP source (Jones et al, 1974). Linearity is also found with the multielement standards provided that;

(i) the total cation concentration is not excessive e.g., not greater than 3400 $mg.\ell^{-1}$ as transport problems may occur (Butler et al, 1980),

(ii) a peristaltic pump is used to minimize viscosity effects on sample uptake rate (vide Chapter 3),

(iii) concentration ratios between different cations in a multielement standard are not excessively different, so as to avoid Aerosol ionic redistribution (AIR) interference, which may occur in high salt content matrices when cation concentrations differ by two or more orders of magnitude (Browner et al, 1983),

(iv) acid matrices between blank, standards and samples are approximately matched, and

(v) element pairs with severe spectral interference are not mixed in the same multielement standard.

Prior to full calibration, or daily sensitivity drift correction (termed normalization in the ARLEB software), the ARL 34000 spectrometer is allowed a warm-up period of two hours following plasma ignition. During this warm-up period compromise analytical conditions are checked (Table 4-4), particularly the accurate adjustment of the aerosol gas flow rate and the profile setting of the spectrometer. For profile adjustment a profile scan is recorded manually across the Y360,073 nm emission line while aspirating a 10 $mg.\ell^{-1}$ Y standard, and the profile position of peak maximum determined. The intensity of the Y360,073 nm emission serves as a guide for the reproducibility of source conditions. During the warm-up period, calibration standards are also prepared.

The high concentration standards used in daily normalization of the ARL 34000 spectrometer are given in Table 5-1, and the serial dilutions of these standards, used in the determination of calibration regressions, i.e., the full calibration procedure, are given in Table 5-2. The cations which are commonly present in environmental water samples are present in the high concentration

TABLE 5-1: Daily calibration (normalization) standards for the ARL 34000 spectrometer.

| | | | |
|---|---|---|---|
| Std., 1: | Ba | 30 | $mg.\ell^{-1}$ |
| | Ca | 600 | " |
| | K | 600 | " |
| | Mg | 600 | " |
| | Na | 600 | " |
| Std., 2: | Cr | 10 | $mg.\ell^{-1}$ |
| | Cu | 10 | " |
| | *Fe | 210 | " |
| | *Mn | 110 | " |
| | Zn | 10 | " |
| Std., 3: | Be | 10 | $mg.\ell^{-1}$ |
| | Cd | 10 | " |
| | Mo | 10 | " |
| | Ti | 10 | " |
| | V | 10 | " |
| Std., 4: | Al | 50 | $mg.\ell^{-1}$ |
| | Co | 50 | " |
| | Ni | 50 | " |
| | Pb | 50 | " |
| | Sr | 5 | " |
| Std., 5: | Si | 100 | $mg.\ell^{-1}$ |
| | B | 10 | " |
| Std., 6: | Hg | 10 | $mg.\ell^{-1}$ |
| | Zr | 10 | " |
| Std., 7: | As | 25 | $mg.\ell^{-1}$ |
| Std., 8: | Se | 50 | $mg.\ell^{-1}$ |
| Std., 9: | Sb | 50 | $mg.\ell^{-1}$ |
| Std., 10: | Y | 10 | $mg.\ell^{-1}$ |

Note: All calibration standards in nitric acid, $\phi$ = 0,01, medium, except for std., 5 and 9 in deionized water. Standards prepared from Titrisol stock solutions., except stds., 6,7 8 and 9, which are prepared from BDH Spectrosol stock solutions, and std., 10, which is prepared from Specpure $Y_2O_3$.

*An alternative calibration std., with 10 $mg.\ell^{-1}$ Fe and Mn is on occasion used, together with Fe and Mn attenuator settings of 726 V and 687 V respectively where greater sensitivity is required for low $\mu g.\ell^{-1}$ concentrations of Fe and Mn. To avoid the necessity of separate mixed stock std solutions, 200 and 100 $mg.\ell^{-1}$ Fe and Mn respectively is added to the lower concentration standard to obtain the 210 and 110 $mg.\ell^{-1}$ Fe and Mn concentrations.

standards (Table 5-1) in concentrations exceeding 100 $mg.\ell^{-1}$ firstly to avoid the necessity of unnecessary sample dilution i.e., Ca, K, Mg, Na, Fe and Mn, and secondly to enable interelement interference corrections to be made from the interfering major elements Ca, Mg, Fe and Mn.

TABLE 5-2: Serial dilutions of the standards (Table 5-1) used for calibrating the ARL 34000 spectrometer.

| Std No., | Dilution factor | | | | | | | |
|---|---|---|---|---|---|---|---|---|
| | (a) | (b) | (c) | (d) | (e) | (f) | (g) | (h) |
| 1 | 1 | 2/3 | 1/2 | 1/3 | 1/6 | 1/8 | 1/12 | 1/24 |
| 2 | 1 | 3/4 | 1/2 | 1/4 | 1/10 | – | – | – |
| 3 | 1 | 3/4 | 1/2 | 1/4 | 1/10 | – | – | – |
| 4 | 1 | 1/2 | 1/4 | 1/10 | 1/20 | – | – | – |
| 5 | 1 | 3/4 | 1/2 | 1/4 | 1/8 | – | – | – |
| 6 | 1 | – | – | – | – | – | – | – |
| 7 | 1 | 1/2 | 1/4 | 1/8 | 3/40 | – | – | – |
| 8 | 1 | – | – | – | – | – | – | – |
| 9 | 1 | – | – | – | – | – | – | – |
| 10 | 1 | – | – | – | – | – | – | – |

The necessity to be able to analyze matrix cations and trace elements on the same sample aliquot without dilution, as far as possible, has a bearing on the choice of analytical emission lines in the wavelength programme of the polychromator. Thus the relatively weak Ca (II) 315,887 nm emission line is used for the Ca analyte channel, rather than the intense Ca (II) resonance line at 396,847 nm for instance. The purpose of analyzing calcium is primarily to correct for interference on the Al(I) 396,18 nm analytical channel. Therefore the need to quantify calcium concentrations without dilution.

The serial dilutions of the calibration standards (Table 5-2) provide, together with a blank solution, 37 calibration solutions for the ARL 34000 polychromator. The ARLEB software allows a maximum of 42 calibration solutions. For stds., 6, 8, 9 and 10 i.e., the stds., for Hg & Zr, Se, Sb and Y, no serial dilutions are made in routine calibration, and a linear two point calibration is used for these elements. The greatest number of serial dilutions are used for std., 1 i.e., the standard containing Ca and Mg, the reason being that these two elements are the most common interferants present in water samples at elevated concentrations. It is consequently necessary to define their concentration to intensity relationship as accurately as possible for the purpose of

interelement interference correction. The ARLEB software fits regressions of the 1st, 2nd or 3rd order to the intensity data, based on minimization of the sum of squares of residuals, obtained on analysis of the serial dilution calibration standards.

In the case of the calibration for Ca, Mg, Na and K, the ARLEB software fits two 3rd order polynomials, one for the lower portion of the curve and one for the upper portion of the calibration curve. Typical calibration data for Ca (II) 315,89 nm analyte emission is shown in Table 5-3. Least squares linear regression does not provide an acceptable fit, the error at zero concentration being 6,2 $mg.\ell^{-1}$ Ca for instance. The deviation from linearity can be seen in Figure 5-1, where the data points for zero and 600 $mg.\ell^{-1}$ Ca have been joined by a straight line. All the intermediate points lie below the straight line, indicating a departure from linearity. The right-hand column in Table 5-3 shows the fit obtained using two 3rd order polynomials of the form;

$$C = C_o + C_1.I + C_2.I^2 + C_3.I^3 \quad \ldots\ldots\ldots \quad (64)$$

where $I$ = gross analyte intensity,

$C_n$ = the $n^{th}$ order coefficient,

and $C$ = the calculated analyte concentration.

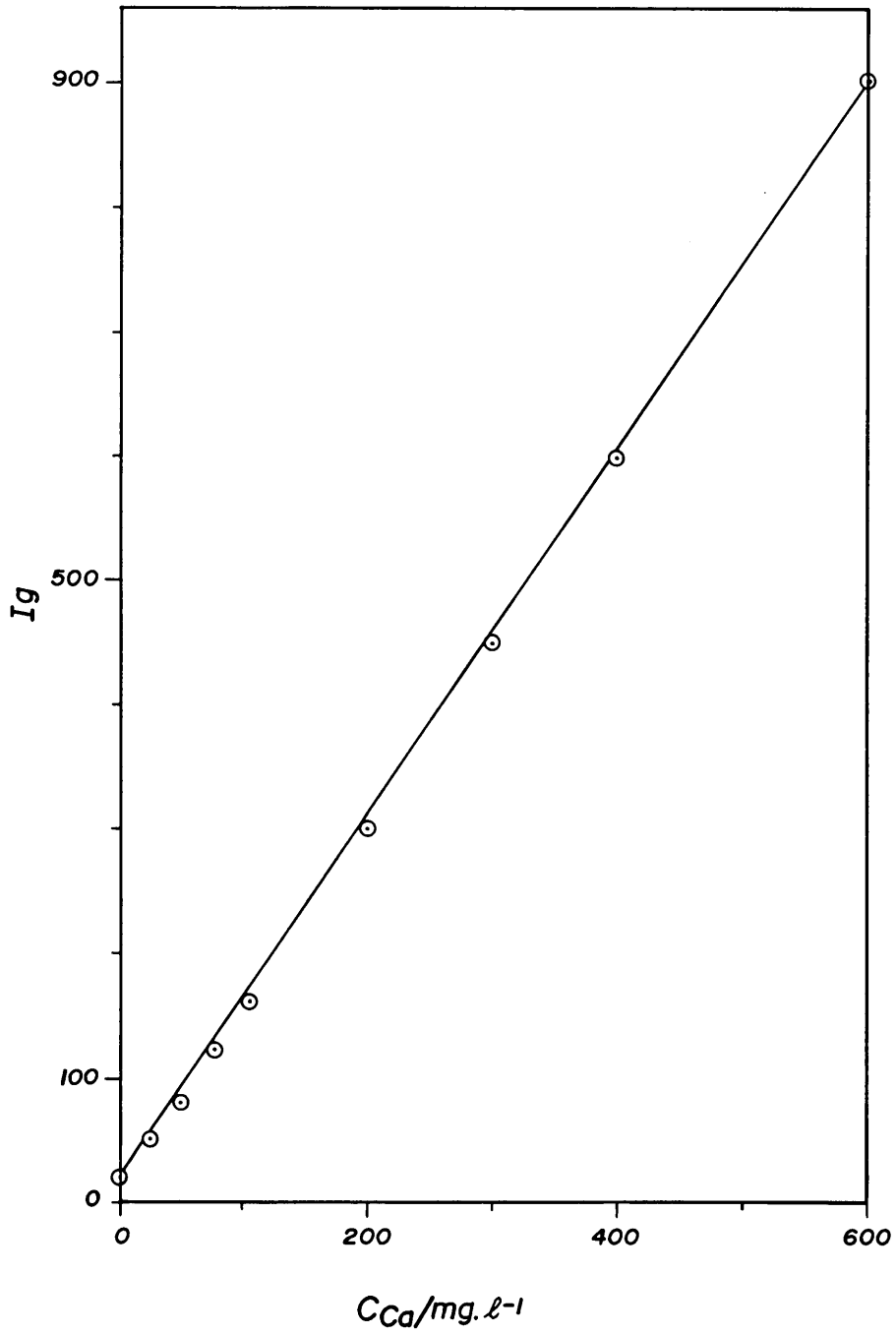


**Figure 5-1:** Calibration intensity data for the Ca(II) 315,89 nm analytical line on the ARL 34000 spectrometer showing the approximate linearity of the gross intensity (Ig) to concentration relationship. Compromise operating conditions (Table 4-3) were used.

As can be seen from Table 5-3, the two 3rd order polynomial regressions provide a better fit than a 1st order regression, particularly for the blank value.

Full calibration of the polychromator is only carried out when some operating parameter has been changed, as preparation of the serial dilutions (Table 5-2) and recording of analyte intensities on these solutions takes serveral hours, and would not be practical in routine analysis.

TABLE 5-3: Typical intensity calibration data for Ca (II) 315,89 nm emission for the serial dilutions of std., 1 (Table 5-2) plus blank run on the ARL 34000 spectrometer under compromise conditions.

| $C_{Ca}$/mg.ℓ$^{-1}$ | I ± σ@ | Calculated $C_{Ca}$/mg.ℓ$^{-1}$ Linear regression | Two 3rd order polynomials |
|---|---|---|---|
| 0 | 19,9 ± 4E-4 | 6,2 | <0,01 * |
| 25 | 49,4 ± 0,3 | 26,1 | 26,1 * |
| 50 | 79,6 ± 0,2 | 46,5 | 49,1 * |
| 75 | 123,6 ± 1,8 | 76,2 | 78,0 * |
| 100 | 158,9 ± 2,2 | 100,0 | 99,2 * |
| 200 | 301,0 ± 0,5 | 195,9 | 199,9 ** |
| 300 | 451,6 ± 6,2 | 297,6 | 300,9 ** |
| 400 | 600,1 ± 32 | 397,8 | 398,1 ** |
| 600 | 906,1 ± 19,9 | 604,4 | 600,3 ** |
| Sum of squares of residuals: | | 100 | 16 |

@ Mean gross intensity ± std., deviation for 3x10s integrations.

* 3rd order polynomial (equation 64) with coefficients;
$C_o$ = -20,13; $C_1$ = 1,069; $C_2$ = -2,99E-3; $C_3$ = 6,21E-6.

** 3rd order polynomial (equation 64) with coefficients;
$C_o$ = -18,28; $C_1$ = 7,765E-1; $C_2$ = -2,05E-4;
$C_3$ = 1,12E-7.

It is impossible, however, to reproduce conditions exactly from day to day, and allowance must be made for calibration drift. Correction for such drift is done on a daily basis (or more often should the concentration readout for a mixed control standard indicate the need for re-correcting drift e.g., a change in the control concentration of greater than 5%), using the normalization routine (NORM) of the ARLEB software. The NORM routine requires only that the ten high concentration mixed standards (Table 5-1) plus a blank solution prior to each standard be analyzed on the ARL 34000 spectrometer. A linear transformation is then used to transform the measured analyte intensities into the virtual equivalent analyte intensities, obtained when the full calibration using the 36 serial dilutions plus blank was made (Table 5-2). The transformation is of the form;

$$I_t(X) = D_1(X).\ I(X) + D_2(X) \qquad \ldots\ldots\ldots\ldots\ldots \quad (65)$$

where $I(X)$ = the actual gross intensity currently recorded for analyte X;

$I_t(X)$ = the transformed, normalized, gross intensity of analyte X,

$D_1(X)$ = the slope term of the normalization routine for analyte X,

and $D_2(X)$ = the intercept term of the normalization routine for analyte X,

where $D_1(X)$ and $D_2(X)$ are defined as follows;

$$D_1(X) = \left( \frac{I(X)_{so} - I(X)_{bo}}{I(X)_{sc} - I(X)_{bc}} \right) \quad \ldots\ldots\ldots\ldots\ldots \quad (66)$$

$$\text{and } D_2(X) = I(X)_{bo} - D_1(X).\ I(X)_{bc} \quad \ldots\ldots\ldots\ldots\ldots \quad (67)$$

where $I(X)_{so}$ = the original gross analyte intensity obtained for the analyte X in the high calibration std.,(s) at the time of the original full recalibration (o),

$I(X)_{bo}$ = the original gross intensity obtained for the blank solution (b) for analyte channel (X) at the time of the original full recalibration (o),

$I(X)_{sc}$ = the current (c) gross analyte (X) intensity obtained for the high concentration standard (s),

and $I(X)_{bc}$ = the current (c) gross intensity measured for the blank solution (b) for analyte channel X.

The transformed gross analyte intensity, $I_t(X)$, is substituted into the calibration polynomial (equation 64) for the given analyte, to obtain the raw i.e., apparent

analyte concentration. By raw concentration is meant the analyte concentration not yet corrected for interelement interferences.

The polynomial regression coefficients of equation 64, constituting the calibration for each analyte element; and the slope and intercept terms of equation 65, constituting the drift correction, are stored in the calibration data file on magnetic disc. Subsequently analyzed samples have their analyte channel intensities processed with equations 65 and 64 to provide concentration readouts. These concentrations must still, however, be corrected for blank drift which may have occurred following normalization, and interelement interferences. These two corrections are discussed in Sections 5.3 and 5.4 respectively.

## 5.3 Analysis of the sample plate

A typical autosampler plate layout for sample analysis is shown in Table 5-4. A high concentration mixed check standard (a) is placed in cup positions 3 and 22 to monitor calibration sensitivity drift. Four blank cups are placed after the first high check standard to ensure that no carry over of analyte or memory signal affects the blank cup in position 7. The blank in position 7 is used for blank subtraction correction for the sample cups which follow. The blank subtraction routine is;

$$C(X)^{c}_{sn} = C(X)^{u}_{sn} - C(X)_{b} \quad \ldots\ldots\ldots\ldots\ldots \quad (68)$$

where $C(X)^{u}_{sn}$ = the analyte concentration C of analyte X in sample Sn, where n = 1 to 10 uncorrected (u) for blank concentration readout change following normalization,

$C(X)^{c}_{sn}$ = the analyte concentration C of analyte X in sample Sn where n = 1 to 10, corrected (c) for blank readout,

and $C(X)_{b}$ = the concentration readout of analyte X in the blank (b) which immediately preceeds the following non-blank samples.

The blank subtraction routine corrects for drift in blank concentration readout occurring in the interval between the preceeding normalization and the given sample sequence.

**TABLE 5-4:** A typical autosampler sample plate layout used on the ARL 34000 spectrometer.

| Cup No. | Contents | Cup No. | Contents |
|---|---|---|---|
| 1 | Blank | 12 | S5 |
| 2 | Blank(b) | 13 | Blank |
| 3 | Std., (a) | 14 | Blank (b)(c) |
| 4 | Blank | 15 | S6 |
| 5 | Blank | 16 | S7 |
| 6 | Blank | 17 | S8 |
| 7 | Blank(b)(c) | 18 | S9 |
| 8 | S1(d) | 19 | S10 |
| 9 | S2 | 20 | Blank |
| 10 | S3 | 21 | Blank(b)(c) |
| 11 | S4 | 22 | Std. (a) |

(a) Std., = a high concentration mixed std., used to monitor sensitivity change.

(b) Blank (nitric acid, $\phi$ = 0,01) cups used in blank subtraction of subsequent non-blank cups.

(c) Blank cups used for the blank drift interpolation routine.

(d) Sample cups annotated S1, S2, S3 ..... etc.

As the blank readout may drift during the analysis of sample sequences S1 to S5 and S6 to S10, a software routine to interpolate for in-plate blank drift was incorporated. This routine applies the following correction;

$$C(X)^{d}_{sn} = C(X)^{c}_{sn} - \frac{l(n)}{m}.\left( C(X)_{bf} - C(X)_{b} \right) \quad \ldots \quad (69)$$

where $C(X)^{c}_{sn}$ is as defined in equation 68,

$C(X)^{d}_{sn}$ = the analyte concentration C, of analyte X, in sample cup Sn where n = 1 to 10, corrected for blank drift (d),

$C(X)_{b}$ is as defined in equation 68,

$C(X)_{bf}$ = the readout for analyte concentration in the second blank of the pair of blanks following (f) the sample cup sequence, i.e., the blank in position 14 for S1 to S5; and the blank in position 21 for S6 to S10,

m = the cup number of $C(X)_{bf}$ minus the cup number $C(X)_{b}$, i.e., 7 for the plate layout given in Table 5-4

and l(n) = the cup number of sample Sn, minus the the cup number of the preceeding blank used for blank subtraction by equation 68.

Correction both for blank change after normalization (equation 68), as well as blank drift during a sample analysis sequence (equation 69) is extremely important at trace analysis concentration levels; as the use of the correct blank value for each sample essentially determines the accuracy of the determination once the second major source of error i.e., interelement spectroscopic interferences have also been dealt with (Section 5.4).

As already pointed out, the sample plate layout contains several blank cups after the 1st high concentration check std., to avoid carry over of signal in the blank used for subtraction from samples S1 to S5. No blanks are included between samples. To reduce the transport system memory between samples, a wash-in time of 80 s is employed. This ensures that the nebulizer system memory, from the previous sample, is reduced to less than 1% (Section 5.5). The original ARLEB software was wasteful of time in that the sample changer moved to the next cup only after printout of the analytical data for the current sample cup. Printout of this data, which includes gross intensity, raw analyte concentration, analyte concentration after interference correction and standard deviation for each of the 28 analytical channels, takes approximately 60 s. The software was modified to move the autosampler to the next cup immediately after the last integration and before printout of the analytical data. In this way the preintegration time could be reduced from 80 s to 20 s, while still allowing a sample wash-in time of 80 seconds.

Typical detection limits for the usual $\phi$ = 0,01 nitric acid matrix and 1 $g.\ell^{-1}$ disodium EDTA matrix is given in Table 5-5. This table gives the mean of 9 determinations of detection limit, calculated using equation 11 (Chapter 2) with a value for the multiple $\kappa$ of 2, for analyte concentration readout of blank solutions

taken from actual analysis plates in June 1985. The detection limits shown in Table 5-5 thus represent the practical analytical detection limits where 3x10 s integrations are used on each blank or sample. There was no statistical difference at the 1% significance level for a two-tailed t-test between the detection limits in the two matrices except for Ca, Ti, Si and Se. The similarity in the detection limits in an EDTA matrix as compared to a nitric acid matrix (Table 5-5) illustrates the relative insensitivity of the ICP emission spectrometric technique to changes in matrix composition.

TABLE 5-5: Comparison of 2σ detection limit (DL) for $\phi$ = 0,01 nitric acid matrix and 1 $g.\ell^{-1}$ disodium EDTA* matrix giving the mean ± std., deviation of 9 determinations of DL on the ARL 34000 spectrometer.

| Analyte | $HNO_3$ matrix $(\overline{DL} \pm \sigma)/\mu g.\ell^{-1}$ | EDTA matrix $(\overline{DL} \pm \sigma)/\mu g.\ell^{-1}$ |
|---|---|---|
| Ba@ | 0,5 ± 0,3 | 0,3 ± 0,1 |
| **Ca | 16 ± 8 | 28 ± 8 |
| K | 854 ± 410 | 1020 ± 600 |
| Mg | 4 ± 1 | 7 ± 4 |
| Na | 126 ± 60 | - |
| Cr | 5,6 ± 3,3 | 5,8 ± 4,0 |
| Cu | 1,3 ± 1,4 | 2,0 ± 1,2 |
| Fe | 5,0 ± 4,4 | 6,0 ± 4,0 |
| Mn | 1,4 ± 0,8 | 1,1 ± 1,0 |
| Zn | 4,4 ± 1,7 | 4,8 ± 2,5 |
| Be | 0,4 ± 0,2 | 0,6 ± 0,2 |
| Cd | 5,4 ± 2,6 | 6,3 ± 4,1 |
| Mo | 7,9 ± 3,5 | 7,4 ± 2,8 |
| **Ti | 0,4 ± 0,2 | 0,7 ± 0,2 |
| V | 1,6 ± 0,6 | 1,6 ± 0,7 |

* Dihydrate salt of disodium ethylenediaminetetraacetic acid.

** DL's significantly different at 1% (two-tailed) level, using a t-test with pooled variance and 18-2 degrees of freedom.

@ Analytical wavelenghts given in Table 4-2.

TABLE 5-5 (Continued)

| Analyte | $HNO_3$ matrix $(\overline{DL} \pm \sigma)/\mu g.\ell^{-1}$ | EDTA matrix $(\overline{DL} \pm \sigma)/\mu g.\ell^{-1}$ |
|---|---|---|
| Al@ | 32 ± 18 | 24 ± 9 |
| Co | 10 ± 3 | 13 ± 7 |
| Ni | 9 ± 4 | 11 ± 8 |
| Pb | 127 ± 95 | 133 ± 52 |
| Sr | 0,1 ± 0,04 | 0,1 ± 0,04 |
| B | 4,0 ± 2,7 | 3,1 ± 2,4 |
| Hg | 14 ± 7 | 18 ± 11 |
| **Si | 77 ± 45 | 17 ± 18 |
| Zr | 15 ± 6 | 16 ± 8 |
| As | 65 ± 38 | 61 ± 29 |
| Sb | 38 ± 25 | 27 ± 17 |
| **Se | 74 ± 39 | 12 ± 28 |
| Y | 0,2 ± 0,1 | 6 ± 17 |

** DL's significantly different at 1% (two-tailed) level, using a t-test with pooled variance and 18-2 degrees of freedom.

@ Analytical wavelengths given in Table 4-2.

## 5.4 Interelement interference correction

As shown in Chapter 4, different analyte elements do not respond identically to change in source conditions. Where the software approach for interelement interference correction is used, therefore, attempts to reproduce source conditions are consequently necessary if relative intensities between analyte emission lines, and thus valid interference correction coefficients are to be maintained.

Interference correction coefficients may also depend critically on profile setting, particularly where an interfering line lies on the edge of the exit slit of the analyte channel e.g., the interference of Mn 203,998 nm on the Se 203,985 nm analytical line as described by Kempster et al (1983), where slight change in profile position may change the magnitude of the Mn on Se interference without significantly affecting the sensitivity of the Se channel.

The determination of interelement interference correction coefficients on a polychromator is, in principle, simple. Net intensities for the programmed elements are recorded on aspiration of a pure, single cation standard solution. The intensities are converted to concentration equivalent units. Positive concentration readout for elements not present in the standard are then taken as interference readouts.

Interference correction coefficients arising from Ca, Mg, Fe and Mn were determined using the procedure outlined by Kempster et al (1983), by analyzing 1000 $mg.\ell^{-1}$ single cation standards prepared from spectroscopically pure $CaCO_3$, MgO, $MnO_2$ and Fe-wire, by dissolution in Analar hydrochloric acid. To enable inpurities in the acid used for dissolution to be subtracted, exactly the same quantity of the same stock of acid was added to the blank solution. Serial dilutions of the single cation standards were then analyzed on the ARL 34000 spectrometer after calibration using mixed standards (Table 5-1). Prior to this analysis, the previously determined interference correction coefficients were zeroed to ensure that the net concentration readout would be the uncorrected concentrations for each analyte channel. In addition, the recording of intensities at a profile position of approximately 0,05 nm either side of central profile for each 1000 $mg.\ell^{-1}$ single cation standard was used in conjuntion with wavelength tables to identify impurities, as well as to distinguish between background elevation and line-wing interferences.

The accurate correction for any error or drift in blank concentration readout is essential in the determination of interference correction coefficients. Table 5-6 illustrates the procedure, using blank error and drift correction analagous to that described for the analysis of

the sample plate in Section 5.3, for the interference of Mg on Mo. The concentration interference data between dotted lines in right hand column of Table 5-6 are used for determination of the interference curve of Mg on Mo, representing concentration equivalent readout on the Mo channel for Mg concentrations of 25 to 1000 $mg.\ell^{-1}$.

TABLE 5-6: Determination of the interference of Magnesium on the Mo(II) 281,615 nm analytical channel of the ARL 34000 polychromator under compromise conditions, showing the blank subtraction and blank drift corrections on concentration equivalent readings (mean ± std., deviation) on the molybdenum channel obtained when aspirating magnesium standards covering the concentration range 5 to 1000 $mg.\ell^{-1}$.

| Sample cup | | | *Mo channel readout | Blank subtraction | Blank drift correction |
|---|---|---|---|---|---|
| No. (n) | Name | Contents $C_{Mg}/mg.\ell^{-1}$ | $/mg.\ell^{-1}(C)$ | $C^a = C-B_O$ | $C^b = C^a - n(B_{10}-B_O)/10$ |
| 0 | BLANK | 0 | -0,3456 ± 0,0035 ($B_0$) | 0 | 0 |
| 1 | S1 | 5 | -0,3439 ± 0,0024 | 0,0017 ± 0,0042 | 0,004 ± 0,004 |
| 2 | S2 | 10 | -0,3519 ± 0,0084 | -0,0063 ± 0,0091 | -0,001 ± 0,009 |
| 3 | S3 | 25 | -0,3400 ± 0,0043 | 0,0056 ± 0,0055 | 0,014 ± 0,005 |
| 4 | S4 | 50 | -0,3210 ± 0,0024 | 0,0246 ± 0,0042 | 0,035 ± 0,004 |
| 5 | S5 | 100 | -0,2808 ± 0,0065 | 0,0648 ± 0,0074 | 0,078 ± 0,007 |
| 6 | S6 | 250 | -0,1769 ± 0,0019 | 0,1687 ± 0,0040 | 0,185 ± 0,004 |
| 7 | S7 | 500 | -0,0010 ± 0,0072 | 0,3446 ± 0,0080 | 0,364 ± 0,008 |
| 8 | S8 | 1000 | 0,3182 ± 0,0085 | 0,6638 ± 0,0092 | 0,685 ± 0,009 |
| 9 | BLANK | 0 | -0,3648 ± 0,0030 ($B_9$) | -0,0192 ± 0,0046 | 0,005 ± 0,005 |
| 10 | BLANK | 0 | -0,3728 ± 0,0044 ($B_{10}$) | -0,0272 ± 0,0056 | 0 |

* Mean ± standard deviation for 3x10 s integrations.

The Mo readout values for cup no., 1 and 2, containing 5 and 10 $mg.\ell^{-1}$Mg respectively, are not used in the determination of the interference curve as these values are less than twice the std., deviation i.e., below the limit of detection.

The use of conventional least squares linear regression to fit the Mg on Mo interference data, while providing a regression coefficient r of 0,9994 (Table 5-7) is nevertheless not an acceptable description of the interference. For low magnesium concentrations a positive deviation ($\Lambda$) is observed while high magnesium concentrations tend to have a negative $\Lambda$ (Table 5-7). Furthermore, the regression does not pass through the origin, resulting in a correction for interference of Mg on Mo even when no Mg is present in a sample.

The fitting of a least squares linear regression of the type advocated by Botto (1983) as given by equation 27 (Chapter 2) results in a good fit near the origin, but shows a tendency for progressively more negative deviations at high magnesium concentrations (Table 5-8). The slope term $C^1$ for a linear regression through the origin is readily calculated by (Green and Margerison, (d), 1978);

$$C^1 = \frac{\sum C_{Mg} \cdot C_{Mo}}{\sum (C_{Mg})^2} \qquad \ldots\ldots\ldots\ldots\ldots \quad (70)$$

where $C^1$ = slope (interference coefficient),

$C_{Mg}$ = Magnesium concentration,

and $C_{Mo}$ = Observed concentration readout on Mo channel.

TABLE 5-7: Difference between observed and calculated values for the interference of Mg on the Mo(II) 281,615 nm analytical channel of the ARL 34000 spectrometer using least squares linear regression(a).

| $C_{Mg}$/mg.ℓ$^{-1}$ | Concentration equiv., interference on Mo 281,615 nm, mg.ℓ$^{-1}$ | | Δ (b) Mo/mg.ℓ$^{-1}$ |
|---|---|---|---|
| | observed(c) | calculated | |
| 0 | 0 | 0,005 | 0,005 |
| 25 | 0,014 ± 0,005 | 0,022 | 0,008 |
| 50 | 0,035 ± 0,004 | 0,039 | 0,004 |
| 100 | 0,078 ± 0,007 | 0,074 | -0,004 |
| 250 | 0,185 ± 0,004 | 0,177 | -0,008 |
| 500 | 0,364 ± 0,008 | 0,349 | -0,015 |
| 1000 | 0,685 ± 0,009 | 0,694 | 0,009 |

(a) $SC_{Mo} = C^1.C_{Mg} + i$; where $C^1$ = 6,89E-4
$i$ = 4,9E-3
and $C_{Mg}$ = magnesium concentration
regression coefficient r = 0,9994 (7 data pairs)

(b) Δ = calculated - observed interference.
Sum of squared residuals; $\sum (-\Delta)^2$ = 4,9E-4.

(c) Mean ± std., deviation (Table 5-6).

TABLE 5-8: Difference between observed and calculated values for the interference of Mg on Mo(II) 281,615 nm analytical channel of the ARL 34000 spectrometer using a least squares linear regression forced through the origin(a).

| $C_{Mg}$/mg.ℓ$^{-1}$ | Concentration equiv., interference on Mo 281,615 nm, mg.ℓ$^{-1}$ | | Δ(b) Mo/mg.ℓ$^{-1}$ |
|---|---|---|---|
| | observed(c) | calculated | |
| 0 | 0 | 0 | 0 |
| 25 | 0,014 ± 0,005 | 0,017 | 0,003 |
| 50 | 0,035 ± 0,004 | 0,035 | 0,000 |
| 100 | 0,078 ± 0,007 | 0,070 | -0,008 |
| 250 | 0,185 ± 0,004 | 0,174 | -0,011 |
| 500 | 0,364 ± 0,008 | 0,348 | -0,016 |
| 1000 | 0,685 ± 0,009 | 0,696 | 0,011 |

(a) $SC_{Mo} = C^1.C_{Mg}$; where $C^1$ = 6,96E-4 and $C_{Mg}$ = magnesium concentration

(b) Δ = calculated - observed interference,
Sum of squares of residuals = $\sum(-\Delta)^2$ = 5,7E-4

(c) Mean ± std., deviation (Table 5-6).

The result of fitting a quadratic regression forced through the origin, of the form given by equation 29 (Chapter 2) is shown in Table 5-9. The quadratic fit clearly extracts maximum information from the data. No residual $(-\Delta)^{@}$ has an absolute value greater than the magnitude of the std., deviation of the observed interference data for Mg on Mo, and the sum of the squared residuals is approximately an order of magnitude smaller than those found for the linear models. Better fit of the interference data is also consistent with the observations of e.g., Dahlquist and Knoll (1978), Garbarino and Taylor (1979) and Larson et al (1983) than non-linear corrections are often required for matrix elements such as Ca. The coefficients of a quadratic fit through the origin (equation 29, Chapter 2) are readily derived as follows:

---

@ The residual is by convention the actual (observed) ordinate value minus the calculated (regression) ordinate value. The deviation, $\Delta$, defined here is the negative residual. This was done so that a positive deviation corresponds to an over-estimated interference, The sum of squares of residuals is thus $\sum(-\Delta)^2$.

Assume a quadratic expression for fitting the interference data of the form;

$$Y = aX + bX^2 \qquad \text{.....} \quad (71)$$

where X = concentration of interferant,

a = dimensionless 1st order interference coefficient,

b = 2nd order interference coefficient, with dimension of reciprocal concentration,

and Y = interference on analyte channel.

**TABLE 5-9:** Difference between observed and calculated values for the interference of Mg on the Mo(II) 281,615 nm analytical channel of the ARL 34000 spectrometer using a quadratic least squares regression through the origin(a)

| $C_{Mg}$/mg.ℓ$^{-1}$ | Concentration equiv., interference on Mo(II) 281,615 nm, mg.ℓ$^{-1}$ | | $\Delta$(b) Mo/mg.ℓ$^{-1}$ |
|---|---|---|---|
| | observed(c) | calculated | |
| 0 | 0 | 0 | 0 |
| 25 | 0,014 ± 0,005 | 0,019 | 0,005 |
| 50 | 0,035 ± 0,004 | 0,038 | 0,003 |
| 100 | 0,078 ± 0,007 | 0,076 | -0,002 |
| 250 | 0,185 ± 0,004 | 0,186 | 0,001 |
| 500 | 0,364 ± 0,008 | 0,363 | -0,001 |
| 1000 | 0,685 ± 0,009 | 0,685 | 0,000 |

(a) $\delta C_{Mo} = C^{1}.C_{Mg} + C^{11}.C_{Mg}$;
where $C^{1} = 7,655E-4$
$C^{11} = 8,03E-8$
and $C_{Mg}$ = magnesium concentration,

(b) $\Delta$ = calculated - observed interference.
Sum of squares of residuals = $\sum(-\Delta)^{2} = 4,0E-5$

(c) Mean ± std., deviation (Table 5-6).

The sum of the squares of the residuals between the observed data points ($X_o$, $Y_o$) and calculated data points ($X_c$, $Y_c$), where $X_c = X_o$ is given by;

$$D = \sum(-\Delta)^2 = \sum(-\overline{Y_c - Y_o})^2$$

$$\text{i.e., } D = \sum(aX_o + bX_o^2 - Y_o)^2 \quad \ldots\ldots\ldots\ldots \quad (72)$$

The partial derivatives of D with respect to a and b are then calculated and set equal to zero, which provides the following two equations;

$$\sum (2a\, X_o^2 + 2b\, X_o^3 - 2Y_oX_o) = 0 \quad \ldots\ldots\ldots\ldots \quad (73)$$

$$\text{from } \frac{\partial D}{\partial a} = 0$$

$$\text{and } \sum (2a\, X_o^3 + 2b\, X_o^4 - 2\, Y_oX_o^2) = 0 \quad \ldots\ldots\ldots\ldots \quad (74)$$

$$\text{from } \frac{\partial D}{\partial b} = 0$$

$$\text{as } \frac{\partial^2 D}{\partial a^2} = \sum(2X_o^2), \text{ which is } \geq 0 \; \forall \; X_o,$$

$$\text{and } \frac{\partial^2 D}{\partial b^2} = \sum(2X_o^4), \text{ which is } \geq 0 \; \forall \; X_o.$$

The solution of equations 73 and 74 for a and b will provide the required expressions for the least squares condition. The first order coefficient $C^1$ is given by the expression for a; and the second order coefficient $C^{11}$ of equation 29 by the value of b:

$$C^{11} = \left( \frac{(\sum X_o^2).\ \sum X_o^2\ .\ Y_o - (\sum X_o.Y_o).\ \sum X^3{}_o}{(\sum X_o^4).\ \sum X_o^2 - (\sum X_o^3)^2} \right) \ldots\ldots \quad (75)$$

$$\text{and } C^1 = \left( \frac{(\sum X_o.Y_o) - (\sum X_o^3).\ C^{11}}{\sum X_o^2} \right) \quad \ldots\ldots \quad (76)$$

Equations 75 and 76 are readily transcribed into computer language statements to facilitate calculation of the coefficients.

In an analagous manner to that illustrated for the interference of Mg on Mo, the interference correction coefficients $C^{1}$ and $C^{11}$ for a quadratic fit through the origin were calculated for the interferences from Ca, Mg, Fe and Mn, and the coefficients obtained compared to those found earlier by Kempster et al (1983). Comparison of the 1983 and 1985 coefficients is given in Tables 5-10 (Ca), 5-11 (Mg), 5-12 (Fe), and 5-13 (Mn). Source conditions for the 1983 and 1985 determinations of interference coefficients were similar, the differences being: (i) An aerosol argon flow rate of 0,40 $\ell.min^{-1}$ was used in 1985 as opposed to 0,41 $\ell.min^{-1}$ in 1983, as the rotameter graduations permitted greater accuracy of adjustment to a flow rate corresponding to a marked division i.e., 0,40.$\ell.min^{-1}$, and (ii) a different Meinhard concentric glass nebulizer.

TABLE 5-10: Linear ($C^{1}$)* and 2nd order ($C^{11}$)** interference correction coefficients from calcium on other analyte element channels on the ARL 34000 spectrometer, showing comparison between coefficients determined in 1983(a) to those found in 1985(b).

| Analyte channel | $*C^{1}(a)$ | $**C^{11}(a)$ | $*C^{1}(b)$ | $**C^{11}(b)$ | $\frac{C^{1}(b)}{C^{1}(a)}$ | $\frac{C^{11}(b)}{C^{11}(a)}$ |
|---|---|---|---|---|---|---|
| Al*** | 6,42E-3@ | -2,0E-6 | 3,91E-3 | -1,2E-6 | 0,61 | 0,60 |
| As | 3,81E-3 | -2,0E-6 | 4,55E-3 | -2,3E-6 | 1,19 | 1,15 |
| B | 9,14E-5 | -5,1E-8 | 6,42E-5 | -1,8E-8 | 0,70 | 0,34 |
| Be | 5,76E-6 | -2,0E-9 | 7,0E-6 | -2,0E-9 | 1,22 | 1,00 |
| Cd | 1,804-4 | -1,1E-7 | 1,51E-4 | -7,2E-8 | 0,84 | 0,65 |
| Co | 3,47E-4 | -1,7E-7 | 2,71E-4 | -9,1E-8 | 0,78 | 0,54 |
| Cr | 1,07E-4 | -6,1E-8 | 1,04E-4 | -4,7E-8 | 0,97 | 0,77 |
| Hg | 1,18E-3 | -9,7E-7 | 4,76E-4 | -2,2E-7 | 0,40 | 0,23 |
| Mn | 1,15E-5 | -2,0E-9 | 2,17E-5 | -1,1E-8 | 1,89 | 5,5 |

* dimensionless
** units of $\ell.mg^{-1}$
*** analytical wavelengths of elements listed shown in Table 4-2.
@ nE - r used as notation for $n.10^{-r}$.

TABLE 5-10 (interference coefficients from calcium, continued)

| Analyte channel | $*C^{1}(a)$ | $**C^{11}(a)$ | $*C^{1}(b)$ | $**C^{11}(b)$ | $\frac{C^{1}(b)}{C^{1}(a)}$ | $\frac{C^{11}(b)}{C^{11}(a)}$ |
|---|---|---|---|---|---|---|
| Mo*** | 1,64E-4@ | -9,7E-8 | 1,63E-4 | -7,2E-8 | 0,99 | 0,74 |
| Ni | 2,04E-4 | -7,6E-8 | 2,05E-4 | -8,4E-8 | 1,00 | 1,10 |
| Pb | 4,85E-3 | -1,8E-6 | 2,33E-3 | -8,5E-7 | 0,48 | 0,47 |
| Sb | 1,17E-3 | -6,2E-7 | 1,22E-3 | -6,0E-7 | 1,04 | 0,97 |
| Se | 6,71E-3 | -4,2E-6 | 8,07E-3 | -3,8E-6 | 1,20 | 0,90 |
| Ti | 1,32E-5 | -6,6E-9 | 1,27E-5 | -3,8E-9 | 0,96 | 0,58 |
| V | 3,91E-5 | -1,7E-8 | 4,61E-5 | -2,2E-8 | 1,18 | 1,29 |
| Y | 1,20E-5 | -5,2E-9 | 9,50E-6 | -3,5E-9 | 0,79 | 0,67 |

* dimensionless

** units of $\ell.mg^{-1}$

*** analytical wavelengths of elements listed shown in Table 4-2.

@ nE - r used as notation for $n.10^{-r}$.

TABLE 5-11: Linear ($C^{1}$)* and 2nd order ($C^{11}$)** interference correction coefficients from magnesium on other analyte element channels on the ARL 34000 spectrometer, showing comparison between coefficients determined in 1983(a) to those found in 1985(b).

| Analyte channel | $*C^{1}$(a) | $**C^{11}$(a) | $*C^{1}$(b) | $**C^{11}$(b) | $\frac{C^{1}(b)}{C^{1}(a)}$ | $\frac{C^{11}(b)}{C^{11}(a)}$ |
|---|---|---|---|---|---|---|
| As*** | 1,34E-3@ | -3,4E-7 | 1,68E-3 | -7,8E-7 | 1,25 | 2,29 |
| B | 5,67E-5 | -7,3E-10 | 5,40E-5 | -1,8E-8 | 0,95 | 2,5E1 |
| Be | 2,97E-6 | 3,0E-10 | 3,00E-6 | - | 1,01 | - |
| Cd | 6,04E-5 | -1,6E-8 | 7,93E-5 | -4,5E-8 | 1,31 | 2,8 |
| Co | 8,55E-5 | 2,6E-8 | 9,96E-5 | -2,4E-8 | 1,16 | -0,92 |
| Hg | 1,48E-4 | 6,8E-9 | 3,78E-4 | -1,5E-7 | 2,55 | -2,2E1 |

* dimensionless

** units of $\ell.mg^{-1}$

*** analytical wavelengths of elements listed shown in Table 4-2.

@ nE - r used for notation for $n.10^{-r}$.

TABLE 5-11 (interference coefficients from magnesium, continued)

| Analyte channel | $*C^{1}(a)$ | $**C^{11}(a)$ | $*C^{1}(b)$ | $**C^{11}(b)$ | $\frac{C^{1}(b)}{C^{1}(a)}$ | $\frac{C^{11}(b)}{C^{11}(a)}$ |
|---|---|---|---|---|---|---|
| Mo*** | 6,82E-4@ | -5,5E-8 | 7,66E-4 | -8,0E-8 | 1,12 | 1,45 |
| Pb | 1,71E-3 | -9,6E-7 | 3,64E-4 | -6,5E-8 | 0,21 | 0,07 |
| Sb | 3,66E-4 | 2,6E-8 | 5,96E-4 | -3,0E-7 | 1,63 | -1,2E1 |
| Se | 1,74E-3 | -1,7E-7 | 4,24E-3 | -2,4E-6 | 2,44 | 1,4E1 |
| V | 1,14E-5 | 6,6E-9 | 2,74E-5 | -1,0E-8 | 2,40 | -1,5 |
| Y | 5,46E-6 | -1,6E-10 | 4,00E-6 | - | 0,73 | - |
| Zr | 5,19E-5 | -9,8E-8 | 3,22E-5 | 8,7E-9 | 0,62 | -0,09 |

* dimensionless

** units of $\ell.mg^{-1}$

*** analytical wavelengths of elements listed shown in Table 4-2.

@ nE - r used as notation for $n.10^{-r}$.

TABLE 5-12: Linear ($C^{1}$)* and 2nd order ($C^{11}$)** interference correction coefficients from iron on other analyte element channels on the ARL 34000 spectrometer, showing comparison between coefficients determined in 1983 (a) to those found in 1985(b).

| Analyte channel | $*C^{1}(a)$ | $**C^{11}(a)$ | $*C^{1}(b)$ | $**C^{11}(b)$ | $\frac{C^{1}(b)}{C^{1}(a)}$ | $\frac{C^{11}(b)}{C^{11}(a)}$ |
|---|---|---|---|---|---|---|
| Al*** | 1,29E-4@ | -9,3E-9 | 4,95E-5 | 2,0E-8 | 0,38 | -2,2 |
| As | 8,26E-4 | -1,8E-7 | 6,26E-4 | -2,0E-8 | 0,76 | 0,11 |
| B | 3,43E-4 | -1,1E-8 | 2,84E-4 | 1,9E-8 | 0,83 | -1,73 |
| Be | 7,12E-5 | 2,9E-9 | 2,66E-4 | 9,8E-9 | 3,74 | 3,38 |
| Cd | 3,36E-4 | -1,4E-8 | 3,11E-4 | 2,5E-9 | 0,92 | -0,18 |
| Co | 1,36E-4 | -3,6E-8 | 7,37E-5 | 1,0E-8 | 0,54 | -0,28 |
| Cr | 2,04E-4 | -4,1E-8 | 4,44E-5 | 1,2E-8 | 0,22 | -0,29 |
| Hg | 1,14E-2 | -1,1E-6 | 6,33E-3 | -8,1E-8 | 0,56 | 0,07 |

* dimensionless

** units of $\ell.mg^{-1}$

*** analytical wavelengths of elements listed shown in Table 4-2.

@ nE - r used as notation for $n.10^{-r}$.

TABLE 5-12 (interference coefficients from iron, continued)

| Analyte channel | $*C^{1}(a)$ | $**C^{11}(a)$ | $*C^{1}(b)$ | $**C^{11}(b)$ | $\frac{C^{1}(b)}{C^{1}(a)}$ | $\frac{C^{11}(b)}{C^{11}(a)}$ |
|---|---|---|---|---|---|---|
| Mo*** | 4,88E-5@ | -1,1E-9 | 4,71E-5 | -1,6E-10 | 0,96 | 0,14 |
| Ni | 1,22E-4 | -2,5E-8 | 1,05E-4 | 8,2E-9 | 0,86 | -0,33 |
| Pb | 9,56E-4 | -1,4E-9 | 5,39E-4 | 2,6E-7 | 0,56 | -1E2 |
| Sb | 2,30E-4 | 5,5E-8 | 2,06E-4 | 8,2E-9 | 0,90 | 0,15 |
| Se | 8,80E-4 | 5,2E-7 | 8,86E-4 | 8,6E-7 | 1,01 | 1,65 |
| V | 5,21E-5 | 2,6E-9 | 3,74E-5 | 5,2E-9 | 0,72 | 2,0 |
| Y | 2,90E-6 | -3,9E-10 | 2,02E-6 | - | 0,70 | - |
| Zn | 1,64E-4 | -4,4E-10 | 8,06E-5 | 4,0E-8 | 4,91 | -9E1 |
| Zr | 7,73E-5 | 3,8E-9 | 7,52E-5 | 2,0E-8 | 0,97 | 5,3 |

* dimensionless

** units of $\ell.mg^{-1}$

*** analytical wavelengths of elements listed shown in Table 4-2.

@ nE - r used as notation for $n.10^{-r}$.

TABLE 5-13: Linear ($C^{1}$)* and 2nd order ($C^{11}$)** interference correction coefficients from manganese on other analyte element channels on the ARL 34000 spectrometer, showing comparison between coefficients determined in 1983(a) to those found in 1985(b).

| Analyte channel | $*C^{1}$(a) | $**C^{11}$(a) | $*C^{1}$(b) | $**C^{11}$(b) | $\frac{C^{1}(b)}{C^{1}(a)}$ | $\frac{C^{11}(b)}{C^{11}(a)}$ |
|---|---|---|---|---|---|---|
| As*** | 8,54E-4@ | -2,4E-7 | 8,18E-4 | -2,6E-7 | 0,96 | 1,08 |
| Be | 2,77E-6 | 5,9E-9 | 9,50E-6 | -3,5E-9 | 3,4 | -0,59 |
| Cr | 2,71E-4 | -5,5E-9 | 3,06E-4 | -4,7E-8 | 1,13 | 8,5 |
| Cu | 3,46E-5 | -1,0E-8 | 3,80E-5 | -2,0E-8 | 1,10 | 2,0 |
| Fe | 7,58E-4 | -1,0E-7 | 4,63E-4 | 2,5E-9 | 0,61 | -2,5E-2 |
| Hg | 1,09E-3 | -6,1E-7 | 5,17E-4 | -8,0E-8 | 0,47 | 0,13 |

* dimensionless

** units of $\ell.mg^{-1}$

*** analytical wavelengths of elements listed shown in Table 4-2.

@ nE - r used as notation for $n.10^{-r}$.

TABLE 5-13: (interference coefficients from manganese, continued)

| Analyte channel | $*C^{1}(a)$ | $**C^{11}(a)$ | $*C^{1}(b)$ | $**C^{11}(b)$ | $\frac{C^{1}(b)}{C^{1}(a)}$ | $\frac{C^{11}(b)}{C^{11}(a)}$ |
|---|---|---|---|---|---|---|
| Mo*** | 3,09E-3[@] | -5,7E-7 | 1,7 E-3 | -1,6E-7 | 0,55 | 0,28 |
| Pb | 9,95E-4 | -1,8E-7 | 5,01E-4 | -3,0E-8 | 0,50 | 0,17 |
| Sb | 3,88E-4 | -1,7E-7 | 3,75E-4 | -2,2E-7 | 0,97 | 1,29 |
| Se | 1,70E-2 | -5,0E-6 | 1,03E-2 | -1,4E-6 | 0,60 | 0,28 |
| V | 2,80E-4 | -7,6E-9 | 3,09E-4 | -6,4E-9 | 1,10 | 0,84 |
| Y | 3,68E-6 | -3,1E-10 | 4,75E-6 | -1,7E-9 | 1,29 | 5,5 |
| Zr | 3,13E-4 | 3,6E-8 | 6,95E-4 | -1,6E-8 | 2,22 | -0,44 |

* dimensionless

** units of $\ell.mg^{-1}$

*** analytical wavelengths of elements listed shown in Table 4-2.

@ nE - r used as notation for $n.10^{-r}$.

The ratio between the 1985 and 1983 determination of interference coefficients for interference from calcium (Table 5-10) shows that the coefficients changed significantly for some analyte elements, whereas little change was observed for others. The coefficients for Ca interference on Sb, for example show a less than 5% change, whereas Ca interference on Al showed a 39% decrease for the linear ($C^1$) coefficient and a 40% decrease for the 2nd order ($C^{11}$) coefficient. The similar change in the 1st and 2nd order coefficients for Ca on Al interference implies that the relative Ca to Al intensities have changed, but not the shape of the interference curve. A linear correlation with r = 0,83 was found between the two ratios $C^1(b)/C^1(a)$ and $C^{11}(b)/C^{11}(a)$ for the interferences from calcium (Table 5-10). This implies a relative stability of the nature of the interferences from calcium.

The interference coefficients with Mg as interferant (Table 5-11) by contrast, however, showed unstable 2nd order coefficients, some changing by more than an order of magnitude for several elements, with a change in sign often being observed. The 1st order coefficients were relatively stable with little change for interference on B or Be, to a two and a half fold increase for interference on Hg.

Correction coefficients for interference from iron (Table 5-12) showed similar behaviour to that observed for Mg as interferant. The stability of the 2nd order coefficients for iron, however, is greater than that for Mg. The linear interference correction coefficient $C^1$, showed less than 10% change for interference of Fe on Cd, Mo, Se and Zr, to an approximately 4 fold increase for Fe interference on Be, and a 5 fold increase for Fe interference on Zn (Table 5-12).

The 1st order interference correction coefficients for manganese as interferant (Table 5-13) showed relative stability of the 1st order coefficients for As, Cr, Cu, Sb and V, with less than 14% change, to an approximately three and a half fold increase of Mn on Be interference. The 2nd order coefficients ranged from an 8% increase for As, to a decrease of two and a half orders of magnitude for Fe.

The observed changes in interference coefficients are partially explained by the different natures of the interferences. All calcium interferences (Tables 5-10) are of the background elevation type, with the exception of Al (interference of the wing of Ca(II) 396,85 nm on Al(I) 396,15 nm) and Ti (interference of Ca(I) 335,02 nm on Ti(II) 334,94 nm) as identified by measurements at offset profile position (Kempster et al, 1983). Interferences of the background elevation type are insensitive to small changes in profile position. The relatively large

wavelength difference of 0,7 nm between Ca(II) 396,85 nm and Al(I) 396,15 nm also causes this particular interference to behave as a background elevation type interference. The observed changes in the interferences are therefore ascribed to source changes, or changes in nebulization characteristics affecting excitation temperatures within the aerosol channel, and therefore affecting relative emission intensities. The implications are that the validity of the interelement interference correction coefficients are dependent on the maintenance of a strictly reproducible inner gas flow rate so that nebulization characteristics and the height at which a given tempertaure is reached within the central channel of the plasma remain invariant.

The interferences from iron and manganese are, however, largely of the spectral overlap type (Kempster et al, 1983), with the exception of Fe on Y and Mn on Cu. Greater instability of interference corrections can therefore be expected, particularly in the light of the fact that exit slit profiles were checked, and adjusted where necessary prior to the 1985 interference coefficient determinations.

The instability of the 2nd order interference correction coefficients for Mg as interferant (Table 5-11) presents something of a puzzle, as these interferences are of the background elevation type with the possible contribution of a spectral overlap component to the interference of Mg on

Mo(II) 281,60 nm. Magnesium shows moderate stability of the 1st order coefficients for interference on other analyte elements, yet great instability of the shape of the interference curve as reflected in the change in the 2nd order coefficients. The latter behaviour is expected for spectral overlap interferences rather than for background elevation type interferences.

The difficulty of exact determination of interference correction coefficients in the software approach, under the given analytical conditions which apply during the analysis of a set of samples results in a deterioration of the detection limit. The approach of Botto (1984) using the criterion that analysis is quantitative when the Percentage interference correction (PIC) $\leq$ 100% (equation 31, Chapter 2) is useful in this regard, but can only be considered as a rule-of-thumb for the following reason: Detection limit in the classical sense is determined by the background noise rather than by the absolute magnitude of the background signal. Likewise, in an analagous sense, the accuracy of an interference correction will depend on the accuracy with which the magnitude of the interference signal is estimated rather than on the relative magnitude of the interference and analyte signals. Where the interference signal is determined at the time of analysis, e.g., in the profile scan mode of analysis on the ARL 3510 spectrometer, then a net analyte signal considerably smaller than the interference background elevation may be quantified. This will be illustrated in the next chapter.

## 5.5 Memory effects in the sample transport system

Memory effects in the nebulizer system following aspiration of a high concentration standard or a sample containing an analyte at high concentration cause carry over of signal to the subsequent sample or samples. Allowance for this carry over requires re-analysis of samples of low concentration which were run on the autosampler of the ARL 34000 spectrometer in a sample cup position immediately following a high concentration sample; or the insertion of one or more blank sample cups on the sampler following a sample of suspected high concentration. The alternative approach to the memory effect phenomenon of correcting mathematically for signal memory as suggested by Dobb and Jenke (1983), using a hyperbolic function (equation 23, Chapter 2) was therefore investigated.

A 1000 $mg.\ell^{-1}$ Hg(II) stock solution was aspirated on the ARL 34000 spectrometer and the Hg 253,65 nm line emission intensity recorded for 2 s integration times. Other operating conditions were those for compromise instrumental operation (Table 4-4). When the Hg gross emission signal had stabilized, the sample aspiration probe was transfered to a $\phi$ = 0,01 nitric acid blank wash solution, and the analyte emission intensity recorded sequentially thereafter for approximately 12 min. The blank emission intensity had also been recorded immediately

prior to aspiration of the Hg standard solution in order to be certain of the blank intensity in the absence of recent exposure of the nebulizing system to high analyte concentration.

In order to avoid aspiration of an air-plug during transference of the aspiration tube from the 1000 $mg.\ell^{-1}$ Hg solution to the wash solution, the peristaltic pump was momentarily switched off. The probe was also dipped for about 1 s into deionized water to rinse its outer surface prior to placement in the blank solution. The washout time t was recorded the instant that the peristaltic pump was restarted. The whole transfer and probe rinse procedure took between 3 and 4 s. Washout intensity data was recorded from the instant when the peristaltic pump was restarted.

The washout curve data for Hg, on aspiration of nitric acid, $\phi$ = 0,01 blank solution is given in Table 5-14.

TABLE 5-14: Washout curve data for Hg, on aspiration of nitric acid, $\phi$ = 0,01, for the ARL 34000 spectrometer[a].

| t/s | I | t/s | I |
|---|---|---|---|
| 4 | 13450* | 76 | 79,37 |
| 12 | 13460* | 116 | 64,14 |
| 20 | 13460* | 156 | 54,97 |
| 28 | 10180 | 196 | 50,75 |
| 36 | 4176 | 276 | 45,30 |
| 44 | 1563 | 356 | 41,74 |
| 52 | 526,7 | 436 | 39,60 |
| 60 | 193,5 | 516 | 33,57 |
| 68 | 87,61 | 596 | 31,40 |
| | | 716 | 33,06 |
| | | 00 | 30,4 $\pm$ 0,2 |

* Initial plateau as a consequence of the washout of 1000 mg.$\ell^{-1}$ Hg solution on the peristaltic pump and apsiration tube.

(a) After the washout time t, the gross intensity, I, was integrated for 2 s, using the QA 34000 assembler software. In Figure 5-2 the gross intensity is plotted against the reciprocal of the mean washout time over the integration.

In Table 5-14, the first three intensities for t = 5 to t = 21 s are constant. This is due to wash-through of 1000 $mg.\ell^{-1}$ Hg solution in the peristaltic pump tube and aspiration tube. The time for this dead volume to be replaced was subsequently measured as 29 s by the timing of an aspirated air plug. A least squares linear regression of the gross intensity (I) to the reciprocal of washout time ($t^{-1}$) for the 16 data points from t = 29 to t = 717s as suggested by Dobb and Jenke (1983) gave a linear regression coefficient of r = 0,794. A plot of I to $t^{-1}$ is given in Figure 5-2 which shows that the I to $^{1}/t$ relationship is clearly not linear and that equation 23 is therefore not suitable to describe the washout curve of mercury. Figure 5-2 indicates that the $^{1}/t$ transformation is not sufficient to linearize the washout curve as suggested by Dobb and Jenke (1983). The possibility of attempting a linearization transformation on both the gross intensity (I) and washout time (t) data values was therefore investigated.

As an experiment, the transformation ln I versus ln t was used. The transformed data for the $\phi$ = 0,01 nitric acid washout being plotted in Figure 5-3. The ln I versus ln t transformation plot has the advantage that detail is not lost for small intensity values at large t. This transformation showed that the washout curve can be divided into three distinct phases (Figure 5-3), i.e., (a)

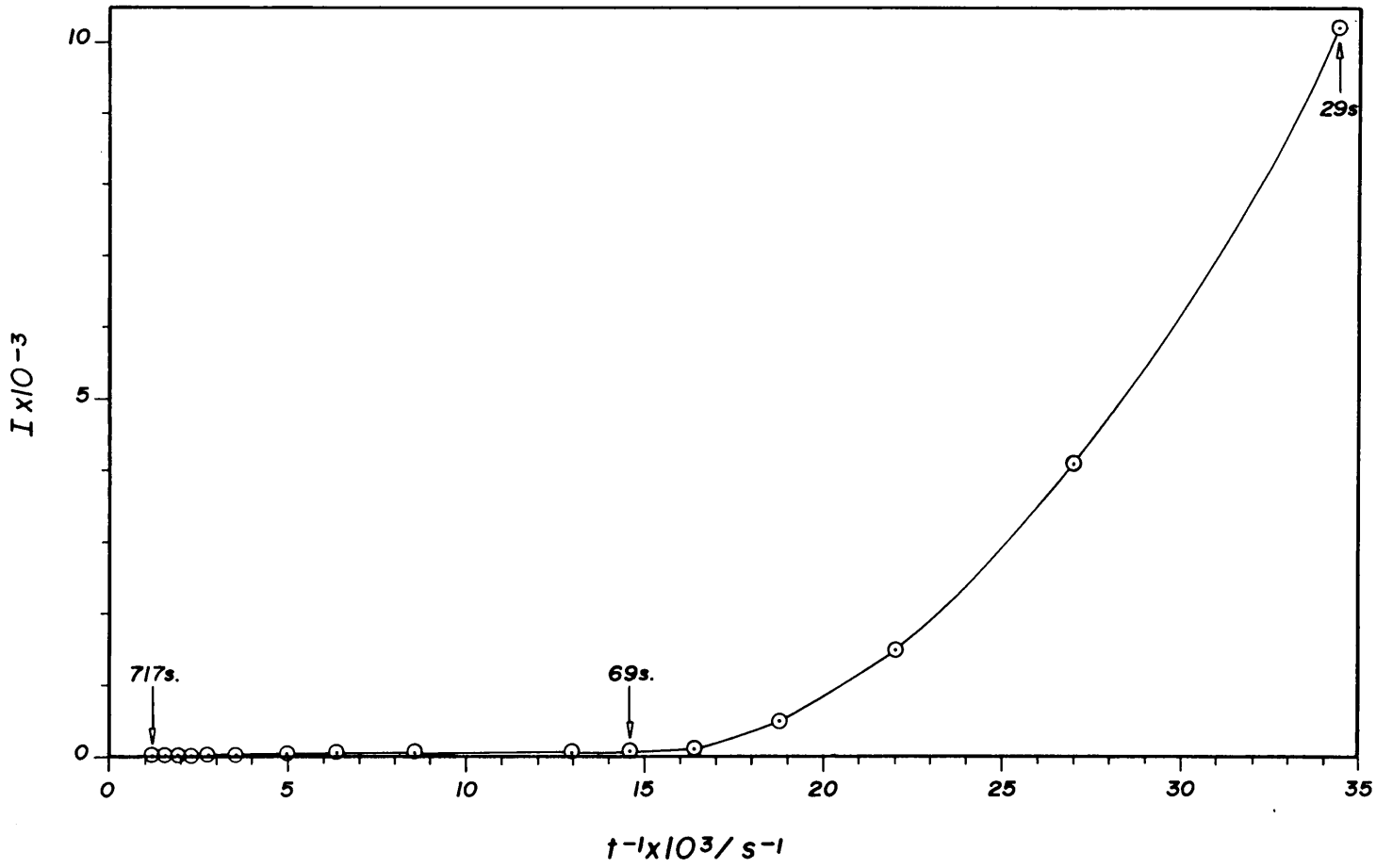


Figure 5-2: Plot of gross intensity (I) of Hg 253,65 nm against the reciprocal of washout time ($t^{-1}$) for nitric acid $\phi$ = 0,01 wash following aspiration of a 1000 mg.$\ell^{-1}$ Hg(II) solution on the ARL 34000 spectrometer; showing firstly the lack of linearity of the I versus $t^{-1}$ plot, and secondly the unsuitability of such a plot for small I and large t, as coincidence with the abscissa occurs for small I.

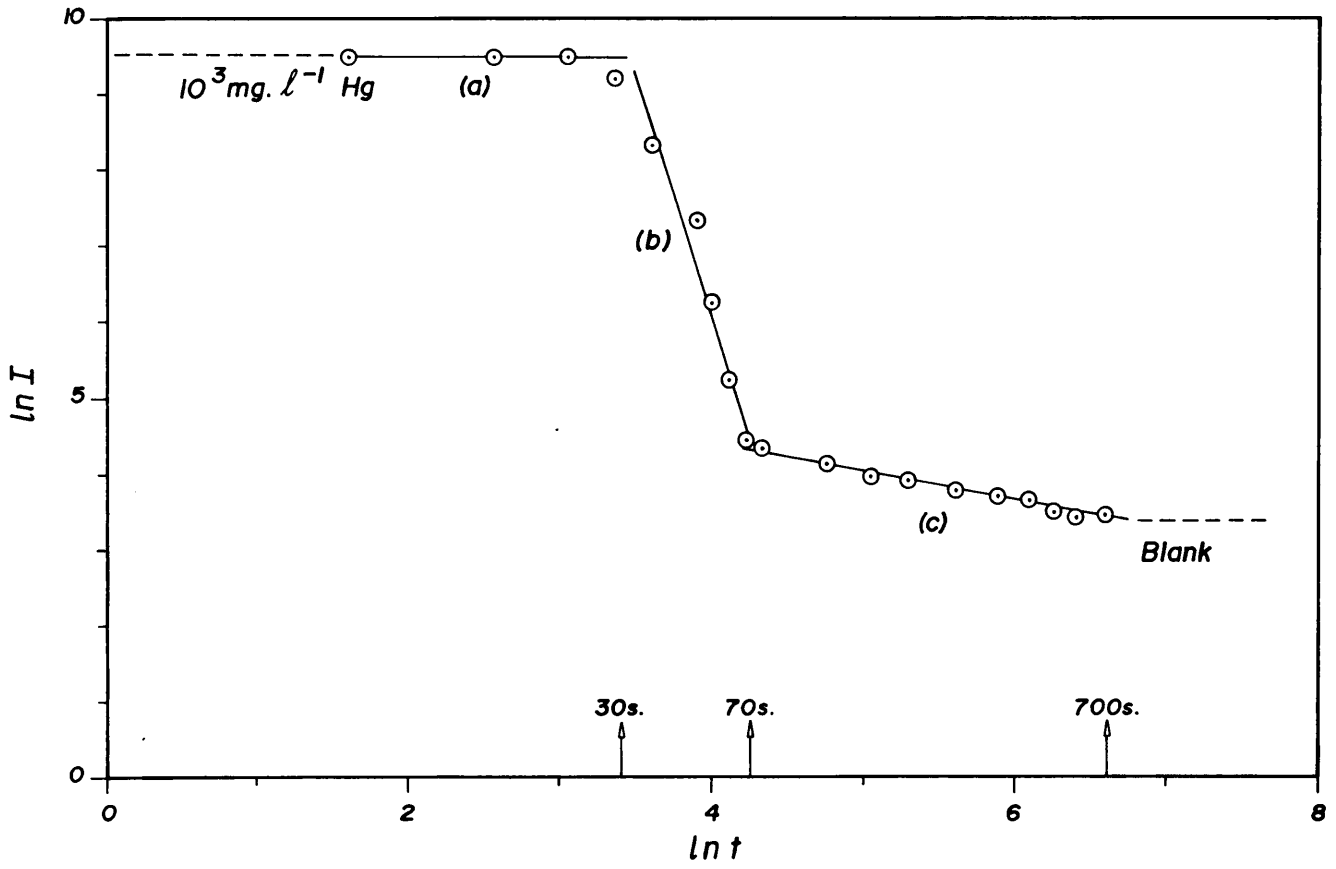


Figure 5-3: Washout memory effect for Hg on the ARL 34000 spectrometer expressed as the natural logarithm of the gross Hg(I) 253,65 nm intensity to the natural logarithm of the washout time in seconds. The plateau (a) represents retention within the aspiration tube; (b) is the rapid washout phase; and (c) the slow washout phase. The wash solution was nitric acid $\phi$ = 0,01.

the pre-washout plateau representing high concentration solution replaced from the dead volume of the pump and aspiration tubing, (b) the rapid washout phase from 30 s to 70 s, and (c) the slow washout phase from 70 to 720 seconds where a more gradual washout occurs. The rapid (b) and slow (c) washout phases are each accurately approximated by a linear function on this plot. A linear regression coefficient of r = -0,992, with slope of - 5,63 (for 6 data points) was found for the rapid washout segment (b); and a linear regression coefficient of r = -0,990, with slope of -0,40 (for 10 data points) was found for the slow washout segment (c) in Figure 5-3. The following two regression equations were obtained:

Rapid washout (b)

$$\ln I = -5{,}63 \ln t + 28{,}5 \quad \ldots\ldots\ldots\ldots\ldots \quad (77)$$

Slow washout (c):

$$\ln I = -0{,}40 \ln t + 6{,}1 \quad \ldots\ldots\ldots\ldots\ldots \quad (78)$$

These equations are of the form:

$$\ln I = -m. \ln t + q \quad \ldots\ldots\ldots\ldots\ldots \quad (79)$$

$$\text{i.e. } \ln I = \ln \left( \frac{e^{q}}{m_{t}} \right)$$

i.e. $I = \frac{Q}{t^m}$ ; where $Q = e^q$ ..... (80)

expressed in the form of equation 80, the rapid washout phase for Hg with nicric acid, $\phi$ = 0, 01 wash solution becomes;

$$I = \frac{2,38 \times 10^{12}}{t^{5,63}} \quad \text{..... (81)}$$

and the slow washout equation 78 becomes;

$$I = \frac{446}{t^{0,4}} \quad \text{..... (82)}$$

Other elements gave similar washout curves e.g., Ti (Figure 5-4).

The determination of memory effect curves was carried out for 17 other analyte elements, in a manner analagous to that used for mercury. The ln I versus ln t transformation gave washout curves similar to that for mercury (Figure 5-3). The Q and m parameters for a fit of equation 80 to the data for the ln I versus ln t washout curves is given in Table 5-15. The initial analyte concentration chosen depended on the intensity of the analyte emission signal and varied from 100 to 1000 $mg.\ell^{-1}$. For K and Si, 1000 $mg.\ell^{-1}$ concentrations did not provide sufficiently intense signals to determine the slow washout portion of the curve accurately.

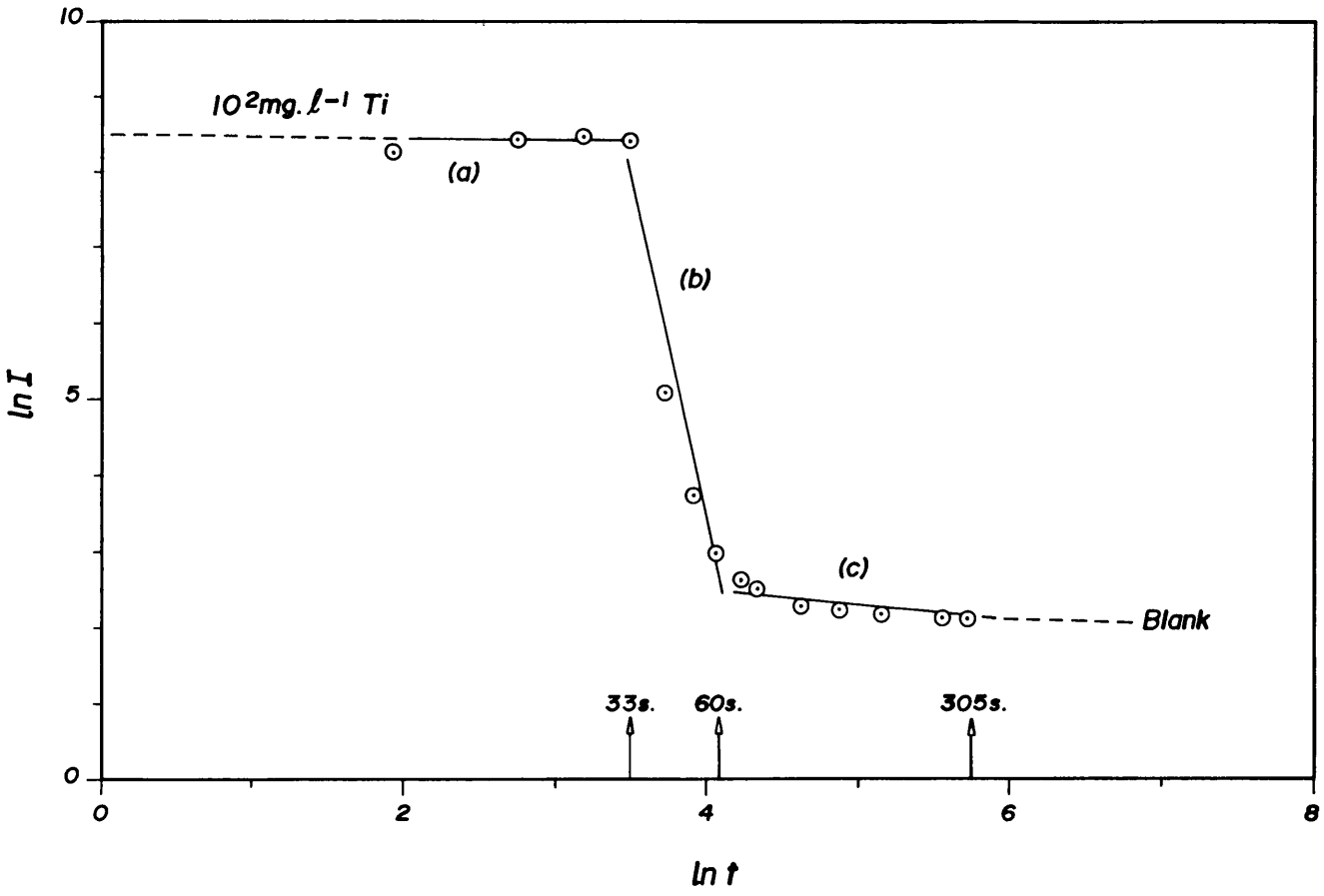


Figure 5-4: Washout memory effect for Ti on the ARL 34000 spectrometer expressed as the natural logarithm of the gross Ti(II) 334,94 nm intensity to the natural logarithm of the washout time in seconds, The initial plateau (a), rapid washout (b) and slow washout phase (c) are similar to those observed for Hg (Figure 5-3). The wash solution was nitric acid $\phi$ = 0,01.

The washout time needed to reach 1% of the initial net analyte intensity ($t_{1\%}$), and 0,1% of the initial net analyte intensity ($t_{0,1\%}$) were determined by interpolation from the ln I versus ln t plots. These washout times are given in Table 5-16. If the time to displace the dead volume in the pump and aspiration tube to the nebulizer is taken into account, then the $t_{1\%}$ and $t_{0,1\%}$ washout times should be decreased by 29 s. As can be seen from Table 5-16 the washout time to 1% of initial net intensity is approximately the same for the various elements, and varies between 48 and 67 s, with a mean of 60 s. The washout time to 0,1% of initial net intensity is between 63 and 85 s, for most elements with the exception of Hg and Mo which gave $t_{0,1\%}$ values of 317 and 171 s, respectively.

The major cause of the memory effect, excluding the dead volume replacement time of the pump and aspiration tubes, was identified as residing distal to the nebulizer <u>per se</u> i.e., in the spray chamber, torch or plasma by an experiment done where the analyte aspiration was interrupted, through switching off the peristaltic pump and then recording the memory curve. Figure 5-5 shows the memory effect when the peristaltic pump was switched off during aspiration of a 1000 $mg.\ell^{-1}$ Hg solution. The initial plateau (a) is absent, with the rapid signal decrease occurring almost immediately, followed by a slow decrease (c). The slope of segments (b) and (c) is -2,46

TABLE 5-15: Memory effect data for washout curves of analyte elements on the ARL 34000 spectrometer giving the Q and m parameters of the equation $I = Q/t^{m*}$ for (a) the fast washout between 30 and 70 s, and (b) the slow washout for t > 70 s. I is the gross analyte intensity.**

| Analyte | Fast wash | | Slow wash | |
|---|---|---|---|---|
| | Q | m | Q | m |
| Al | 2,64E11@ | 5,77 | 1,08E1 | 0,40 |
| B | 8,77E11 | 5,98 | 3,21E1 | 0,42 |
| Ca | 1,78E9 | 4,59 | 8,67E0 | 0,03 |
| Cd | 1,77E12 | 6,24 | 1,82E1 | 0,09 |
| Co | 3,21E13 | 6,64 | 1,99E1 | 0,32 |
| Fe | 3,58E9 | 4,93 | 9,56E1 | 0,94 |
| Hg | 2,38E12 | 5,63 | 4,37E2 | 0,40 |
| K | 2,18E7 | 3,64 | - | - |
| Mg | 7,16E12 | 6,60 | 5,47E0 | 0,16 |
| Mn | 2,92E11 | 5,82 | 3,99E2 | 1,16 |
| Mo | 5,35E9 | 4,79 | 3,52E1 | 0,22 |
| Na | 7,18E11 | 6,37 | 3,32E0 | 0,04 |
| Ni | 1,30E13 | 6,47 | 1,68E1 | 0,31 |
| Pb | 2,94E9 | 4,96 | 5,36E0 | 0,25 |
| Si | 4,38E9 | 5,08 | - | - |
| Sr | 1,18E14 | 6,74 | 8,43E3 | 1,76 |
| Ti | 1,59E15 | 7,82 | 3,96E1 | 0,29 |
| V | 1,44E13 | 6,78 | 1,58E1 | 0,08 |

* See equation 80

** Washout solution nitric acid, $\phi$ = 0,01 except for B and Si where deionized water was used.

@ nE - r used as notation for $n.10^{-r}$.

**TABLE 5-16:** Washout times to 1% of initial net analyte intensity ($t_{1\%}$) and 0,1% of initial intensity ($t_{0,1\%}$) for various elements using nitric acid, $\phi$ = 0,01 wash solutions except for B and Si where deionised water was used, on the ARL 34000 spectrometer.

| Analyte | $t_{1\%}$/s | $t_{0,1\%}$/s |
|---|---|---|
| Al | 67 | 81 |
| B | 63 | 85 |
| Ca | 61 | 72 |
| Cd | 48 | 63 |
| Co | 64 | 75 |
| Fe | 66 | 82 |
| Hg | 63 | 317 |
| K | 53 | 66 |
| Mg | 61 | 73 |
| Mn | 64 | 75 |
| Mo | 63 | 171 |
| Na | 56 | 65 |
| Ni | 64 | 76 |
| Pb | 66 | 81 |
| Si | 63 | - |
| Sr | 66 | 77 |
| Ti | 48 | 75 |
| V | 48 | 64 |

and -0,39 (Figure 5-5). Other elements showed similar behaviour (Figure 5-6).

From a practical analytical viewpoint, the use of equation 80 for correction for signal memory during the rapid washout phase for t < 70 s would be undesirable as the high order of the exponent of t renders correction very sensitive to exact timing. Use of this equation during the slow washout phase for t > 70 s, where the slope is much less steep may be feasible, however.

## 5.6 Use of internal standardization to correct for error in ion-line readout caused by slight change in aerosol gas flow rates.

As pointed out in Section 4.8 of the previous chapter, change in aerosol gas flow rate results in change in emission intensities of varying degree, depending on the analyte emission line concerned. This change is particularly pronounced in the case of ionic lines. A correlation between the degree of change in emission intensity for ionic emission and the excitation potential allowed a mathematical relationship to be constructed which may prove useful as a type of weighted internal standardization formula (equation 62, section 4.9).

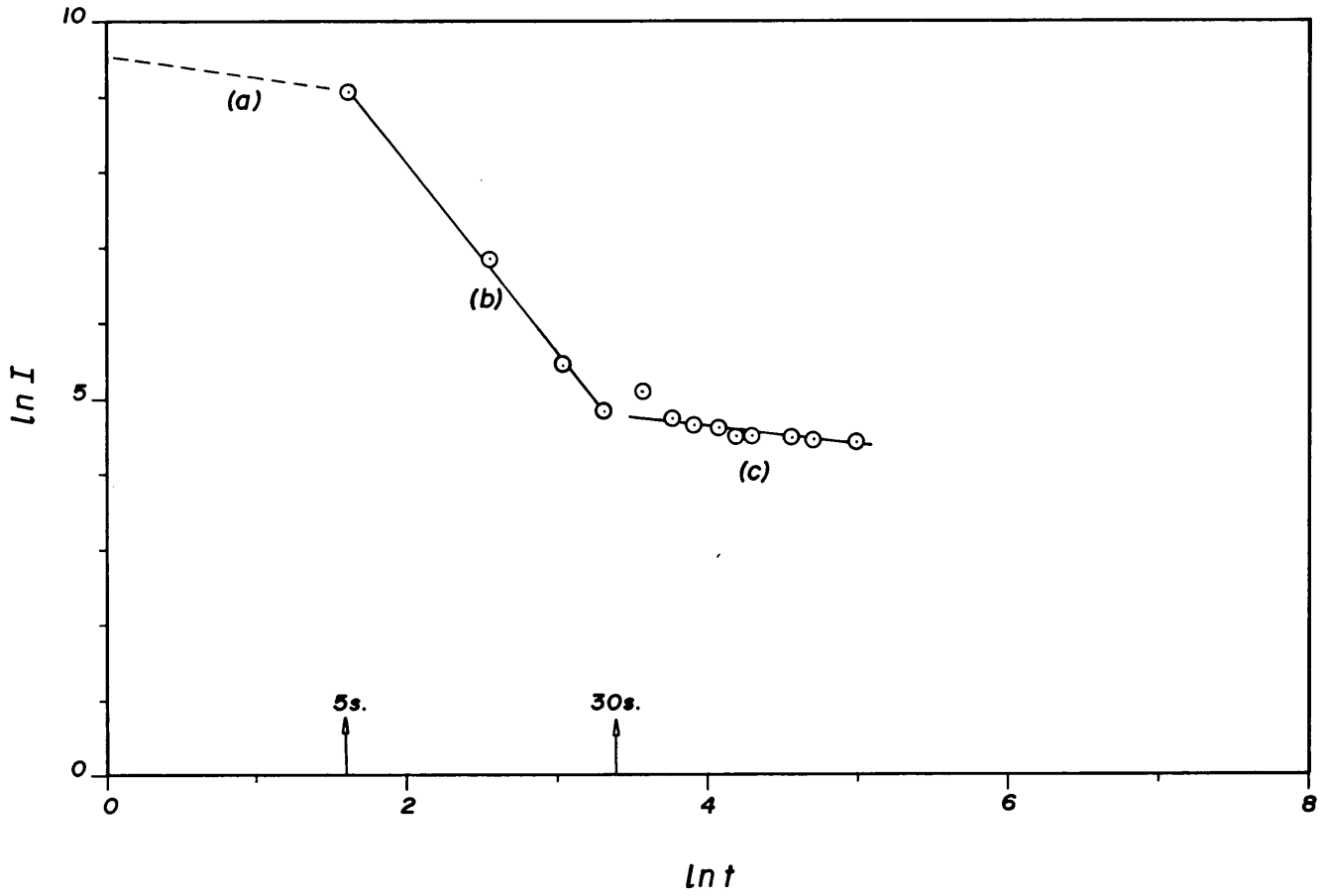


Figure 5-5: Memory effect within the nebulizing chamber for Hg on the ARL 34000 spectometer expressed as the natural logarithm of Hg(II) 253,65 nm intensity to the natural logarithm of the time (t) in seconds following switching off the peristaltic pump and cessation of aspiration. The initial plateau (a) is almost absent, with the aerosol fog dissipating rapidly (b); followed by a slow decline of residual memory (c). The initial Hg concentration was 1000 mg.$\ell^{-1}$.

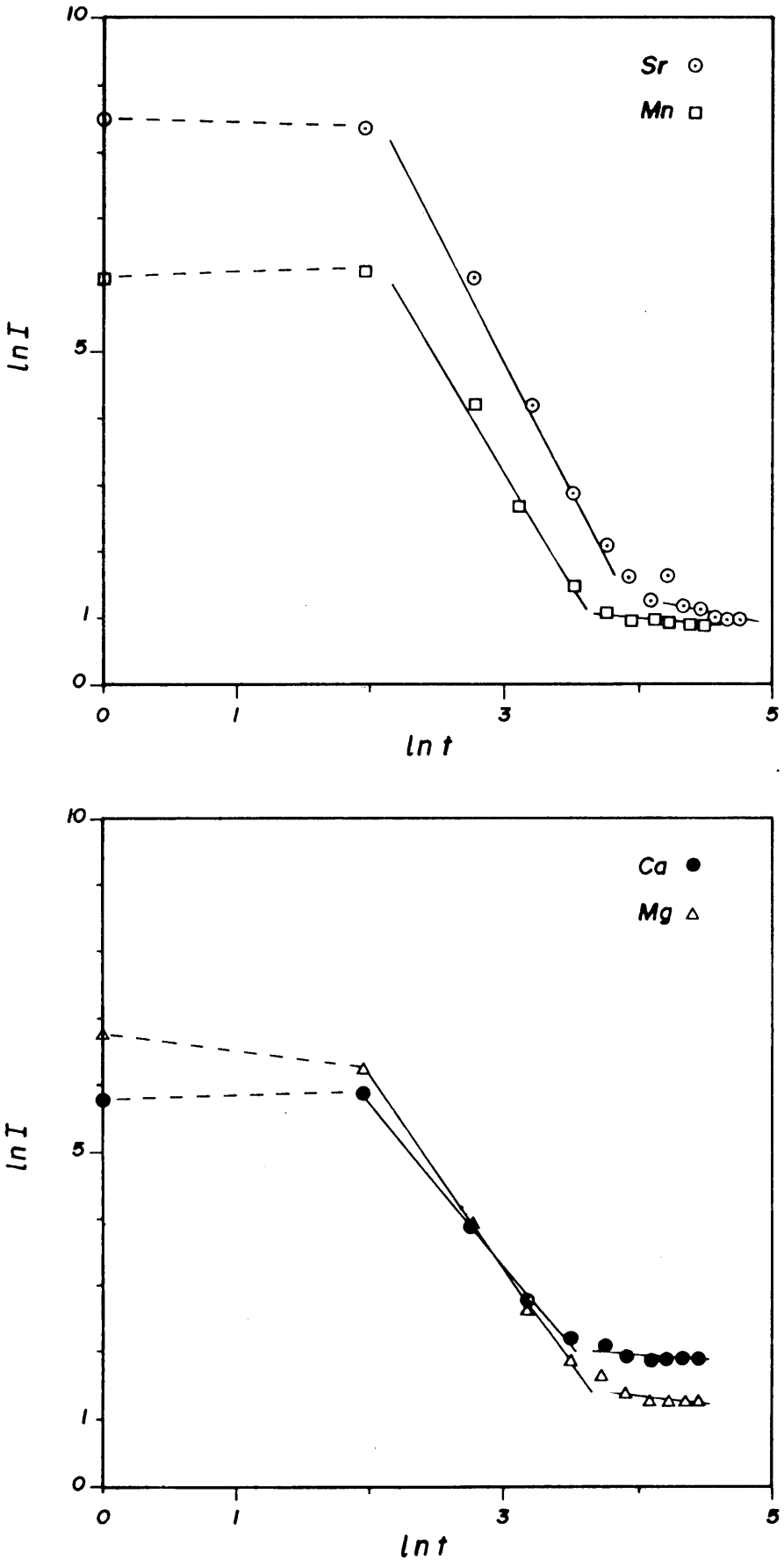


Figure 5-6: Memory effect within the nebulizing chamber for Sr and Mn (upper diagram), and Ca amd Mg (lower diagram) following switching off the peristaltic pump; showing analagous behaviour to that described in Figure 5-5. The initial concentrations of Sr, Mn, Ca and Mg were 100; 110; 600 and 600 mg.$\ell^{-1}$ respectively.

Equation 62 was tested by analyzing a set of standard solutions at an aerosol flow rate of 380 mℓ.min$^{-1}$ i.e., 5% less than the flow rate of 400 mℓ.min$^{-1}$ used for normalization of the ARL 34000 polychromator. The standards were prepared by dilution of the mixed calibration standards (Table 5-1); standard 2 being prepared without manganese. Each solution was spiked with 10 mg.ℓ$^{-1}$ Mn, for the purpose of internal standardization. The concentration readout data, together with the true analyte concentration, percentage error and concentration readout for the added manganese is shown in Table 5-17. As can be seen from this table, the concentration readout error without use of the internal standardization correction is unacceptably large, with only two of the eleven ion-line channels showing <5% error i.e., Zr(II) 349,62 nm and Mo(II) 281,62 nm. The remaining ion-line channels all have an error of greater than 10%, with Ca(II) 315,89 nm showing an error of + 56%. The recovery of the 10 mg.ℓ$^{-1}$ manganese spike varied between 119,3% and 123,0%.

Application of the weighted internal standardization correction given by equation 62, resulted in a dramatic reduction in overall error for the ion-line analyte channels (Table 5-18). Seven channels now produced acceptable results, with the error being numerically less than 5%. The error in calcium concentration was also reduced from +56% to +21%. The calculation of the corrected concentrations with the aid of equation 62 is illustrated in Table 5-19.

TABLE 5-17: Error in ion line analyte concentration readout (mean of 3x10s integrations) caused by a 5% reduction in aerosol gas flow rate from 400 mℓ.min$^{-1}$ to 380 mℓ.min$^{-1}$ on the ARL 34000 spectrometer, following calibration under compromise conditions (Table 4-4). Errors numerically <5% underlined.

| Analyte | $C_b$ | $C_t$ | Error | $C_a$ |
|---|---|---|---|---|
| Ba(II)@ | 3,694 | 3,00 | +23% | 11,93 |
| Ca(II) | 93,71 | 60,00 | +56% | 11,93 |
| Cd(II) | 1,286 | 1,00 | +29% | 12,29 |
| Cr(II) | 13,21 | 10,00 | +32% | 12,00 |
| Fe(II) | 11,66 | 10,00 | +17% | 12,00 |
| Mo(II) | 1,038 | 1,00 | + 4% | 12,29 |
| Sr(II) | 0,567 | 0,50 | +13% | 12,30 |
| Ti(II) | 1,161 | 1,00 | +16% | 12,29 |
| V (II) | 1,188 | 1,00 | +19% | 12,29 |
| Y (II) | 1,184 | 1,00 | +18% | 12,30 |
| Zr(II) | 1,003 | 1,00 | 0% | 12,27 |

$C_b$ = analyte concentration readout /mg.ℓ$^{-1}$; The RSD of all concentration readouts was less than 1% except for Mo and Zr which gave RSD's of 4% and 2% respectively.

$C_t$ = true analyte concentration /mg.ℓ$^{-1}$

$C_a$ = apparent concentration of 10 mg.ℓ$^{-1}$ Mn.

@ analytical wavelengths of elements listed shown in Table 4-2.

TABLE 5-18: Reduction in error, due to analysis at an aerosol flow rate of 380 mℓ.min$^{-1}$ after calibration at a flow rate of 400 mℓ.min$^{-1}$, after applying the weighted internal standardization correction (equation 62) to the analyte concentration readout $C_b$ (Table 5-17) using manganese as internal stanard. Errors numerically <5% underlined.

| Analyte | $C_{ob}$ | $C_t$ | Error |
|---|---|---|---|
| Ba(II)@ | 3,35 | 3,00 | +12% |
| Ca(II) | 72,5 | 60,00 | +21% |
| Cd(II) | 1,018 | 1,00 | + 2% |
| Cr(II) | 10,47 | 10,00 | + 5% |
| Fe(II) | 9,74 | 10,00 | - 3% |
| Mo(II) | 0,802 | 1,00 | -20% |
| Sr(II) | 0,500 | 0,50 | 0% |
| Ti(II) | 0,989 | 1,00 | - 1% |
| V (II) | 0,985 | 1,00 | - 2% |
| Y (II) | 1,012 | 1,00 | + 1% |
| Zr(II) | 0,856 | 1,00 | -14% |

$C_{ob}$ = corrected analyte concentration /mg.ℓ$^{-1}$, following application of equation 62 with manganese as internal standard (see Table 5-19).

$C_t$ = true analyte concentration /mg.ℓ$^{-1}$.

@ analytical wavelengths of elements listed shown in Table 4-2.

TABLE 5-19: Conversion of apparent analyte concentration, $C_b$ (Table 5-17) to corrected analyte concentration, $C_{ob}$ (Table 5-18) using the weighted internal standardization equation (62), with Mn as internal standard*.

| Analyte | $E_b$ | $(E_a-E_b)$ | P | Q | R | F | $C_b$/mg.ℓ$^{-1}$ | $C_{ob}$/mg.ℓ$^{-1}$ |
|---|---|---|---|---|---|---|---|---|
| Ba** | 2,72 | 2,09 | 1,193 | 0,847 | 0,767 | 0,906 | 3,694 | 3,35 |
| Ca | 7,05 | -2,24 | 1,193 | 0,991 | 0,767 | 0,774 | 93,71 | 72,5 |
| Cd | 5,47 | -0,66 | 1,229 | 0,969 | 0,767 | 0,792 | 1,286 | 1,018 |
| Cr | 6,18 | -1,37 | 1,200 | 0,968 | 0,767 | 0,792 | 13,21 | 10,47 |
| Fe | 4,77 | 0,04 | 1,200 | 0,919 | 0,767 | 0,835 | 11,66 | 9,74 |
| Mo | 6,06 | -1,25 | 1,229 | 0,992 | 0,767 | 0,773 | 1,038 | 0,802 |
| Sr | 2,94 | 1,87 | 1,230 | 0,871 | 0,767 | 0,881 | 0,567 | 0,500 |
| Ti | 3,74 | 1,07 | 1,229 | 0,900 | 0,767 | 0,852 | 1,161 | 0,989 |
| V | 4,33 | 0,48 | 1,229 | 0,925 | 0,767 | 0,829 | 1,188 | 0,985 |
| Y | 3,62 | 1,19 | 1,230 | 0,897 | 0,767 | 0,855 | 1,184 | 0,102 |
| Zr | 3,58 | 1,23 | 1,227 | 0,899 | 0,763 | 0,853 | 1,003 | 1,856 |

*Note: (i) $E_a$ = excitation potential (eV) of Mn(II) 257,61 nm i.e., 4,81 eV; $E_b$ = excitation potential of analyte line (eV) from Zaidel' et al, (1970);
(ii) P = $C_a/C_{oa}$ i.e., apparent Mn concentration/true Mn concentration;
(iii) Q = denominator of correction factor in equation 62;
(iv) R = numerator of correction factor in equation 62;
(v) F = R/Q i.e., correction factor;
(vi) $C_{ob}$ = $C_b$.F (equation 62).

** analytical wavelengths of elements listed shown in Table 4-2.

Use of the conventional internal standardization method, as given by equation 63 (Section 4.9) to the analyte concentration data of Table 5-17 is shown in Table 5-20. The conventional internal standardization technique produced five acceptable results, with errors numerically less than 5%. The calcium error was reduced to +30% (Table 5-20) as opposed to +21% for the weighted method (Table 5-19).

Both internal standardization methods, while transforming unacceptable results to values with acceptable error for the majority of ion-line analyte channels, resulted in increased error for the Mo(II) 281,62 nm and Zr(II) 349,62 nm channels.

TABLE 5-20: Reduction or error, due to analysis at an aerosol flow rate of 380 mℓ.min$^{-1}$ after calibration at a flow rate of 400 mℓ.min$^{-1}$, after applying conventional internal standardization (equation 63) to the analyte concentration readout $C_b$ (Table 5-17), using manganese as internal standard. Errors numerically <5% underlined.

| Analyte | $C_{ob}$ | $C_t$ | Error |
|---|---|---|---|
| Ba(II)@ | 3,08 | 3,00 | + 3% |
| Ca(II) | 78,1 | 60,00 | +30% |
| Cd(II) | 1,07 | 1,00 | + 7% |
| Cr(II) | 11,0 | 10,00 | + 10% |
| Fe(II) | 9,72 | 10,00 | - 3% |
| Mo(II) | 0,865 | 1,00 | - 14% |
| Sr(II) | 0,472 | 0,50 | - 6% |
| Ti(II) | 0,968 | 1,00 | - 3% |
| V (II) | 0,990 | 1,00 | - 1% |
| Y (II) | 0,987 | 1,00 | - 1% |
| Zr(II) | 0,836 | 1,00 | -16% |

$C_{ob}$ = corrected analyte concentration /mg.ℓ$^{-1}$, following application of equation 63.

$C_t$ = true analyte concentration.

@ analytical wavelengths of elements listed shown in Table 4-2.

## 5.7 Evaluation of internal standardization to correct for error in atomic-line readout caused by slight change in aerosol gas flow rate.

A weighted internal standardization correction analagous to equation 62 (Section 4,9) for ion lines may be derived for atomic lines from equation 49 (Section 4.8) The equation for atomic lines is:

$$C_{ob} = C_b \cdot \left( \frac{0{,}136 \cdot E_a - 0{,}37}{0{,}136 \cdot (E_a - E_b) + (0{,}136E_b - 0{,}37)\left(\frac{C_a}{C_{oa}}\right)} \right) \quad \ldots\ldots\ldots\ldots\ldots\ldots\ldots\ldots \quad (83)$$

Where $C_{oa}$ = true concentration of the internal standard (analyte a), $C_a$ = the apparent concentration of the internal standard; $C_b$ = apparent concentration of analyte b, and $C_{ob}$ = corrected concentration of analyte b. Using beryllium as internal standard, with the excitation potential of the Be(I) 234,86 nm line of 5,28 eV (Zaidel' et al, 1970) substituted for $E_a$, equation 83 becomes:

$$C_{ob} = C_b \cdot \left( \frac{0{,}348}{0{,}136 \cdot (5{,}28 - E_b) + (0{,}136 \cdot E_b - 0{,}37)\left(\frac{C_a}{C_{oa}}\right)} \right) \quad \ldots\ldots\ldots\ldots\ldots\ldots\ldots \quad (84)$$

The use of equation 84 as well as the conventional internal standardization formula (equation 63) was evaluated for atomic lines on the ARL 34000 spectrometer in an analagous fashion to that described for ionic lines in Section 5.6 using a 5 $mg.\ell^{-1}$ Be spike as internal standard. The concentration readout data at the 5% reduction in aerosol gas flow rate is given in Table 5-21. Error in atomic analyte concentration readout ranged from -5% for Pb to +64% for Zn, with the beryllium spikes showing recoveries between 120% and 139%. The calculation of the weighted internal standardization correction is given in Table 5-22, with the error after correction being given in Table 5-23. The error after use of conventional internal standardization is given in Table 5-24.

Both the weighted (equation 83) and conventional (equation 63) internal standardization formulas showed a tendency to over-correct the atomic line analyte concentration readout values. The weighted method gave errors ranging from -22% to +18%; and the conventional internal standardization method gave errors ranging from -29% to +23%.

TABLE 5-21: Error in atomic line analyte concentration readout (mean of 3x10 s integrations) caused by a 5% reduction in aerosol gas flow rate from 400 $m\ell.min^{-1}$ to 380 $m\ell.min^{-1}$ on the ARL 34000 spectrometer, following calibration under compromise conditions (Table 4-4). Errors numerically < 5% underlined.

| Analyte | $C_b$ | $C_t$ | Error | $C_a$ |
|---|---|---|---|---|
| As(I)@ | 13,53 | 10,00 | +35% | 6,940 |
| Al(I) | 9,745 | 10,00 | - 3% | 6,663 |
| B (I) | 6,22 | 5,00 | +24% | 5,990 |
| Co(I) | 11,29 | 10,00 | +13% | 6,663 |
| Cu(I) | 1,034 | 1,00 | + 3% | 6,654 |
| Hg(I) | 6,68 | 5,00 | +34% | 6,869 |
| Mg(I) | 71,79 | 60,00 | +20% | 6,730 |
| Ni(I) | 10,07 | 10,00 | + 1% | 6,663 |
| Pb(I) | 9,466 | 10,00 | - 5% | 6,663 |
| Sb(I) | 12,77 | 10,00 | +28% | 6,603 |
| Se(I) | 12,31 | 10,00 | +23% | 6,958 |
| Si(I) | 57,9 | 50,00 | +16% | 5,990 |
| Zn(I) | 1,642 | 1,00 | +64% | 6,654 |

$C_b$ = analyte concentration readout /$mg.\ell^{-1}$;
The RSD of concentration readouts were < 1% except for Pb (3%) and Sb (7%)

$C_t$ = true analyte concentration /$mg.\ell^{-1}$

$C_a$ = apparent concentration of 5 $mg.\ell^{-1}$ Be spike

@ analytical wavelengths of elements listed shown in Table 4-2.

TABLE 5-22: Conversion of $C_b$ (Table 5-21) to $C_{ob}$ (Table 5-23) using the weighted internal standardization equation (83) for atomic lines, with Be as internal standard*.

| Analyte | $E_b$ | $(E_a-E_b)$ | P | Q | R | F | $C_b$/mg.ℓ$^{-1}$ | $C_{ob}$/mg.ℓ$^{-1}$ |
|---|---|---|---|---|---|---|---|---|
| As** | 6,40 | -1,12 | 1,388 | 0,543 | 0,348 | 0,641 | 13,53 | 8,67 |
| Al | 3,14 | 2,14 | 1,333 | 0,367 | 0,348 | 0,948 | 9,745 | 9,24 |
| B | 4,96 | 0,32 | 1,198 | 0,408 | 0,348 | 0,853 | 6,22 | 5,30 |
| Co | 4,07 | 1,21 | 1,333 | 0,410 | 0,348 | 0,849 | 11,29 | 9,58 |
| Cu | 3,78 | 1,50 | 1,331 | 0,396 | 0,348 | 0,879 | 1,034 | 0,909 |
| Hg | 4,88 | 0,40 | 1,374 | 0,458 | 0,348 | 0,760 | 6,680 | 5,08 |
| Mg | 5,94 | -0,66 | 1,346 | 0,499 | 0,348 | 0,697 | 71,79 | 50,04 |
| Ni | 3,54 | 1,74 | 1,333 | 0,385 | 0,348 | 0,904 | 10,07 | 9,10 |
| Pb | 4,34 | 0,94 | 1,333 | 0,422 | 0,348 | 0,825 | 9,466 | 7,81 |
| Sb | 5,98 | -0,70 | 1,321 | 0,491 | 0,348 | 0,709 | 12,77 | 9,05 |
| Se | 6,32 | -1,04 | 1,392 | 0,540 | 0,348 | 0,644 | 12,31 | 7,93 |
| Si | 5,08 | 0,20 | 1,198 | 0,411 | 0,348 | 0,847 | 57,9 | 49,04 |
| Zn | 5,80 | -0,52 | 1,331 | 0,486 | 0,348 | 0,716 | 1,642 | 1,18 |

* Notes: (i) $E_a$ = excitation potential (eV) of Be(I) 234,86 nm i.e., 5,28 eV; $E_b$ = excitation potential of analyte line (eV) from Zaidel' et al (1970);
(ii) P = $C_a/C_{oa}$ i.e., apparent Be concentration/true Be concentration;
(iii) Q = denominator of correction factor in equation 83;
(iv) R = numerator of correction factor in equation 83;
(v) F = R/Q i.e., correction factor;
(vi) $C_{ob}$ = $C_b$.F (equation 83).

** analytical wavelengths of elements listed shown in Table 4-2.

TABLE 5-23: Effect of weighted internal standardization (equation 83) on atomic analyte concentration readout $C_b$ (Table 5-21), showing corrected analyte concentration, $C_{ob}$. Beryllium used as internal standard. Errors numerically < 5% underlined.

| Analyte | $C_{ob}$ | $C_t$ | Error |
|---|---|---|---|
| As(I)@ | 8,67 | 10,00 | -13% |
| Al(I) | 9,24 | 10,00 | - 8% |
| B (I) | 5,30 | 5,00 | + 6% |
| Co(I) | 9,58 | 10,00 | - 4% |
| Cu(I) | 0,909 | 1,00 | - 9% |
| Hg(I) | 5,08 | 5,00 | + 2% |
| Mg(I) | 50,04 | 60,00 | -17% |
| Ni(I) | 9,10 | 10,00 | - 9% |
| Pb(I) | 7,81 | 10,00 | -22% |
| Sb(I) | 9,05 | 10,00 | -10% |
| Se(I) | 7,93 | 10,00 | -21% |
| Si(I) | 49,04 | 50,00 | - 2% |
| Zn(I) | 1,18 | 1,00 | +18% |

$C_{ob}$ = corrected analyte concentration /mg.$\ell^{-1}$ following application of weighted internal standardization (equation 83)

$C_t$ = true analyte concentration/mg.$\ell^{-1}$.

@ = analytical wavelengths of elements listed shown in Table 4-2.

TABLE 5-24: Effect of conventional internal standardization (equation 63) applied to atomic analyte concentration readout $C_b$ (Table 5-21), showing corrected analyte concentration, $C_{ob}$. Beryllium used as internal standard. Errors numerically < 5% underlined.

| Analyte | $C_{ob}$ | $C_t$ | Error |
|---|---|---|---|
| As(I)@ | 9,75 | 10,00 | - 3% |
| Al(I) | 7,31 | 10,00 | -27% |
| B (I) | 5,19 | 5,00 | + 4% |
| Co(I) | 8,47 | 10,00 | -15% |
| Cu(I) | 0,777 | 1,00 | -22% |
| Hg(I) | 4,86 | 5,00 | - 3% |
| Mg(I) | 53,3 | 60,00 | -11% |
| Ni(I) | 7,56 | 10,00 | -24% |
| Pb(I) | 7,10 | 10,00 | -29% |
| Sb(I) | 9,67 | 10,00 | - 3% |
| Se(I) | 8,85 | 10,00 | -12% |
| Si(I) | 48,3 | 50,00 | - 3% |
| Zn(I) | 1,23 | 1,00 | +23% |

$C_{ob}$ = corrected analyte concentration /mg.$\ell^{-1}$, following application of equation 63.

$C_t$ = true analyte concentration/mg.$\ell^{-1}$

@ analytical wavelengths of elements listed shown in Table 4-2.

## 5.8 Summary

In this chapter the calibration of the polychromator to provide concentration readout was described. The determination of interference correction coefficients required for interelement interfrence correction was illustrated for the interference of Mg on Mo(II) 281,62 nm, it being shown that the smallest sum of squared residuals for the Mg on Mo interference curve were obtained for a quadratic regression forced through the origin. The importance of maintaining invariant source and nebulization conditions so as to prevent change in relative element intensities and thus change in interference correction coefficients was illustrated; the correction coefficients for Ca, Mg, Fe and Mn as determined in 1983 at an aerosol flow rate of 0,41$\ell.min^{-1}$, and in 1985 at an aerosol flow rate of 0,40$\ell.min^{-1}$, being shown.

The analysis of a sample plate was discussed, and the importance of correction for drift in the concentration readout of a water blank emphasized. The two-sigma detection limits for nitric acid, $\phi$ = 0,01 and 1 $g.\ell^{-1}$ disodium EDTA matrix were compared and found to be similar, except for Ca, Ti, Si and Se. This illustrated a relative insensitivity of detection limit on the polychromator to change in composition of the matrix.

An investigation of the memory effects in the sample transport system showed that the washout curve was biphasic, and that the rapid and slow washout phases gave a linear plot when the natural logarithm of intensity was plotted against the natural logarithm of washout time. A hyberbolic washout curve as found by Dobb and Jenke (1983) failed to provide an adequate model for the washout curve. The washout time needed for the net analyte intensity to decay to 1% of initial intensity was ca., 60s for the elements studied.

The chapter was concluded with a study of the use of the weighted internal standardization correction (equation 62 for ion lines; and equation 83 for atomic lines) described in Chapter four to correct for change in analyte signal caused by a change in inner (aerosol) gas flow rate. The weighted correction for ion lines provided better results than conventional internal standardization. This finding is not surprising in view of the high correlation found between change in analyte intensity and excitation potential for ion lines when aerosol flow changes (section 4.8). For atomic lines, both the weighted and conventional internal standardization formulas gave poor results, with overcorrection of the change in analyte signal brought about by change in aerosol gas flow rate.

# CHAPTER 6: QUANTITATIVE ANALYSIS NEAR THE DETECTION LIMIT ON THE SCANNING MONOCHROMATOR

## 6.1 Introduction.

This chapter concerns primarily the determination of precision and detection limit at low analyte concentrations on the ARL 3510 ICP scanning monochromator. The precision, linearity and detection limit for the Co 238,89 nm analytical line as measured at line centre profile position, is followed by a development of the theory of measurement of precision in the profile scan mode. This involves the use of an inverse Gaussian transformation to obtain estimates of intensity at line centre from off-centre intensity data of a profile scan. Examples of the application of this transformation follow, with an illustration of the problems created by baseline elevation interference, background structure, and relative profile misalignment between a sample and blank profile. The chapter includes a discussion on the use of the $\Omega$ function[@] for estimating detection limit from a blank profile scan, the theory of which was described in Chapter two.

---

@ The $\Omega$ function is the standard deviation of n values of the intensity readout of a blank recorded at wavelength intervals of $\delta\lambda$ across the window $\lambda_o$ - m. $\delta\lambda$ to $\lambda_o$ + m.$\delta\lambda$, where n = 2m+1 (equation 20, section 2.10).

The chapter is concluded with an illustration of the use of inverse Gaussian transformation in the analysis of Pb and Cr in a digest of a polluted sediment, and shows that the method is not only applicable to analysis near the detection limit.

## 6.2 Linearity and detection limit of the ARL scanning monochromator at line centre position.

The use of the ARL 3510 scanning monochromator for integration measurements at peak maximum provides, as expected, a linear calibration at low concentration, for net analyte intensity against concentration. This is illustrated, for example, in data obtained at line centre for the Co(II) 238,89 nm analytical line for cobalt concentrations between 0 and 2 $mg.\ell^{-1}$ (Table 6-1), where a linear regression correlation coefficient value r, of 0,9999 was obtained. The 2 sigma detection limit, determined in the manner of Butler et al (1980) for a RSD value for a net analyte signal of 50%, is around 0,01 $mg.\ell^{-1}$ Co. A plot of RSD against $\log_{10} C_{Co}$ shown in Figure 6-1, illustrates the method of Butler et al (1980), where the 2 sigma deletion limit is given by the concentration where the RSD value is 50%.

While the use of the ARL 3510 spectrometer at peak centre position is useful where no significant line overlap or baseline-shift interferences occur, the major

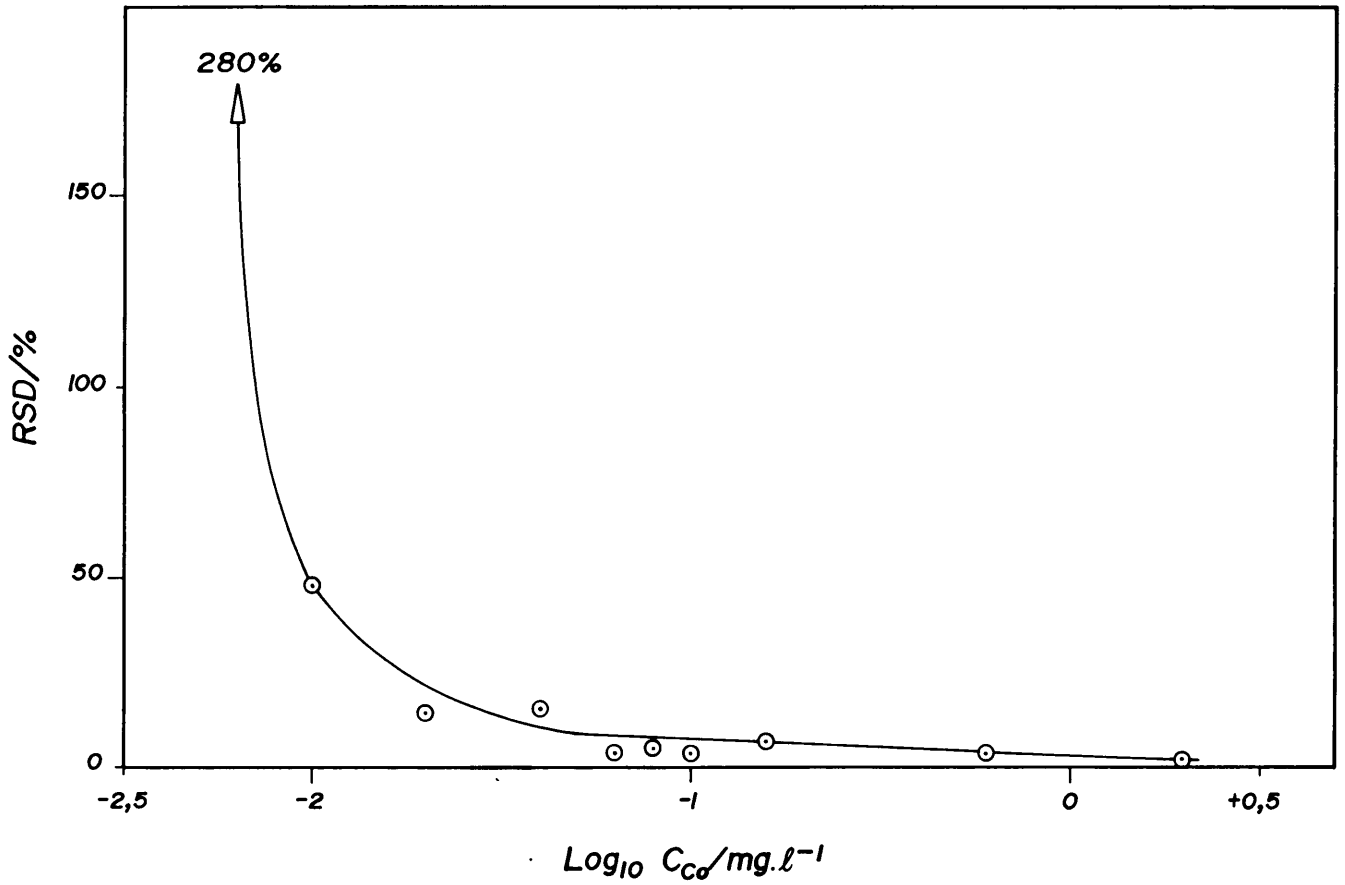


Figure 6-1: Plot of the percent relative standard deviation (RSD %) for the Co(II) 238,89 nm line (Table 6-1) against the logarithm of cobalt concentration ($mg.\ell^{-1}$) showing the lower portion of the analytical range.

attractiveness of the scanning facility is to allow for quantification of emission at profile-offset positions, and thus detect and correct for interferences where necessary by the background subtraction technique. In Section 6.5 the measurement of the same serial dilution standards of cobalt, analyzed here at line centre, Table 6-1, will be demonstrated for analysis in the profile scan mode.

TABLE 6-1: Serial dilutions of cobalt standards in nitric acid, $\phi$ = 0,01 showing the mean net intensity (I), std., deviation ($\sigma$), and percentage relative std., deviation (RSD) for 3x1 s integrations at peak maximum of the Co(II) 238,89 nm emission line on the ARL 3510 spectrometer, at attenuator setting of 12*.

| $C_{Co/mg.\ell^{-1}}$ | I | $\sigma$ | RSD |
|---|---|---|---|
| 2,00 | 14170 | 318 | 2,2% |
| 0,60 | 4320 | 182 | 4,2% |
| 0,16 | 1310 | 95 | 7,2% |
| 0,10 | 870 | 36 | 4,1% |
| 0,08 | 630 | 29 | 4,6% |
| 0,06 | 420 | 16 | 3,8% |
| 0,04 | 310 | 49 | 15,8% |
| 0,02 | 110 | 16 | 14,5% |
| 0,01 | 56 | 27 | 48 % |
| 0,005 | 24 | 69 | 290 % |

* Correlation between Co concentration and I is 0,9999 with a linear regression equation,

$$I = 7073.C_{Co} + 47$$

## 6.3 Use of an inverse Gaussian transformation for estimation of line centre intensity in the profile scan mode of measurement.

The central portion of a line profile may be considered as approximately Gaussian in shape[@], i.e., the net intensity, I, may be expressed as;

$$I = a.e^{-bx^2} \qquad \ldots\ldots\ldots\ldots\ldots \quad (85)$$

where a and b are constants,

and x is the offset from central profile position.

If $I_o$ is the net intensity of peak maximum when x = 0, then $a = I_o$. When x = h, where h is the half width at half peak maximum height, i.e., when $I = I_o/2$, then:

$$I_o/2 = I_o.e^{-bh^2}$$

$$\text{i.e., } b = (\ln 2)/h^2 \qquad \ldots\ldots\ldots\ldots\ldots\ldots \quad (86)$$

Equation 85 may thus be written;

$$I = I_o.e^{-(\ln 2).\, x^2/h^2} \qquad \ldots\ldots\ldots\ldots\ldots\ldots \quad (87)$$

where I is the net intensity at profile offset x,

---

@ J.M. Mermet, personal communication. April 1985.

Equation 87 by rearrangement yields;

$$I_o = I.(e^{-(\ln 2).x^2/h^2})^{-1}$$

i.e., $$I_o = I.e^{(\ln 2).x^2/h^2} \quad \text{.....} \quad (88)$$

or $$I_o = I.f(x)$$

where $$f(x) = e^{(\ln 2).x^2/h^2} \quad \text{.....} \quad (89)$$

The function f(x) is an inverse Gaussian function, and may be used in the manner of equation 88, to estimate the peak maximum intensity $I_o$ where the intensity I at profile offset position x is given, provided that h is known. Equation 88 may be used to transform a set of n net intensity values obtained from a profile scan across an emission line into a set of n calculated values for the peak maximum intensity $I_o$, at line centre.

The mean, std., deviation and relative standard deviation may be calculated from this set of transformed intensities serving as predictors for $I_o$ in the usual manner, thus providing a measure of the precision of measurement for use in the profile scan mode of analysis. Precision data may be obtained from a single profile scan of a std., or sample together with a blank scan to provide net intensities. This provides a considerable time saving, as the time required to plot a single scan on the ARL 3510 spectrometer is alone several minutes, and the necessity for replication of scans is avoided.

The half width at half height value h, is readily measured geometrically from a hard copy plot of the scan across the given emission line while aspirating a standard, followed by a superimposed blank scan, provided the line has been accurately profiled prior to recording of the scan so that central profile step position corresponds to peak maximum.

In the practical use of the inverse Gaussian transformation, the determination of the profile position where the profile offset x = 0, is critical. Due to mechanical play in the worm gear successive profile scans across an emission line on the ARL 3510 monochromator may be out of register on occasion by as much as 2 profile steps or 0,0056 nm. It is thus necessary to determine the profile position of peak centre, where x = 0, for a recorded scan prior to application of the inverse Gaussian transformation, as described in Section 6.4.

## 6.4 Determination of the profile position of line centre

If the set of net intensities at the profile step positions across an emission line is expressed as;

$$S_n = \left\{ (x, I_x) \;\middle|\; x = o, \pm 1, \pm 2, \ldots, \pm m \right\} \quad \ldots \quad (90)$$

where $n = 2m + 1$ and $I_o > I_x$, $\forall\, x \neq 0$,

then if $I_x - I_{-x} \neq 0$ ..... (91)

then the scan is asymmetrical. The true line centre position has been missed and $I_o$ does not represent the true maximum intensity for the emission line @.

The profile position of line centre is readily estimated by using the subset $S_3$ of the three central values of $S_n$;

$$S_3 = \left\{ (x, I_x) \;\middle|\; x = 0, \pm 1 \right\} \quad \ldots \quad (92)$$

where $I_o > I_x$ for $x \neq 0$

---

@ The symmetry of the Gaussian profile function implies that $I_x = I_{-x}$ if x is measured from line centre.

by fitting a quadratic function * of the form;

$$I = U.x^2 + V.x + W \qquad \ldots\ldots\ldots\ldots \quad (93)$$

where the position of inflextion,

when $\partial I/\partial x = 0$ gives the position of line centre i.e., where;

$$x_{central} = -V/2U \qquad \ldots\ldots\ldots\ldots \quad (94)$$

Substitution of the 3 central data points of $S_3$ in equation 93 and solution for the constants, together with condition 94, readily provides the formula for the estimated position of central profile as:

$$x_{central} = \frac{(I_{-1} - I_{+1})}{2(I_{-1} + I_{+1} - 2.I_o)} \qquad \ldots\ldots\ldots\ldots \quad (95)$$

In actual use of the scan technique, instrumental wavelength selection error, as well as drift, may result in the experimental peak maximum intensity value $I_o$ at $x = 0$ not lying at the computer profile plot step position 0 but at some other step position $P_o$. The corrected profile step position $x_{cor.}$ for each intensity data point is then given by;

---

* The lst two term of the series expansion of $a.e^{(x-\delta)^2}$ are $a + a.(x-\delta)^2$ which is a polynomial of 2nd order, i.e. $ax^2-2a\delta x + a(\delta^2+1)$.

$$x_{cor.} = P - (P_o + x_{central}) \quad \ldots\ldots\ldots\ldots \quad (96)$$

where $x_{central}$ is as defined by equation 95,

$P_o$ is the apparent experimental profile step position of maximum intensity,

and $P$ is the apparent profile step position of the given intensity data point whose corrected profile position is to be calculated.

## 6.5 Application of the inverse Gaussian transform to profile scan data of the Co(II) 238,89 nm line.

The cobalt standards from 0 to 2 $mg.\ell^{-1}$ Co, prepared for the experiment at the peak maximum profile position as described in Section 6.2, were also analyzed in the profile scan mode across the Co(II) 238,89 nm line at profile step intervals corresponding to 0,0028 nm and the intensity recorded for a 1 s integration time at each position at an attenuator setting of 12 on the ARL 3510 spectrometer, other conditions being those described in Table 4-5. The gross intensity data for these scans across the wavelength profile of the cobalt line are given in Table 6-2.

If the assumption is made that the effect of any lateral shift in the blank profile with respect to the profile of the standard on the net intensities is negligible, if it occurred, then the net intensity data given in Table 6-3 are obtained.@

---

@ Relative profile shift between a blank and standard/sample cannot be ignored where the background under the emission line is noticeably sloped or structured. In this situation relative profile misalignments must first be corrected for, before net intensities are calculated. See Section 6.7.

TABLE 6-2: Gross intensities of Co standards in nitric acid, $\phi$ = 0,01 , for 1 s integration time for profile scans across the Co(II) 238,89 nm emission line at attenuator setting 12 on the ARL 3510 spectrometer.

| P | $I_b$ | $I_{2,0}$ | $I_{0,6}$ | $I_{0,16}$ | $I_{0,10}$ | $I_{0,08}$ | $I_{0,06}$ | $I_{0,04}$ | $I_{0,02}$ | $I_{0,01}$ | $I_{0,005}$ |
|---|---|---|---|---|---|---|---|---|---|---|---|
| -5 | 1471 | 1475 | 1449 | 1379 | 1423 | 1365 | 1401 | 1410 | 1459 | 1408 | 1427 |
| -4 | 1317 | 1516 | 1474 | 1452 | 1440 | 1452 | 1447 | 1403 | 1441 | 1449 | 1396 |
| -3 | 1268 | 1617 | 1446 | 1423 | 1378 | 1381 | 1381 | 1427 | 1305 | 1391 | 1316 |
| -2 | 1169 | 2757 | 1610 | 1333 | 1311 | 1276 | 1277 | 1308 | 1278 | 1293 | 1280 |
| -1 | 1217 | 6019 | 2346 | 1517 | 1390 | 1364 | 1272 | 1264 | 1223 | 1249 | 1255 |
| 0 | 1304 | 11622 | 3830 | 1913 | 1633 | 1526 | 1431 | 1403 | 1327 | 1249 | 1241 |
| +1 | 1407 | 14818 | 5177 | 2318 | 1897 | 1770 | 1657 | 1574 | 1453 | 1389 | 1383 |
| +2 | 1329 | 11718 | 4754 | 2317 | 1955 | 1885 | 1709 | 1608 | 1456 | 1419 | 1411 |
| +3 | 1272 | 6685 | 3177 | 1934 | 1718 | 1714 | 1599 | 1490 | 1399 | 1415 | 1332 |
| +4 | 1231 | 2796 | 1860 | 1484 | 1424 | 1434 | 1328 | 1321 | 1294 | 1303 | 1333 |
| +5 | 1193 | 1664 | 1374 | 1349 | 1240 | 1273 | 1281 | 1233 | 1200 | 1209 | 1218 |
| +6 | 1231 | 1363 | 1246 | 1203 | 1199 | 1174 | 1182 | 1167 | 1193 | 1169 | 1188 |

P = profile step position, uncorrected.
$I_b$ = intensity of nitric acid, $\phi$ = 0,01 , blank.
$I_C$ = gross intensity at Co - concentration of C mg.$\ell^{-1}$.

TABLE 6-3: Net intensities of Co standards for 1 s integration for profile scans across the Co(II) 238,89 nm emission line, obtained by subtracting blank intensity from the gross std., intensities (Table 6-3). The maximum net intensity for each standard is underlined.

| P | $I_{2,0}$ | $I_{0,6}$ | $I_{0,16}$ | $I_{0,10}$ | $I_{0,08}$ | $I_{0,06}$ | $I_{0,04}$ | $I_{0,02}$ | $I_{0,01}$ | $I_{0,005}$ |
|---|---|---|---|---|---|---|---|---|---|---|
| -5 | 4 | -22 | -92 | -48 | -106 | -70 | -61 | -12 | -63 | -44 |
| -4 | 199 | 157 | 135 | 123 | 135 | 130 | 86 | 124 | 132[a] | 79 |
| -3 | 349 | 178 | 155 | 110 | 113 | 113 | 159 | 37 | 123 | 48 |
| -2 | 1588 | 441 | 164 | 142 | 107 | 108 | 139 | 109 | 124 | 111[a] |
| -1 | 4802 | 1129 | 300 | 173 | 147 | 55 | 47 | 6 | 32 | 38 |
| 0 | 10318 | 2526 | 609 | 329 | 222 | 127 | 99 | 23 | -55 | -63 |
| +1 | 13411 | 3770 | 911 | 490 | 363 | 250 | 167 | 46 | -18 | -24 |
| +2 | 10389 | 3425 | 988 | 626 | 556 | 380 | 279 | 127 | 90 | 82 |
| +3 | 5413 | 1905 | 662 | 446 | 442 | 327 | 218 | 127 | 143 | 60 |
| +4 | 1565 | 629 | 253 | 193 | 203 | 97 | 90 | 63 | 72 | 102 |
| +5 | 471 | 181 | 156 | 47 | 80 | 88 | 40 | 7 | 16 | 25 |
| +6 | 132 | 15 | -28 | -32 | -57 | -49 | -64 | -38 | -62 | -43 |

P = profile step position, uncorrected
$I_C$ = net intensity at Co - concentration of C $mg.\ell^{-1}$.
(a) noise maxima.

In Figure 6-2, a plot is shown of the net intensity data for the 2 $mg.\ell^{-1}$ Co std., against profile position, taken from Table 6-3. The half width at half height value h, as determined from Figure 6-2, is 1,70 profile steps for the Co(II) 238,89 nm line on the ARL 3510 scanning monochromator.

The application of equation 96 in determining the true profile positions from line centre profile position, taken as zero, is shown in Table 6-4.

The application of the inverse Gaussian transformation, equation 88, to the data in Table 6-4 is shown in Table 6-5. The effect of the transformation on line profile is shown graphically in Figures 6-3 and 6-4 for the 2 $mg.\ell^{-1}$ Co and 0,6 $mg.\ell^{-1}$ Co standards respectively.

The mean, std., deviation and RSD for the data in Table 6-5 is given in Table 6-6. A comparision with Table 6-2 shows that the analysis by conventional measurement at peak maximum and analysis using the inverse Gaussian transformation on profile scan data give comparable results. Both calibration techniques are linear with r = 0,9999; and use of the F-test (Table 6-7) shows that the precision of the conventional peak maximum integration method (Table 6-2) and that of the profile scan method with inverse Gaussian transformation (Table 6-6) shows no statistical difference at the 5% two-tailed level, except for the 0,16 $mg.\ell^{-1}$ Co std, where the profile method shows the better precision.

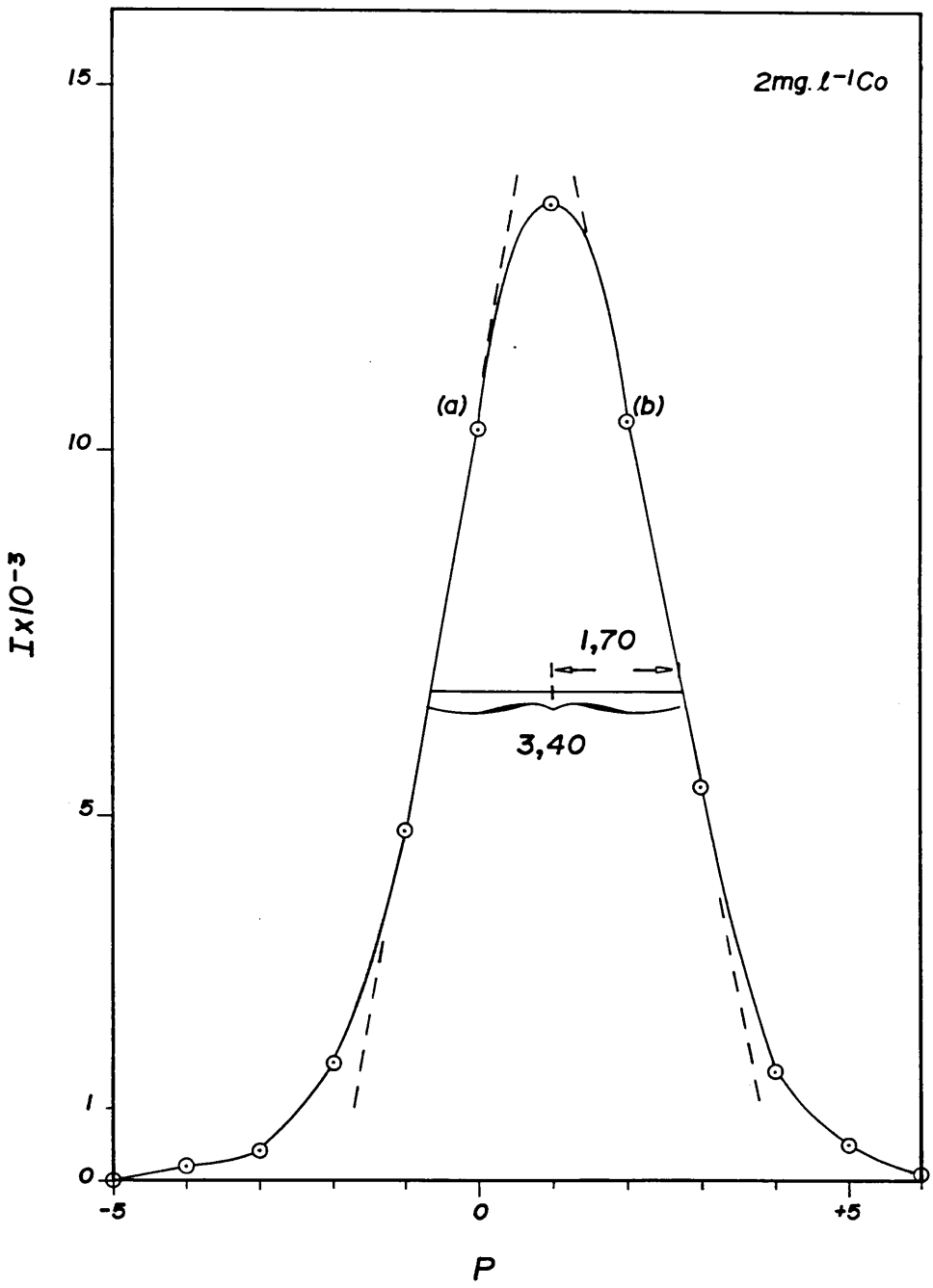


**Figure 6-2:** Determination of half width at half height for the Co(II) 238,89 nm emission line on the ARL 3510 spectrometer. Net intensity (I) is plotted against profile step position (P). Note symmetry of profile adjustment, i.e., (a) and (b) at the same height. Half width at half height = 1,70 profile steps.

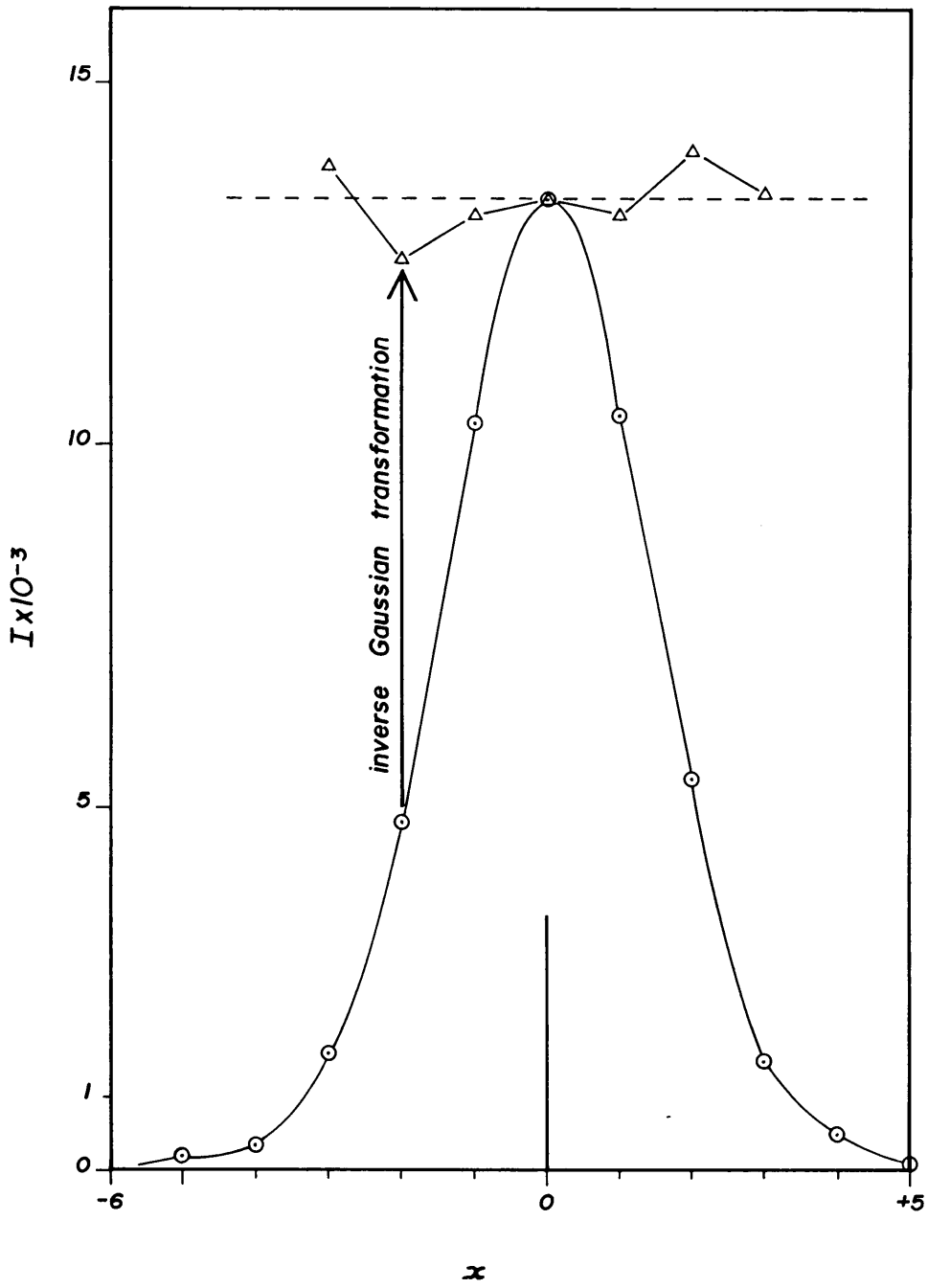


Figure 6-3: Net intensity data for a profile scan of the Co(II) 238,89 nm line with a 2 mg.$\ell^{-1}$ Co std (⊙—⊙), and the inverse Gaussian transformation (Δ·—Δ), providing predicted peak max., values.

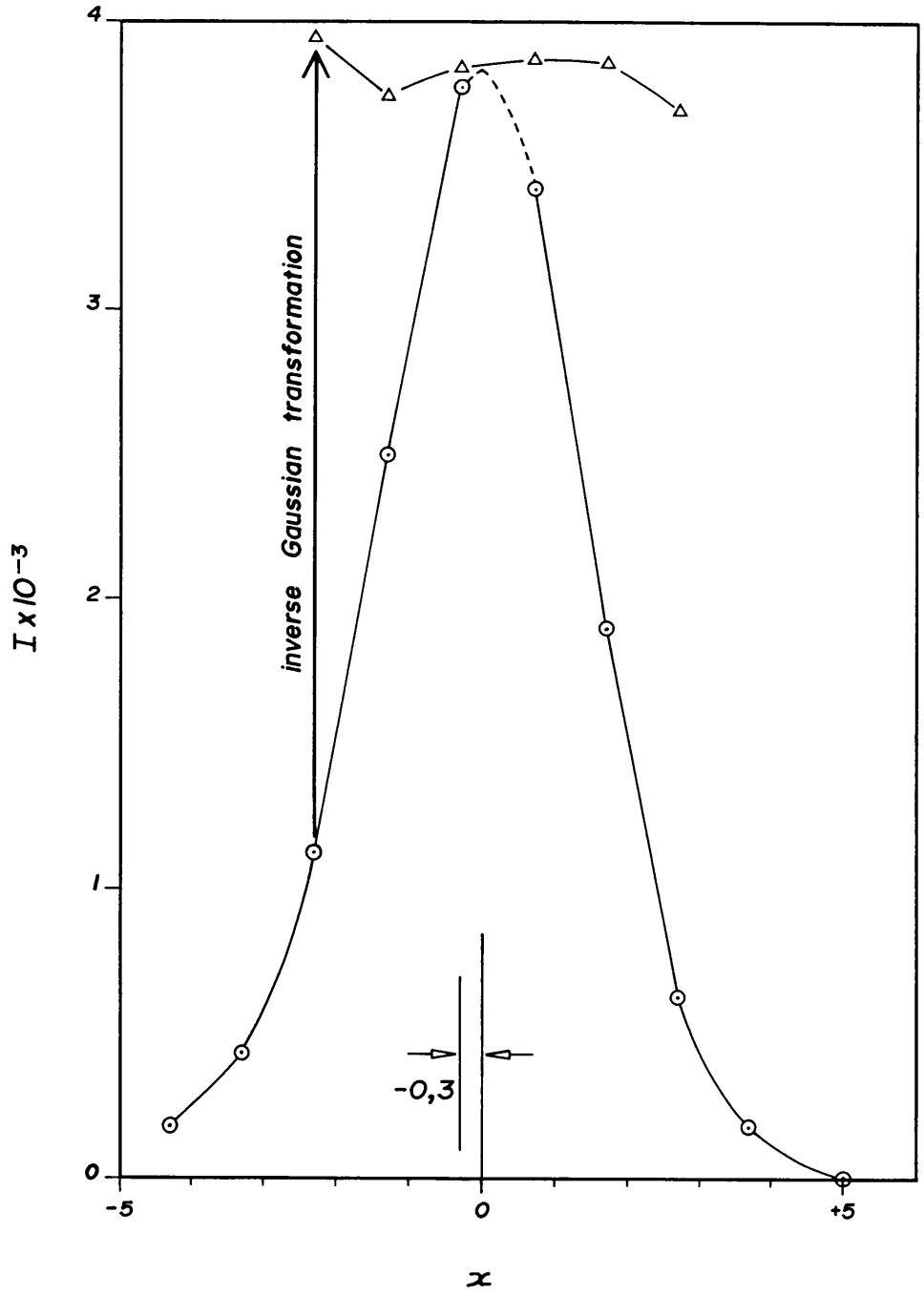


Figure 6-4: Net intensity profile scan data for the Co(II) 238,89 nm line with a 0,60 mg.ℓ$^{-1}$ Co std (⊙—⊙), showing the profile drift error of 0,3 profile steps and the inverse Gaussian transformed profile (Δ—Δ).

The implications of this experiment, where it was shown that the precision of measurement at line centre may be estimated by applying an inverse Gaussian transformation to a single wavelength scan of the analyte sample peak, are; firstly that analytical time may be saved, the time to display a wavelength scan on the videoscreen of the ARL 3510 spectrometer being several minutes, and secondly, that less sample volume is used for a single scan than for replicate scans. This may be important where sample volume is at a premium. A further advantage of the profile scan method of quantitative analysis over intergration at line centre only, is that the profile method is not affected by slight profile drift, whereas with integration at line centre error is introduced.

TABLE 6-4: Net intensities versus profile step position P, showing corrected position x as calculated from equation 96. Maximum net intensities are underlined.

| P | x | $I_{2,0}$ | x | $I_{0,6}$ | x | $I_{0,16}$ | x | $I_{0,10}$ | x | $I_{0,08}$ |
|---|---|---|---|---|---|---|---|---|---|---|
| -1 | -2,006 | 4802 | -2,283 | 1129 | -2,691 | 300 | -2,930 | 173 | -3,129 | 147 |
| 0 | -1,006 | 10318 | -1,283 | 2526 | -1,691 | 609 | -1,930 | 329 | -2,129 | 222 |
| +1 | -0,006 | <u>13411</u> | -0,283 | <u>3770</u> | -0,691 | 911 | -0,930 | 490 | -1,129 | 363 |
| +2 | 0,994 | 10389 | 0,717 | 3425 | 0,309 | <u>988</u> | 0,070 | <u>626</u> | -0,129 | <u>556</u> |
| +3 | 1,994 | 5413 | 1,717 | 1905 | 1,309 | 662 | 1,070 | 446 | 0,871 | 442 |
| +4 | 2,994 | 1565 | 2,717 | 629 | 2,309 | 253 | 2,070 | 193 | 1,871 | 203 |

P = profile step position, uncorrected.
x = corrected profile position, as steps from line centre.
$I_C$ = net intensity of a C mg.$\ell^{-1}$ Co - solution.

TABLE 6-4 (continued)

| P | x | $I_{0,06}$ | x | $I_{0,04}$ | x | $I_{0,02}$ | x | $I_{0,01}$ |
|---|---|---|---|---|---|---|---|---|
| -1 | -3,210 | 55 | -3,147 | 47 | -3,500 | 6 | -3,927 | 32 |
| 0 | -2,210 | 127 | -2,147 | 99 | -2,500 | 23 | -2,927 | -55 |
| +1 | -1,210 | 250 | -1.147 | 167 | -1,500 | 46 | -1,927 | -18 |
| +2 | -0,210 | 380 | -0,147 | 279 | -0,500 | 127 | -0,927 | 90 |
| +3 | 0,790 | 327 | 0,853 | 218 | 0,500 | 127 | 0,073 | 143* |
| +4 | 1,790 | 97 | 1,853 | 90 | 1,500 | 63 | 1,073 | 72 |

P = profile step position, uncorrected.
x = corrected profile position, as steps from line centre.
$I_C$ = net intensity of a C mg.$\ell^{-1}$ Co - solution.

TABLE 6-5: Application of the inverse Gaussian transform (equation 88) to the net intensity data from Table 6-4, using a half width at half height value (h) of 1,70 (Figure 6-2). Only the 3 intensity values centred around the underlined maximum intensities in Table 6-4 are shown here.

| P | $I_{2,0}$ | $I_{0,6}$ | $I_{0,16}$ | $I_{0,10}$ | $I_{0,08}$ | $I_{0,06}$ | $I_{0,04}$ | $I_{0,02}$* | $I_{0,01}$ |
|---|---|---|---|---|---|---|---|---|---|
| 0 | 13160 | 3748 | - | - | - | - | - | - | - |
| 1 | 13410 | 3842 | 1021 | 603 | 493 | 355 | 229 | 79 | - |
| 2 | 13170 | 3874 | 1011 | 627 | 558 | 384 | 280 | 135 | 111 |
| 3 | - | - | 999 | 587 | 530 | 380 | 260 | 135 | 143 |
| 4 | - | - | - | - | - | - | - | 108 | 95 |

$I_C$ = transformed net intensity for a C mg.$\ell^{-1}$ Co-solution.

* 4 intensity values taken as the two central values are identical.

**TABLE 6-6:** Mean ($\bar{I}$) std., deviation ($\sigma$) and relative standard deviation (RSD) of the transformed intensity values from Table 6-5*.

| $C_{Co}$/mg.ℓ$^{-1}$ | $\bar{I}$ | $\sigma$ | RSD |
|---|---|---|---|
| 2,0 | 13250 | 140 | 1,0% |
| 0,6 | 3820 | 65 | 1,7% |
| 0,16 | 1010 | 11 | 1,1% |
| 0,10 | 606 | 20 | 3,3% |
| 0,08 | 527 | 33 | 6,3% |
| 0,06 | 373 | 16 | 4,3% |
| 0,04 | 256 | 26 | 10,2% |
| 0,02 | 114 | 27 | 24 % |
| 0,01 | 116 | 24 | 21 % |

* Linear correlation coefficient between cobalt concentration (mg.ℓ$^{-1}$) and mean transformed intensity ($\bar{I}$) is 0,9999; with a mean sum of squared residuals value of 2800.

TABLE 6-7: Standard deviations ($\sigma$) of intensity I, for the integration at (a) central profile position (Table 6-1), and (b) with inverse Gaussian transformation after profile scanning (Table 6-6) for the Co(II) 238,89 nm analytical line, showing associated F-values*.

| $C_{Co}$/mg.$\ell^{-1}$ | $\sigma_{I,a}$ | $\sigma_{I,b}$ | F-value** |
|---|---|---|---|
| 2,0 | 318 | 140 | 5,2 |
| 0,6 | 182 | 65 | 7,8 |
| 0,16 | 95 | 11 | 74,6*** |
| 0,10 | 36 | 20 | 3,2 |
| 0,08 | 29 | 33 | 1,3 |
| 0,06 | 16 | 16 | 1,0 |
| 0,04 | 49 | 26 | 3,6 |
| 0,02 | 16 | 27 | 2,9 |
| 0,01 | 27 | 24 | 1,3 |

* Green and Margerison, (e), 1978

** $F = \sigma_a^2/\sigma_b^2$ where $\sigma_a^2 \geq \sigma_b^2$; and
$F = \sigma_b^2/\sigma_a^2$ where $\sigma_b^2 > \sigma_a^2$.

*** significant at 5% two-tailed level where F critical = 39,0 for 2 degrees of freedom for each variance. (Netter and Wasserman, (b), 1974).

## 6.6 Treatment of profile scan data where baseline elevation occurs.

The method of quantitative use of profile scan data illustrated in Section 6.5 requires the use of net intensity data. Where baseline changes e.g., from matrix effects or stray light from neighbouring lines occur, then a baseline interpolation and subtraction procedure must be used prior to application of the inverse Gaussian function.

An example is provided where 500 $mg.\ell^{-1}$ Al results in a background elevation at the As(I) 193,76 nm analytical line (Figure 6-5). The presence of 500 $mg.\ell^{-1}$ Al results in a baseline elevation equivalent to approximately 3 $mg.\ell^{-1}$ As, when no arsenic is present in the sample. A sample containing 2 $mg.\ell^{-1}$ As and 500 $mg.\ell^{-1}$ Al will, in the profile centre method of measurement, without correction for baseline elevation, provide a false As readout of 5 $mg.\ell^{-1}$ As (Figure 6-5).

In practical analysis, the sample with a high concentration of aluminium, when scanned across the As(I) 193,76 nm line, is observed to show a peak under the As line but with a marked background elevation (Figure 6-6). The elevated background must be subtracted using the points shown as (a) and (b) in Figure 6-6 for example, in a baseline shift interpolation routine, before the inverse Gaussian

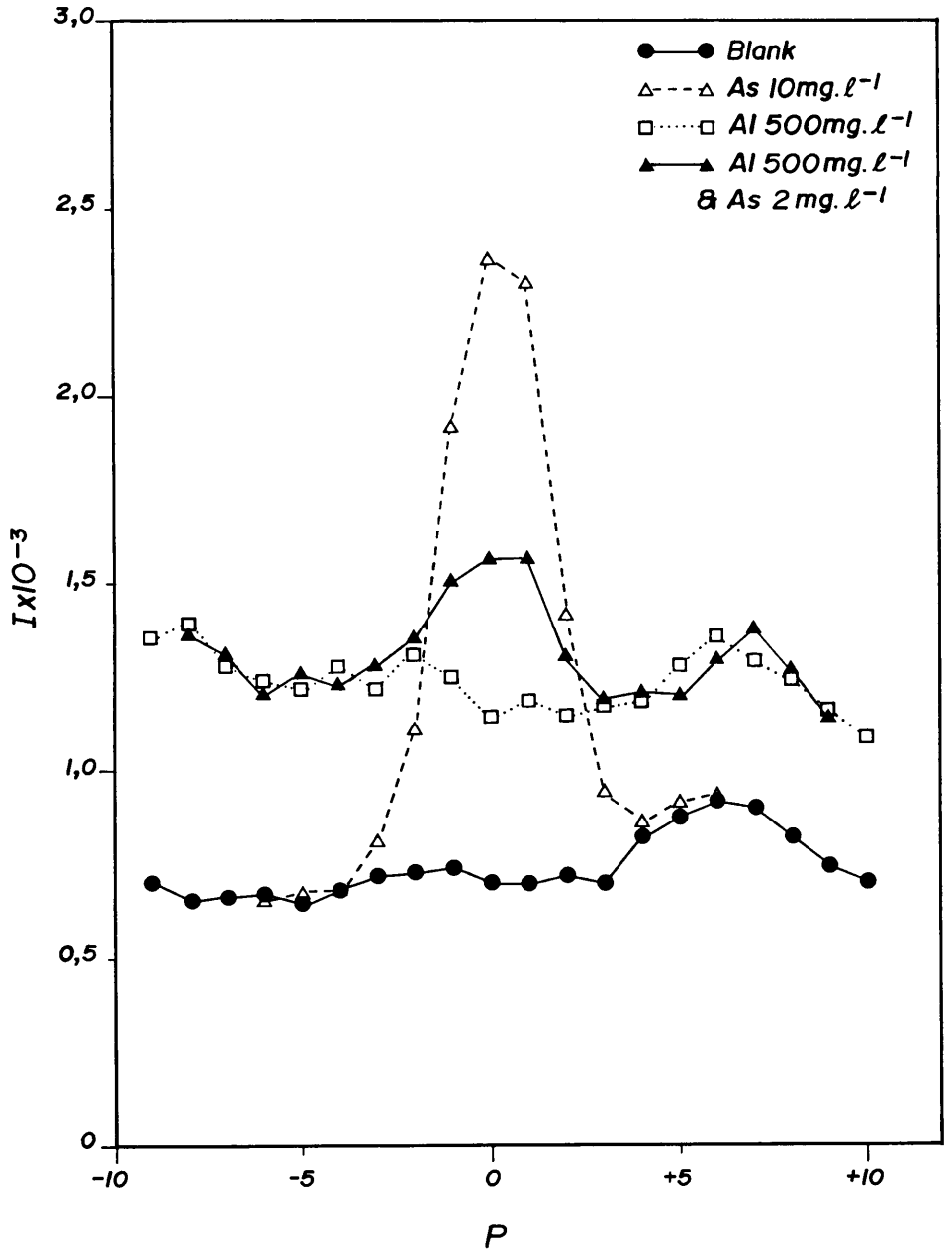


**Figure 6-5:** Profile scan data for the As(I) 193,76 nm emission line showing the baseline shift caused by 500 mg.ℓ$^{-1}$ Al (□....□), and the spiking of the Al std with 2 mg.ℓ$^{-1}$ As (▲——▲).

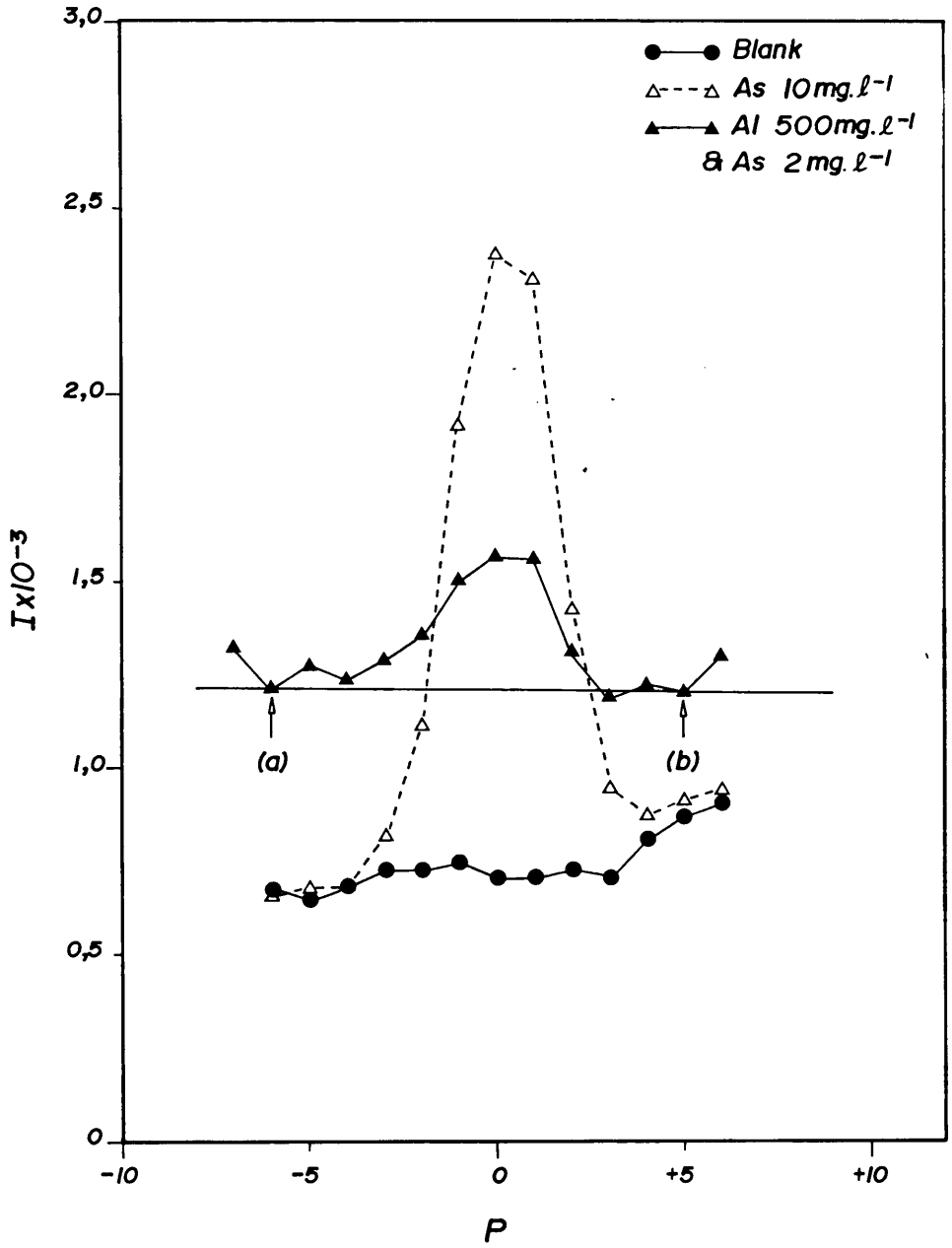


**Figure 6-6:** Profile scan data for the As(I) 193,76 nm line with 10 mg.ℓ$^{-1}$ As (△---△), blank (●–●) and 2 mg.ℓ$^{-1}$ As in 500 mg.ℓ$^{-1}$ Al (▲——▲), showing positions for baseline shift interpolation (a & b).

transformation is applied. The net intensity data for the 500 $mg.\ell^{-1}$ Al std., spiked with 2,0 $mg.\ell^{-1}$ As after baseline interpolation subtraction, with application of the profile correction (equation 96) and inverse Gaussian function (equation 88) is shown in Table 6-8. This provides a value for the transformed net intensity of the 10 $mg.\ell^{-1}$ As std., of 1791 $\pm$ 88 and for the 500 $mg.\ell^{-1}$ Al plus 2 $mg.\ell^{-1}$ As std., of 420 $\pm$ 58, giving a calculated arsenic concentration in the latter spiked solution of 2,34 $\pm$ 0,03 $mg.\ell^{-1}$ As. The 2 $mg.\ell^{-1}$ As spike is thus determined with a RSD of 1,3% and an error of +0,34 $mg.\ell^{-1}$ As in 2,0 $mg.\ell^{-1}$As or 17% error.

The arsenic in an aluminium matrix is thus quantifiable despite the fact that the baseline elevation interference is greater than the signal produced from the small quantity of arsenic present. This example illustrates that the degree of spectral interference does not always determine the ability to quantify traces as pointed out in Section 5.5 for the approach used by Botto. Provided that the baseline intensity under the peak can be determined by baseline interpolation from near peak positions, analyte peaks superimposed on baseline elevated data may be quantified.

TABLE 6-8: The three central values for net intensity I, corrected profile position x, and inverse Gaussian transformed intensity G, for (a) 10 $mg.\ell^{-1}$ As; and (b) 2 $mg.\ell^{-1}$ As in the presence of 500 $mg.\ell^{-1}$ Al.@

| P | $I_a$ | $x_a$ | $G_a$ | $I_b$ | $x_b$ | $G_b$ |
|---|---|---|---|---|---|---|
| -1 | 1169 | -1,4 | 1892 | 301 | -1,4 | 487 |
| 0 | 1661 | -0,4 | 1728 | 365 | -0,4 | 380 |
| +1 | 1606 | 0,6 | 1754 | 360 | 0,6 | 393 |

@ I = net intensity calculated as for Co in Table 6-3 following subtraction of elevated baseline as illustrated in Figure 6-6.

x = Profile position corrected with equation 96

G = Intensities after transformation with inverse Gaussian transform, equation 88, with h = 1,68 profile step units for the As 193,76 nm line.

## 6.7 The problem of relative profile shift for sloped or structured backgrounds in the profile scan mode of measurement.

The measurement of concentration of an analyte in ICP emission spectrometry is dependent on the determination of the net intensity i.e., the increase in intensity above background emission produced by the analyte. Where a profile scan of a blank solution across an analytical wavelength shows a sloped background, there should be no relative profile shift between blank and sample solution profiles, as such a shift will affect the accuracy of measurement of net intensity.

Consider for example the profile across the Hg(I) 184,95 nm line on the ARL 3510 spectrometer (Figure 6-7). The background slope (2) implies that there should be no profile shift between the blank scan (2) and sample scan (3) if a correct value for net intensity at line centre position is to be obtained. Quantification of the precision in an analagous fashion to that shown in section 6.6 gave a RSD, for the 0,2 $mg.\ell^{-1}$ Hg scan, of 48% implying that peak 3 (Figure 6-7) is at the detection limit (Table 6-9).

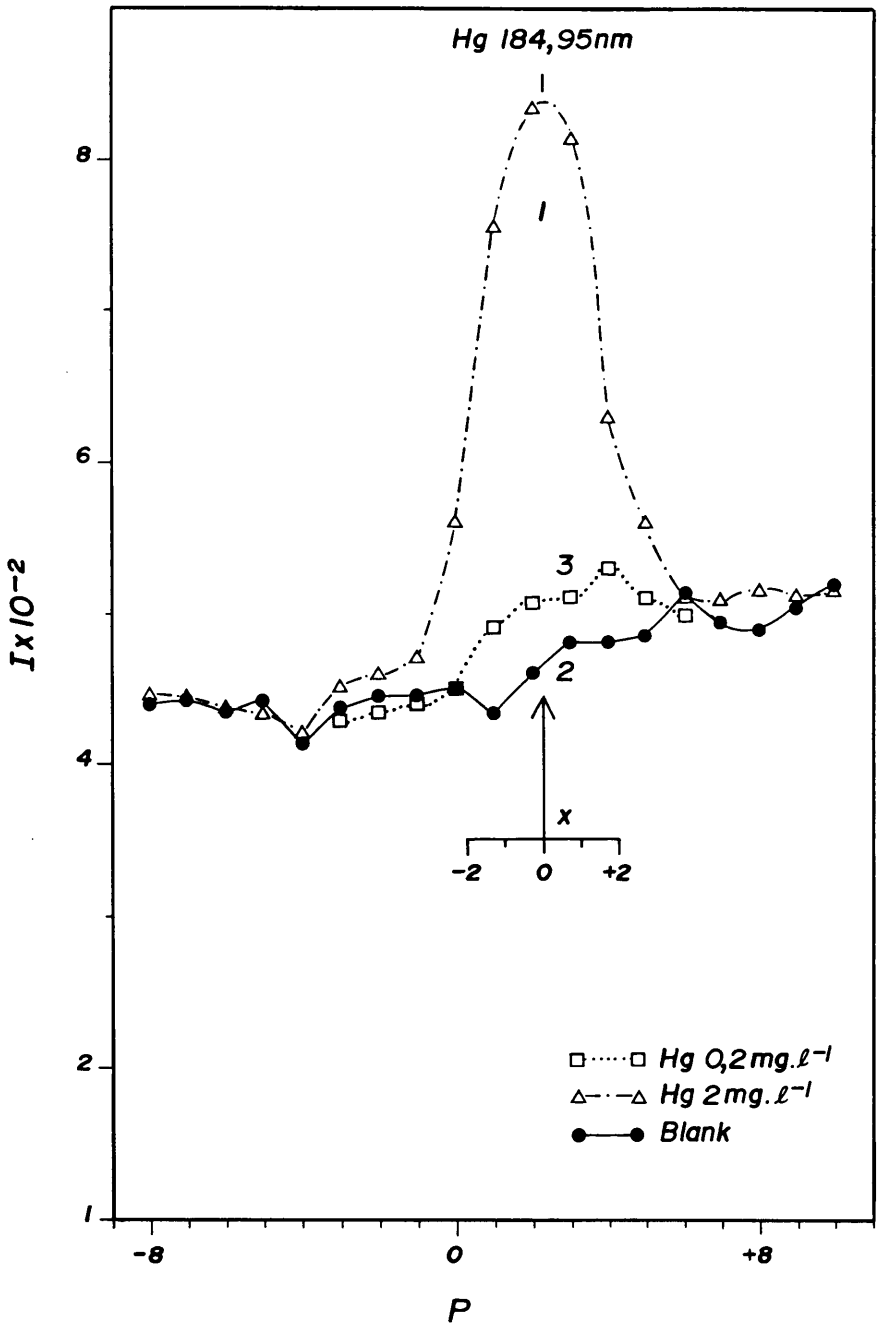


Figure 6-7: Profile scan across the Hg(I) 184,95 nm line showing a plot of gross intensity (I) against profile step position for 1 s integration time at attenuator setting 12 on the ARL 3510 spectrometer showing Hg std (1) and sloped background (2). The background slope results in deterioration in detection limit due to dependence of net intensities on exact profile setting. The solution (3) containing 0,2 mg.$\ell^{-1}$ Hg is at the detection limit.

TABLE 6-9: Calculation of precision from a profile scan, using inverse Gaussian transformed intensities G, for (a) 2 mg.$\ell^{-1}$ Hg and (b) 0,2 mg.$\ell^{-1}$ Hg, showing the percent relative standard deviation (RSD) obtained.

| P | $I_{2,0}$ | x | $G_{2,0}$ | $I_{0,2}$ | $G_{0,2}$ |
|---|---|---|---|---|---|
| +1 | 320 | -1,3 | 480 | 58 | 87 |
| 2 | 371 | -0,3 | 479 | 48 | 49 |
| 3 | 333 | +0,7 | 374 | 30 | 34 |
| | | Mean: | 444 | Mean: | 56 |
| | | σ | ±61 | σ | ±27 |
| | | RSD : | 14% | RSD : | 48% |

P = profile step position, uncorrected.

$I_C$ = net intensity for a C mg.$\ell^{-1}$ Hg solution.

x = corrected profile position from line centre, profile step units, using equation 96.

$G_C$ = net intensity of a C mg.$\ell^{-1}$ Hg solution after inverse Gaussian transformation, equation 88, with h = 1,7 for the Hg 184,96 nm, line.

It is not only sloped backgrounds which present difficulty in the accurate measurement of net intensity, but any background structure under the analyte line which will imply a critical sensitivity to exact profile registration between successive scans, particularly at concentrations near the limit of detection.

As an illustration of this problem, consider scans across the As 193,76 nm line on the ARL 3510 spectrometer for 1 s integration times and attenuator setting of 12, for low As concentrations (Figure 6-8). This figure shows a 5 $mg.\ell^{-1}$As (1) and 0,5 $mg.\ell^{-1}$As (2) scan plus two scans of a blank solution of $\phi$ = 0,01 nitric acid (3), with one blank solution showing profile misalignment of +3 steps, as indicated by the shift in the neighbouring background peak (4), +3 steps to the right (5).

If calculation of the concentration of arsenic in the solution containing 0,5 $mg.\ell^{-1}$ As is done using blank (a) and the 5 $mg.\ell^{-1}$ As scan as calibration standard (Figure 6-8); by means of the inverse Gaussian method as illustrated in Section 6.5, and assuming linearity, an arsenic concentration of 0,59 $\pm$ 0,08 $mg.\ell^{-1}$ is obtained (Table 6-10). There is thus a positive error of 0,09 $mg.\ell^{-1}$ As which is just greater than one std., deviation unit for the measurement.

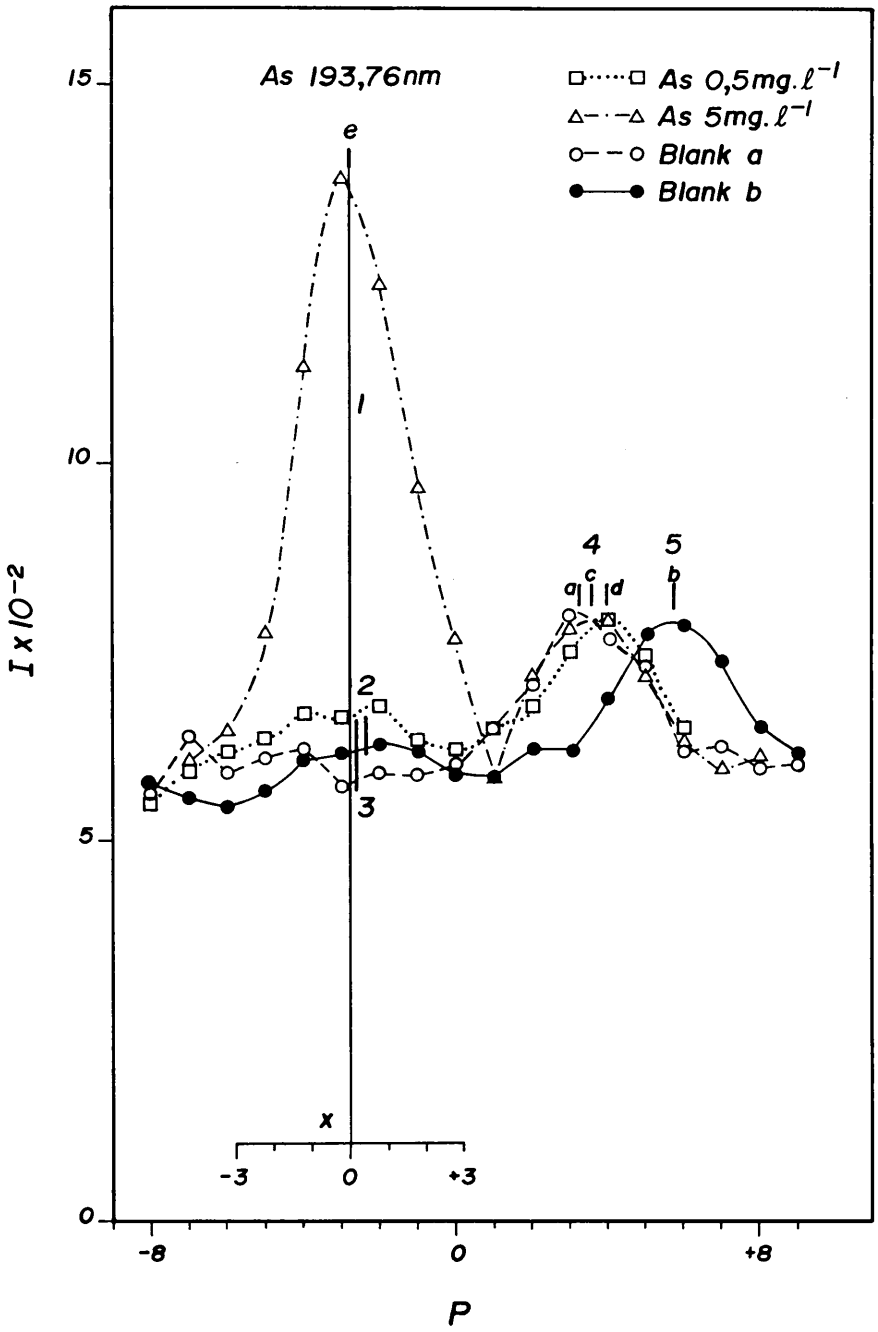


**Figure 6-8:** Profile scans across the As(I) 193,76 nm line showing a plot of gross intensity (I) against profile step position (P) with As std., peak (1), with line centre in position e, where x=0. Quantification of the net intensity for a sample containing a small quantity of arsenic (2) is critically dependent on the accuracy with which blank intensity is defined (3). An adjacent background peak (4) may be used to detect profile registration shifts (eg. 5) in the blank or sample scan data.

TABLE 6-10: Calculation of inverse Gaussian transformed intensities, G, from single scans across the As(I) 193,76 nm line, of two As-solutions viz., 5 mg.ℓ$^{-1}$ As and 0,5 mg.ℓ$^{-1}$ As.

As, 5 mg.ℓ$^{-1}$

| P | $I_g$ | $I_b$ | $I_n$ | x | G |
|---|---|---|---|---|---|
| -4 | 1124 | 623 | 501 | -1,15 | 693 |
| -3 | 1380 | 574 | 806 | -0,15 | 810 |
| -2 | 1236 | 592 | 644 | 0,85 | 769 |
| | | | | $\overline{G}$ : | 757 |
| | | | | σ : | 59 |

As, 0,5 mg.ℓ$^{-1}$

| P | $I_g$ | $I_b$ | $I_n$ | x | G |
|---|---|---|---|---|---|
| -4 | 670 | 623 | 47 | -1,46 | 79 |
| -3 | 665 | 574 | 91 | -0,04 | 96 |
| -2 | 681 | 592 | 89 | 0,54 | 96 |
| | | | | $\overline{G}$ : | 90 |
| | | | | σ : | 10 |

Intensity (I) subscripts: g-gross, b-blank, n-net.

x Profile position from line centre (equation 96)

G Inverse Gaussian transform (equation 88) with h = 1,68 profile steps for the As 193,76 nm line.

Transformed net intensity for 5 mg.ℓ$^{-1}$ As = 757 ± 59
Transformed net intensity for 0,5 mg.ℓ$^{-1}$ As = 90 ± 10
Apparent arsenic concentration in 0,5 mg.ℓ$^{-1}$ As solution

$$= \left( \frac{90 \pm 10}{757 \pm 59} \right) \times 5 \quad \text{i.e.,} \quad 0{,}59 \pm 0{,}08 \text{ mg.ℓ}^{-1} \text{ As}$$

**TABLE 6-11:** Quantification of arsenic concentrations near the detection limit of the As(I) 193,76 nm line, showing how use of a misaligned blank profile b (Figure 6-8) results in an inability to identify peak max., position for the low concentration of 0,5 $mg.\ell^{-1}$ As solution.

| P | $I_g$ | $I_b$ | $I_n$ | |
|---|---|---|---|---|
| -6 | 623 | 550 | 73 | |
| -5 | 637 | 566 | 71 | |
| -4 | 670 | 606 | 64 | |
| -3 | 665 | 616 | 49 | * |
| -2 | 681 | 626 | 55 | |
| -1 | 629 | 619 | 10 | |
| 0 | 621 | 590 | 31 | |
| 1 | 647 | 586 | 61 | |

Intensity (I) subscripts: g-gross, b-blank, n-net

* No maximum intensity identifiable near the profile position of line centre for the As 193,76 nm line(P=-3).

If the misaligned blank scan (blank b, Figure 6-8) is used to calculate net intensities for the 0,5 $mg.\ell^{-1}$ As solution, erroneous net intensities result with no peak maximum identifiable near the profile position for line centre (Table 6-11).

The use of the background peak neighbouring the arsenic analytical line may be used, however, to realign the profile scan blank (b) if the profile for this scan is shifted 3 steps to the left (Figure 6-8). The corrected net intensity values may then be obtained for the 0,5 $mg.\ell^{-1}$ As solution (Table 6-12). The transformed net intensity of 94±9 obtained with the realigned blank profile (Table 6-12) does not differ significantly@ from that obtained with blank (a) (Table 6-10) of 90±10 intensity units for the 0,5 $mg.\ell^{-1}$ As solution. The transformed net intensities for the 5 $mg.\ell^{-1}$ As calibration standard viz., 757±59 using blank (a) (Table 6-10) and 758±46 using realigned blank (b) show no significant difference.

---

@ $|t| = 0,51$ with $t_{critical}$ $(0,975) = 2,78$ for 2n-2
i.e. 4 degress of freedom.

TABLE 6-12: Correction for relative profile misalignment in the determination of net intensity for the 0,5 mg.$\ell^{-1}$ As profile scan and blank by shifting the blank profile 3 steps to the left so that background peaks 4 and 5 as shown in Figure 6-8, coincide.

| P | $I_g$ | P | $I_b$ | $I_n$ | | | |
|---|---|---|---|---|---|---|---|
| -6 | 623 | -3 | 616 | 7 | | | |
| -5 | 637 | -2 | 626 | 11 | | x | G |
| -4 | 670 | -1 | 619 | 51 | | -1,68 | 102 |
| -3 | 665 | 0 | 590 | 75 | | -0,68 | 84 |
| -2 | 681 | 1 | 586 | 95 | @ | 0,32 | 97 |
| -1 | 629 | 2 | 624 | 5 | | 1,32 | |
| 0 | 621 | 3 | 622 | - 1 | | | |
| | | | | | | $\bar{G}$ : | 94 |
| 1 | 647 | 4 | 691 | -44 | | $\sigma$ : | 9 |

@ Peak identifiable with maximum near profile position for line centre (P= -3) for As 193,76 nm.

x Profile position from peak max., equation (96)

G Inverse Gaussian transform, equation 88.

Transformed net intensity for 0,5 mg.$\ell^{-1}$ As = 94$\pm$9.

In conclusion, in the use of the profile scan method for quantitation of analyte concentrations near the limit of detection; the presence of profile misalignment greater than 1 profile division should be corrected for prior to blank subtraction so that valid net intensities are obtained.

## 6.8 Detection limit from blank profile scan data

In Section 2.10 (Chapter 2), the possibility of defining the variable $\Omega_b$ (equation 20) in order to estimate detection limit from blank readings in the profile scan mode of measurement was raised. Application of this function to the blank intensity data for the Co 238,89 nm scan data (Table 6-2), centred around profile step position P = +1 for x ~ 0, provides $\Omega_b$ values shown in Tables 6-13.

TABLE 6-13: Calculation of $\Omega_b$ (equation 20, Chapter 2) for the blank intensity data for a scan across Co(II) 238,89 nm centred around line centre at P = +1 (Table 6-2).

| m | n | $\Omega_b$* | $\Omega_b$/mg.$\ell^{-1}$Co | $2\Omega_b$/mg.$\ell^{-1}$Co |
|---|---|---|---|---|
| 1 | 3 | 54 | 0,008 | 0,016 |
| 2 | 5 | 70 | 0,010 | 0,020 |
| 3 | 7 | 79 | 0,012 | 0,024 |

$\Omega_b$* calculated from intensity data.

For n = 3 a $2\Omega_b$ value of 0,016 mg.$\ell^{-1}$ Co as an estimate of detection limit in the scan mode is in reasonable agreement with a DL of 0,010 mg.$\ell^{-1}$ Co for integration at central profile position (Table 6-1 and Figure 6-1).

In the case of Hg, the following was found:

For a profile of a blank solution across Hg(I) 184,95 nm (Figure 6-7) an $\Omega_b$ value of 0,11 $mg.\ell^{-1}$ Hg was obtained for n = 5 and 0,12 $mg.\ell^{-1}$ Hg for n = 3, implying estimated detection limits of 0,22 and 0,24 $mg.\ell^{-1}$ Hg respectively. These values are similar to the inverse Gaussian transformation estimate of DL in the scan mode as 0,2 $mg.\ell^{-1}$ Hg where the RSD is ~ 50% (Table 6-9).

The profile data for Hg(I) 184,95 nm shows a sloped background under the line (Figure 6-7) which results in over-estimation of the DL using $\Omega_b$. In the case of sloped backgrounds equation 20 may be applied to the residual intensities remaining after application of linear regression to the profile intensity data for the blank, rather than to the blank intensities <u>per se</u> (Table 6-14). This provides an $\Omega_b$ value of 0,03 $mg.\ell^{-1}$ Hg, giving an estimated DL of 0,06 $mg.\ell^{-1}$ Hg. This detection limit is representative of the detection limit which may be achieved provided that no shift in profile occurs between sample, std., and blank.

TABLE 6-14: Calculation of $\Omega_b$* (equation 20) for blank intensity data for a scan across Hg(I) 184,95 nm (Figure 6-7) from residuals after linear regression.

| P | $I_b$ | $I_{b,r}$ | R |
|---|---|---|---|
| 0 | 450 | 440,6 | 9,4 |
| 1 | 436 | 451,4 | -15,4 |
| 2 | 462 | 462,2 | - 0,2 |
| 3 | 482 | 473,0 | 9,0 |
| 4 | 481 | 483,8 | - 2,8 |

r = 0,86
a = 440,6
b = 10,8
(where $I_{b,r} = b.P + a$)

$\Omega_b$ = 6,0 intensity units = 0,03 mg.$\ell^{-1}$ Hg.

* standard deviation of the blank taken across a wavelength window (see section 2.10).

$I_b$ - blank intensity
$I_{b,r}$ - regressed blank intensity
R - residual.

## 6.9 Assurance of analyte element identity by use of the profile scan technique at more than one analytical wavelength.

While background elevation or wing overlap interferences are readily identified by the use of a wavelength scan across an analytical emission line, the problem still remains where only one analytical line of a given element is investigated, that an exact spectral line coincidence may occur. Such exact coincidences cannot be identified by means of a scan across one analytical line only. A ready solution to this problem is provided by the use of scans at two or more emission lines of the same element. If several scans, at different analytical wavelengths for a given element all show the presence of that element, with the determined concentrations in approximate agreement, the certainty of element identity can be regarded as established beyond reasonable doubt.

The extra effort required to record scans at multiple wavelengths for a given element is particularly important where toxic elements such as arsenic, for example, are found in concentrations presenting a health hazard in environmental samples. In such cases element identity and concentration must be ascertained with great accuracy, both qualitative and quantitative.

## 6.10 Application of the inverse Gaussian transformation to the determination of chromium and lead in a sediment digest.

The inverse Gaussian transformation on profile scan data is not only valuable for quantitative analysis near the detection limit, but may also be used at higher concentrations. In this section, the use of the method is illustrated for the determination of chromium and lead in a sediment digest. The sediment sample used was obtained from a river in an industrially polluted area.

After air drying at 105°C to constant mass, the sample was thoroughly mixed before taking a 0,500 g aliquot for analysis. The dried material had the appearance of grey powder. To the sample aliquot, in a 100 mℓ beaker, was added 12 mℓ freshly prepared aqua regia, and three glass anti-bumping beads. The beaker was covered with a watch glass and placed on a hot plate at low-heat. After the contents were allowed to simmer for 30 min, the heat setting was turned up and the contents evaporated to near dryness. After cooling, 5 mℓ deionized water was added and the contents quantitatively transfered to a filter funnel with a Whatman No., 42 paper. Nitric acid, $\phi$ = 0,01, was used to rinse the beaker, watchglass and filter. The filtrate was collected in a 200 mℓ volumetric flask and made up to volume with nitric acid, $\phi$ = 0,01. A blank was similarly prepared, but without adding the sample.

The prepared aqua regia digest was analyzed for Cr and Pb by the profile scan method, as well as by conventional integration at line centre, on the ARL 3510 scanning monochromator in a manner analagous to that used for Co in section 6.5. The half-width at half-height value h, as determined experimentally for the Cr(II) 206,154 nm and Pb(II) 220,351 nm analytical line was 1,60 and 1,65 profile steps respectively. Chromium was determined without dilution of the digest, while for Pb a fivefold dilution was used. Integration times used were 1s per profile step position in the case of the profile scan, and 10s at line centre in the case of the conventional integration method.

The calculation of the inverse Gaussian transformed net intensities from the profile scan data for a 5,0 $mg.\ell^{-1}$ Cr standard and four replicate scans of the sample digest is given in Table 6-15, concentration being determined in the manner illustrated for Co in section 6.5. The chromium concentrations obtained from the profile scan data, and by conventional integration at line-centre are shown in Table 6-16. There was no significant difference, at the two-tailed 1% level, between the mean chromium concentrations found by the two methods, and precision was similar viz., a 1,8% RSD in the case of the profile scan method and 1,5% RSD in the case of integration at line centre.

The lead concentrations found in the digests by the inverse Gaussian scan method and conventional integration method are shown in Table 6-17. Both methods gave the same lead concentration viz., 21,27 $mg.\ell^{-1}$ Pb in the digest, with a RSD of 1,8% for the scan method and 0,6% for conventional integration.

Repetition of the whole procedure on a second 0,5 aliquot of the sediment sample gave Pb and Cr concentrations in the prepared digest as shown in Table 6-18. In this case Cr concentrations showed a significant difference, but with similar precision i.e., 1,6% RSD for the scan method, and 1,4% RSD for the conventional integration method. The Pb concentrations were not significantly different from each other, but were slightly lower than the value determined on the 1st sediment aliquot.

The concentrations of Cr and Pb found by the scan and conventional methods for the two sediment aliquots, expressed as $\mu g.g^{-1}$ concentration in the air dried sample, are shown in Table 6-19, the overall mean concentration of Cr and Pb being 496 $\pm$ 6 and 8420 $\pm$ 100 $\mu g.g^{-1}$ respectively as determined by the scan method; and 472 $\pm$ 5 and 8330 $\pm$ 50 $\mu g.g^{-1}$ respectively as determined by the conventional integration method.

Of the two methods, the collection of profile scan data for the inverse Gaussian method is experimentally easier than integration at line centre, as profile drift in the

collected data does not affect the inverse Gaussian calulation; whereas in conventional integration at line-centre, this is not the case. In line-centre integration, the exit slit must coincide exactly with line-centre, and must not drift from this position. The inability of the ARL 3510 scanning monochromator to allow for profile step settings of less than 0,0028 nm makes this experimentally difficult.

TABLE 6-15: Calculation of inverse Gaussian transformed net intensities (G) from profile scan net intensity data of a 5,0 $mg.\ell^{-1}$ Cr-standard and four replicate scans of an aqua regia digest of a sediment sample.

| P | $I_{5,0}$ | $x_{5,0}$ | $G_{5,0}$ | $I_{s,1}$ | $x_{s,1}$ | $G_{s,1}$ | $I_{s,2}$ | $x_{s,2}$ | $G_{s,2}$ |
|---|---|---|---|---|---|---|---|---|---|
| 0 | 2556 | 1,362 | 4224 | 698 | 1,346 | 1140 | 650 | 1,286 | 1017 |
| -1 | 4282 | 0,362 | 4437 | 1077 | 0,346 | 1112 | 1007 | 0,286 | 1030 |
| -2 | 4006 | -0,638 | 4473 | 1008 | -0,654 | 1132 | 910 | -0,714 | 1045 |
| | | $\overline{G}_{5,0}$ | 4378 | | $\overline{G}_{s,1}$ | 1128 | | $\overline{G}_{s,2}$ | 1031 |
| | | $\sigma$ | 134 | | $\sigma$ | 14 | | $\sigma$ | 14 |
| | | RSD | 3% | | RSD | 1% | | RSD | 1% |

Subscripts: 5,0 - $C_{Cr}/mg.\ell^{-1}$ for scan of standard:

s,n - $n^{th}$ replicate scan of sample digest s, across Cr(II) 206,154 nm line.

P - uncorrected profile step position.

I - net intensity, uncorrected.

x - corrected profile step position, equation 96.

G - net intensity transformed with inverse Gaussian function, equation 88, using

TABLE 6-15 (continued):

| P | $I_{s,3}$ | $x_{s,3}$ | $G_{s,3}$ | $I_{s,4}$ | $x_{s,4}$ | $G_{s,4}$ |
|---|---|---|---|---|---|---|
| 0 | 788 | 1,142 | 1122 | 680 | 1,360 | 1122 |
| -1 | 1068 | 0,142 | 1074 | 1124 | 0,360 | 1164 |
| -2 | 912 | -0,858 | 1113 | 1052 | -0,640 | 1175 |
| | | $\overline{G}_{s,3}$ | 1103 | | $\overline{G}_{s,4}$ | 1154 |
| | | $\sigma$ | 26 | | $\sigma$ | 28 |
| | | RSD | 2% | | RSD | 2% |

Subscripts: s,n - $n^{th}$ replicate scan of sample digest, across Cr(II) 206,154 nm line.

P - uncorrected profile step position.

I - net intensity, uncorrected.

x - corrected profile step position, equation 96.

G - net intensity transformed with inverse Gaussian function, equation 88, using h-value of 1,60 for the Cr(II) 206,154 nm line.

**TABLE 6-16:** Chromium concentrations found in the aqua regia digest of a sediment sample using (a) the profile scan method and mean inverse Gaussian transformed net intensity, G; and (b) conventional integration at peak maximum, M, with 3 x 10s integrations, and linear interpolation between the 5,0 $mg.\ell^{-1}$ Cr standard and blank.

| n | $C_{Cr}$/$mg.\ell^{-1}$; G | $C_{Cr}$/$mg.\ell^{-1}$; M |
|---|---|---|
| 1 | 1,288 ± 0,042 | 1,291 ± 0,038 |
| 2 | 1,177 ± 0,039 | 1,291 ± 0,057 |
| 3 | 1,260 ± 0,049 | 1,279 ± 0,024 |
| 4 | 1,318 ± 0,051 | 1,235 ± 0,023 |
| Mean*: | 1,261 ± 0,023 | 1,274 ± 0,019 |

n - replicate number

$$C_{Cr;G} = \left( \frac{\bar{G}_{s,n} \pm \sigma}{\bar{G}_{5,0} \pm \sigma} \right) \times 5$$ ; data from Table 6-15.

$C_{Cr;M}$ - conventional determination of concentration from the ratio of sample net intensity to standard net intensity, multiplied by standard's concentration; from intensities measured at peak maximum.

* Difference between means not significant at 1% two-tailed level ($|t| = 0,872$).

TABLE 6-17: Lead concentrations found in the aqua regia digest of a sediment sample using (a) the profile scan method and mean inverse Gaussian transformed net intensity, G; and (b) conventional integration at peak maximum, M, with 3 x 10s integrations, and linear interpolation between 10,0 $mg.\ell^{-1}$ Pb standard and blank.

| n | $C_{Pb}/mg.\ell^{-1}$; G | $C_{Pb}/mg.\ell^{-1}$; M |
|---|---|---|
| 1 | 20,15 ± 0,48 | 20,55 ± 0,14 |
| 2 | 21,38 ± 1,23 | 21,71 ± 0,10 |
| 3 | 22,94 ± 0,66 | 20,88 ± 0,26 |
| 4 | 20,60 ± 0,33 | 21,95 ± 0,48 |
| Mean: | 21,27 ± 0,38 | 21,27 ± 0,14 |

n - replicate number

$C_{Pb;G}$ - lead concentration determined by profile scan method using Pb(II) 220,351 nm line, with h = 1,65 and 1s integration time at attenuator setting 12. Analagous procedure used to that shown for Cr in Table 6-15 and 6-16, except that a 10 $mg.\ell^{-1}$ Pb standard was used and sample digest was diluted fivefold prior to profile scan.

$C_{Pb;M}$ - conventional analysis at peak maximum, determined analagously to the method used for Cr; as given in footnotes to Table 6-16.

TABLE 6-18: Chromium and lead concentrations found in a 2nd aqua regia digest prepared from the sediment sample, as determined by inverse Gaussian method (G) and conventional integration at line centre (M). See Tables 6-16 and 6-17 for explanatory notes.

A) Chromium concentrations in duplicate digest

| n | $C_{Cr}$/mg.ℓ$^{-1}$; G | $C_{Cr}$/mg.ℓ$^{-1}$; M |
|---|---|---|
| 1 | 1,338 ± 0,018 | 1,025 ± 0,026 |
| 2 | 1,329 ± 0,041 | 1,122 ± 0,038 |
| 3 | 1,112 ± 0,015 | 1,075 ± 0,029 |
| 4 | 1,103 ± 0,062 | 1,112 ± 0,013 |
| Mean*: | 1,220 ± 0,019 | 1,084 ± 0,014 |

B) Lead concentrations in duplicate digest

| n | $C_{Pb}$/mg.ℓ$^{-1}$; G | $C_{Pb}$/mg.ℓ$^{-1}$; M |
|---|---|---|
| 1 | 19,49 ± 0,37. | 20,45 ± 0,48 |
| 2 | 22,60 ± 0,70 | 20,03 ± 0,47 |
| 3 | 20,94 ± 0,95 | 20,55 ± 0,30 |
| 4 | 20,28 ± 0,68 | 20,50 ± 0,39 |
| Mean: | 20,83 ± 0,35 | 20,38 ± 0,21 |

* difference between means significant at 1% two-tailed level.

TABLE 6-19: Overall mean concentrations of Cr and Pb in the sediment sample found using the inverse Gaussian method (a), and conventional integration at line centre (b). Data from Table 6-16 to 6-18.

Chromium:

| Aqt* | $C_{Cr}$/mg.g$^{-1}$, dry weight | |
|---|---|---|
| | a | b |
| 1 | 504 ± 9 | 510 ± 8 |
| 2 | 488 ± 8 | 434 ± 6 |
| Mean: | 496 ± 6 | 472 ± 5 |

Lead:

| Aqt* | $C_{Pb}$/µg.g$^{-1}$, dry weight | |
|---|---|---|
| | a | b |
| 1 | 8510 ± 150 | 8510 ± 60 |
| 2 | 8330 ± 140 | 8150 ± 80 |
| Mean: | 8420 ± 100 | 8330 ± 50 |

* Aqt - digestion aliquot.

## 6.11 Summary

In this chapter, the use of the wavelength scan mode of measurement was addressed as a means of quantitative analysis. It was shown, using the Co 238,89 nm line, how linearity, precision and detection limit are similar when determined by conventional measurement at line centre or by use of a wavelength scan, with the aid of an inverse Gaussian transformation as a means of estimating line centre intensity and precision.

The use of profile scan data for quantitative analysis has the advantage over the software approach of interference correction used on the polychromator (Chapter five) that quantitative analysis may be achieved by baseline interpolation and subtraction, and is not limited by the criterion of Botto (1984) that the percentage interference correction should not exceed 100%. This was illustrated in section 6.6, where the example was given of the determination of arsenic in a matrix containing aluminium at high concentration.

A difficulty inherent in the use of profile scan data, obtained on a Czerny-Turner type monochromator for quantitative analysis is the relative profile misalignment which may arise between sample, standard, and blank solution scans. Where sloped backgrounds are encountered, this results in deterioration of the detection limit and accuracy as illustrated in section 6.7. The deterioration of detection limit may be quantified through definition of detection limit as twice the omega value, where omega is defined as the standard deviation of n blank measurements recorded across a wavelength window, rather than at the central wavelength position. Where no profile shift occurs between successive scans, then omega may be alternatively defined as the standard deviation of the residuals remaining after application of linear regression to the blank reading taken across a wavelength window as discussed in section 6.8.

The chapter was concluded with an example illustrating the use of the inverse Gaussian transformation for quantitative analysis of lead and chromium in a sediment digest, and showed that the scan method and conventional integration method provided similar concentrations and precision.

# CHAPTER 7: QUALITY CONTROL

## 7.1 Introduction

As discussed in section 2.13, quality control may be divided into within-laboratory or internal procedures, which includes instrumental quality control; and inter-laboratory or external quality control. The instrumental quality control procedures used for the routine analysis of samples on the polychromator have essentially already been dealt with in Chapters three to five. The major points of importance in internal quality control are summarized in section 7.2. Specific assurance procedures for a given element in a particular sample are discussed in section 7.3, which includes a discussion on the use of wavelength scanning procedures on the monochromator as a means of internal quality control. Thereafter follow some examples of external quality control in section 7.4. A discussion on the type of quality control procedure needed where unusual matrices are encountered is given in section 7.5. A short conclusion follows in section 7.6.

## 7.2 Internal quality control

Internal quality control procedures used during routine analysis of samples on the polychromator may be subdivided into:

(a) Control of sample preparation.

(b) Instrumental control.

(c) Decision to use further procedures, based on analytical results.

The major points in these three subdivisions are discussed below:

(a) Control of sample preparation

This entails the control of procedures designed to present the sample in the form of a clear solution, free of suspended particulates, with a total cation concentration not exceeding 3400 $mg.\ell^{-1}$ (section 3.4) in a dilute acid matrix, usually $\phi$ = 0,01 nitric acid. It also entails the necessity to avoid loss of analyte and minimize contamination, especially in the case of the digestion of solid samples; plus the need to correct for impurities in the reagents used through use of a reagent blank and blank subtraction. The reagent blank should be prepared and analyzed at least in duplicate.

In the case of water samples, where enrichment procedures are used, then the use of analyte element additions (spikes) to an aliquot of the sample prior to the concentration step is necessary as a control on

the efficacy of the enrichment step (Kempster and Van Vliet, 1978; Watling and Watling, 1976). The use of spikes is likewise needed where separation techniques are applied to solid sample digests.

The need to approximately match the acid strengths of samples and calibration standards so as to avoid the acid matrix effect was shown in Chapter three.

(b) Instrumental control

The need to carefully control instrumental parameters was demonstrated in Chapter four, where the sensitivity of analyte element emission to (i) change in sample uptake rate (ii) change in input mains voltage to the rf generator, and (iii) change in inner (aerosol) gas flow to the plasma torch was shown. Thus the need to check compromise instrumental operation parameters (Table 4-3), particularly those related to sample introduction and the plasma source.

Prior to calibration or daily normalization of the polychromator with known standards (Table 5-1), the spectrometer's profile setting must be carefully checked; in this case the Y(II) 360,073 nm line was used (section 5.2).

An important quality control check in the analysis of the sample plate (Table 5-4, section 5.3) is the inspection of the analyical results obtained for the mixed element control standard, which is placed near the start and end on an analysis plate, to ascertain whether sensitivity change has occurred or not. Should the analyzed concentration of an element in the control standard differ by more than 5% from the true concentration, then the instrument should be re-normalized after the compromise operating conditions have been checked (Table 4-3).

As shown in section 5.4, the interelement interference correction coefficients are affected by slight change in source conditions i.e., aerosol gas flow rate and incident rf power, as well as by changes in nebulization. The accuracy of the correction coefficients is central to valid analytical results, and such correction coefficients must therefore be redetermined should any nebulization or source parameter condition be changed.

(c) Decision to use further procedures, based on analytical results

Once the sample plate (section 5.3) has been analyzed, and the analyst has inspected the results to ensure that the element concentrations found for the control standard are within the 5% limit of the true value, as

described above, then the analyst should inspect the individual sample results as follows:

(i) Are the analyzed concentrations within the maximum concentration limits as defined by the mixed calibration set (Table 5-1)? If this is not so, then the sample must be reanalyzed after appropriate dilution.

(ii) Where the major interferants encountered in water samples i.e., Ca, Mg, Fe or Mn are present at relatively high concentration, in practice in excess of ca., 100 $mg.\ell^{-1}$, then care should be taken in the reporting of results for trace elements where large interference from the matrix elements is encountered. Here, the approach of Botto (1984) is useful, where an analysis may be considered quantitative when the Percentage Interference Correction, PIC (equation 31, Chapter two), does not exceed 100%. To facilitate use of this check, the raw or uncorrected element concentrations should be printed out adjacent to the corrected concentrations on the analysis result sheet. Should the PIC exceed 100%, then direct analysis of the given element in that sample on the

polychromator by the software approach, is not possible. An alternative techniques should then be employed.

Alternative techniques used are (i) the ARL 3510 scanning monochromator, where the degree of interelement interference can often be reduced due to the higher resolution of the monochromator as compared to the ARL 34000 polychromator (Table 4-1); or (ii) other analytical techniques such as flameless atomic absorption spectrometry.

## 7.3 Specific quality control procedures

The determination of percentage recovery following the addition of a known amount of an element to a sample (spiking) is of rather limited usefulness in the instrumental aspect of the ICP emission spectrometric analysis *per se** as a consequence, firstly of the linearity of the method and secondly of the relative insensitivity

---

* Not to be confused with the usefulness of recovery tests in ascertaining the efficacy of enrichment or separation procedures applied during sample preparation, as mentioned in section 7.2(a).

of the analyte emission signal to matrix differences, where aspiration rate is controlled with the aid of a peristaltic pump (Chapter three). Recovery tests may, however, serve to detect changes in sensitivity where matrices have not been suitably matched. Butler, Mathews and Kempster (1980), using the ARL 34000 ICP polychromator instrument as described by Kempster and de Villiers (1978) carried out recovery tests on spiking, for Cd, Cr, Co, Cu, Fe, Pb, Mn, Ni, Sr and Zn in fish, algae and sediment digests and showed that satisfactory recoveries were obtained for these elements, with the exception of Pb, Cr and Zn in some of the digests, which may be attributed to acid matrix differences between the digests and the calibration standards.

It is very important to realize that recovery on spiking in ICP emission spectrometric analysis provides no information on the presence or absence of spectral overlap or background elevation type interferences, which constitute the central problem in trace element analysis of environmental samples by ICP emission spectrometry. Thus for example, Butler et al (1980) found recoveries for Co in fish digest of 100%, yet the ICP technique gave a cobalt concentration of 0,003 $mg.g^{-1}$ while the atomic absorption method gave a cobalt concentration of 0,00003 $mg.g^{-1}$ i.e., two orders of magnitude lower.

The detection and correction of background elevation or line overlap type interferences is readily achieved using the profile scan mode of analysis, as described in Chapter six. The determination of the amount of background to subtract under the analyte element peak may be established for individual samples, and is not limited by the criterion of Botto (1984). For instance in section 6.6 the example is given of the determination of arsenic in an aluminium matrix at the As(I) 193,76 nm analytical line, where the Percentage Interference Correction (PIC) exceeds 100%.

While the use of profile scans for quantitative analysis provide a means of distinguishing between analyte element emission and background elevation or line-wing overlap interferences, the problem of exact line co-incidence requires the use of an alternative analytical line (section 6.9).

Other quality control procedures are the use of alternative analysis techniques such as atomic absorption spectrometry. In a comparison of ICP emission spectrometry and atomic absorption spectrometry in the analysis of fish, algal and sediment digests, Butler et al (1980) concluded that the limiting problem in direct analysis rests on the inability of the concentric glass nebulizer to handle total cation concentrations greater than 3400 $mg.\ell^{-1}$ without changes in sensitivity.

## 7.4 External quality control

External or inter-laboratory quality control provides an excellent means of checking the analytical procedures, firstly as analyses are done blind i.e., without prior knowledge of the result and secondly because the opportunity is presented of comparing one's results with those obtained by other laboratories, often using alternative analytical techniques. The inter-laboratory comparisons organized by the International Atomic Energy Agency (IAEA) are especially attractive due to the wide range of analytical methods employed by the participating laboratories. One disadvantage is that only a limited number of elements are adequately covered, and insufficient data to obtain statistically meaningful results commonly occurs, for example for such elements as Be, B, Y, Si, Zr, Sb, Se and V in samples of interest in environmental analysis (Pszonicki and Hanna, 1985).

The results achieved in some external quality control studies for (a) hay powder, (b) river sediment, (c) sewage sludge and (d) water are presented below:

(a) Hay powder - International Atomic Energy Agency (IAEA) study V-10 (Pszonicki and Hanna, 1985):

A test of the analytical performance of the ARL 34000 spectrometer, using the calibration procedures as

described in Chapter five was made in 1984, when a sample of powdered hay was analyzed for IAEA study No. V-10. The results of this comparison became available in July 1985. For this intercomparison, two different sample digestion techniques were used viz., (i) a nitric/perchloric acid digestion, and (ii) an aqua regia digestion.

The sample pretreatment procedure was as follows:

(i) For the nitric/perchloric acid digestion ca., 250 mg accurately weighed hay powder was placed in a Technicon digestion tube. To the digestion tube was added 10 mℓ redistilled nitric acid and 5 mℓ perchloric acid. After allowing the mixture to stand overnight, boiling chips were added and the digestion tube heated to 100°C in a Technicon Digestion Block. When evolution of brown-fumes had ceased, the temperature was raised to 150°C, where it was maintained for 35 min., after which the temperature was increased to 225°C. After 60 min., at the latter temperature the digestion tube and its contents was cooled to ambient temperature, the contents quantitatively transferred to a 100 mℓ volumetric flask and diluted to volume with deionized water. Five replicate sample digests were prepared.

(ii) For the aqua regia digest, a weighed quantity of the hay sample was pre-ashed in a porcelain crucible in a muffle furnance at 600°C for 1h. To three 0,1g subsamples of the ash in a porcelain crucible was added 15 mℓ freshly prepared aqua regia. The crucible was covered with a watch glass and allowed to stand overnight. The watch glass was then removed and the digest evaporated to near-dryness on a water bath. A further three aliquots of 5 mℓ aqua regia was added with evaporation between each addition. The residue was dissolved in $\phi$ = 0,01 nitric acid, filtered through Whatman No., 42 paper and made up to 200 mℓ in a volumetric flask with $\phi$ = 0,01 nitric acid.

Blank digests were also prepared by omitting the hay sample from the digestion procedure.

The sample digests were analyzed on the ARL 34000 ICP spectrometer using the calibration method as described in Chapter five, with quadratic interference coefficient corrections (Kempster et al, 1983).

The analytical results obtained for the hay sample are shown in Table 7-1, while Table 7-2 gives the range of the accepted means for the

IAEA study as well as showing the type of analytical methods employed (Pszonicki and Hanna, 1985). The concentrations reported for the digestion methods (i) and (ii) as described above, all lay within the range of accepted means except for Al using sample pretreatment (i), and Zn using sample pretreatment (ii). The aluminium concentration using pretreatment (ii) was within the 95% confidence interval of the accepted mean (Table 7-1). The results for Cr, Fe, Mn and Sr were satisfactory using pretreatment (i), but were low using pretreatment (ii), particularly in the case of Cr. Calcium and magnesium were equally well determined by either pretreatment, while Cu was best determined using pretreatment (ii). The results for Na and K were not accurate with either pretreatment. Zinc was best determined using pretreatment (i).

The elements As, Cd, Co, Ni, Mo, Pb and V were also included in this intercomparison, the concentrations were, however, below the limit for detection on the ARL 34000 spectrometer and the concentrations of these elements could not be quantified.

The overall intelaboratory number of outliers reported for this study by Pszonicki and Hanna (1985) was 10%.

TABLE 7-1: Concentrations (µg/g, dry weight) obtained for analysis of Hay Powder on the ARL 34000 spectrometer after nitric/perchloric acid digestion (i) and aqua regia digestion (ii) during participation in IAEA study V-10, showing comparison with the interlaboratory means reported for this study (Pszonicki and Hanna, 1985). The calibration method described in Chapter five was used, with quadratic interference coefficient correction (Kempster et al, 1983).

| Element | Pretreatment employed (i)** mean ± σ µg/g | (ii)*** mean ± σ µg/g | Overall interlaboratory accepted mean µg/g | 95% confidence interval of mean µg/g |
|---|---|---|---|---|
| Al | *128±12 | 66±3 | 53,2(a) | 33,3 to 73,2 |
| Ca | 23200±200 | 20800±700 | 21700(b) | 21300 to 22200 |
| Cr | 5,0±1,9 | 2,0±0,1 | 6,06(b) | 5,4 to 7,1 |
| Cu | 9,8±1,6 | 9,0±1,0 | 9,27(b) | 8,91 to 9,64 |
| Fe | 177,4±7,0 | 170,3±15,0 | 180,8(b) | 173,1 to 188,4 |

(a) un-certified, information only

(b) satisfactory degree of confidence

* outlier

** (i) = nitric/perchloric acid

*** (ii) = aqua regia

TABLE 7-1 (continued):

| Element | Pretreatment employed (i)** mean ± σ µg/g | (ii)*** mean ± σ µg/g | Overall interlaboratory accepted mean µg/g | 95% confidence interval of mean µg/g |
|---|---|---|---|---|
| K | 14600±300 | 15300±400 | 20700(a) | 19400 to 22000 |
| Mg | 1408± 15 | 1343± 46 | 1380(b) | 1320 to 1450 |
| Mn | 43,4±2,1 | 39,3±2,1 | 47,4(a) | 44,1 to 50,6 |
| Na | 793± 29 | 874± 66 | 548(a) | 483 to 614 |
| Sr | 38,6±0,6 | 36,3± 1,2 | 40,2(b) | 38,1 to 42,4 |
| Zn | 21,6±3,8 | *33,3± 14 | 24,3(b) | 23,5 to 25,2 |

(a) un-certified, information only

(b) satisfactory degree of confidence

* outlier

** (i) = nitric/perchloric acid

*** (ii) = aqua regia

TABLE 7-2: Range of accepted laboratory means and method types showing number of accepted laboratory means with no's of outliers in brackets, for the IAEA intercomparison study V-10, trace elements in Hay Powder (Pszonicki and Hanna, 1985).

| Element | Range of accepted lab., means (µg/g) | Number of accepted means and number of outliers (bracketed) | | | | | |
|---|---|---|---|---|---|---|---|
| | | NAA[a] | AAS[b] | AES[c] | XRS[d] | EL[e] | MS[f] |
| Al | 30,0 to 87,0 | 2(0) | - | 5(1) | - | - | - |
| Ca | 19800 to 24400 | 5(1) | 10(0) | 6(2) | 3(5) | - | - |
| Cr | 2,0 to 9,3 | 11(0) | 12(0) | 6(0) | 2(0) | - | - |
| Cu | 7,2 to 12,1 | 1(0) | 17(1) | 7(0) | 6(3) | 1(0) | 0(1) |
| Fe | 123,4 to 231,2 | 11(0) | 12(1) | 7(0) | 7(2) | - | - |
| K | 12600 to 27700 | 7(1) | 4(0) | 8(0) | 7(1) | - | - |

(a) Neutron activation analysis
(b) Atomic absorption spectrometry
(c) Atomic emission spectroscopy
(d) X-ray spectroscopy
(e) Electrochemical methods
(f) Spark source mass spectrometry

TABLE 7-2 (continued):

| Element | Range of accepted lab., means (µg/g) | Number of accepted means and number of outliers (bracketed) | | | | | |
|---|---|---|---|---|---|---|---|
| | | NAA[a] | AAS[b] | AES[c] | XRS[d] | EL[e] | MS[f] |
| Mg | 1097 to 1681 | 3(0) | 9(0) | 6(0) | - | - | - |
| Mn | 26,2 to 72,1 | 6(0) | 14(0) | 7(0) | 5(0) | - | 1(0) |
| Na | 375 to 874 | 7(0) | 4(0) | 8(0) | - | - | - |
| Sr | 32,1 to 48,2 | 5(0) | 2(0) | 5(0) | 5(1) | - | - |
| Zn | 19,2 to 31,0 | 9(0) | 16(3) | 5(1) | 8(1) | - | - |

(a) Neutron activation analysis

(b) Atomic absorption spectrometry

(c) Atomic emission spectroscopy

(d) X-ray spectroscopy

(e) Electrochemical methods

(f) Spark source mass spectrometry

(b) River sediment - National Institute for Water Research (NIWR) study No. 83/A, (Smith, 1984a).

Smith (1984a) ran an interlaboratory comparison study for trace metals in a river sediment during 1983. For this study a subsample of the NBS Standard Reference Material 1645 (River Sediment) was distributed to the participating laboratories, with the request that the sample be analyzed for As, Cd, Co, Cu, Pb, Mn, Hg, Ni and Zn. As mercury was present at a concentration below the detection limit of the ICP emission spectrometer, it is not included here.

This sample was interesting as being characteristic of a polluted sediment, having been dredged from the bottom of the Indiana Harbour Canal, Indiana, USA. The material contained a considerable quantity of iron and chromium viz., ca., 11% Fe and 3% Cr (m/m), and would therefore constitute a test of interference correction procedures.

The digestion procedures suggested by Smith (1984a) were used, with the modification that no interference suppressants as required for atomic absorption spectroscopy were added. An aqua regia digestion was used for Cd, Co, Cu, Pb, Mn, Ni and Zn, while a sulphuric acid/potassium persulphate digestion procedure was used for As (Smith, 1984a). Due to the limited quantity of sample supplied, digests were only carried out in duplicate.

Copper, Mn, and Zn were determined by analysis on the ARL 34000 spectrometer using quadratic interference correction as described in Chapter five, while As, Cd, Co, Pb and Ni were determined by the profile scan mode of analysis on the ARL 3510 scanning monochromator, using blank subtraction and linear interpolation at line centre between the intensity of the standard and interpolated blank (Chapter six). The analytical wavelengths employed on the monochromator were As(I) 193,76 nm; Cd(II) 226,50 nm; Co(I) 340,51 nm; Pb(I) 217,00 nm and Ni(I) 352,45 nm.

The results of the analysis for As, Cd, Co, Cu, Pb, Mn, Ni and Zn are shown in Table 7-3. Acceptable quantitation of the elements shown was observed, with the exception of Cd and Zn which gave concentrations that were too high and too low respectively compared with the interlaboratory means. The positive Cd - error may be due to the almost exact line coincidence of the weak Fe(I) 226,505 nm line with the Cd(II) 226,502 nm analytical line used (Ziadel' et al, 1970). The scan mode of analysis with background subtraction using the background near the analytical line as a measure of the background under the line (or the mean of the background at each side of the line), will not correct for line coincidence interferences.

The concentration found for Cu was in excellent agreement with that given by the NBS, while As, Co, Pb, Mn and Ni gave acceptable values. The overall number of outliers found for the trace elements in this study was 10% (Smith 1984a). Almost all the laboratories in this study employed atomic absorption spectrometry as the method of analysis.

TABLE 7-3: Concentrations (mg/kg dry weight) found in NBS-1645 river sediment by ICP emission spectrometric analysis during participation in the National Institute for Water Research interlaboratory study No., 83/A (Smith 1984a).

| Element | This study | Interlaboratory mean | Range of accepted values | NBS certified value |
|---|---|---|---|---|
| As | $44^{(b)} \pm 14$ | 41 | 37 to 44 | (66)* |
| Cd | $**23^{(b)} \pm 7$ | 8,6 | 4,0 to 10,6 | 10,2 |
| Co | $5^{(b)} \pm 2$ | 11,5 | 4,9 to 22,0 | (8)* |
| Cu | $108^{(a)} \pm 3$ | 107 | 84 to 132 | 109 |
| Pb | $670^{(b)} \pm 40$ | 720 | 534 to 880 | 714 |
| Mn | $588^{(a)} \pm 6$ | 655 | 499 to 750 | 785 |
| Ni | $37^{(b)} \pm 5$ | 46 | 24 to 68 | 45,8 |
| Zn | $**1188^{(a)} \pm 56$ | 1676 | 1392 to 1984 | 1720 |

* uncertified value

** outlier

(a) determined on ARL 34000 spectrometer

(b) determined on ARL 3510 scanning monochromator by blank subtraction and linear interpolation using scan mode of analysis.

(c) Sewage sludge - National Institute for Water Research (NIWR) comparison study no., 83/B, (Smith, 1984b).

In this interlaboratory comparison study, a homogenized air dried sample of Daspoort sewage sludge was distributed to 29 laboratories, 26 of whom reported results for trace metals. Smith (1984b) requested that the following metals be determined on this sample: Ca, Mg, Cd, Cr, Cu, Pb, Ni. Zn, Hg, As, Se, Mo and B. As an insufficient number of laboratories determined Se, Mo and B to enable a reliable mean to be calculated, the results for these three elements are not reported here. Further, as Hg was not determined by emission spectrometry, it will also not be discussed here..

For the determination of Ca, Mg, Cd, Cr, Cu, Pb, Ni and Zn an aqua regia digestion procedure was used, with a sulphuric acid/persulphate digestion procedure being employed for As (Smith, 1984b). Calcium, Mg, Cr, Cu and Zn were determined with the ARL 34000 spectrometer using the calibration procedure described in Chapter five, while Cd, Pb, Ni and As were determined on the ARL 3510 scanning monochromator using the scan mode of analysis with off-peak blank subtraction and linear interpolation between a

calibration standard and the blank value at line centre. The analytical wavelengths employed on the scanning monochromator were Cd(II) 226,50 nm; Pb(I) 217,00 nm; Ni(I) 352,45 nm and As(I) 193,76 nm.

A comparison of the results obtained by the ICP emission spectrometric technique with the interlaboratory mean is shown in Table 7-4. The accuracy of the Ca, Mg, Cr, Cu and As determinations was within one standard deviation of the interlaboratory mean; and for Cd, Pb and Ni within two standard deviations of this mean (Table 7-4). Only zinc showed poor accuracy, with the ICP emission spectrometric value being considerably lower than the interlaboratory mean. In this study the overall interlaboratory outlier average for the metals shown was 10%, the other laboratories all employing atomic absorption spectrometry as the method of analysis for the sample.

TABLE 7-4: Concentrations (mg/Kg dry weight) found in Daspoort sewage sludge sample by ICP emission spectrometric analysis during participation in the National Institute for Water Research interlaboratory study no. 83/B (Smith 1984b).

| Element | This study | Interlaboratory mean ± std., dev. | Range of accepted values |
|---|---|---|---|
| Ca | 39500[a] ± 600 | 40600 ± 6100 | 25100 to 56300 |
| Mg | 6400[a] ± 100 | 7400 ± 1200 | 5000 to 10000 |
| Cd | 8,0[b] ± 4 | 5,4 ± 1,7 | 2,0 to 9,0 |
| Cr | 127[a] ± 2 | 141 ± 48 | 60 to 253 |
| Cu | 590[a] ± 12 | 601 ± 88 | 467 to 827 |
| Pb | 234[b] ± 20 | 305 ± 58 | 174 to 395 |
| Ni | 36[b] ± 14 | 50 ± 12 | 33 to 77 |
| Zn | 1313[a] ± 11 | 1888 ± 253 | 1313 to 2250 |
| As | 6[b] ± 3 | 5,5 ± 1,4 | 4,0 to 8,0 |

(a) determined on ARL 34000 spectrometer

(b) determined on ARL 3510 scanning monochromator by blank subtraction and linear interpolation using scan mode of analysis.

(d) Water - International Atomic Energy Agency (IAEA) study no W-3/1. (Pszonicki et al, 1982).

The IAEA comparision study for trace elements in water provided the opportunity of assessing the analytical performance of the ARL 34000 ICP spectrometer for the determination of Ba, Cd, Cr, Cu, Fe, Mn, Mo, V and Zn in a simulated fresh water sample after calibration as described in Chapter five, with the exception that the interference corrections did not include manganese. The elements As and Se were also analyzed, but using flameless atomic absorption spectrometers and not ICP emission spectrometry, and they will not be discussed here. Other trace metals present in the sample were below the limit of detection of the polychromator.

The results of this interlaboratory comparision are shown in Table 7-5. The concentrations found for Ba, Cd, Fe, Mn and Zn were within one standard deviation unit of the interlaboratory mean. The values found for Cr and Cu were slightly high, but within two standard deviation units of the interlaboratory mean. For Mo and V, erroneously high values were obtained.

TABLE 7-5: Comparison of concentrations (µg/ℓ) found in a simulated water sample with the true values and those reported during the interlaboratory comparison study IAEA W-3/1, trace elements in water (Pszonicki et al, 1982).

| Element | ARL 34000 mean ± std., dev. | true value | Overall interlabratory mean ± std., deviation |
|---|---|---|---|
| As@ | 26,8 ± 4,4 | 22,4 | 20,8 ± 7,2 |
| Ba | 123 ± 1 | 99,60 | 96,2 ± 31,2 |
| Cd | 4,0 ± 1,7 | 3,98 | 3,89 ± 1,6 |
| Cr | 3,2 ± 1,7 | 2,02 | 2,55 ± 0,95 |
| Cu | 12,5 ± 2,7 | 9,06 | 8,74 ± 1,79 |
| Fe | 132,7 ± 1,7 | 125,80 | 122,3 ± 18,1 |
| Mn | 9,2 ± 0,8 | 9,56 | 8,41 ± 2,02 |
| Mo | * 8,2 ± 2,7 | 2,28 | 3,62 ± 1,22 |
| Se@ | *30,2 ± 9,0 | 21, 2 | 20, 0 ± 2, 5 |
| V | * 4,7 ± 1,4 | 2,00 | 1,93 ± 0,44 |
| Zn | 21,8 ± 4,3 | 23,20 | 22,86 ± 2,38 |

* outlier
@ determined by flameless AAS.

Other laboratories also found positively biased outliers for Mo and V. Pszonicki et al (1982) speculate that this may indicate a contamination problem, although these two elements are not among the usual components of environmental impurities.

In study W-3/1, Pszonicki et al (1982) reported that the overall outlier percentage was 15%. The major technique employed by the 58 participating laboratories was flameless atomic absorption spectrometery followed by neutron activation analysis. Forty percent of the results were obtained by direct analysis without separation or preconcentration. Pszonicki et al (1982) concluded that the prevention of accidental contamination is a major problem in the determination of trace elements in water.

## 7.5 Approach to quality control in unusual matrices.

The software approach for interference correction is only valid where interference correction coefficients have been determined for the major interfering matrix elements present in a water or environmental sample. These are the four elements, Ca, Mg, Fe and Mn as discussed in Chapter five. Occassionally, however, the laboratory is presented with samples for analysis containing high concentrations of transition elements such as Cr, V or Ni e.g., in industrial waste material. Analysis of a digest of such material on

the polychromator as described in Chapter five is unwise unless the major interference effects arising from the matrix element in question have been identified. As the determination of quadratic interference coefficients for such occassionally present matrix elements is a tedious process, the analyst is advised to identify major interferences through the preparation and analysis of a single element standard containing the matrix element in question and then analyzing those trace elements, where unacceptable interference is found on the polychromator, by using the scanning technique with background correction on the monochromator.

## 7.6 Conclusion

There is no question that the ICP spectrometric emission technique is one well suited for the analysis of environmental samples firstly because of its multielement nature and secondly because of the relatively good limits of detection. This was shown for instance by Butler, Mathews and Kempster (1982), and confirmed by blind interlaboratory studies, e.g., as discussed in section 7.4. The emphasis, in practical application of the techniques lies however, with the analytical service provided, as the requestor of the analyses is interested in the correctness of his results, rather than in the fact that the technique performed satisfactorily in some quality

control study. For this reason, close attention to instrumental quality control procedures is extremely important. In particular the use of the blank interpolation subtraction routine (equation 69, section 5.3) to correct for drift in emission intensity of the blank standard, and thus correct subtraction of the blank intensity, is extremely important, as error in blank subtraction has a far greater effect at trace concentration levels, than error at the high concentration end of the calibration. Associated with this need to correctly determine the blank intensity under the analyte element line-peak is the need to correct for change in the baseline caused by spectral interference, either through the use of software correction as discussed in Chapter five, or through the use of wavelength profiles for quantitative analysis with off-peak background correction as shown in Chapter six.

Effective quality control requires attention to the total analytical procedure. Thus while doing the required instrumental analysis, the analyst should at all times keep the five corollaries to accurate trace analysis stated in section 2.15 in mind viz;

(i) that the concentration sought should be greater than the detection limit,

(ii) that operating parameters be kept constant in the interests of a stable calibration,

(iii) that correction is made for spectral interferences from matrix elements,

(iv) that the detection limit in the sample matrix be established, and

(v) that where new or unusual matrices are encountered, that analyte element identity be confirmed by methods other than direct analysis on the polychromator.

# CHAPTER 8: CONCLUSIONS

## 8.1 Significance of findings

In the application of ICP emission spectrometry for the analysis of environmental samples, a central problem is the occurrence of spectral interferences, as a consequence of the rich line spectra of an ICP source (Anderson *et al*, 1982), as pointed out in section 1.1, where it was stated that the achievement of analytical accuracy required primarily the identification and quantification of sources of error and interferences.

The analytical problem was further clarified in the evaluation of the present status of the application of the ICP emission spectrometric method (section 2.15) where it was stated that the accurate determination of elements at trace concentration levels in the presence of high concentrations of interfering matrix elements, required that five corollaries be dealt with. These corollaries, which were discussed in detail in section 2.15 are given here in abbreviated form for the convenience of the reader:

(i) Analytical sensitivity, enabling direct determination.

(ii) A stable calibration, which is insensitive to small changes in operating parameters, and invariant to change in sample composition.

(iii) Avoidance of interferences from matrix elements, failing which quantification of such interferences is necessary.

(iv) Definition of the precision and detection limit.

(v) Certification of element identity.

The experimental work undertaken in this study may be viewed in relation to these five corollaries as follows:

The requirement of analytical sensitivity, suitable for direct determination of trace elements, without preconcentration, was shown to apply to a large number of analytical channels on the ARL 34000 polychromator. The detection limit of eleven channels in $\phi$ = 0,01 nitric acid matrix was less than 5 $\mu g.\ell^{-1}$ i.e., Ba, Mg, Cu, Mn, Zn, Be, Ti, V, Sr, B and Y; while a further eleven channels showed a detection limit less than 50 $\mu g.\ell^{-1}$ i.e., Ca, Cr, Fe, Cd, Mo, Al, Co, Ni, Hg, Zr and Sb. Six channels i.e., Na, Pb, Si, As, Se and K showed detection limits greater than 50 $\mu g.\ell^{-1}$ (Table 5-5, section 5.3). That the ICP emission spectrometric technique may be successfully applied to real world environmental samples was illustrated in section 7.4, where examples were given of results from inter-laboratory quality control studies.

A major portion of this thesis was devoted to a study of the factors which have a bearing on the stability of the analyte emission signal, and thus by implication, on the stability of the calibration. The findings which have relevance to the second corollary are firstly, the demonstration (section 3.5) that a residual acid matrix effect for nitric and sulphuric acid is present where the sample uptake rate is controlled by a peristaltic pump, although the magnitude of this effect is smaller than that reported by Dahlquist and Knoll (1978); secondly, that change in sample uptake rate influences the degree of ionization of manganese (section 4.4) and thus the fraction of analyte whose emission signal is recorded; thirdly, that change in aerosol gas flow rate has an effect on analyte emission intensity and that this effect is greater for analyte lines with high excitation potential than those with low excitation potential (section 4.8); fourthly, that a change in input voltage to the rf generator, which was too small to cause a visible change in the metered reading of rf input power, had a marked effect on analyte emission intensity (section 4.6). The fact that the analyte emission intensity of eight out of the twenty channels tested for sensitivity to change in the mains input voltage of the rf generator on the ARL 34000 spectrometer showed a significant change for a mains voltage change of only 2,3% or 5 volt, demonstrates the importance of stabilizing the mains voltage supply to the rf generator in the interest of stable emission signals.

The demonstration that there is a statistically significant correlation between the first, third and fourth parameters mentioned above i.e., degree of matrix suppression of analyte signal (section 3.5), percent change in analyte signal consequent to a change in aerosol gas flow rate (section 4.8), and change in analyte signal consequent to change in input voltage to the rf generator (section 4.6); and excitation potential is a new finding. The fact that these three different parameters all showed similar behaviour with regard to the correlation of a signal change with excitation potential value argues for a similar mechanism of action within the plasma source. This relationship with excitation potential has bearing on the choice of analytical emission lines, as lines with a lower excitation potential can be expected to be less sensitive to change in the parameters mentioned above than lines with high excitation potential.

The fact that the change in emission intensity consequent to change in inner (aerosol) gas flow rate showed a particularly good correlation with excitation potential in the case of ion-lines (equation 48, section 4.8) allowed the development of a weighted internal standardization formula (equation 62, section 4.9). It was shown in section 5.6 that this weighted formula achieved better correction of the concentration readout for ion-lines than conventional internal standardization. An analagous formula for atomic-line weighted internal standardization did not provide effective correction (section 5.7).

The question of establishment of the blank emission signal obtained when for instance $\phi$ = 0,01 nitric acid is aspirated in the absence of analyte elements, also has a bearing with respect to the second corollary i.e., establishment and stability of the calibration of instensity readout in concentration units. Related to this is the need to establish the memory effect within the sample transport system. A study of the memory effect (section 5.5) showed a high-order dependence on washout time for the rapid washout phase (equation 81) which argued against accurate correction for the memory effect and argued for the allowing of a sufficient washout time of ca., 80 s to achieve washout to within 0,1% of initial intensity, for the preceeding sample, for most elements. Two elements which showed prolonged memory within the system were Hg and Mo (Table 5-16). The memory effect found in this study (equations 81 and 82) was considerably more complicated than the simple hyperbolic washout function found by Dobb and Jenke (1983).

A study of the spectral interferences arising from the major matrix interferents commonly present in water samples i.e., Ca, Mg, Mn and Fe (section 5.4) showed that often large differences in the linear and 2nd order correction coefficients were present for interference coefficient determinations in 1983 and in 1985. These differences are thought to be due largely to a difference in aerosol gas flow rate i.e., 410 $m\ell.min^{-1}$ in 1983 as

against 400 mℓ.min$^{-1}$ in 1985, Accurate interference correction coefficients are central to valid analytical results in the software approach (Anderson et al, 1982). Thus the importance of keeping operating conditions affecting relative emission intensities unchanged in the interest of invariant interference correction coefficients. As the factors mentioned in connection with the stability of the calibration above, showed analyte specific changes, these factors may also contribute to correction coefficient change.

The study on the use of the scan mode of analysis as a means of quantifying analyte concentration as given in Chapter six of this thesis has relevance to the fourth and firth corollaries mentioned above. The detection limit is relatively easily quantified in analysis at line centre in terms of the standard deviation of the background (Table 5-5, section 5.3). The analysis of samples using the software approach of interference correction is, however, limited by the criterion of Botto (1984) that the percentage interference correction (equation 31, section 2.12) should not exceed 100 % for accurate determination of an analyte. The software approach of interference correction also has the disadvantage that any interfering matrix element must be quantified and its interference effect on an analyte element must also be quantified for valid determination. The scan mode of analysis has the

advantage that line wing interference from any element may be corrected by off-peak background subtraction. The disadvantage is, however, that precision of line centre intensity readout, used for concentration determination, requires that multiple scans be recorded. As demonstrated in section 6.3 an alternative approach to this problem is the use of an inverse Gaussian transformation to estimate precision of the line-centre readout from a single scan. An example, showing the potential of this procedure, was given for the Co(II) 238,89 nm line, where the equivalence in detection limit as determined by conventional replicate measurement at line centre as opposed to the use of the inverse Gaussian technique on a single scan was shown (section 6.5). An example was also given in section 6.10 of the determination of Cr and Pb in a polluted river sediment by the scan technique. The practical significance of the inverse Gaussian transformation is that sample volume, which may be at a premium, may be saved and further, a saving in analytical time is also implied.

The use of the omega function (equation 20, section 2.10) as a means of estimating detection limit from a single blank scan across the analyte line was shown in section 6.8. This function has the advantage that a deterioration in detection limit is given for sloped backgrounds, a

phenomenon which is of practical significance as wavelength profile drift results in an error in background signal for sloped backgrounds. This type of error does not occur in the case of a flat background under the analyte line.

The use of a visually displayed wavelength scan across an analyte line for quantitative analysis as described in Chapter six, may also be seen as a form of certification of the presence of the analyte, as any background elevation or wing overlap interferences are visually obvious to the analyst. A wavelength scan around a single analytical line of an element will not, however, detect exact line overlap interferences, and in such cases a scan at an alternative wavelength for the analyte element is necessary (section 6.9). As shown in section 7.4, for determination of Cd in a river sediment from a scan, the almost exact coincidence of Fe(I) 226,505 nm with the Cd(II) 226,502 nm analytical line was the probable source of the positive Cd-error.

The question of quality control, which is of relevance too, to the fifth corollary, was addressed in Chapter seven, where examples were given on the performance of the ICP analytical technique using the software approach in interlaboratory studies, plus the use of the scan method at line centre for a river sediment (section 7.4).

Interlaboratory studies are a check not only on an individual analytical procedure, but may also reflect problems in sample preservation or contamination such as the high incidence of positive molybdenum and vanadium outliers in IAEA intercomparison study on water (Pszonicki et al, 1982) as shown in section 7.4(d).

As regards internal quality control, the criterion of Botto (1984) frequently prevents quantification of arsenic or lead concentrations around 0,2 $mg.\ell^{-1}$ as these concentrations are near the detection limit (Table 5-5, section 5.3). It is here that the use of the scanning monochromator may prove useful, as re-analysis of the sample by the scan techniques described in Chapter six is not limited by the criterion of Botto (1984).

## 8.2 Summary

The two main findings of significance in this study were:

Firstly, the demonstration that element specific changes in analyte emission intensity, which show a correlation with excitation potential, occur where (a) the inner (aerosol) gas flow rate is changed, (b) the input mains voltage to the rf generator is changed, and (c) where the volume fraction for a nitric or sulphuric acid matrix is not

matched between calibration standards and samples. The validity of the software approach for interference correction on the polychromator is dependent on accurate interference correction coefficients, which again depend on constant plasma source conditions with unvarying interelement emission intensity ratios. Thus accurate control over the three parameters mentioned above is essential for accurate analysis.

Secondly, that the use of an inverse Gaussian transformation enables quantitative analysis with calculation of precision to be carried out using a single profile scan of a sample, standard and blank solution. This manner of using profile scan data extends the usefulness of a profile scan from the conventional semi-quantitative approach of investigating background elevation and line-wing interferences, to quantitative use of a profile scan for practical analytical use. The significance of the determination of analytical precision from a single scan of the sample lies in the potential saving of sample volume, which may be critical when many analyte elements are to be analyzed on a single sample.

In conclusion, both the simultaneous multichannel type polychromator and the wavelength scanning monochromator type spectrometers are of practical value in the application of ICP emission spectrometry to environmental

sample analysis. The former is of value for the analysis of large numbers of samples, particularly for those elements where the detection limit for direct analysis was found to be less than 5 $\mu g.\ell^{-1}$ i.e., Ba, Mg, Cu, Mn, Zn, Be, Ti, V, Sr, B and Y, but also for the detection of elevated concentrations for the elements with a detection limit below 50 $\mu g.\ell^{-1}$ i.e., Ca, Cr, Fe, Cd, Mo, Al, Co, Ni, Hg, Zr and Sb. The scanning monochromator type spectrometer has its value firstly, in the determination of elements in unusual matrices, where uncertainty of the spectral corrections render the software approach used with the polychromator inapplicable, and secondly, in the determination of an analyte element in the presence of severe background elevation or wing overlap interference, where the criterion of Botto (1984) that when the percentage interference correction (PIC) exceeds 100% then the software approach, as used on the polychromator, is not valid. The profile scan mode of analysis is not limited by the criterion of Botto, as shown in Chapter six.

Finally, the establishment of the detection limit is of fundamental importance in the application of the ICP emission spectrometric analysis technique to trace element analysis of environmental samples. In addition to establishing detection limit by the conventional

integration of emission signals at line centre, the estimation of the detection limit from a profile scan was discussed in Chapter six, where the $\Omega^*_b$ function was introduced to account for deterioration of detection limit where profile shift occurs with sloped or structured backgrounds.

---

* Standard deviation of background intensity readings taken across a wavelength window or interval, rather than at line-centre.

## LITERATURE REFERENCES

ABERCROMBIE, F.N., SILVESTER, M.D., MURRAY, A.D., and BARRINGER, A.R. (1978) A new multielement technique for the collection and analysis of airborne particulates in air quality surveys, in: Applications of inductively coupled plasmas to emission spectroscopy (Ed., R.M. Barnes), Eastern Analytical Symposium (1977), Franklin Institute Press, Philadelphia, p121-145.

ANDERSON, T.A., FORSTER, A.R., and PARSONS, M.L. (1982) ICP emission spectra: II. Alkaline earth elements, Appl. Spectrosc., 36(5), p504-509.

ANGLEYS, G., and MERMET, J.M. (1984) Theoretical aspects and design of a low-power, low-flow-rate torch in inductively coupled plasma atomic emission spectroscopy, Appl. Spectrosc., 38(5), p647-653.

BAGINSKI, B.R., and MEINHARD, J.E. (1984) Some effects of high-solids matrices on the sample delivery system and the Meinhard concentric nebulizer during ICP emission analyses, Appl. Spectrosc., 38(4), p568-572.

BARNES, R.M. (1978) Review of the applications of the inductively coupled plasma, in: Applications of inductively coupled plasmas to emission spectrometry (Ed., R.M. Barnes), Eastern Analytical Symposium (1977), Franklin Institute Press, Philadelphia, p3-49.

BARNES, R.M. (Ed.) (1983) Developments in atomic plasma spectrochemical analysis; proc., of International Winter Conference, San Juan, Puerto Rico, 7 to 11 January 1980, Wiley Heyden, N.Y., p1-751.

BATAL, A., JAROSZ, J., and MERMET, J.M. (1983) Study of the continuum in an argon inductively coupled plasma, in: Developments in atomic plasma spectrochemical analysis, (Ed., R.M. Barnes), proc., of International Winter Conference, San Juan, Puerto Rico, 7 to 11 January 1980, Wiley Heyden, N.Y., p68-71.

BERMAN, S.S., McLAREN, J.W., and RUSSEL, D.S. (1983) Application of the inductively coupled plasma to the analysis of marine samples, in: Developments in atomic plasma spectrochemical analysis, (Ed., R.M. Barnes), proc., of International Winter Conference, San Juan, Puerto Rico, 7 to 11 January 1980, Wiley Heyden, N.Y., p586-600.

BERMAN, S.S., McLAREN, J.W., and WILLIE, S.N. (1980) Simultaneous determination of five trace metals in seawater by inductively coupled plasma atomic emission spectrometry with ultrasonic nebulization, Anal. Chem., 52(3) p488-492.

BLACK, A.P., SINGLEY, J.E., WHITTLE, G.P., and MAULDING, J.S. (1963). Stoichiometry of the coagulation of color-causing organic compounds with ferric sulphate, Jour. AWWA., 55, p1347-1366.

BLADES, M.W. (1982) Some considerations regarding temperature, electron density, and ionization in the argon inductively coupled plasma, Spectrochim. Acta, 37B(10), p869-879.

BLADES, M.W., and HIEFTJE, G.M. (1982) On the significance of radiation trapping in the inductively coupled plasma, Spectrochim. Acta, 37B(3), p191-197.

BLADES, M.W., and HORLICK, G. (1981) Interference from easily ionizable element matrices in inductively coupled plasma emission spectrometry - a spatial study, Spectrochim. Acta, 36B(9), p881-900.

BOCK, R. (1979). A handbook of decomposition methods in analytical chemistry, translated and revised by I.L.Marr, International Textbook Co., Glasgow, p1-444.

BOTTO, R.I. (1983) Interference correction for simultaneous multielement determinations by inductively coupled plasma, in: Developments in atomic plasma spectrochemical analysis, (Ed., R.M. Barnes), proc., of International Winter Conference, San Juan, Puerto Rico, 7 to 11 January 1980, Wiley Heyden, N.Y., p141-166.

BOTTO, R.I. (1984) Quality assurance in operating a multielement ICP emission spectrometer, Spectrochim. Acta, 39B(1), p95-113.

BOUMANS, P.W.J.M. (1966) Theory of spectrochemical excitation, Hilger and Watts Ltd., London, (a) p98-99; (b) p160; (c) p94.

BOUMANS, P.W.J.M. (1974) Multielement analysis by optical emission spectrometry-rise or fall of an empire? Philips Tech. Rev., 34(11/12), p305-321.

BOUMANS, P.W.J.M., McKENNA, R.J., and BOSVELD, M. (1981) Analysis of the limiting noise and identification of some factors that dictate the detection limits in a low-power inductively coupled argon plasma system, Spectrochim. Acta, 36B(11), p1031-1058.

BOUST, D., and SAAS, A (1981). A selective chemical extraction procedure applied to trace metals; comparison between several reagents on two types of sediments (Seine and Gironde Estuaries); in Proc., of International Conference on Heavy Metals in the Environment, Amsterdam, Sept., 1981, C.E.P. Consultants, Edinburgh, p709-712.

BUREAU INTERNATIONAL TECHNIQUE du CHLORE. (1979). Standardization of methods for the determination of traces of mercury; Part 5. Determination of total mercury in water, Anal. Chim. Acta, 109, p209-228.

BRENNER, I.B. (1985) A spectral line atlas for multitrace and minor element analysis of geological and ore mineral samples by ICP-AES, in: Extended abstracts of the 2nd International Symposium on Analytical Chemistry in the exploration, mining and processing of materials, CSIR, Pretoria, 15 to 19 April 1985, p166-168.

BROEKAERT, J.A.C., WOPENKA, B., and PUXBAUM, H. (1982) Inductively coupled plasma optical emission spectrometry for the analysis of aerosol samples collected by cascade impactors, Anal. Chem., 54(13), p2174-2179.

BROWNER, R.F. (1978) Sampling approaches for the inductively coupled plasma in practical analysis, in: Applications of inductively coupled plasmas to emission spectroscopy (Ed., R.M. Barnes), Eastern Analytical Symposium (1977), Franklin Institute Press, Philadelphia, p51-63.

BROWNER, R.F., BLACK, M.S., and BOORN, A.W. (1983) Recent studies with sample introduction into the RFICP, in: Developments in atomic plasma spectrochemical analysis (Ed., R.M. Barnes), proc., of International Winter Conference, San Juan, Puerto Rico, 7 to 11 January 1980, Wiley Heyden, N.Y., p238-244.

BRUWER, C.A., VAN VLIET, H.R., SARTORY, D.P., KEMPSTER, P.L. (1985) An assessment of water related problems of the Vaal River between Barrage and Douglas Weir, Technical report No. TR121 of the Dept., of Water Affairs, Pretoria, p1-185.

BURRELL, D.C. (1974) Atomic spectrometric analysis of heavy-metal pollutants in water, Ann Arbor Science, Michigan, p47-85; p166.

BUTLER, L.R.P., LAQUA, K and STRASHEIM, A. (1985) Nomenclature, symbols, units and their usage in spectrochemical analysis-V radiation sources, Pure & Appl. Chem., 57(10), p1453-1490.

BUTLER, L.R.P., MATTHEWS, P.M., and KEMSPTER, P.L. (1980) The application of an ICP-optical emission spectrometer to the analysis of water and environmental samples: Paper presented at the Symposium on Recent Developments in Emission Spectroscopy, National Institute for Metallurgy, Randburg, April 1980. Paper subsequently written up as an NPRL internal report, Pretoria (1982) on: The investigation of the inductively coupled plasma for the analysis of fresh water, fresh water sediments and biological materials in connection with pollution studies, p1-35.

CAPAR, S.G., and DUSOLD, L.R. (1979) APL applied to processing data from an inductively coupled plasma emission spectrometer, Int. Lab., 9(2), p71-84.

CHASE, J.D. (1971) Theoretical and experimental investigation of pressure and flow in induction plasmas, J. Appl. Phys., 42(12), p4870-4879.

CHURCH, S.E. (1983) Trace element determinations in geological reference materials - an evaluation of the ICP-AES method for geochemistry applications, in: Developments in atomic plasma spectrochemical analysis (Ed., R.M. Barnes), proc., of International Winter Conference, San Juan, Puerto Rico, 7 to 11 January 1980, Wiley Heyden, N.Y., p410-434.

CHRISTMAN, R.F., and GHASSEMI, M. (1966). Chemical nature of organic color in water, Jour. AWWA., 58, p723-741.

CHRISTMANN, D.R., and INGLE, J.D. (1976). Problems with sub-p.p.b. mercury determinations: Preservation of standards and prevention of water mist interferences, Anal. Chim. Acta, 86, p53-62.

DAHLQUIST, R.L., and KNOLL, J.W. (1978) Inductively coupled plasma-atomic emission spectrometry: Analysis of biological materials and soils for major, trace and ultra-trace elements, Appl. Spectrosc., 32(1), p1-29.

DE GALAN, L. (1984) Some considerations on the excitation mechanism in the inductively coupled argon plasma, Spectrochim. Acta, 39B(4), p537-550.

DE GROOT, A.J., ZSCHUPPE, K.H., and SALOMONS, W. (1982). Standardization of methods for heavy metals in sediments, Hydrobiologica, 92, p689-695.

DICKINSON, G.W., and FASSEL, V.A. (1969) Emission spectrometric detection of the elements at the nanogram per milliliter level using induction-coupled plasma excitation, Anal. Chem., 41(8), p1021-1024.

DOBB, D.E., and JENKE, D.R. (1983) Characterization of and correction for memory effects produced by pneumatic nebulizers in inductively coupled plasma emission spectroscopy. Appl. Spectrosc., 37(4), p379-384.

ECKERT, H.U., and PRIDMORE-BROWN, D.C. (1971) Temperature profiles in argon induction plasmas: Theory and experiment, J. Appl. Phys., 42(12), 5051-5054.

ECKSCHLAGER, K. (1969) Errors, measurement and results in chemical analysis, translated by Chalmers, R.A., Van Nostrand Reinhold Co., London, p94.

EPA (1980) Inductively coupled plasma-atomic emission spectrometric method for trace element analysis of water and wastes (interim), United States Environmental Proctection Agency (EPA), Environmental Monitoring and Support Laboratory, Cincinnati, Ohio, p1-29.

EPA (1982) Environmental Protection Agency, Test Method 200.7, Inductively coupled plasma atomic emission spectrometric method for trace element analysis of water and wastes, U.S. EPA Environmental Monitoring and Support Laboratory, Cincinnati, Ohio.

FASSEL, V.A., PETERSON, C.A., ABERCROMBIE, F.N., and KNISELEY, R.N. (1976) Simultaneous determination of wear metals in lubricating oils by inductively-coupled plasma atomic emission spectrometry, Anal. Chem., 48(3), p516-519.

FLOYD, M.A., FASSEL, V.A., WINGE, R.K., KATZENBERGER,. J.M., and D'SILVA, A.P. (1980) Inductively coupled plasma-atomic emission spectroscopy: A computer controlled, scanning monochromator system for the rapid sequential determination of the elements, Anal. Chem., 52(3), p431-438.

FORSTER, A.R., ANDERSON, T.A., and PARSONS, M.L. (1982) ICP spectra: I. Background emission, Appl. Spectrosc., 36(5), p499-504.

FÖRSTNER, U., CALAMANO, W., CONRADT, K., JAKSCH, H., SCHIMKUS, C., and SCHOER, J. (1981). Chemical speciation of heavy metals in solid waste materials (sewage sludge, mining wastes, dredged materials, polluted sediments) by sequential extraction; in Proc., of International Conference on Heavy Metals in the Environment, Amsterdam, Sept., 1981, C.E.P. Consultants, Edinburgh, p698-704.

FÖRSTNER, U., PATCHINEELAM, S.R., and SCHMOLL, G. (1979). Chemical forms of heavy metals in natural and polluted sediments, in: Management and Control of Heavy Metals in the Environment, Proc., of International Conference on Heavy Metals in the Environment, London, Sept., 1979, C.E.P., Consultants, Edinburgh, p316-319.

GARBARINO, J.R., and TAYLOR, H.E. (1979) An inductive-coupled plasma atomic-emission spectrometric method for routine water quality testing, Appl. Spectrosc., 33(3), p220-226.

GARBARINO, J.R., and TAYLOR, H.E. (1980) A Babington-type nebulizer for use in the analysis of natural water samples by inductively coupled plasma spectrometry, Appl. Spectrosc., 34(5), p584-590.

GOLDFARB, V.M. (1983) Non-equilibrium effects in plasma discharges for atomic emission spectroscopy, in: Developments in atomic plasma spectrochemical analysis (Ed., R.M. Barnes), proc., of International Winter Conference, San Juan, Puerto Rico, 7 to 11 January 1980, Wiley Heyden, N.Y., p725-739.

GOLIGHTLY, G.W. (1978) Recent geochemical applications of the inductively coupled plasma, in: Applications of inductively coupled plasmas to emission spectroscopy (Ed., R.M. Barnes), Eastern Analytical Symposium (1977), Franklin Institute Press, Philadelphia, p107-119.

GOULDEN, P.D., and ANTHONY, D.H.J. (1982) Determination of trace metals in freshwaters by inductively coupled plasma atomic emission spectrometry with a heated spray chamber and desolvation. Anal. Chem., 54, p1678-1681.

GREEN, J.R., and MARGERISON, D. (1978) Statistical treatment of experimental data, Elsevier, Amsterdam, (a) p126-142; (b) p104-106; (c) p189-196; (d) p201-203; (e) p163-173.

GREENFIELD, S. (1983) Detection limits and other figures of merit, in: Developments in atomic plasma spectrochemical analysis (Ed., R.M. Barnes), proc., of International Winter Conference, San Juan, Puerto Rico, 7 to 11 January 1980, Wiley Heyden, N.Y., p1-19.

GREENFIELD, S., JONES, I. LL., and BERRY, C.T.. (1964) High-pressure plasmas as spectroscopic emission sources, Analyst, 89, p713-720.

GREENFIELD, S., JONES, I. LL., McGEACHIN, H. McD., and SMITH, P.B. (1975) Automatic multi-sample simultaneous multielement analysis with a H.F. plasma torch and direct reading spectrometer, Anal. Chim. Acta, 74, p225-245.

GREENFIELD, S., and McGEACHIN, H. McD. (1978) Calorimetric and dimensional studies on inductively coupled plasmas, Anal. Chim. Acta, 100, p101-119.

GREENFIELD, S., and THORBURN BURNS, D. (1980) A comparison of argon-cooled and nitrogen-cooled plasma torches under optimised conditions based on the concept of intrinsic merit, Anal. Chim. Acta, 113, p205-220.

HAMILTON, E.I. (1980a) The need for trace element analyses of biological materials in the environmental sciences, in: Elemental analysis of biological materials, International Atomic Energy Agency, Technical Report IAEA No. 197, Vienna, Austria, p39-54.

HAMILTON, E.I. (1980b). The chemical laboratory and trace element analysis, in: Elemental analysis of biological materials, International Atomic Energy Agency, Technical Report IAEA No. 197, Vienna, Austria, p303-315.

HEIDEN, R.W., and AIKENS, D.A. (1977). Composition differences in commercial polyethylene bottles and their relation to the stability of stored part-per-billion mercury (II) solutions, Anal. Chem., 49(4), p668-670.

HESSE, P.R. (1971) A textbook of soil chemical analysis, John Murray, London, p301-331.

IYENGAR, G.V., and SANSONI, B. (1980) Sample preparation of biological materials for trace element analysis, in: Elemental analysis of biological materials, International Atomic Energy Agency, technical report IAEA no., 197, Vienna, Austria, p73-101.

JOHNSON, G.W., TAYLOR, H.E., and SKOGERBOE, R.K. (1979) Determination of trace elements in natural waters by the d.c. argon plasma, multielement atomic emission spectrometer (DCP-MAES) technique, Spectrochim. Acta, 34B, p197-212.

JONES, J.L., DAHLQUIST, R.L., KNOLL, J.W., and HOYT, R.E. (1974) Liquids analysis with the inductively coupled plasma torch - a multichannel optical emission system, paper presented at the 1974 Pittsburgh Conference, Cleveland, Ohio.

KEMPSTER, P.L. (1979). Health implications of using bitumen, coal-tar, asbestos and plastic materials in water distribution systems, Technical Report No. 101, Dept. of Water Affairs, Pretoria, p1-8.

KEMPSTER, P.L., and DE VILLIERS, D.B. (1980) Evaluation of ICP spectrometry for water analysis. Internal report, Hydrological Research Institute, Dept., of Water Affairs, Pretoria. Paper presented at Symposium on Recent Developments in Emission Spectroscopy, National Institute of Metallurgy, Randburg, April 1980.

KEMPSTER, P.L., MALLOCH, J.D.R., and DE KLERK, M.V.D.S. (1983) Determination of interference correction coefficients for routine trace element analysis of surface water by inductively coupled plasma emission spectrometry, Spectrochim. Acta, 38B (5/6), p967-972.

KEMPSTER, P.L., and VAN VLIET, H.R. (1978). A semi-automated resin concentration method for the preconcentration of trace metals in fresh water, prior to atomic absorption analysis, Water SA, 4(3), p125-128.

KENNY, J.F., and KEEPING, E.S. (1964) Mathematics of statistics, 3rd edition, Van Nostrand, N.Y., p182-186.

KIRKBRIGHT, G.F., and WARD, A.F. (1974) Atomic-emission spectrometry with an induction-coupled high-frequency plasma source. Comparison with the inert-gas shielded premixed nitrous oxide acetylene flame for multi-element analysis, Talanta, 24(11), p1145-1165

KIRKBRIGHT, G.F., WARD, A.F., and WEST, T.S. (1973) Atomic emission spectrometry with an induction-coupled high-frequency plasma source. The determination of iodine, mercury, arsenic and selenium, Anal. Chim. Acta, 64, p353-362

KLOPPER, B.C., and MARCHANT, J.W. (1977). Some adsorption/-contamination phenomena observed in dilute trace element solutions stored in high-density polyethylene containers, Internal Report, Geological Survey, Pretoria, p1-97.

KNOTT, A.R. (1975). Investigation of a high purity water system, At Absorpt. Newslett., 14(5), p126-127.

KORNBLUM, G.R. (1977) Physical characterization of an inductively coupled plasma for analytical atomic spectroscopy, Doctoral thesis, Delf University, p1-106.

KUENNEN, R.W., WOLNIK, K.A., FRICKE, F.L. (1982) Pressure dissolution and real sample matrix calibration for multielement analysis of raw agricultural crops by inductively coupled plasma atomic emission spectrometry, Anal. Chem., 54(13), p2146-2150.

LARSON, G.F., and FASSEL, V.A. (1979) Line broadening and radiative recombination background interferences in inductively coupled plasma-atomic emission spectroscopy, Appl. Spectrosc., 33(6), p592-599.

LARSON, G.F., FASSEL, V.A., SCOTT, R.H., and KNISELEY, R.N. (1975) Inductively coupled plasma-optical emission analytical spectrometry. A study of some interelement effects, Anal. Chem., 47(2), p238-243.

LARSON, G.F., GOODPASTURE, R.T., and MORROW, R.W. (1983) Simultaneous multielement analysis of natural waters by inductively coupled plasma-optical emission spectrometry (ICP-OES), in: Developments in atomic plasma spectrochemical analysis (Ed., R.M. Barnes), proc., of International Winter Conference, San Juan, Puerto Rico, 7 to 11 January 1980, Wiley Heyden, N.Y. p611-626.

LOWE, M.D. (1981) A low argon flow inductively coupled plasma torch utilizing a flame-atomic absorption spectrometry nebulizer, Appl. Spectrosc., 35(1), p126-128.

L'VOV, B.V. (1970) Atomic absorption spectrochemical analysis, Soviet Acadamy of Sciences translated by J.H. Dixon, Adam Hilger, London, (a) p47-50; (b) p132-133.

MAESSEN, F.J.M.J., BALKE, J., and DE BOER, J.L.M. (1982) Preservation of accuracy and precision in the analytical practice of low power ICP-AES, Spectrochim. Acta, 37B(6), p517-526.

MAHAN, K.I., and MAHAN, S.E. (1977). Mercury retention in untreated water samples at the part-per-billion level, Anal. Chem, 49(4), p662-664.

McKINNON, P.J., GIESS, K.C., and KNIGHT, T.V. (1983) A clog-free nebulizer for use in inductively coupled plasma-atomic emission spectroscopy, in: Developments in atomic plasma spectrochemical analysis (Ed., R.M. Barnes), proc., of International Winter Conference, San Juan, Puerto Rico, 7 to 11 January 1980, Wiley Heyden, N.Y., p287-301.

MEDDINGS, B., ANDERSON, H., KAISER, H., and NG, R. (1985) Design and use of a high precision, low operating cost nebulizer/torch system for ICP analysis, in: Extended abstracts of the 2nd International Symposium on Analytical Chemistry in the Exploration, Mining and Processing of Materials, CSIR, Pretoria, 15 to 19 April, p153-154.

MERMET, J.M., and TRASSY, C. (1981) A spectrometric study of a 40 MHz inductively coupled plasma-V. Discussion of spectral interferences and line intensities, Spectrochim. Acta, 36B(4), p269-292.

MERRYFIELD, R.N., and RUNNELS, J.H. (1983) The inductively coupled plasma-an important and versatile analytical tool for the petroleum industry, in: Developments in atomic plasma spectrochemical analysis (Ed., R.M. Barnes), proc., of International Winter Conference, San Juan, Puerto Rico, 7 to 11 January 1980, Wiley Heyden, N.Y. p396-403.

MICHAUD, E., and MERMET, J.M. (1982) Iron spectrum in the 200-300 nm range emitted by an inductively coupled argon plasma, Spectrochim. Acta, 37B (2), p145-164.

MIKA, J., and TöRöK, T. (1974) Analytical emission spectroscopy fundamentals: translated by P.A. Floyd, London, Butterworths, p1-529.

MONTASER, A., FASSEL, V.A., ZALEWSKI, J. (1981) A critical comparison of Ar and Ar-$N_2$ inductively coupled plasmas as excitation sources for atomic emission spectrometry, Appl. Spectrosc., 35(3), p292-302.

MOORE, W.J. (1966) Physical chemistry, 4th edition, Longmans, London, p230-231.

MOTOOKA, J.M., MOSIER, E.L., SUTLEY, S.J., and VIETS, J.G. (1979) Induction-coupled plasma determination of Ag, Au, Bi, Cd, Cu, Pb and Zn in geologic materials using a selective extraction technique-preliminary investigation, Appl. Spectrosc., 33(5), p456-460.

MUNTER, R.C., and GRANDE, R.A. (1983) Plant tissue and soil extract analysis by ICP-atomic emission spectrometry, in: Developments in atomic plasma spectrochemical analysis (Ed., R.M. Barnes), proc., of International Winter Conference, San Juan, Puerto Rico, 7 to 11 January 1980, Wiley Heyden, N.Y., p653-672.

NAKAHARA, T. (1981) Application of hydride generation to the determination of trace concentrations of arsenic by inductively-coupled plasma atomic emission spectrometry, Anal. Chim. Acta, 131, p73-82.

NETTER, J., and WASSERMAN, W. (1974). Applied linear statistical models, Richard D. Irwin Inc., Illinois, (a) p804-805; (b) p807-813.

NHRMWDA. (1977). National handbook of recommended methods for water-data acquisition (NHRMWDA); Ch 5, chemical and physical quality of water and sediment, office of water data coordination, Geological Survey, U.S. Dept., of the Interior, Reston, Virginia, p5-1 to 5-16.

NORTHWAY, S.J., BROWN, R.M., and FRY, R.C. (1980) Atomic nitrogen spectra in the argon inductively coupled plasma (ICP), Appl. Spectrosc., 34(3), p338-348.

NORTHWAY, S.J., and FRY, R.C. (1980) Atomic oxygen spectra in the argon inductively coupled plasma (ICP), Appl. Spectrosc., 34(3), p332-338.

OHLS, K., KOCH, K.H., GROTE, H. (1977) Einsatz der ICP--emissionsspektometrie zur simultanen multielementanalyse, Z. Anal. Chem., 284, p177-187.

OHLS, K., and SOMMER, D. (1983) Analysis of liquid, solid and gaseous samples using a high-power nitrogen/argon ICP system, in: Developments in atomic plasma spectrochemical analysis (Ed., R.M. Barnes), proc., of International Winter Conference, San Juan, Puerto Rico, 7 to 11 January 1980, Wiley Heyden, N.Y., p321-336.

PARSONS, M.L., FORSTER, A., and ANDERSON, D. (1980) An atlas of spectral interferences in ICP spectroscopy, Plenum Press, N.Y., p1-644.

PSZONICKI, L., and HANNA, A.N. (1985) Report on intercomparison IAEA/V-10 of the determination of trace metals in hay powder, International Atomic Energy Agency, Vienna, Report No., IAEA/RL/123.

PSZONICKI, L., HANNA, A.N., and SUSCHNY, O. (1983a) Report on intercomparison V-9 of the determination of trace elements in cotton cellulose, International Atomic Energy Agency, Laboratory Seibersdorf, Report No. IAEA/RL/97, p1-23.

PSZONICKI, L., HANNA, A.N., and SUSCHNY, O. (1983b) Report on intercomparison A-13 of the determination of trace elements in freeze dried animal blood, International Atomic Energy Agency, Laboratory Seibersdorf, Report No., IAEA/RL/98.

PSZONICKI, L., VEGLIA, A., and SUSCHNY, O. (1982) Report on intercomparison W-3/1 of the determination of trace elements in water, International Atomic Energy Agency, Laboratory Seibersdorf, Report No., IAEA/RL/94.

REED, T.B. (1961) Induction-coupled plasma torch, J. Appl. Phys., 32(5), p821-824.

REED, T.B. (1962) Plasma torches, Int. Sci., & Tech., June 1962, No. 6, p42-48.

REEVES, R.D., NIKDEL, S., and WINEFORDNER, J.D. (1980) Molecular emission spectra in the radiofrequency excited inductively coupled argon plasma, Appl. Spectrosc., 34(4), p477-483.

REZAAIYAAN, R., and HIEFTJE, G.M. (1985) Analytical characteristics of a low-flow, low-power inductively coupled plasma, Anal. Chem., 57, p412-415.

REZAAIYAAN, R., HIEFTJE, G.M., ANDERSON, H., KAISER, H., and MEDDINGS, B. (1982) Design and construction of a low-flow, low-power torch for inductively coupled plasma spectrometry, Appl. Spectrosc., 36(6), p627-631.

ROEDERER, J.E., BASTIAANS, G.J., FERNANDEZ, M.A., and FREDEEN, K.J. (1982) Spatial distribution of interference effects in ICP emission analysis, Appl. Spectrosc., 36(4), p383-389.

RONAN, R. (undated) Simultaneous multielement analysis of liquid samples by inductively coupled plasma atomic-emission spectroscopy, Internal report of the Environmental Protection Agency, EPA, Central Regional Laboratory, Chicago, Illinois.

SABS (1984) Specification for water for domestic supplies, South African Bureau of Standards, Specification No., SABS 241-1984.

SACHS, L. (1982) Applied statistics a handbook of techniques, translated by Reynarowych, Z., 5th edition, Springer-Verlag, New York, p94-96.

SANEMASA, I., DEGUCHI, T., URATA, K., TOMOOKA, J., and NAGAI, H. (1976). Loss and recovery of mercury from sea water during storage, Anal. Chim. Acta, 87, p479-481.

SCOTT, R.H., FASSEL, V.A., KNISELEY, R.N., and NIXON, D.E. (1974) Inductively coupled plasma-optical emission analytical spectrometry, Anal. Chem., 46(1), p75-80.

SKOGERBOE, R.K., LAMOTHE, P.J., BASTIAANS, G.J. FREELAND, S.J., and COLEMAN, G.N. (1976) A dynamic background correction system for direct reading spectrometry, Appl. Spectrosc., 30(5), p495-500.

SLAVIN, M. (1978) Atomic absorption spectroscopy, 2nd edition, John Wiley & Sons, New York, p1-14.

SMITH, R. (1984a) NIWR interlaboratory comparison study no., 83/A: Determination of trace metals in river sediment, Council for Scientific and Industrial Research, Research Report No., 602, Pretoria, p1-33.

SMITH, R. (1984b) NIWR interlaboratory comparison study no., 83/B: Analysis of a sewage sludge for inorganic chemical contaminants and nutrients, Council for Scientific and Industrial Research, Research Report No., 603, Pretoria, p1-33.

STANDARD METHODS (1975) Standard methods for the examination of water and wastewater, 14th edition, published jointly by the American Public Health Association, American Water Works Association and the Water Pollution Control Federation, Washington D.C., p141.

STANDARD METHODS (1980) Standard methods for the examination of water and wastewater, 15th edition, published jointly by the American Public Health Association, American Water Works Association and the Water Pollution Control Federation, Washington D.C., (a) p24-30; (b) p35-39; (b) p141-142.

SUBRAMANIAN, K.S., and MERANGER, J.C. (1982) Simultaneous determination of 20 elements in some human kidney and liver autopsy samples by inductively coupled plasma atomic emission spectrometry, Sci. Tot. Environ., 24, p147-157.

SUMMERHAYS, K.D., LAMOTHE, P.J., and FRIES, T.L. (1983) Volatile species in inductively coupled plasma atomic emission spectroscopy: Implications for enhanced sensitivity, Appl. Spectrosc., 37(1), p25-28.

TAYLOR, H.E. (1983) Current status of plasma emission spectroscopy in water analysis , in: Developments in atomic plasma spectrochemical analysis (Ed., R.M. Barnes), proc., of International Winter Conference, San Juan, Puerto Rico, 7 to 11 January 1980, Wiley Heyden, N.Y., p575-585.

TAYLOR, C.E., and FLOYD, T.L. (1980) Evaluation of a multichannel inductively coupled-optical emission spectrometer modified to minimize and correct scattered light effects., Appl. Spectrosc., 34(4), p472-477.

TAYLOR, P., JANSSENS, E., DAMS, R., and HOSTE, J. (1984) Wavelength accuracy and reproducibility of a high resolution computer controlled monochromator, Spectrochim. Acta, 39B(7), p867-878.

THOMPSON, M., PAHLAVANPOUR, B., WALTON, S.J., and KIRKBRIGHT, G.F. (1978a) Simultaneous determination of trace concentrations of arsenic, antimony, bismuth, selenium and tellurium in aqueous solution by introduction of the gaseous hydrides into an inductively coupled plasma source for emission spectrometry, Analyst, 103, p568-579.

THOMPSON, M., PAHLAVANPOUR, B., WALTON, S.J., and KIRKBRIGHT, G.F. (1978b) Simultaneous determination of trace concentrations of arsenic, antimony, bismuth, selenium and tellurium in aqueous solution by introduction of the gaseous hydrides into an inductively coupled plasma source for emission spectrometry, part II-interference studies, Analyst, 103, p705-713.

THOMPSON, M., RAMSEY, M.H., and PAHLAVANPOUR, B. (1982) Water analysis by inductively coupled plasma atomic-emission spectrometry after a rapid pre-concentration, Analyst, 107, p1330-1334.

TRAIN, R.E. (1979) Quality criteria for water, U.S. Environmental Protection Agency, Castle House Publications, London, p54-64.

TRASSY, C., and MERMET, J.M. (1984) Les applications analytiques des plasmas haute-frequence, Lavoisier, Paris, p1-327.

TRUITT, D., and ROBINSON, J.W. (1970a) Spectroscopic studies of radio-frequency induced plasma. Part I. Development and characterization of equipment, Anal. Chim. Acta, 49, p401-415.

TRUITT, D., and ROBINSON, J.W. (1970b) Spectroscopic studies of organic compounds introduced into a radiofrequency induced plasma - part II. Hydrocarbons, Anal. Chim. Acta, 51, p61-67.

VAN MONTFORT, P.F.E., and AGTERDENBOS, J., (1981) Some fundamental considerations on analytical high-frequency plasmas, Talanta, 28 p629-635.

WALLACE, G.T., FLETCHER, I.S., and DUCE, R.A. (1977). Filter washing, a simple means of reducing blank values and variability in trace metal environmental samples, J. Environ. Sci. Health, A12(9), p493-506.

WATLING, H.R., and WATLING, R.J. (1976). Preconcentration and extraction techniques for the determination of trace elements in water, 1. Sodium diethyldithiocarbamate - chloroform; Special Report Fis 83, National Physical Research Laboratory, Council for Scientific and Industrial Research, Pretoria, p1-70.

WATTERS, R.L., and NORRIS, J.A. (1978) Factors influencing precision and accuracy of analysis with inductively coupled plasmas, in: Applications of inductively coupled plasmas to emission spectroscopy (Ed., R.M. Barnes), Eastern Analytical Symposium (1977), Franklin Institute Press, Philadelphia, p65-81.

WEAST, R.C. (Ed.,) (1980) CRC handbook of chemistry and physics, 60th edition, CRC Press, Boca Raton, Florida, pE-35-350 to E-378.

WEHR, M.R., and RICHARDS, J.A. (1964) Physics of the atom, Addison-Wesley Inc., London, p404-407.

WEISS, H.V., SHIPMAN, W.H., and GUTTMAN, M.A. (1976). Effective storage of dilute mercury solutions in polyethylene, Anal. Chim. Acta, 81, p211-217.

WHO. (1973). World Health Organization International Reference Centre for Community Water Supply, Technical Paper No. 4 on Health aspects relating to the use of uPVC pipes for community water supply, The Hague, p1-54.

WINDSOR, D.L., and DENTON, M.B. (1979) Empirical formula determination with an inductively coupled plasma gas chromatographic detector, Anal. Chem., 51(8), p1116-1119.

WINGE, R.K., FASSEL, V.A., KNISELEY, R.N., DE KALB, E., and HAAS, W.J. Jr. (1977) Determination of trace elements in soft, hard and saline waters by the inductively coupled plasma, multi-element atomic emission spectroscopic (ICP-MAES) technique, Spectrochim. Acta, 32B, p327-345.

WOLNIK, K.A., KUENNEN, R.W., FRICKE, F.L. (1983) Determination of toxic and nutritional elements in raw agricultural crops using ICAP spectroscopy, in: Developments in atomic plasma spectrochemical analysis (Ed., R.M. Barnes), proc., of International Winter Conference, San Juan, Puerto Rico, 7 to 11 January 1980, Wiley Heyden, N.Y., p 685-696.

ZAIDEL', A.N., PROKOF'EV, V.K., RAISKII, S.M., SLAVNYI, V.A., and YA SCHREIDER, E. (1970) (The Russian) tables of spectral lines, IFI/Plenum, N.Y., 3rd edition, p1-782.

ZAMECHEK, W., LEWANDOWSKI, R.J., PARKHURST, R.G., and ELLGREN, A.J. (1978) Trace metals analysis in silicon and aluminum metals by inductively coupled plasma, in: Applications of inductively coupled plasmas to emission spectroscopy (Ed., R.M. Barnes), Eastern Analytical Symposium (1977), Franklin Institute Press, Philadelphia, p169-185.